THE UNIVERSITY *of* EDINBURGH

This thesis has been submitted in fulfilment of the requirements for a postgraduate degree (e. g. PhD, MPhil, DClinPsychol) at the University of Edinburgh. Please note the following terms and conditions of use:

- This work is protected by copyright and other intellectual property rights, which are retained by the thesis author, unless otherwise stated.
- A copy can be downloaded for personal non-commercial research or study, without prior permission or charge.
- This thesis cannot be reproduced or quoted extensively from without first obtaining permission in writing from the author.
- The content must not be changed in any way or sold commercially in any format or medium without the formal permission of the author.
- When referring to this work, full bibliographic details including the author, title, awarding institution and date of the thesis must be given.

Unravelling the proteomic landscape in Interferon Stimulated Gene 15 deficient cancer cellular models

Ainhoa Gonzalez Urionabarrenetxea

Doctor of Philosophy

University of Edinburgh

August 1, 2023

“The good thing about science is that it’s true whether or not you believe in it”

Neil deGrasse Tyson

“Nothing in life is to be feared, it is only to be understood. Now is the time to understand more, so that we may fear less”

Marie Skłodowska Curie

Dedicated to my parents, who have given me everything

Declaration

I declare that this thesis was composed by myself, that the work contained herein is my own except where explicitly stated otherwise in the text, and that this work has not been submitted for any other degree or professional qualification except as specified.

Ainhoa Gonzalez Urionabarrenetxea

August 1, 2023

Acknowledgements

First and foremost, I want to thank Professor Kathryn Ball for everything she has done for me, both inside and outside this PhD. I am immensely grateful to have had you through this rocky process full of surgeries, back injuries, worldwide pandemics and more. You always remained calmed, supportive and understanding, and I would not have been able to take this project to term without your encouragement and guidance. Thank you for believing in me when I did not, for helping me build up my confidence and for our conversations about science, plants and life.

I would like to extend my sincere thanks to Professor Ted Hupp for always being available to provide insight into this project. Thank you for your advice and suggestions when things did not go to plan and for your enthusiasm when addressing the mysteries of science. I gratefully acknowledge the support of my partner institution, the University of Gdansk, and everyone at the International Centre for Cancer Vaccine Science. I want to thank Dr. Sachin Kote and Dr. Jakub Faktor for welcoming me in their lab, taking the time to teach me, and for their valuable contribution to this thesis. Likewise, I want to thank Professor Lenka Hernychová and Mr. Tomáš Henek for their work, contribution and patience explaining every little detail of the process, answering my (many) questions.

My warmest thanks to everyone who has made this thesis possible, and to all my lab colleagues for creating such a wonderful and safe working environment. Special thanks to Jack for always making time to help me with a smile, and to Ashita, who has been there for me through the good and the bad, both professionally and personally. I really appreciate the time you have taken to patiently teach me and all the advice and guidance you have given me when I felt lost - thank you for not giving up on me. Equally, many thanks to Janet for the emotional support and for always making me laugh when I need it the most, and to Maria for being there for me no matter how far apart we are.

I am deeply grateful to my husband, who has listened to all my biology related problems with immeasurable patience, always making his best effort to understand the science behind only to help me solve them. Thank you for your love and support, for being by my side through all the stages of this journey picking me up when I thought I could not make it, and for the late-night work and data analysis sessions.

Finally, I want to thank my parents, to who I dedicate this piece of work, for their unconditional love and support. Thank you for being there through the good and the bad, for enduring my moods in the bad days and for your continuous encouragement over the years. I would not be anything of what I am today without you.

Lay summary

The variety of cancer treatments available nowadays have greatly increased the life expectancy of patients with certain tumour types, but developing treatment resistance is not uncommon. Understanding the molecular changes that drive resistance is essential to design therapies that work appropriately. The interferon Stimulated Gene 15 (ISG15) is a well-known antiviral protein that helps the immune system clear infections, but it has also been found to be involved in cancer progression and treatment resistance. ISG15 is capable of attaching to other proteins to alter their function, which means it interacts with hundreds of different proteins with an extensive range of biological jobs. This fact makes it hard to study and understand the role of ISG15 in cancer. As suggested by its full name, the expression of ISG15 is induced by interferons (IFNs), small proteins whose main function is the activation and enhancement of the innate immune system, which have been extensively used as treatment for pathogenic infections and cancers.

This study aims to analyse what proteins and biological processes get altered in the absence of ISG15 in two different cancer models – cervical cancer and brain cancer - in order to shed light on the role and mechanism of this protein in IFN treatment resistance. For this, different mass-spectrometry (MS) approaches were used. MS is a technique capable of precisely identifying what proteins and in what amount are present at a given time in a complex biological mixture. Comparing what proteins appear or disappear and in what amounts, when we remove ISG15 and treat the cells with IFN, can help us understand what processes get activated and deactivated upon treatment, providing insights into the resistance mechanism(s).

Abstract

The Interferon Stimulated Gene 15 (ISG15) is a ubiquitin-like protein that can be found both conjugated to target proteins, in a process known as ISGylation, and in a non-conjugated "free" form where it can act as a cytokine. Even though ISG15 has been widely studied for its antiviral properties, recent research has implicated ISG15 in many more biological processes, including the development and progression of cancer. In this area, research is divided between studies that suggest ISG15 is a tumour suppressor and immune system enhancer, and those that claim it relates to tumour aggressiveness and treatment resistance. The extensive number of modification targets and variety of roles of ISG15 makes it challenging to determine its molecular mechanisms in cancer.

The aim of this study is to shed light on the role of this ubiquitin-like protein in cancer cell models and to provide insights into the mechanisms of action that leads to ISG15 function in interferon (IFN) resistance. Clustered Regularly Interspaced Short Palindromic Repeats (CRISPR) / Cas9 gene-editing technology was used to ablate ISG15 expression in a cervical cancer cellular model (SiHa cells). Once a stable knock-out was obtained, a variety of analysis were performed with and without interferon treatment to try to identify any biological difference between the wild type cells and the ISG15 deficient cells, including cell growth and cell cycle analysis and colony formation assays. After identifying ISG15 deficient cells as sensitive to IFNα treatment, which was confirmed in a variety of cellular models, three different proteomic approaches were used to try to address the proteomic landscape in two ISG15 deficient cell backgrounds in the presence and absence of IFNα treatment. a) First, a stable isotope labelling by amino acids in cell culture (SILAC) technique was used in wild-type (WT) and ISG15 deficient cervical cancer (SiHa) cells, either untreated or treated for 24 or 48 hours, to look at recently synthesised protein changes. Results showed significant increased expression of other ISGs like IFIT1 and MX1, but also of other less expected proteins such as NQO1, MT1G and MT1F, all of which are involved in oxidative stress response and detoxification. This was reflected in the analysis of the dysregulated biological processes performed with the identified targets, which revealed upregulated response to stress. This analysis also revealed upregulated processes related to antigen processing and presentation, downregulated processes related to response to wounding and wound healing and various dysregulated metabolic processes. b) Second, in order to find out what proteins and processes were commonly altered upon depletion of ISG15 in different cancer models, a steady state whole proteomics approach was used in ISG15 deficient patient-derived glioblastoma stem cells (GSCs). Again, the upregulation of a IFN stimulated signature was detected in the absence of ISG15, as well as processes related to the positive regulation of IFN production. Several metabolic processes were also

found to be dysregulated, and processes related to antigen processing and presentation were also detected to be upregulated upon IFN treatment. c) Finally, as the previous results suggested the involvement of ISG15 in MHC class I antigen presentation, a state-of-the-art immunopeptidomic method was used to elute and analyse the peptides presented by MHC-I in ISG15 deficient versus wild-type GSCs in the presence or absence of IFNα treatment. The presentation of peptides derived from several proteins were found significantly altered in the absence of ISG15 (e.g. GAPDH), and peptide length distribution analysis suggested an increased and sustained expression of MHC-I presented peptides upon IFN treatment.

Overall, results suggest that the loss of ISG15 results in an amplified IFN response promoting sensitivity, probably due to the loss of the role of ISG15 as a negative regulator of this pathway. At the same time, the absence of ISG15 seems to be involved with mitochondrial and metabolic dysregulation, as well as altered antigen peptide expression. Further researching these findings could be useful in the field of immune based and peptide targeted therapies.

Abbreviations

μg	Microgram
μL	Micro-Litre
μM	Micromolar
μm	Micrometer
4EHP	Eukaryotic Initiation Factor 4E Homologous Protein
A-T	Ataxia-telangiectasia
ACN	Acetonitrile
AMP	Adenosine Monophosphate
APS	Ammonium Persulfate
ATP	Adenosine Triphosphate
ATR	Ataxia-Telangiectasia and Rad3-Related
BCA	Bicinchoninic acid
bMercETOH	Beta-mercaptoethanol
bp	Base pairs
BSA	Bovine Serum Albumin
CCL18	Chemokine (C-C motif) Ligand 18
CD	Cluster of Differentiation
cDNA	Complementary DNA
CENP-A	Centromere Protein A
CHIP	Carboxy-terminus of Hsp70-Interacting Protein

CLL	Chronic Lymphocytic Leukemia
cm	Centimetre
COVID	Coronavirus Disease
CRISPR	Clustered Regularly-Interspaced Short Palindromic Repeat
CTLA4	Cytotoxic T-lymphocyte Associated protein 4
CTP	Camptothecin
Da	Dalton
DAPI	4,6-diamidino-2-phenylindole
DMSO	Dimethyl Sulfoxide
DNA	Deoxyribonucleic Acid
DSB	Double-strand DNA Breaks
DTT	Dithiothreitol
E1	Ubiquitin-activating enzyme
E2	Ubiquitin-conjugating enzyme
E3	Ubiquitin ligase enzyme
E6AP	E6-associated protein
ECL	Enhanced Chemiluminescence
EDTA	Ethylenediaminetetraacetic acid
EFP	Estrogen-responsive Finger Protein
EGF	Epidermal Growth Factor
eIF4E	Eukaryotic Initiation Factor 4E
eIF4G	Eukaryotic Initiation Factor 4G
ER	Endoplasmic Reticulum
ERK1/2	Extracellular Signal-Regulated Kinase 1/2
EV	Empty Vector
FACS	Fluorescence-Activated Cell Sorting

FASP	Filter Aided Sample Preparation
FBS	Fetal Bovine Serum
FGF	Fibroblast Growth Factor
FISH	Fluorescence In Situ Hybridization
FITC	Fluorescein Isothiocyanate Conjugated
FLAG	Anti-FLAG antibody
FLICA	Fluorescent Labeled Inhibitor of Caspases
FSC	Forward Scatter
GAF	Gamma activated factor
GAPDH	Glyceraldehyde-3-phosphate dehydrogenase
GAS	Gamma Activated Sequence
GFP	Green Fluorescent Protein
gRNA	Guide RNA
GSC	Glioblastoma Stem Cells
Gy	Gray
HCV	Hepatitis C Virus
HDR	Homology-Directed Repair
HECT	Homologous to E6-AP Carboxyl Terminus
HER2	Human Epidermal growth factor Receptor 2
HERC5	HECT Domain and RCC1-Like Domain-Containing Protein 5
HHARI	Human Homolog of Drosophila Ariadne
HIV-1	Human Immunodeficiency Virus 1
HLA-ABC	Human Leukocyte Antigen Class I ABC
HUSH	Human Silencing Hub
IFI	Interferon Induced Protein
IFIT1	Interferon-induced protein with tetratricopeptide repeats 1

IFITM1	Interferon Induced Transmembrane Protein 1
IFN	Interferon
IFNAR	Interferon alpha/beta receptor
IFNGR	Interferon gamma receptor
IL	Interleukin
IL-12R	Interleukin 12 Receptor
IRDS	Interferon Related DNA-damage Resistance Signature
IRF	Interferon Regulatory Factor
IRG	Interferon Regulated Gene
ISG	Interferon Stimulated Gene
ISG15	Interferon Stimulated Gene 15
ISGF3	Interferon Stimulated Gene Factor 3
ISRE	Interferon Stimulated Response Element
IU	International Unit
JAK	Janus kinase
kb	Kilo-base pairs
kDa	Kilo Dalton
kg	Kilogram
KI	Knock-in
KLD	Kullback-Leibler Distance
KO	Knock-out
kV	Kilovolts
LB	Lysogeny Broth
LC	Liquid Chromatography
LC-MS	Liquid chromatography-mass spectrometry
LCMV	Lymphocytic Choriomeningitis Virus

LFA-1	Leukocyte Function Associated Antigen-1
LS-MS	Laser desorption/ionization mass spectrometry
M	Molar
M2	Macrophage M2 subtype
mA	Milliamp
MAPK	Mitogen-Activated Protein Kinase
MDA5	Melanoma Differentiation-Associated protein 5
MEF	Mouse Embryonic Fibroblasts
MEF	Murine Embryonic Fibroblasts
MEM NEAA	Minimum Essential Medium Non-Essential Amino Acids
MET	Mesenchymal-epithelial transition factor
MHC	Major Histocompatibility Complexes
mL	Milli-Litre
mL	Millilitre
mM	Millimolar
mRNA	Messenger RNA
MS	Mass Spectrometry
MSMD	Mendelian Susceptibility to Mycobacterial Disease
MT	Metallothionein
MX1	Myxovirus resistance protein 1
NDUA4	NADH dehydrogenase [ubiquinone] 1 alpha subcomplex subunit 4
ng	Nanogram
NHEJ	Non-Homologous End-Joining
NK	Natural Killer
nm	Nanometer
NP	Nucleoprotein

NSC	Neural Stem Cells
OAS1	2'-5' oligoadenylate synthase 1
OAS2	2'-5' oligoadenylate synthase 2
OAS3	2'-5' oligoadenylate synthase 3
OASL	2'-5' oligoadenylate synthase-like protein
PAM	Protospacer Adjacent Motif
PBMC	Peripheral Blood Mononuclear Cells
PBS	Phosphate Buffered Saline
PCNA	Proliferating Cell Nuclear Antigen
PCR	Polymerase Chain Reaction
PD-L1	Programmed death-ligand 1
PD1	Programmed Death 1
PD1	Programmed cell death protein 1
Pen-Strep	Penicillin-Streptomycin
PEV	Position Effect Variegation
PFU	Plaque-Forming Unit
PKR	Protein Kinase R
Plpro	Papain-like Proteases
PPHLN	Periphilin-1
Ppi	Inorganic Pyrophosphate
pSTAT1	Phosphorylated Signal Transducer and Activator of Transcription 1
PTEN	Phosphatase and tensin homolog
qRT-PCR	Quantitative Reverse Transcription Polymerase Chain Reaction
RIG-I	Retinoic Acid-Inducible Gene I
RING	Really Interesting New Gene
RNA	Ribonucleic Acid

ROS	Reactive oxygen species
rpm	Revolutions per Minute
SARS-CoV-2	Severe Acute Respiratory Syndrome Coronavirus 2
SDS-PAGE	Sodium Dodecyl Sulphate - Polyacrylamide Gel Electrophoresis
sgRNA	Single Guide RNA
shRNA	Short hairpin RNA
SILAC	Stable Isotope Labelling by Amino Acids
siRNA	Small interfering RNA
SIV	Simian Immunodeficiency Virus
SKP2	S-phase Kinase-associated Protein 2
SLE	Systemic Lupus Erythematosus
SOC	Super Optimal Broth with Catabolite repression
SSC	Side Scatter
ssODN	Single-Stranded Oligodeoxynucleotide
STAT	Signal Transducer and Activator of Transcription
T1	Transmembrane protein 1
T2	Transmembrane protein 2
T4	Transmembrane protein 4
Ta	Tubulointerstitial nephritis antigen
TAE	Tris-acetate-EDTA
TAM	Tumor-Associated Macrophages
TAP	Transporter associated with Antigen Processing
TCR	T Cell Receptor
TEMED	Tetramethylethylenediamine
TGF	Transforming Growth Factor
TIL	Tumour Infiltrated Lymphocites

TMA	Tissue microarray
TNF	Tumour Necrosis Factor
TRIM	Tripartite Motif
TSA	Tumour Specific Antigen
UBAIT	Ubiquitin Activated Interaction Trap
UbcH8	Ubiquitin-conjugating enzyme H8
UBE1L	Ubiquitin-activating enzyme E1-like protein
UCRP	Ubuquitin Cross-Reactive Protein
USP	Ubiquitin Specific Protease
UV	Ultra-Violet
V	Volts
VSV	Vesicular Stomatitis Virus
WB	Western Blot
WT	Wild Type

Contents

List of Figures

List of Tables

Chapter 1

Introduction

1.1 Interferons and Interferon Stimulated Genes

The human immune system is an intricate machinery with several means to defend the body from pathogenic infections and malignancies, one of which is the interferon (IFN) system. First described by Isaacs & Lindenmann in 1957, these small signalling cytokines play a very important role in the first lines of the immune defence, triggering and stimulating both the innate and adaptive responses. Interferons are classified in three different types based on the structure of their membrane receptors, sequence homology and functional activity. The human type I IFN group is composed of 13 subtypes of IFNα plus IFNβ, IFNω, IFNϵ and IFNκ, all of which signal through the type I IFN receptor IFNAR consisting of IFNAR1 and IFNAR2 transmembrane proteins (Weerd *et al.*, 2007). IFNγ signals through a different heteromeric receptor formed of two chains of interferon gamma receptor 1 (IFNGR1) and two chains of interferon gamma receptor 2 (IFNGR2), and is the only member of the type II IFN group (Platanias, 2005). Finally, four subtypes of IFNλ compose the type III IFNs, which signal through yet another heterodimeric receptor composed of IL-28RA and IL-10R2 (Kotenko, 2011; Prokunina-Olsson *et al.*, 2013). All three receptor complexes for type I, type II and type III IFNs signal through the Janus kinase (JAK)/signal transducer and activator of transcription (STAT) pathway. Type I and type III IFNs activate the transcription factor complex IFN-stimulated gene factor 3 (ISGF3), composed of phosphorylated STAT1/STAT2/IRF9, while interactions through the receptor for IFNs type II lead to the formation of phosphorylated STAT1 homodimers, also known as gamma-interferon activation factor (GAF). Both ISGF3 and GAF then translocate to the nucleus to bind to IFN-stimulated response elements (ISRE) and to gamma-activated sequences (GAS), respectively. As seen in Figure 1.1, ISGF3 induces transcription of the Interferon Stimulated Genes (ISGs) and GAF induces the IFNγ stimulated genes. This thesis will fo-

cus on type I IFNs, henceforth IFN unless otherwise stated in the text.

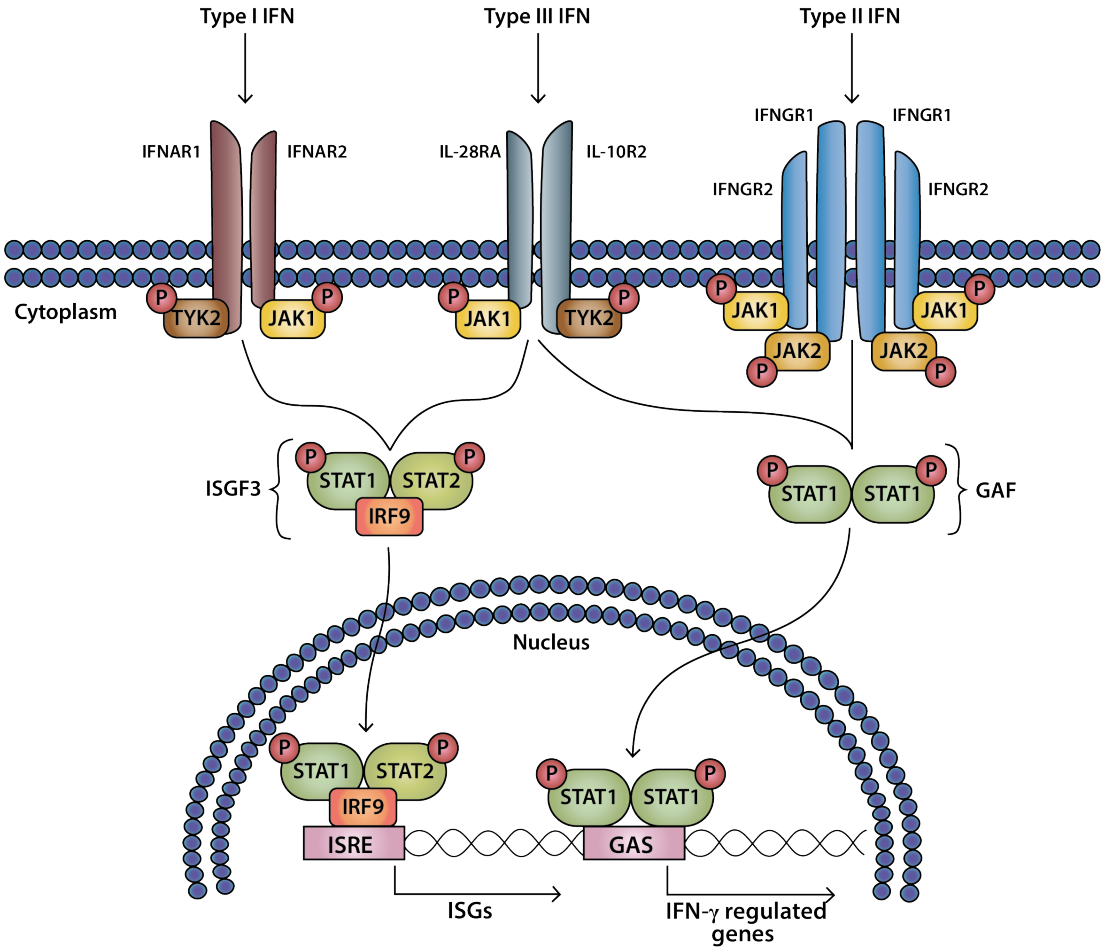

Figure 1.1: The different signalling pathways of interferon. All three receptor complexes for type I, II and III IFNs signal through the JAK/STAT pathway, but while type I and III activate the transcription factor complex ISGF3, composed by phosphorylated STAT1/STAT2/IRF9, interactions through the receptor complexes for IFNs type II lead to the formation of phosphorylated STAT1 homodimers, also known as GAF. ISGF3 and GAF translocate to the nucleus to bind to IFN-stimulated response elements (ISRE) and to gamma-activated sequences (GAS) respectively to induce transcription of ISGs.

According to the work carried out by Shaw *et al.* in 2017, humans differentially express 2048 ISGs and 1484 interferon regulated genes (IRGs) in response to IFN type I, which accounts for around 10 and 7% of the genome respectively (Nurk *et al.*, 2022). Although the exact percentage varies from study to study depending on what threshold they consider to define an ISG (a specific fold change or statistical cutoff), it can be affirmed that ISGs and IRGs play a critical physiological role in humans. In their study, Shaw *et al.* analysed the interferome triggered by IFN type I in fibroblasts derived from ten different vertebrate animal species (nine mammals and one bird) using RNAseq and comparative analysis. Figure 1.2 shows the number of shared ISGs identified at the nodes of the phylogeny tree of the species studied, suggesting that the interferomes in the different species have evolved

by linage-specific pressure. Although they identified unique ISGs upregulated by IFN in each species, they also found upregulated core sets on vertebrates (62 genes) and mammals (28 genes) involved in a variety of ancestral functions of the IFN system such as antigen presentation, IFN induction and suppression, ubiquitination, apoptosis and antiviral response, proving the central role of this essential system. Among these genes, they also found several ISGs involved in suppression of the IFN response upregulated as part of the core vertebrate ISG set, such as USP18, USP25 and IFI35, confirming that the negative regulation of the IFN system is an essential ancestral process.

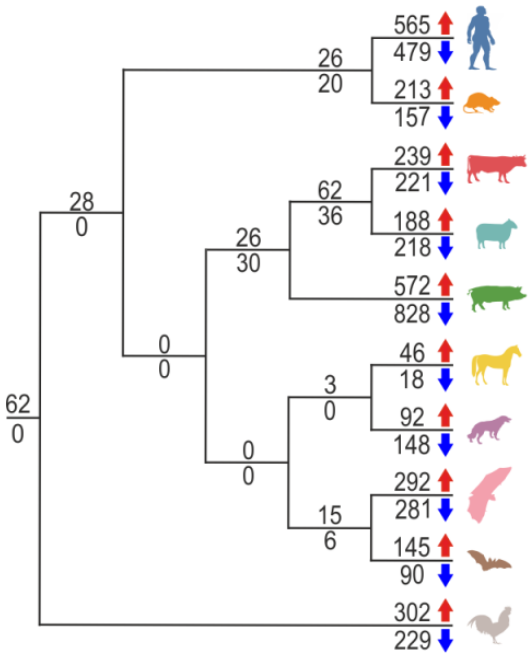

Figure 1.2: Number of ISGs identified by RNAseq in the different vertebrates studied by Shaw *et al.* (2017) (human, rat, cow, sheep, pig, horse, dog, micro-bat, fruit bat and chicken). This phylogeny tree shows the number of ISGs upregulated (above the line, red arrow) and downregulated (below the line, blue arrow) in each species and in the nodes that relate them evolutionary. 62 common upregulated genes were identified in all the species, defined as the "core vertebrate ISG set".

The strong antiviral and immunomodulatory properties of IFN have been widely reviewed over the years (Theofilopoulos *et al.*, 2005; Stetson & Medzhitov, 2006; González-Navajas *et al.*, 2012; Ivashkiv & Donlin, 2014; López de Padilla & Niewold, 2016; Schoggins, 2019), but IFNs have also been found to be involved in the development of disease, as discussed in the following section.

1.1.1 Interferon Stimulated Genes in disease

Although IFNs and ISGs are key in fighting and eradicating pathogens and infections, their dysregulation has also been linked to inflammatory and autoimmune disorders, chronic infections, and cancer.

An autoimmune disease is a condition controlled both by host genes and the environment in which the organism's immune system cannot differentiate its own cells from the foreign, resulting in an unnecessary antigen-driven immune response towards healthy tissue (Marrack *et al.*, 2001). A self-sustaining and auto-amplifying chronic dysregulated IFN signalling has been linked to many autoimmune disorders, including systemic lupus erythematosus (SLE), myositis, rheumatoid arthritis, Sjögren's syndrome (SS) and systemic sclerosis (SSc) (Hall & Rosen, 2010; Crow & Ronnblom, 2019). SLE is one of the most studied diseases regarding the involvement of IFN signalling in the autoimmune pathology. Studies have shown that SLE patients with an increased expression of IFNα and ISGs were linked to a more aggressive disease, flares and tissue damage, which makes them good biomarkers for indication of the severity as well as for the prognosis prediction of the pathology (Petri *et al.*, 2009; Bauer *et al.*, 2009; Banchereau & Pascual, 2006; Crow, 2010). This has been proven through gene expression profiling studies, showing that SLE patients have an upregulated IFN signature and increased expression of IFN regulated mRNA transcripts, suggesting that the blockade of such pathway with anti-IFNα antibodies could be of major therapeutic benefit (Kennedy *et al.*, 2015; Chyuan *et al.*, 2019).

Even though the IFN pathway is key in fighting viral infections as part of the immune response system, dysregulated hyperactive IFN signalling has also been linked to persistent chronic infections (Lukhele *et al.*, 2019; Murira & Lamarre, 2016; Snell *et al.*, 2017) and to IFN treatment resistance (Chen *et al.*, 2005). Two studies published simultaneously in Science in April 2013 revealed that lymphocytic choriomeningitis virus (LCMV) infected mice showed steady type I IFN signalling, which resulted in increased expression of immune suppressive factors such as IL-10 and PD-L1 (Wilson *et al.*, 2013; Teijaro *et al.*, 2013). Both of these studies proved that blocking type I IFN signalling with an anti-IFNAR1 antibody in LCMV-C113 infected mice resulted in a significant decrease on immunosuppression and chronic inflammation, assisting with the clearance of the persistent infection. Experiments by Fallet *et al.* (2016) showed that mice infected with such LCMV chronic infections also presented type I IFN-I signalling driven virus-specific B cell deficiency, which was also restored upon IFN-I receptor blockade. On the other hand, similar experiments by Sandler *et al.* (2014) in rhesus macaques infected with simian immunodeficiency virus (SIV) showed varying results. Blocking the type I IFN receptor resulted in reduced antiviral gene expression, greater viral reservoir and increased T-cell deficiency, while IFNα treatment induced the expression of antiviral genes, preventing systemic infection. How-

ever, continuous IFNα treatment shifted this initially beneficial response resulting in IFN desensitisation, which lead to decreased expression of antiviral genes, increased the viral reservoir and accelerated T-cell depletion.

As described in section 1.1, IFNs also play an important role as therapeutic agents in different cancers. Although it may sound contradictory, many tumours are characterised by simultaneous immunosuppression and inflammation (Snell *et al.*, 2017; Hanahan & Weinberg, 2011), and IFNs might have an important role in this dichotomy. Persistent IFN signalling has been proven to provoke resistance to immune checkpoint blocking therapies such as PD1 pathway blockade as well as to combination therapies such as radiation and CTLA4 blockade (Benci *et al.*, 2016). On that note, Terawaki *et al.* (2011) performed an analysis of the PD-1 gene that revealed an IFN stimulation response element (ISRE) responsible of triggering gene transcription in a mouse T cell line (2B4.11). This was confirmed by the fact that IFNα treatment resulted in increased expression of PD-1 through binding of IRF9 to the ISRE in the PD-1 promoter, resulting in an attenuated T cell response. On the other hand, Zaretsky *et al.* (2016) analysed samples from four relapsed melanoma patients resistant to PD-1 blockade therapy and found that samples from two of them had resistance associated loss of function mutations in either JAK1 or JAK2, which resulted in lack of response to IFNγ.

The mechanisms and circumstances by which type I IFNs can be beneficial or detrimental in a cancer background are still to be completely understood. Nevertheless, it is clear that they play an important role in utilising the immune system to fight this disease, and further exploring IFN administration or blockade therapies could be key for its treatment. The following section will discuss the role of a specific subset of IFN stimulated / regulated genes in cancer development and progression.

1.2 Interferon Related DNA-damage Resistance Signature (IRDS)

In 2004, Khodarev *et al.* selected a radioresistant cancer cell line from parental radiosensitive human head and neck squamous carcinoma cells (SCC61) by injecting them into nude mice and exposing the tumours to a 5 Gy radiation treatment. After exposure to radiation, cells were separated *in vitro*, reinjected into mice, treated and excised again another seven times. The resistant cell line obtained after eight cycles of radiation was designated as Nu61. RNA analysis of the gene expression on Nu61 vs SCC61 cells identified 49 statistically relevant genes expressed differently between the two cell lines, many of which were ISGs - this group of genes was designated the Interferon Related DNA-damage Resistance Signature (IRDS). Among them, STAT1 was the most highly upregulated one, and transfection of the cDNA of both of its isoforms (α and β) in radiosensitive SCC61 cells

resulted in increased radioresistance upon a 3Gy radiation treatment. They later reported that radiation does indeed activate an IFN-inducible and STAT1 dependant pathway and that constitutive overexpression of this pathway induces resistance to radiation (Khodarev *et al.*, 2007). Based on this work, and in an effort to identify new therapy-predictive markers, Weichselbaum *et al.* (2008) analysed a variety of cancer cell lines and found 36 genes among the top 25% identified in the surviving fraction of cells after radiation treatment (2 Gy), 32 of which were a subset of the genes identified by Khodarev *et al.* Here, STAT1 also ranked in the top 1% of the genes analysed, and its silencing by shRNAs in Nu61 cells resulted in downregulation of other IRDS genes and in resensitisation of the cells to the chemotherapeutical drug doxorubicin. To test if the expression of these IRDS genes was a consequence of the upregulation of STAT1 or could themselves mediate treatment resistance, this group targeted another two members that seemed to be regulated by STAT1 with shRNA - ISG15 and IFIT1. The silencing of both genes individually resensitised Nu61 resistant cells to doxorubicin without affecting the levels of STAT1. This was the first report of these two IFN stimulated genes with roles in antiviral immunity being related with DNA damage resistance. After experimentally proving that the upregulation of several members of the IRDS mediate experimental resistance to DNA-damaging treatments, Weichselbaum *et al.* tested if the IRDS profile and response to treatment in different primary human tumours resembled that in either SCC61 or NU61 cells. Patient samples from a variety of human cancers (breast, head and neck, prostate, lung, glioma) were analysed and categorised in two different groups - one resembling SCC61 cells, classified as IRDS (-), and one resembling Nu61 cells, classified as IRDS (+) (Figure 1.3). To determine if the IRDS state of certain cancers can be used as a predictive marker for therapy, they analysed the data from 295 early stage breast cancer patients to study the relation between the patients IRDS profile and a multivariable proportional-hazards model for metastatic risk, which showed a correlation between the two. Further analysis of databases and prognostic criteria showed that the IRDS state could be a therapy-predictive marker for DNA-damaging treatments, helping to stratify patients that can benefit from such treatments.

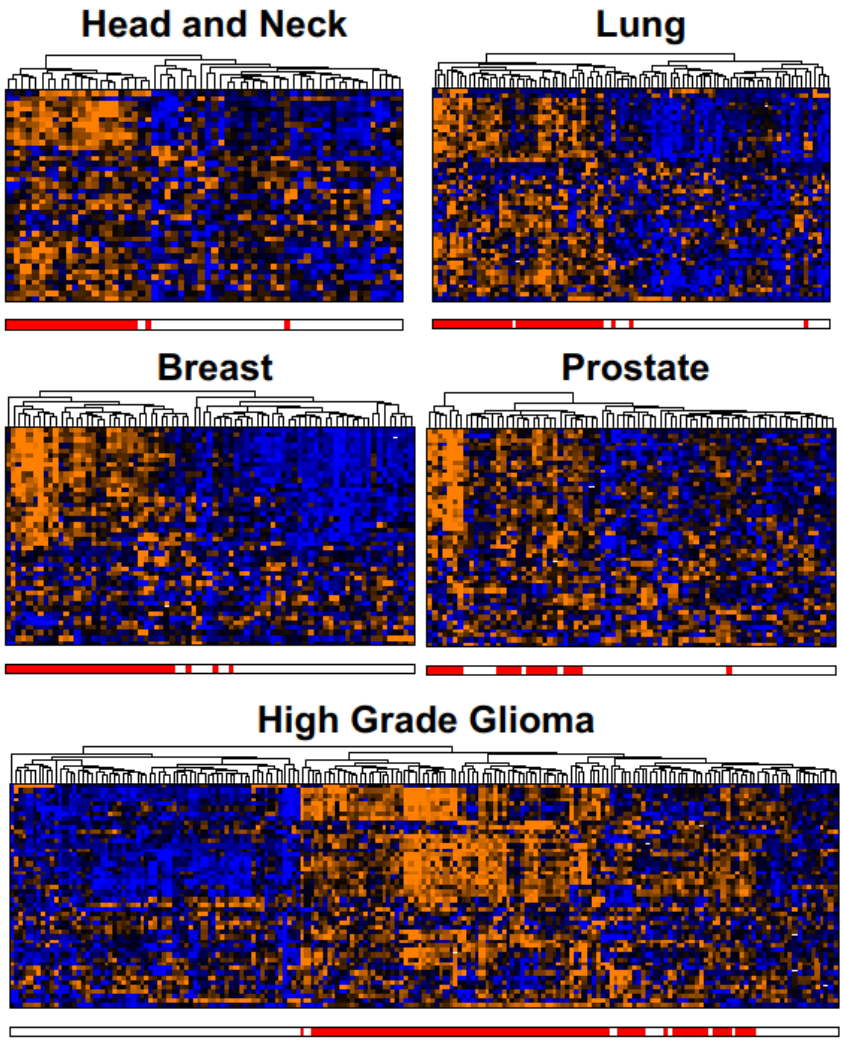

Figure 1.3: Clustering of microarray data showing the expression pattern of the IRDS genes in different primary human tumours. Each column represents a primary tumour and each row represents an IRDS gene, orange indicating high expression and blue indicating low expression. Tumours marked in red (below each dendogram) are the ones classified as IRDS (+). Figure by Weichselbaum *et al.* (2008).

The IRDS has been further studied as a signature in the context of cancer. In 2014, Boelens *et al.* tested whether stromal cells in the microenvironment communicate with cancer cells to upregulate the IRDS. For this, they used metastatic human breast adenocarcinoma cells (MDA-MB-231) as a cancer model and human diploid fibroblasts as stromal cells. They subcutaneously injected the cancer cells either alone or with the stromal cells into mice to find out that the formed tumours containing fibroblasts showed a higher expression of IRDS members such as STAT1, MX1 or OAS1 when compared with tumours composed of breast cancer cells alone. On top of this, they found that the stromal cells enhanced the growth rate of the cancer cells and protected them against radiation and cell death. The study of different co-cultures of breast cancer cells and fibroblasts *in vitro*

showed that breast cancer cells can be categorised in two groups - the IRDS responders which are mainly composed of basal-like cells and upregulate IRDS genes upon interaction with stromal cells, and the IRDS non-responders which are composed mainly of non-basal-like with some basal-like subtypes and do not induce IRDS genes. In these experiments, only the IRDS responders were protected against radiation and chemotherapy by stromal cells, but the knock-out of STAT1 repressed the expression of the rest of IRDS genes and inhibited stromal cell mediated treatment resistance. This group concluded that stromal cells transfer exosomes to cancer cells to promote a STAT1 dependant IRDS induction and subsequent resistance to radiotherapy and chemotherapy in a subset of basal subtype breast cancers, which requires live stromal cells and is not associated with expression and/or function of IFNs or their receptors.

In contrast with the data described above, other studies have shown that IFNs have an important role in the induction of the IRDS. In 2013 Cheon *et al.* investigated how continuous exposure of cells to a low level of IFNβ affected the expression of ISGs. As described in section 1.1, in the canonical IFN pathway, STAT1 and STAT2 are phosphorylated and combined to IRF9 to form ISGF3 in response to IFN type I, which then binds to ISRE to induce the expression of hundreds of ISGs. This group had previously showed (Cheon & Stark, 2009) that the lack of phosphorylation of STAT1 at tyrosine 701 (U-STAT1) prolonged the IFNβ response for several days, and they later found that IFNβ also induced the expression of unphosphorylated STAT2 (U-STAT2, without the usual phosphorylation at Y690). The combination of U-STAT1, U-STAT2 and IRF9 resulted in unphosphorylated ISGF3 (U-ISGF3), which extended the expression of a subset of the initially induced ISGs despite the usual negative regulatory effect of the IFN response. When comparing the genes induced by ISGF3 vs U-ISGF3, they found 48 genes induced only by ISGF3 and 29 genes induced by U-ISGF3 (Figure 1.4a). They reported that the system driven by U-ISGF3 sustains the expression of these ISGs for at least 12 days with no increase in STAT phosphorylation, and that although this prolonged expression did not harm cells it did provide them with an extended resistance to virus infection and DNA damage. Interestingly, they revealed that the members of the IRDS previously described are exclusively U-ISGF3-induced genes. This could help explain the contradiction that IFNs are described as tumour suppressors that inhibit proliferation and promote apoptosis and yet the expression of many ISGs are related with bad prognosis and therapy resistance, since the U-ISGF3-induced IRDS subset does not include many of the other ISGs known to confer such traits. They concluded that the continuous exposure of cells to low levels of IFN often seen in cancer could result in the induction of U-STAT, formation of U-ISGF3 and long-term upregulation of the IRDS, which promotes oncogenesis and therapy resistance (Figure 1.4b).

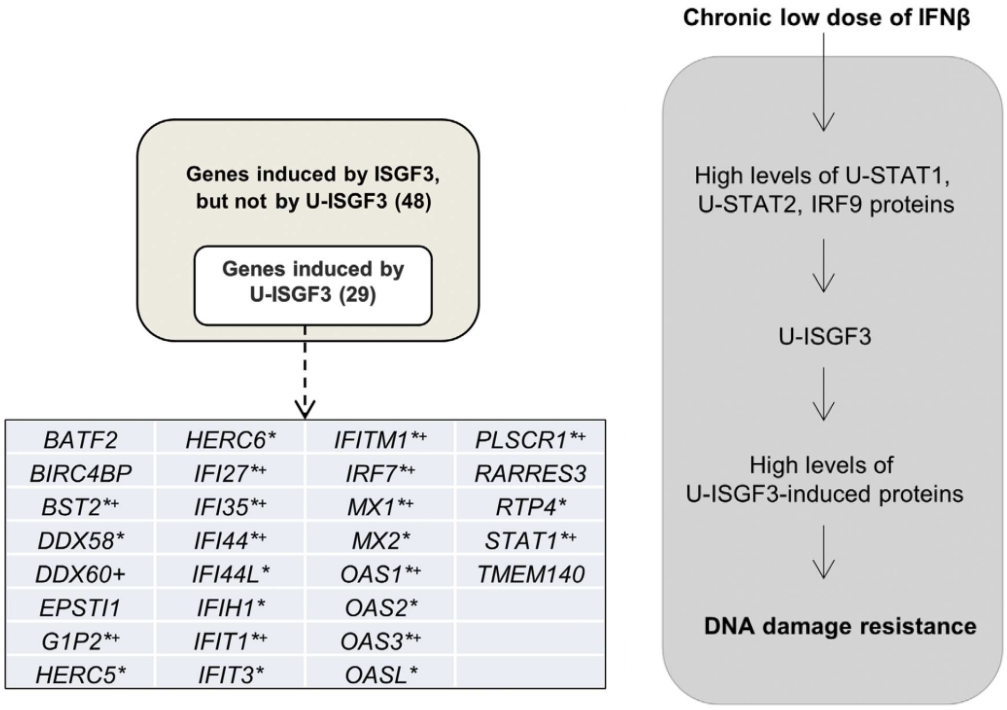

Figure 1.4: Figures by Cheon *et al.* (2013) on the expression of U-ISGF3 and the consequent upregulation of the IRDS. **(a)** Microarray analysis of the genes induced by ISGF3 and U-ISGF3 on normal human fibroblast BJ cells and list of genes identified to be induced by U-ISGF3. To identify the genes induced by ISGF3, cells were treated for 6 hours with 3 IU/mL IFNβ prior analysis. To identify U-ISGF3 induced genes, cells were transfected with a lentiviral vector encoding a mutant STAT1 protein that cannot be phosphorylated at Y701 without IFN treatment. The genes marked with an (*) are those known to have anti-viral functions, while those marked with a (+) are the ones that had been reported to be upregulated in DNA damage-resistant cancer cells at the time the paper was published. **(b)** Chronic exposure to low doses of IFN results in high levels of U-STATs that lead to increased expression of U-ISGF3 and consequent upregulation of the IRDS, which mediates resistance to DNA-damage.

It is well known that upon viral infection, the presence of exogenous DNA in the cytoplasm of cells can trigger IFN signalling. Similarly, the "self" DNA derived from DNA damage, double-strand breaks and the DNA repair systems can also activate type I IFN signalling. This was demonstrated by Erdal *et al.* (2017), who showed that ssDNA accumulated in the cytosol as a result of DNA-damaging agents, like radiation or chemotherapeutic drugs, activated an innate IFN type I driven immune response. They determined that therapeutic DNA-damaging agents such as ionising radiation (tested at high levels of 10 Gy but also at therapeutic levels of 2 Gy and 6 Gy), mitomycin C (3 μM) or cisplatin (15 μM) caused the accumulation of cytosolic ssDNA, that the DNA end resection factors BLM and EXO1 are key for the generation of such fragments and that cytoplasmic exonuclease Trex1 is necessary to degrade them. To prove that such fragments activate the IFN type I immune response and more specifically the IRDS, they analysed the basal and DNA-

damaging treatment induced mRNA expression of several type I IFN target IRDS member genes (MX1, ISG15, OAS1, IFIT1, IFI6, IFI44 and BST2), as well as the levels and phosphorylation status of STAT1, on the breast cancer cell lines and on one radio-resistant glioblastoma cell line. They found that all the three treatments induced phosphorylation of STAT1 at Y701, a known marker for type I IFN signalling activation. Nevertheless, this was identified in the first 24 hours and the long term phosphorylation state or the activation of the pathway by unphosphorylated STAT1 was not analysed. On the conditions studied, they did however detect the expression of the IRDS members analysed by qRT-PCR in the first 24 hours, which with the exception of IFIT2 showed a two to six-fold increase upon 10 Gy radiation treatment. Although delayed, the chemotherapeutic agents mitomycin C and cisplatin showed similar results. They noticed that Trex1 deficient breast cancer cells, which presented an accumulation and persistence of cytosolic DNA due to the absence of the main exonuclease that degrades it, showed an increased radioresistance. To test if the IRDS expression resultant from the accumulation of cytosolic DNA was responsible for such resistance, they tested Trex1 double negative cells that also had IRF3 disrupted to find out that this loss reversed the radioresistance previously observed. Interestingly, they reported that those breast cancer cell lines with lower Trex1 expression and higher BLM and EXO1 expression were the ones associated with a poorer prognosis. This information, along with the previously described data, could help explain the mechanism by which the IRDS mediates resistance to DNA-damaging agents.

The role of IFNs in the tumour microenvironment and the pathways and regulations of ISGs and the IRDS in cancer cells have been reviewed by Cheon *et al.* (2014) and more recently by Padariya *et al.* (2021). The research on the individual members of the IRDS outside their canonical roles, sparked by the studies presented in this section, has demonstrated the involvement in emergence and progression of malignancies of many of them. The IFN-induced transmembrane protein 1 (IFITM1), for example, has been repeatedly reported to be involved in tumour proliferation, angiogenesis, metastasis and resistance to DNA-damaging treatments. This 17 kDa transmembrane protein known to modulate immune and antiviral responses has been found overexpressed in many different solid human tumours such as gastroesophageal adenocarcinoma, hepatocellular and nasopharyngeal carcinoma, glioma and lung, breast, head and neck, ovarian, grastric and colorectal cancers, as recently reviewed in detail by Liang *et al.* (2020). Three out of the four members of the oligoadenylate synthase (OAS) family of IFN-induced antiviral enzymes (OAS1, OAS3 and OASL, but not OAS2), which also are IRDS members, have likewise been linked to tumourgenesis and bad prognosis. Zhang & Yu (2020) have recently presented their bioinformatics and statistics based study on the role of the OAS family as biomarkers in breast cancer, in which they concluded that high mRNA expression of OAS1 and OAS3 correlates with worse prognosis in all breast cancers while overexpression of OAS2 is associated with a better prognosis in some subtypes. Zhang *et al.* (2021a), on the other hand, reported

the correlation between high expression of mRNA encoding MET (a proto-oncogene encoding a receptor tyrosine kinase), OAS1 and OASL with an unfavourable prognosis and tumour progression in pancreatic cancer. This thesis will focus on the Interferon Stimulated Gene 15 (ISG15), another IRDS member that has also been consistently linked with tumour proliferation, therapy resistance and aggressiveness and whose mechanism of action in disease is still poorly understood.

1.3 ISG15

In 1979, Farrell *et al.* found a novel protein by detecting its increased mRNA levels on IFN treated Ehrlich ascites carcinoma cells, but did not identify such protein. Later in 1984, Korant *et al.* reported the induction of the 15 kDa protein in various IFN treated human and animal cells in culture, such as human fibroblasts, WISH cells (human amnion-derived cells) and Madin-Darby Bovine Kidney (MDBK) cells, and described it to be only in very small amounts if any at all in untreated cells. They also found induction on Daudi (human African-American Burkitt's lymphoma) cells upon IFNα and IFNβ treatment, and to a much lower extent upon IFNγ treatment. Most importantly, they suggested its involvement in antiviral immunity for the first time, and purified it from the cytoplasmatic fraction from Daudi cells. However, it was not until 1986 that this mysterious protein was sequenced from the mRNA isolated from the same IFN treated cells (Blomstrom *et al.*, 1986). This 15 kDa protein was named ubiquitin cross-reactive protein (UCRP) by Haas *et al.* (1987), who first suggested it was a functionally distinct ubiquitin-like protein. We know now that UCRP, known nowadays as ISG15, is indeed an ubiquitin-like protein modifier that regulates the function and fate of its target proteins by binding to them in a process similar to ubiquitination. This process, called ISGylation, can lead to both loss and gain of function. The ability of ISG15 to conjugate other proteins was first described by Loeb & Haas (1992), who studied the induction and conjugation of ISG15. They reported the temporal induction of free ISG15 within 30 minutes of IFN treatment followed by a delayed increase of ISG15 conjugates between 12 and 72 h after treatment, but the levels and ratios of free vs conjugated ISG15 varied among the different cell lines studied.

All the work described above was the base of future research to study and better understand ISG15. This 165 amino acid (17,890 Da) protein is composed of two ubiquitin like domains connected by a central hinge. The nascent ISG15 is synthesised as an inactive precursor that gets processed into a 156 amino acid protein by removing the last 8 amino acids of the C-terminus and the methionine of the N-terminus (Knight Jr. *et al.*, 1988). This cleavage, performed between ^{157}Gly-^{158}Gly by a poorly characterised 100-kDa thiol protease enzyme, exposes the mature carboxyl terminus ^{152}LRLRGG essential for the ligation of ISG15 to target proteins, which is the same 6 amino-acid sequence found in mature

ubiquitin (Potter *et al.*, 1999). The details of the crystal structure of ISG15 were revealed in 2005 by Narasimhan *et al.* Each of the tandem ubiquitin homology domains is a β-grasp fold comprised of five β-strands and one α-helix (Figure 1.5), each of which share around 30-36% identity with ubiquitin (Blomstrom *et al.*, 1986).

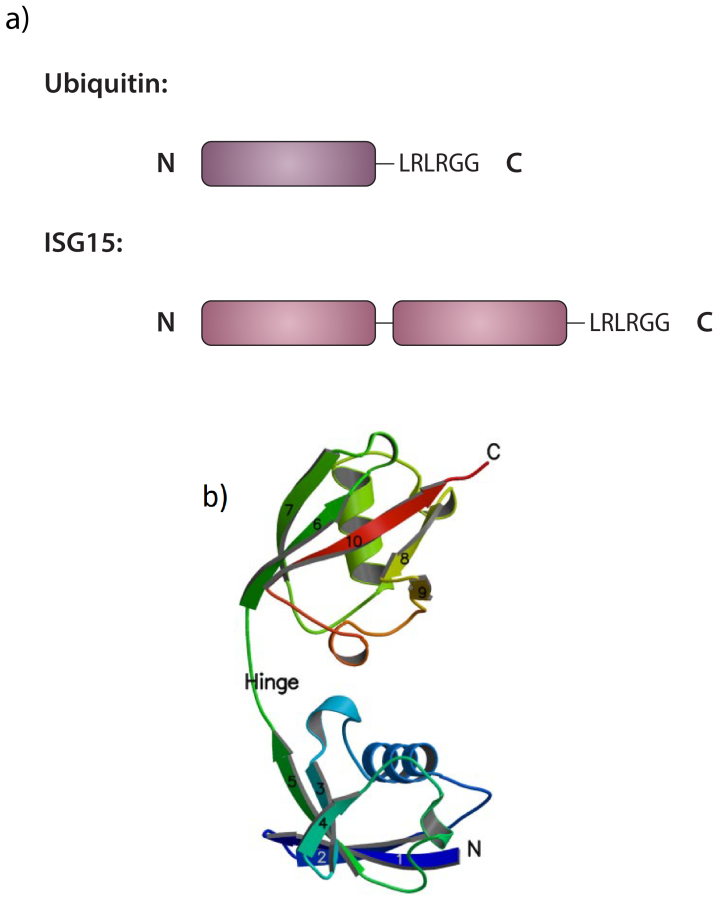

Figure 1.5: Structure of human ISG15 (PDB 1Z2M) and its similarity with human ubiquitin (PDB 1UBQ). **a)** ISG15 is composed of two ubiquitin-like domains connected with a central hinge, and it shares the ^{152}LRLRGG C-terminal motif of ubiquitin. **b)** Ribbon diagram by Narasimhan *et al.* (2005) showing the structure of ISG15, with the two ubiquitin-like β-grasp domains, each comprised of five β-sheets and one α-helix, orientated differently and coloured from blue in the N-terminus to red in the C-terminus.

Ubiquitin binds to lysines on target proteins and is capable of forming linear (C-terminal to N-terminal), heterogeneous (linking at different lysines through the chain) or branched chains by linking onto its own N-terminal and lysines. Linkage through the different lysines and the chains and branches that are formed can trigger different biological responses. When comparing the structure and sequence of each of the ubiquitin-like ISG15 domains with those of ubiquitin (Figure 1.6), four conserved lysines can be identified. Lys^{27}, involved in non-canonical ubiquitination, has been related with the regulation of the immune signalling response and fusion induced degradation (Komander, 2009;

Zhou & Zhang, 2022). This lysine is conserved in both ISG15 domains, corresponding to Lys^{29} in the N-domain and to Lys^{108} in the C-domain. The other two conserved ubiquitin lysines in the N-terminal, also involved in non-canonical ubiquitination, are Lys^{6} and Lys^{33}, which correspond to Lys^{8} and Lys^{35} respectively. Polyubiquitination via Lys^{6} has been linked to DNA repair and mitophagy, while Lys^{33}-linked ubiquitination, the least explored polyubiquitination type, has also been implicated in the regulation of innate immune pathways and autophagy (Tracz & Bialek, 2021). The final conserved ubiquitin lysine, corresponding to Lys^{129} in the C-terminal domain of ISG15, is one of the two sites for canonical polyubiquitination, Lys^{48}. Protein targeting by Lys^{48}-linked chains for proteasomal degradation is the best-known role of ubiquitin (Komander, 2009; Swatek & Komander, 2016).

ISG15 has also been reported to both induce and prevent target degradation and to be involved in mitophagy, immune response regulation and DNA-damage repair, as will be discussed in this thesis. However, the involvement of ISG15 in most of these biological processes has been proved to be a result of covalent modification of target proteins (e.g.: the ISGylation of PCNA aids on regulating its role in DNA repair (Park *et al.*, 2014) and the ISGylation of misfolded p53 leads to its degradation (Huang *et al.*, 2014)). In fact, although ISG15 also modifies other proteins by binding onto lysines in target proteins like ubiquitin, no ability of ISG15 to self-ISGylate and form dimers or chains has been reported to date. However, ISG15-ubiquitin mixed chains have been described, where ISG15 binds to ubiquitin locking it onto the substrate and inhibiting its degradation. Fan *et al.* (2015a) reported that this binding mainly occurs at Lys^{29} of ubiquitin, and Lys^{48} was reported to be the secondary ISGylation site, although at a much lower level. While Lys^{29} is not conserved in any of the ISG15 domains, Lys^{48} corresponds to Lys^{129} in the C-terminal. This means that, even though ISG15 is not directly involved in bulk protein degradation like ubiquitin is (Held *et al.*, 2020), it can compete with ubiquitin both blocking lysines in the target proteins (Desai *et al.*, 2006) and locking it in the substrates, as proved by Fan *et al.* At the same time, the ISGylation of ubiquitin in Lys^{29} and Lys^{48} would also impede auto-ubiquitination and chain formation at these sites, preventing the roles associated with these lysines.

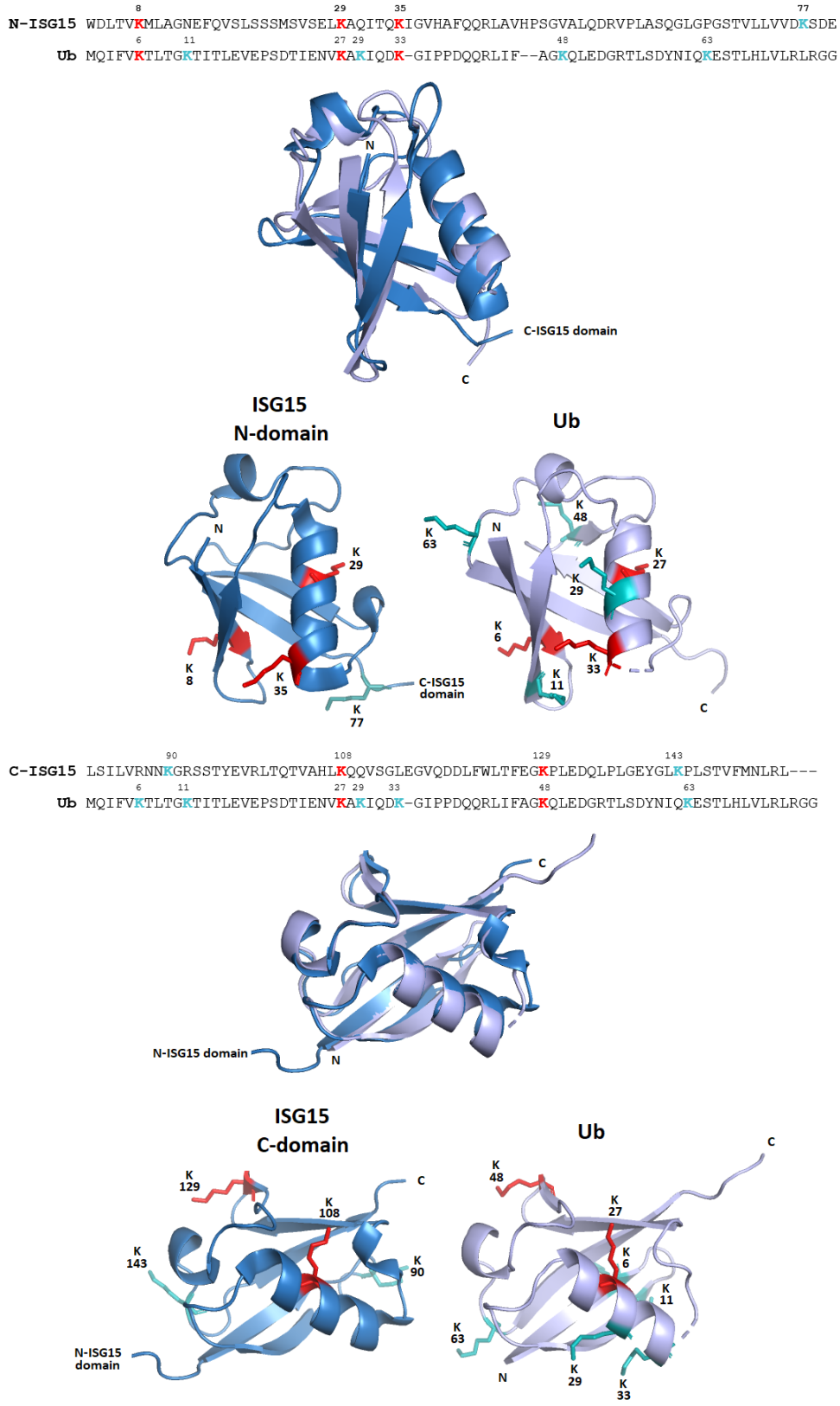

Figure 1.6: Sequence, structure and lysine content of ISG15 (PDB 1Z2M) vs ubiquitin (PDB 1UBQ). The structures of each of the ISG15 domains are superimposed, ISG15 in dark blue and ubiquitin in light blue, to show their structural similarities. Conserved lysines are shown in red in both the ISG15 and ubiquitin aligned sequences and structures, while non-conserved lysines are shown in turquoise.

Each of the two domains in ISG15 has a different role in the ISGylation process. Just like ubiquitination, the ISGylation mechanism also requires an E1 activating enzyme to catalyse adenylation and form a thioester bond with the C-terminal of ISG15, an E2 conjugating enzyme to transfer ISG15 via a transthiolation reaction and an E3 ligase enzyme to aid in the transfer and conjugation of ISG15 to the target protein by covalently linking the C-terminus of ISG15 to the ϵ-amine group of a lysine on the target substrate (Zhang & Zhang, 2011). When the removal of ISG15 from target proteins is required for regulatory purposes, the equivalent role to that performed by deubiquitinating enzymes is carried out by the ubiquitin-specific protease 18 (USP18). Notwithstanding its name, and even though it shows a significant homology to well characterised ubiquitin-specific proteases, USP18 is not a deubiquitylating enzyme, but the main specific deISGylating isopeptidase enzyme (Figure 1.7). Other USPs such as USP2, USP5, USP13, USP14 USP21 have exhibited the ability to recognise ISG15 (Catic *et al.*, 2007; Ye *et al.*, 2011), but only USP18 has been demonstrated to be the *bona fide* deconjugating enzyme for ISG15 in a cellular context (Basters *et al.*, 2014). All of the enzymatic members of the ISGylation machinery, as well as the deISGylating enzyme USP18, are ISGs.

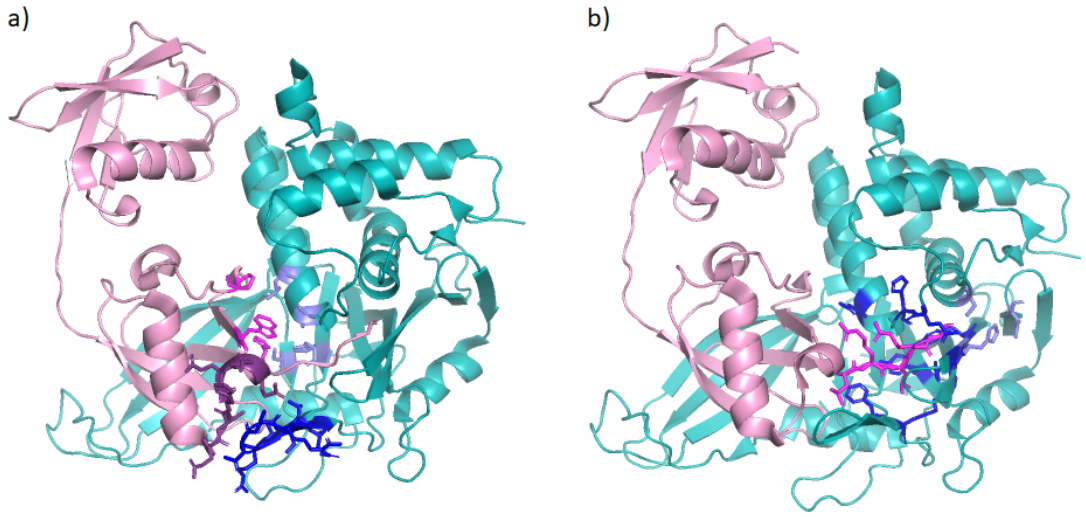

Figure 1.7: Structure of the ISG15:USP18 complex (PBD 5CHV). **a)** Binding boxes on USP18 (green), defined as the groups of amino acids unique to this protein that are required for the binding of ISG15 and are proposed to confer its specificity, are coloured light and dark blue. The equivalent binding boxes in ISG15 (light pink) are shown in bright pink and purple. ISG15 residues coloured in bright pink bind USP18 residues coloured in light blue, and ISG15 residues coloured in purple bind USP18 residues coloured in dark blue. **b)** USP18 catalytic triad is shown in light blue. USP18 residues coloured in dark blue are the ones that bind the C-terminal tail of ISG15, shown in bright pink. The crystal structure of this murine complex was solved and published by Basters *et al.* (2017).

Despite the high similarity between the ubiquitination and ISGylation processes, ubiquitin performs as a single domain molecule, while each ubiquitin-like domain in ISG15 is involved in different steps of the process. A study by Chang *et al.* in 2008 showed that the C-terminus is the one involved in the interaction between ISG15 and the E1 and E2 enzymes, while the N-terminal domain is not essential in these processes but is the one responsible for the efficient transfer of ISG15 from the E2 to the target substrate through an E3 ligase. The E1 activating enzyme of ISG15 is a monomeric protein of 120 kDa called UBE1L, which was first identified as such by Yuan & Krug in 2001. This group later confirmed their findings with subsequent experiments (Zhao *et al.*, 2004) where they also identified UbcH8 as the E2 enzyme for ISG15. They showed that UBE1L, which is specific to ISG15 and does not activate ubiquitin, transfers ISG15 mainly to UbcH8 both *in vitro* and *in vivo*, while the E1 activating enzymes for ubiquitin transfer it to many different E2 enzymes (Pickart, 2001). Silencing of UbcH8 resulted in the inhibition of IFN induced ISGylation proving that it serves as the major E2 enzyme for ISG15 conjugation *in vivo*. The identification of UbcH8 as the main E2 enzyme of the ISGylation system was simultaneously confirmed by Kim *et al.* in the same year. The last step of the ISGylation process requires an E3 ligase to form an isopeptide covalent bond between the C-terminal glycine of the ISG15 LRLRGG motif and a lysine of the target protein. E3 ligases are classified in two major groups based on their structure - the homologous to the E6AP carboxyl terminus (HECT) domain family and the group of really interesting new gene (RING) finger domain and RING-related E3s, although the vast majority of the E3 ligases encoded by the human genome are RING finger E3s (Metzger *et al.*, 2012). Because UbcH8 also works as an E2 enzyme for ubiquitin, Zhao *et al.* (2004) hypothesised that the ISGylation and ubiquitination pathways somewhat overlap, and proceeded to test whether the ISGylation pathway uses UbcH8-competent ligases known to conjugate ubiquitin to conjugate ISG15. They found that one ubiquitin-competent E3 ligase, Rsp5p, also conjugates ISG15 *in vitro*. Although they concluded through two different assays that this E3 ligase, capable of catalysing the ubiquitination of human WBP2 *in vitro*, could also function with UbcH8 to conjugate ISG15 to WBP2 *in vitro*, no further evidence or *in vivo* experiments have been described supporting this data.

To date, three different E3 ligases have been established to operate with ISG15 *in vivo*: Tripartite Motif Containing 25 (TRIM25), Human homolog of Drosophila Ariadne (HHARI) and HECT Domain and RCC1-Like Domain-Containing Protein 5 (HERC5). TRIM25, also known as Estrogen-responsive Finger Protein (EFP), was the first E3 ligase proven to conjugate ISG15 to 14-3-3σ *in vivo* in 293T human embryonic kidney cells and MCF-7 breast cancer cells as part of the ISGylation process (Zou & Zhang, 2006), although the biological consequence of such interaction was not determined. 14-3-3σ is a p53 dependent negative cell cycle regulator and tumour suppressor (Hermeking *et al.*, 1997) that has been shown to be downregulated through TRIM25-mediated ubiquitination and consequent

proteolysis in breast cancer cells (Urano *et al.*, 2002), even though other studies suggest it could have different roles in different tumours (Ko *et al.*, 2014). Interestingly, at the time TRIM25 was identified as an E3 ligase for ISG15, another paper was published simultaneously in the same journal identifying HERC5 as the main E3 ligase for ISGylation (Dastur *et al.*, 2006). In this paper, they tested the overall ISG15 conjugate levels after targeting several E3 ligases known to interact with UbcH8 using siRNAs and also after transfecting them into human cells. Targeting of TRIM25 and TRIM22 resulted in no significant alteration in the accumulation of ISG15 conjugates, and the transfection of these ligases did not boost or alter the level of ISGylated proteins. Therefore, they concluded that none of these E3 ligases played an essential or broad role in the ISGylation process. They were not wrong, since Zou & Zhang showed that the function of TRIM25 is substrate specific and the prevention of the ISGylation of 14-3-3σ would not have a huge impact on the overall ISGylation levels. The silencing of HERC5 did however have a very significant impact on the total level of ISG15 conjugated proteins in human cells, and co-transfection of the E1 and E2 enzymes of the ISGylation process along with ISG15 and HERC5 resulted in a strong ISGylation response even in non-IFN-treated cells. This proved that, even if there are other E3 ligases capable of ISGylating specific substrates, HERC5 is the main ligase in human cells, which has been confirmed several times since (Wong *et al.*, 2006; Takeuchi *et al.*, 2006; Tang *et al.*, 2010; Mathieu *et al.*, 2021). The third E3 ligase identified to function as part of the ISGylation process is also substrate specific. HHARI has been shown to aid in the covalent modification of the Eukaryotic translation initiation factor 4E (eIF4E)-homologous protein (4EHP), one of the three eIF4E-family members found in mammals (Okumura *et al.*, 2007). eIF4E is part of the eukaryotic translation initiation factor eIF4F, and interacts with eIF4G to enhance the binding between eIF4E and the RNA cap structure to initiate translation (Raught & Gingras, 1999). It has been found, however, that out of the three eIF4E, 4EHP (also known as eIF4E-2) does not interact with eIF4G like the other two members do (eIF4E-1 and eIF4E-3), and it has been suggested that it actually competes with them for binding to the RNA structure preventing translation (Christie & Igreja, 2023). Interestingly, Okumura *et al.* showed that the ISGylation of 4EHP enhances its RNA cap structure-binding activity, which was the first report of gain of function following ISG15 modification.

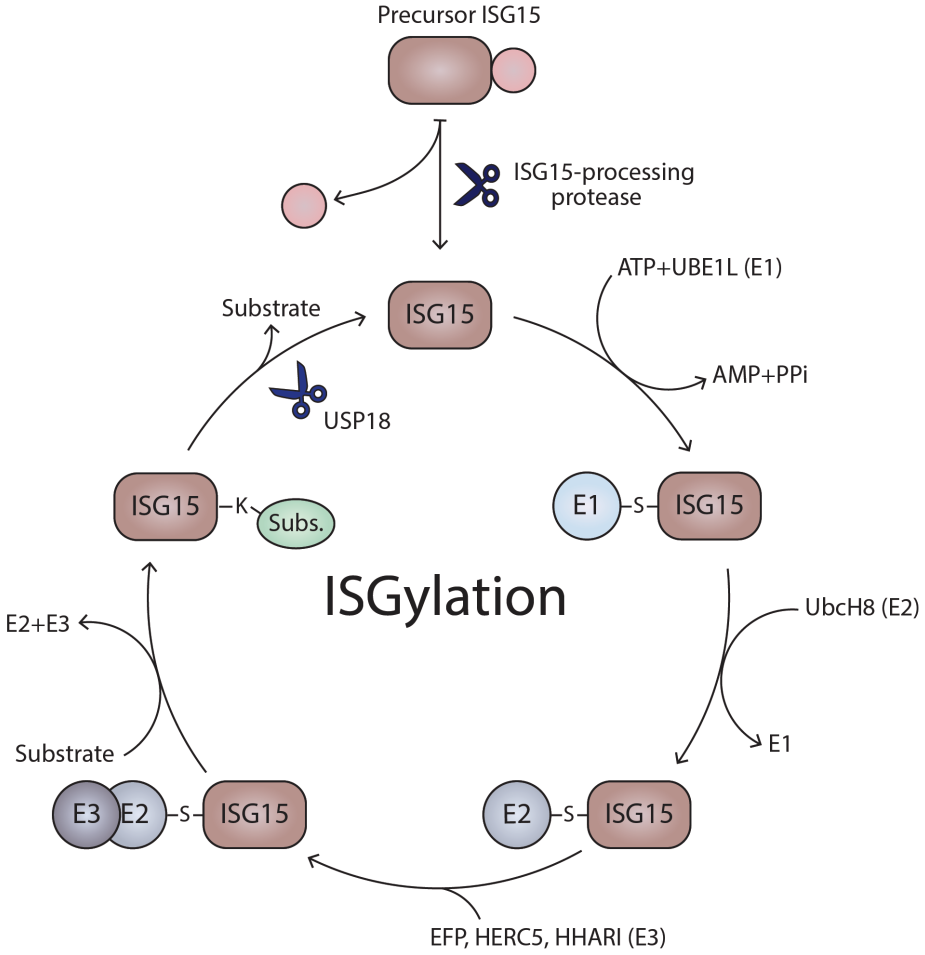

Figure 1.8: Enzymatic machinery of the ISGylation and de-ISGylation system. Upon synthesis, the inactive precursor of ISG15 gets cleaved on the N-terminus removing the initial methionine and on the C-terminus between ^{157}Gly-^{158}Gly exposing the ^{152}LRLRGG sequence essential for the ligation of ISG15 to the target proteins. The mature ISG15 protein its activated by the E1 enzyme of the ISGylation machinery, UBE1L, by catalysing adenylation and forming a thioester bond with its C-terminal. ISG15 is then transferred and linked to the ISG15 conjugating enzyme, UbcH8, via a new covalent thioester bond. Finally, one of the E3 ligases (three different E3 ligases have been identified to date to operate with ISG15 - TRIM25, HHARI, HERC5) gets recruited to aid in the transfer and conjugation of ISG15 to the target protein by covalently linking the C-terminus of ISG15 to the ϵ-amine group of a lysine on the target substrate. When necessary for regulation, the specific isopeptidase USP18 removes ISG15 from the substrate. This diagram has been slightly adapted from a figure created by myself for my MScR thesis, still relevant for the work presented here.

Free ISG15 also has a role other than covalently modifying other proteins. The secretion of free ISG15 from cells was first described in 1991 by Knight Jr. & Cordova, when they reported that the secretion of ISG15 from human lymphocytes and monocytes can be induced by IFN. This was the first time ISG15 was suggested to have a role in cell to cell signalling. Later that year, the same group reported that this immune cell secreted ISG15 could, at the same time, induce the secretion of IFNγ from human lymphocytes, suggesting that ISG15 could play a role as an intercellular immune system effector (Recht *et al.*,

1991). In 1996, they proved that ISG15 could be released from several different types of cells, including monocytes, T lymphocytes, B lymphocytes and epithelial cells, and that secreted free ISG15 could stimulate the proliferation of natural-killer (NK) cells (D'Cunha *et al.*, 1996a; D'Cunha *et al.*, 1996b). Although the way ISG15 gets released from cells has not been discovered, studies suggested that this protein, which does not contain a signal peptide, is not secreted through the canonical transport pathway of the Golgi apparatus (D'Cunha *et al.*, 1996b; Knight Jr. & Cordova, 1991).

During the early 00s, the study of the role of ISG15 as a cytokine was mainly set aside and most research on ISG15 focused on its role in viral immunity as a protein modifier. In 2012, a study by Bogunovic *et al.* revived the discussion when they reported that inherited ISG15 deficiency made patients were more susceptible to mycobacterial infection (subsection 1.3.4). The fact that Mendelian Susceptibility to Mycobacterial Disease (MSMD) is associated with deficiencies in genes involved with IL-12 and IFNγ production and response lead to a re-examination of the role of ISG15 as a cytokine capable of inducing the expression of IFNγ. Studies by Bogunovic *et al.* (2012) suggested that free ISG15 acts synergistically with IL-12 to induce secretion of IFNγ by NK and T cells. Although they did not discern the mechanism by which this synergy stimulates production and secretion of IFNγ, they concluded that the ISGylating ability of ISG15 did not play a role in it since the combination of IL-12 with a mutated version of ISG15, incapable of conjugating, also induced secretion of IFNγ. They also reported the co-localisation of high concentrations of ISG15 in granulocytes compared to other leukocytes, suggesting that granules and microvesicles could be one the ways ISG15 is released from the cells. However, this does not explain how ISG15 gets secreted from other types of cells and thus could be just one of its means of secretion.

To try to elucidate the mechanism of the synergism between ISG15 and IL-12, Swaim *et al.* (2017) studied the response of a non-Hodgkin's lymphoma derived natural-killer cell line, NK-92, and peripheral blood mononuclear cells (PBMC) to different combinations of IL-12 and ISG15. They found that both cell lines produced a low level of IFNγ in the presence of IL-12 alone, and that ISG15 alone did not elicit any secretion. However, their combination lead to a 5 to 10-fold increase in IFNγ secretion when compared to the level produced of IL-12 alone from both PBMCs and NK-92 cells, confirming the findings of Bogunovic *et al.* Using a panel of mutated variants of ISG15, they identified the key surface residues required for this process. They found that all the alterations studied that resulted in a strong defect in the induction of IFNγ were located in the C-terminal domain of ISG15 (Figure 1.9a), and that all the mutant variants studied, defective or competent on stimulating production of IFNγ, supported ISGylation. In an effort to identify a putative surface receptor for ISG15, they fused a FLAG tagged ISG15 to an Ubiquitin-Activated Interaction Trap (UBAIT). An UBAIT is a short flexible linker bound to a C-terminal ubiquitin moiety

that, upon activation by E1 and E2 enzymes, is capable of trapping transiently interacting proteins through a stable amide bond in a proximity ligation reaction. This method was originally designed by O'Connor *et al.* (2015) for the identification of ubiquitin ligase substrates, but its adaptation allowed Swaim *et al.* (2017) to identify the Leukocyte Function-associated Antigen-1 (LFA-1), an heterodimeric complex composed of CD11a (αL integrin) and CD18 (β2 integrin), as a membrane receptor for extracellular ISG15. This was confirmed by blocking LFA-1 with antibodies and/or small molecules, which significantly reduced the ability of ISG15 to stimulate the production of IFNγ in NK-92 cells. Regarding the synergy between ISG15 and IL-12, the authors showed that the signalling pathways by which they stimulate the production/secretion of IFNγ are different and independent, with IL-12 activating transcription of the gene for IFNγ (which ISG15 does not do on its own) and ISG15 stimulating and significantly increasing the level of secreted IFNγ via activation of the Src family kinases. To make sure ISG15 did not interact with the IL-12 receptor (IL-12R) and to make sure the interaction was specific for CD11a/CD18, they transfected CD11a, CD18, IL-12R as well CD11b and CD11c, which can also heterodimerise with CD18, into HEK293T cells (a highly transfectable derivative of human embryonic kidney 293 cells), known not to express LFA-1. ISG15 only bound to the cells when both CD11a and CD18 were expressed at the same time, but not when CD18 was co-expressed with CD11b or CD11c, and expression of IL-12R alone did not lead to binding of ISG15. Finally, since IL-12 also induces the expression of IL-10, they also tested if ISG15 was capable of enhancing the secretion of this cytokine, which was indeed the case only with the wild-type ISG15 but not with the IFNγ patch defective mutant variant (Figure 1.9b). This work sets the base for the understanding of ISG15 as a free extracellular signalling molecule capable of inducing secretion of not only IFN but other cytokines as well. Since then, other cytokines have been reported to be induced by ISG15. Østvik *et al.* (2020) reported that HT29 (human intestinal epithelial) cells and human 3D colonoids express and release free ISG15, and that free ISG15 can induce inflammatory bowel disease relevant proinflammatory cytokines such as CXCL1, CXCL5, CCL20, IL-1β, tumour necrosis factor (TNF), IL-6, IL-10 and IFNγ from PBMCs. Consistent with previous reports, they showed that IL-12 and ISG15 together resulted in a stronger effect on the secretion of IFNγ.

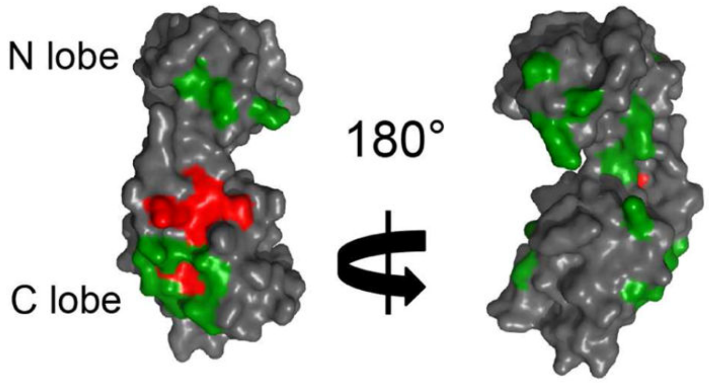

(a)

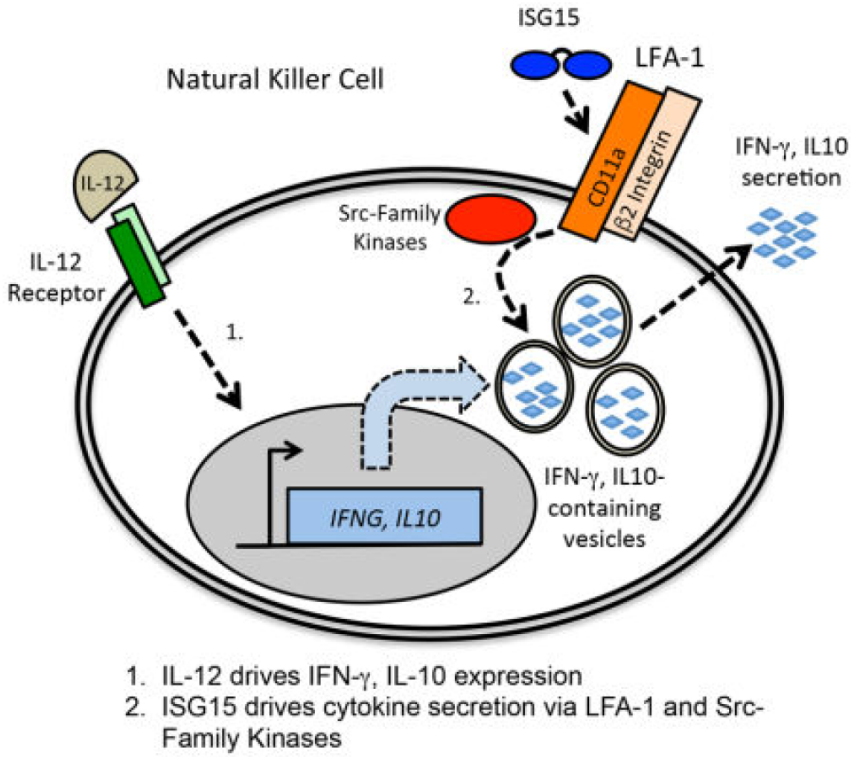

(b)

Figure 1.9: Figures by Swaim *et al.* (2017). **(a)** ISG15 mutated variants tested for their ability to stimulate IFNγ production from NK-92 cells synergistically with IL-12.Those mutations that lead to no production or significantly decreased production of IFNγ (shown in red) were considered as signalling defective, while those that did not affect the ability of ISG15 to induce production of IFNγ (shown in green) were considered as competent variants. All the mutations detected to affect such ability are clustered in the C-domain of ISG15. This cluster was denominated as the "IFN γ patch". **(b)** Proposed model for extracellular free ISG15 recognition by the LFA-1 membrane receptor on NK-92 cells. While IL-12 induces expression of IFNγ and IL-10, ISG15 significantly enhances the secretion of these cytokines upon interaction with LFA-1.

After publishing their work identifying LFA-1 as an ISG15 receptor, Swaim *et al.* (2020) went a step further and studied the determinant ISG15 residues required for its secretion from cells. This time, they used HEK293T cells to transfect a subset of the mutated ISG15 variants they used to find LFA-1 to try to identify mutants specifically defective for release of ISG15. They identified three different variants to be defective (L72, S83 and L85), all of which were competent for receptor binding and retained the ability to ISGylate intracellularly. These residues are located at the surface of ISG15 close to the hinge of the protein, with S83 and L75 being on the C-lobe and L-72 in the N-lobe (Figure 1.10). None of them are in the IFNγ patch, consistent with the fact that the variants were still able to induce secretion of IFNγ when added directly to NK-92 cells. Experiments with transfected ISG15 alone or ISG15 with is conjugating system components (UBE1L, UbcH8 and either WT HERC5 or inactive mutant HERC5) lead to the conclusion that intracellular ISGylation inhibits ISG15 secretion and signalling, which could be just a result of the unavailability of free ISG15 to be secreted instead of a direct inhibition. To date, the exact secretion pathway of ISG15 remains unclear.

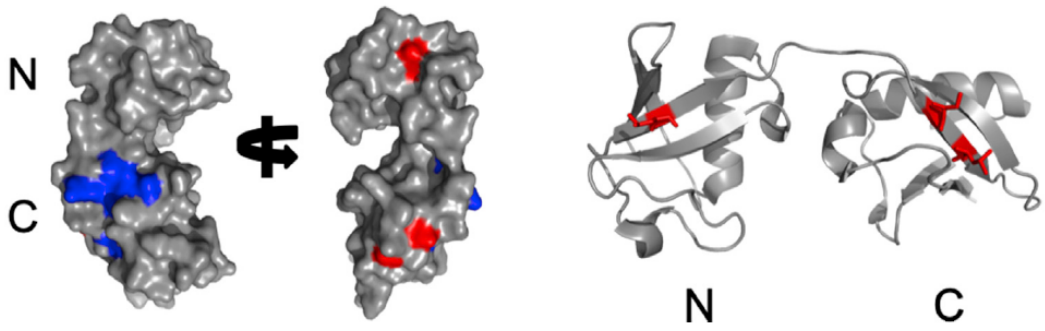

Figure 1.10: Figures by Swaim *et al.* (2020). ISG15 structure highlighting the surface residues of ISG15 required for IFNγ signalling (IFNγ patch, shown in blue) and the residues required for ISG15 secretion (shown in red).

1.3.1 ISG15 in virology

The involvement of ISG15 in the immune response was implied by its discovery as an IFN stimulated protein. Conclusions by Kunzi & Pitha in 1996 indicated that ISG15 played a role in inhibiting the expression of HIV-1 by trapping HIV-1 transcripts in the nucleus, resulting in low cytoplasmic HIV-1 RNA and a decrease in HIV-1 protein synthesis. Since then, the role of ISG15 in antiviral immunity has been its most studied function and has been widely reviewed (Harty *et al.*, 2009; Skaug & Chen, 2010; Morales & Lenschow, 2013; Perng & Lenschow, 2018; Freitas *et al.*, 2020b) as one of the most highly expressed proteins upon IFN treatment and viral infection (Der *et al.*, 1998; Johnston *et al.*, 2001; Labrada *et al.*, 2002). This section will review some of the studies performed to analyse the role of

ISG15 in the immunity against a variety of viruses.

Evidence that ISGylation could have a key role in antiviral immunity was published in 2004, when Ritchie *et al.* observed that USP18$^{-/-}$ mice were resistant to LCMV and vesicular stomatitis virus (VSV) infections when compared with wild-type mice which developed lethal infections, showing a significantly increased inhibition of viral RNA that correlated with increased protein ISGylation. They also observed type I mediated IFN resistance to VSV and Sindbis virus on Mouse Embryonic Fibroblasts (MEF) derived from USP18$^{-/-}$ mice, which also showed higher amounts of ISGylated proteins than the MEFs derived from wild-type mice. Shortly after, Lenschow *et al.* (2005) used a chimeric recombinant version of the Sindbis virus system to express ISG15 in mice lacking the IFNα/β receptor (IFNα/βR$^{-/-}$) in order to analyse the antiviral properties of ISG15. Their results showed that the reconstitution by overexpression of ISG15 in mice unable to trigger the IFN response was enough to attenuate Sindbis viral infection, manifested by lower viral titres and antigen levels as well as decreased lethality. Using mutant versions of ISG15, they also concluded that the antiviral activity was largely dependent on the ubiquitin homolog C-terminal motif ^{152}LRLRGG, essential for the ISGylation process, suggesting that the conjugating role of ISG15 is the responsible for the antiviral protection observed here. In 2007, Lenschow *et al.* (2007) published another piece of research in which they tested the susceptibility of ISG15$^{-/-}$ mice to a variety of double-stranded DNA and single-stranded RNA viruses. Their experiments showed that ISG15 deficient mice were more susceptible to both influenza A and B, herpes simplex type I, murine gammaherpesvirus 68 and, again, Sindbis virus. When they used recombinant viruses expressing wild-type ISG15, the susceptibility to Sindbis virus was rescued, but this was not the case when expressing a mutated version of ISG15 uncapable of conjugating (C-terminal mutated to ^{152}LRLRAA).

Further investigations using human embryonic kidney (293T) cells revealed that R153A mutation on ISG15 impaired the binding to the E1 enzyme UBE1L and the consequent transthiolation of the E2 enzyme UbcH8 (Giannakopoulos *et al.*, 2009). IFNα/βR$^{-/-}$ and ISG15$^{-/-}$ mice infected with Sindbis virus expressing the R153A mutated ISG15 showed a significant decrease in viral protection when compared to mice infected with virus expressing wild-type ISG15 (Figure 1.11). At the same time, UBE1L$^{-/-}$ also showed increased susceptibility to Sindbis infection and a higher lethality rate compared to wild-type mice. Altogether, this data shows that Arg153 on ISG15 and its interaction with UBE1L are essential for the antiviral immunity observed, demonstrating again that the protein conjugation plays a key role in the antiviral function of ISG15 against Sindbis virus. Nevertheless, ISG15 does not seem to be the most efficient antiviral protein to fight Sindbis infection. After assessing 44 different antiviral protein candidates, Zhang *et al.* (2007) selected and analysed the properties of a range of proteins, including ISG15, against Sindbis virus both *in vitro* and *in vivo*. Their findings on infected neonatal mice, proven to be defective in IFNα/β

antiviral activities, showed that although ISG15 did indeed protect the animals from mortality, other proteins like zinc-finger antiviral protein (ZAP) and ISG20 had greater antiviral protection. Nevertheless, recent publications have established that ISG15 deficient patients do not exhibit the viral susceptibility observed in mice, challenging the central role of ISG15 in antiviral immunity in humans, further discussed in subsection 1.3.4.

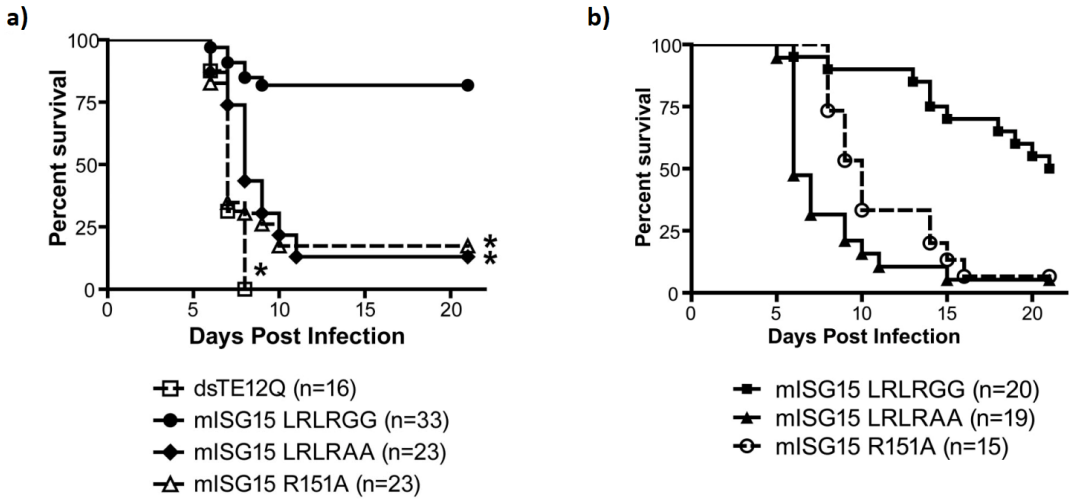

Figure 1.11: Survival rate of mice upon infection with Sindibis virus expressing wild-type or mutated ISG15, by Giannakopoulos *et al.* (2009). **a)** IFNα/βR$^{-/-}$ mice infected with Sindibis virus ($5x10^6$ PFU) using the virus vector dsTE12Q. The unaltered version was used as a control, while altered versions were produced to express wild-type (LRLRGG) and mutated versions of ISG15 (LRLRAA, uncapable of conjugating to target proteins and R151A, uncapable of binding to the E1 enzyme UBE1L). **b)** Survival rates on ISG15$^{-/-}$ mice infected intracerebrally with Sindibis virus vector dsTE12Q ($1x10^3$ PFU) either unaltered or altered to express the different versions of ISG15.

ISG15 and COVID-19

While the focus on the study of ISG15 as an antiviral molecule slightly faded over the last decade to focus on the identification of new potential targets and roles for this protein, the quick spread of the severe acute respiratory syndrome coronavirus 2 (SARS-CoV-2) (also known as COVID or COVID-19) re-kindled research on ISG15 regarding its role in fighting viral infection. This disease shook the world in 2019 causing a worldwide pandemic and infecting millions of people. The main symptoms of this RNA betacoronavirus, at the time of its discovery, were fever (presented by 88.7% of patients) and cough (67.8%), while nausea or vomiting and diarrhoea were rare (5.0% and 3.8% respectively) (Guan *et al.*, 2020). The median incubation period was of four days and severe illness developed in 15.7% of the patients after hospitalisation, this situation being more common among those patients with at least one coexisting condition such as hypertension and chronic ob-

structive pulmonary disease (23.7% of all the patients) (Guan *et al.*, 2020). An early COVID study by Hadjadj *et al.* (2020), which included 50 COVID-19 patients (15 mild to moderate, 17 severe and 18 critical patients) and 18 healthy controls, showed that IFN type I response characterised by lack of IFNβ and low production and activity of IFNα highly correlated with severe and critical COVID-19 disease. This phenomenon exacerbated inflammatory response, while mild to moderate patients presented a high IFN response.

Papain-like proteases (PLpro) are responsible for cleaving pp1a and pp1ab viral polypeptides to form replicase complexes essential for successful viral replication. Nevertheless, these proteases have also been found to be involved in host innate immune response suppression in some coronaviruses by reversing the ubiquitin and ISG15 post tranlational modifications. Freitas *et al.* (2020a) found that the PLpro in SARS-CoV-2 (SCoV2-PLpro) has a reduced activity when it comes to cleaving K48 linked ubiquitin compared to SARS-CoV, although it shows a higher specificity towards ISG15, potentially inhibiting its antiviral effects. On top of this, Shin *et al.* (2020) showed that SCoV2-PLpro also cleave ISG15 from the interferon regulatory factor 3 (IRF3). The ISGylation of IRF3 enhances its activity resulting in a positive regulation of the IFN pathway (Shi *et al.*, 2010). Therefore, as described by Shin *et al.*, cleaving ISG15 from IRF3 in SARS-CoV-2 resulted in attenuated type I IFN response. Similarly, the ISGylation dependent activation of the MDA5 mediated antiviral state gets compromised by the deISGylation activity carried out by SCoV2-PLpro (Liu *et al.*, 2021). Moreover, Munnur *et al.* (2021) confirmed in their study the strong deISGylating activity of SCoV2-PLpro when compared to their deubiquitylating activity and showed that the increased levels of free ISG15 generated as a result of enhanced deISGylation dysregulated macrophage response, suggesting that the unbalanced free to ISGylated ISG15 ratio contributed to the pro-inflammatory cytokine storms sometimes observed in SARS-CoV-2 patients. In order to examine if protein ISGylation is exacerbated in SARS-CoV-2 infected cells, causing an unproportioned level of free ISG15 when cleaved, Schwartzenburg *et al.* (2022) measured the levels of ISGylation in peripheral blood mononuclear cells from symptomatic COVID-19 patients and compared them to those found in asymptomatic and uninfected patients. Their results revealed that the infected patients with symptoms did indeed show increased levels of ISGylation, even when compared to infected patients with no symptoms. Here again, they proposed that that these increased level of ISG15 conjugation and consequent elevated levels of free ISG15 upon deISGylation by SCoV2-PLpr could be partially responsible of the cytokine storms. These conclusions could have promising therapeutic implications for the most severe unresponsive patients presenting pro-inflammatory cytokine storms.

1.3.2 ISG15 in cancer

The role of ISG15 as part of the IFN stimulated antiviral immune response has been broadly reviewed. However, ISG15 has also been related with the progression, prognosis and treatment response of human cancers. The study of this role in the last two decades has been quite contradictory - many studies conclude that ISG15 exhibits anti-tumour and pro-immune system properties, while many others maintain the expression of ISG15 is directly related with bad prognosis, therapy resistance and advanced metastatic level. This section will critically discuss some of the literature published describing the involvement of ISG15 in cancer development and treatment response.

One of the earliest studies on the role of ISG15 in cancer progression was performed by Andersen *et al.* (2006), who identified ISG15 as being significantly upregulated in a stage associated manner in bladder cancer samples when compared to healthy samples. Their results showed no IFN or inflammatory response related gene expression, suggesting that the overexpression of ISG15 transcripts found in 93% of Ta, 100% of Ta and 98% of T2-T4 samples was not a product of the general immune and inflammatory response. The measurements of protein expression also showed a significant upregulation of ISG15, with a mean 4.1 fold expression in Ta and T1 samples and a mean 12.1 fold expression in T2-T4 samples. Similarly, Satake *et al.* (2010) found that ISG15 was highly expressed only in high-grade prostate cancer samples and not in the normal prostate tissue. Silencing of ISG15 in 22Rv1 cells (human prostate carcinoma epithelial cells) using shRNA resulted in decreased colonies and reduced number of viable cells survival, while overexpression of ISG15 promoted cell growth suggesting its involvement in carcinogenesis. Overexpression of ISG15 in breast cancer both at the mRNA and protein level was reported by Bektas *et al.* (2008), who described ISG15 as overexpressed in breast carcinoma cells when compared with healthy breast samples. Results from the study showed that ISG15 mRNA levels were low in non-cancerous breast cell lines HMEC and MCF12A, but significantly elevated in breast malignant cell lines BT20, MDAMB468, MDA-MB231, T47D and MCF7, with a median fold change of 2.5. The analysis of cancerous and healthy primary samples also revealed significantly increased ISG15 mRNA levels in the malignant samples, with a median fold change of 10.3. Protein expression studies by immunohistochemistry of TMAs also revealed ISG15 to be upregulated in breast carcinoma samples, revealing a significant correlation between increased expression level and unfavourable prognosis. Research of oral squamous cell carcinoma reported that ISG15 was significantly overexpressed, which was again related to poor prognosis. Although the knock-out of ISG15 did not result in significant changes in growth rate, it did reduce tumour lymphangiogenesis and cell migration (Chen *et al.*, 2019).

ISG15 in cancer cell stemness

Very recent studies have linked the overexpression of ISG15 with the progression of other types of cancer such as glioblastoma (Tecalco-Cruz *et al.*, 2022), cervical cancer (Tao *et al.*, 2022) and solitary fibrous tumours (Mondaza-Hernandez *et al.*, 2022), the latter proving the relation between the increased expression of ISG15 and the upregulation of cancer stem cell related genes and subsequent stem cell-like properties. Other studies have also reported ISG15 to promote cancer stem cell like phenotypes. Sainz *et al.* (2014) found that tumour associated macrophages (TAMs) polarized towards an M2 protumour state promote self-renewal, migration, and tumorigenesis in pancreatic adenocarcinoma models by secreting ISG15 and USP18. Co-culturing pancreatic adenocarcinoma cells with recombinant ISG15 resulted in increased self-renewal capacity, migration and expression of pluripotency-associated genes, as well as in the activation of the activation of the p44/42 MAPK (ERK1/2) signalling pathway, known to be important for neoplastic cells (Figure 1.12). To confirm these findings, they analysed the tumorigenic effect of pancreatic adenocarcinoma cells injected with ISG15$^{-/-}$ TAMS into ISG15$^{-/-}$ mice, which showed to be reduced in comparison with the effect observed in mice co-injected with tumour cells and wild-type TAMs. Further research by the same group studying the role of ISG15 in pancreatic cancer stem cells (Alcalá *et al.*, 2020) revealed increased ISG15 mRNA and protein levels, both free and ISGylated, in these tumour stem cells when compared to the control cells. At the same time, they identified increased mRNA levels of IFN regulators pSTAT1 and IRF9, indicating a pancreatic cancer stem cell specific upregulation of the type I IFN pathway. The evaluation of the ISG15 transcriptional levels across public databases revealed that the expression of ISG15 is significantly increased in tumour samples and metastases compared to adjacent normal tissue, the higher levels correlating with worse disease prognosis. The knock-out of ISG15 using CRISPR in pancreatic cancer stem cell lines resulted in reduced self-renewal and *in vivo* tumorigenic capacity. Interestingly, the addition of recombinant free ISG15 to the cell cultures did not restore these properties nor the intracellular ISGylation, suggesting that the latter is responsible for the enhanced cancer stem cell like phenotypes. This hypothesis was supported by the partial rescue of the tumourgenic potential of one of the cell lines they used in their study through the overexpression of intracellular ISG15 transfecting a V5-tagged ISG15 construct.

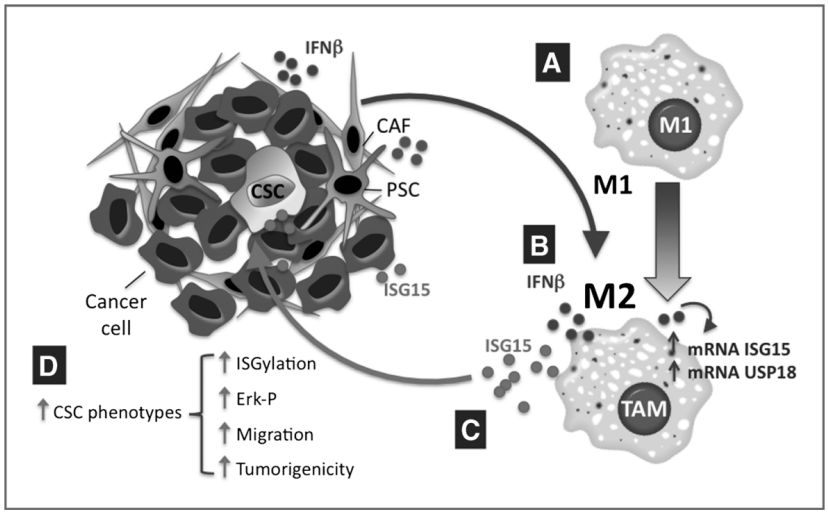

Figure 1.12: Model proposed by Sainz *et al.* (2014) of ISG15 promoting pro-tumour effects in pancreatic adenocarcinoma. M1 macrophages infiltrated within the tumour microenvironment are polarised towards a M2 pro-tumour state by tumour secreted factors like TGFβ1. Tumour cell secreted type I IFN stimulates TAMs to upregulate ISG15 and USP18. Secretion of free ISG15 acts on tumour cells promoting stem-like properties, such as self-renewal, migration, tumorigenesis and activation of the p44/42 MAPK (ERK1/2) signalling pathway.

Another example of ISG15 driven cell stemness in cancer is the research by Chen *et al.* (2016), who identified ISG15 as being significantly overexpressed in both nasopharyngeal carcinoma biopsy samples and cell lines. They found it to promote cancer stem cell-like properties in these tumours, including increased ability to form colonies and tumourspheres, both in number and size, and enhanced expression of pluripotency associated genes. These phenotypes were attenuated upon knock down of ISG15. Similar to many of the studies previously described, the overexpression of ISG15 also correlated with more frequent disease recurrence and lower disease-free and overall survival rates in nasopharyngeal carcinomas. An expansion of this study published in 2020 (Chen *et al.*) reported that ISG15 is also expressed in nasopharyngeal carcinoma associated macrophages inducing a M2 state, consistently with the data published by Sainz *et al.* and Alcalá *et al.* They proved that this response is dependant on the interaction of ISG15 with LFA-1, resulting in the secretion of CCL18 and subsequent promotion of tumour cell migration. Dai *et al.* (2022) also proved that ISG15 positively regulated stem-like phenotypes in glioma samples and proposed the ISGylation and subsequent enhanced stability of Oct4, a transcription factor critically involved in stemness, as a possible mechanism. Due to the significant evidence on the involvement of ISG15 in carcinogenesis, aggressiveness and therapy resistance, ISG15-targeting cancer vaccines have been developed and tested.

Anti-ISG15 vaccines in cancer

Wood *et al.* (2012) developed an anti-ISG15 vaccine and proved that its use in primary and metastatic breast cancer mouse models resulted in significant CD8 mediated tumour reduction. After confirming that ISG15 mRNA and protein was also significantly upregulated in breast different cancer mouse models when compared to normal mouse mammary tissue, they showed that the anti-ISG15 vaccine generated an ISG15 specific IFNγ response and a significant CD8 dependant regression of the primary tumour burden and metastatic spread with good epitope spreading. These findings are particularly meaningful since most of the immunotherapy advances at the time were HER2 related, while the ISG15 overexpression identified the breast cancer samples were HER2, progesterone receptor, and oestrogen receptor status independent, meaning that this therapy could benefit a wider range of patients. More recently, Nguyen *et al.* (2022) developed a listeria-based vaccine targeting ISG15 to be tested in renal cell carcinoma mouse models overexpressing it. The treatment resulted in a significant polyfunctional T cell immune and anti-tumour response, comparable to the one obtained with the current frontline anti-PD1 immunotherapies used in patients suffering from this disease. However, the use of this vaccine promoted PD1 expression, and its combination with anti-PD1 therapy did not result in a synergistic effect. Although further research is required to find the best therapy combination, the results presented by this group set a promising background for the use of anti-IS15 vaccines as treatment in renal cell carcinoma.

ISG15 in drug resistance

As detailed in section 1.2, Weichselbaum *et al.* (2008) described the relation between the overexpression of the IRDS and cellular resistance to DNA-damaging therapies. They also identified ISG15 as one of the members of this group, which they found to be one of top overexpressed proteins in a series of human tumour samples (Figure 1.13). Because STAT1 was identified as a member of the IRDS as well, they experimentally tested if ISG15 was able to mediate the treatment resistance by itself or was just a marker of the STAT1 activity. Their results showed that knock down of ISG15 resulted in cells being resensitised to DNA-damaging drugs. As part of the research on nasopharyngeal carcinoma described earlier in this section, Chen *et al.* also found that the overexpression of ISG15 promoted resistance to DNA-damaging treatments such radiation and the chemotherapy agent cisplatin. Other studies, however, have described ISG15 to be involved in sensitising cancer cells to DNA-damaging treatments as well as in repair upon DNA damage. Desai *et al.* (2008) established a relation between high ISG15 expression and sensitivity to the chemotherapeutic drug camptothecin (CTP) in several cancer types including glioblastoma, colorectal cancer and breast cancer. They tested this premise analysing the ISG15

expression levels in ZR-75-1 and BT474 breast cancer cell lines, the first one being much more sensitive to CTP than the second one (>50 fold). After proving that the expression of ISG15 and ISGylated proteins were indeed very high in ZR-75-1 cells and very low in BT474 cells, they used shRNA targeting ISG15 in ZR-75-1 cells, which resulted in significant resistance to CTP. They also proved the relation between the sensitivity/resistance to CTP and the expression of topoisomerase I, and proposed that ISG15 could be antagonising its ubiquitination and consequent downregulation (required to mediate resistance) as a possible working mechanism. Huo *et al.* (2017) also presented ISG15 as a mediator of sensitivity to chemotherapeutic drugs, as they found it downregulated in cisplatin resistant lung carcinoma cells (A549/DDP) when compared to sensitive A549 cells, and ISG15 knock down in the latter cell model resulted in increased resistance to cisplatin. Here, they suggested that the cell cycle arrest induced by the silencing of ISG15 allowed time to repair the DNA-damage caused by the chemotherapeutic drug. Consistent with this data, Zhang *et al.* (2021b) also demonstrated that ISG15 was significantly downregulated in other cisplatin-resistant cell lines, SKOV3/DDP and A2780/DDP, compared to the sensitive partner cell lines. Expression of wild-type ISG15 in the resistant cell lines upon cisplatin treatment lead to reduced cell viability and increased apoptosis, but the expression of a mutated version incapable of ISGylating did not restore drug sensitivity. On top of this, the expression of both wild-type and mutated ISG15 in the resistant cell lines led to reduced cancer stem cell like phenotypes such as colony formation ability, migration, invasion and spheroid formation. Interestingly, the knock down of ISG15 in the sensitive cell lines did not result in cisplatin resistance, but it did enhance these cancer stem like properties.

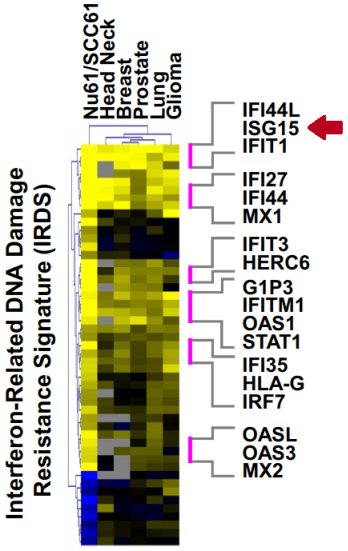

Figure 1.13: Heat map showing the expression of different IRDS genes (rows) in five different types of tumours (columns) using their expression on Nu61 vs SCC61 (radiation resistant vs radiosensitive) cell lines as a reference. ISG15, one of the top overexpressed genes in all the tumour types, is marked with a red arrow. Yellow indicates high expression and blue indicates low expression. Figure by Weichselbaum *et al.* (2008).

ISG15 as an anti-cancer and pro-immunity protein

A proposed mechanism by which ISG15 aids DNA repair was described by Park *et al.* (2014), who showed how the ISGylation of the Proliferating Cell Nuclear Antigen (PCNA), a DNA replication machinery element crucial for translesion DNA synthesis, helped regulate its activity by terminating the process after DNA repair had taken place. The impairment this modification either by mutating residues essential for the ISGylation of PCNA or by knocking down any of the elements required for the adequate processing of the modification, resulted in the faulty termination of the repair process and subsequent increase in mutation frequency upon UV-mediated DNA-damage. The same group also investigated the effects of the tumour suppressor activities of ISG15 by studying the effect of the ISGylation on p63 and p53. Particularly, they showed how the treatment of cells with a chemotherapeutic drug induced ISGylation of an alternative splicing of p63 (ΔNp63α) capable of suppressing p53 family members and found to be significantly upregulated in many human epithelial tumours, leading to its inhibition (Jeon *et al.*, 2012). On the other hand, the ISGylation of p53, also DNA-damage induced, leads to significantly enhancing its tumour suppressor activity (Park *et al.*, 2016). The ISGylation of CHIP, an E3 ligase responsible of the ubiquitination of c-Myc among other roles, has also been reported to promote its activity upon IFN type I treatment, leading to growth inhibition in A549 lung cancer cells (Yoo *et al.*, 2018). Another example of the tumour suppressive role of ISG15 through target modification was reported by Yeung *et al.* (2018), who showed that ISGylation of ERK in high grade serous ovarian cancer lead to growth suppression and apoptosis induction. They also showed an association between elevated ISG15 protein expression in the tumour with increased CD8+ lymphocyte count and with improved overall and progression free survival.

Conclusion

The data presented here paints a confusing picture. ISG15 has been proved to be pro- and anti-tumourgenic in different cancer backgrounds and conditions. Although it seems clear that both free ISG15 and ISGylation have immune boosting properties under a healthy environment, the first as a cytokine and the second by targeting different proteins to inhibit or enhance their functions, the link of an altered or uncontrolled ISG15 pathway with tumour progression and aggressiveness is undeniable. To study the role of ISG15 in cancer, understanding the IFN signalling state of tumour cells (mutation or dysregulation) as well as the level and ratio of free versus conjugated protein seems crucial. Some studies have suggested that ISG15 promotes cancer through its conjugation and consequent stabilisation of pro-tumour proteins, but performs as a tumour suppressor when acting free as a cytokine (Burks *et al.*, 2015; Desai, 2015). While there is not much known regarding the

expression levels of free vs conjugated ISG15 and in human cancers, Desai *et al.* (2006) did find that some of the tumour samples they analysed expressed significantly different free to conjugated ISG15 ratios (very high levels of ISGylation and low levels of free ISG15 and *vice versa*), although they could not explain the reason. On the other hand, Tecalco Cruz & Mejía-Barreto (2017) suggested that the balance of free and conjugated ISG15 and their roles in cancer were highly dependent on the cell and tumour type. Further research to investigate if the difference in protein state ratios correlate with better or worse prognosis and the tumour specific patterns is needed.

1.3.3 ISG15 and USP18 as negative regulators of the IFN pathway

As described in Figure 1.8, USP18 is the isopeptidase responsible of removing ISG15 from its target proteins in a process known as deISGylation. However, USP18 has shown to have a role independent of its isopeptidase activity. Malakhova *et al.* (2003) were the first to identify USP18 as a novel negative regulator of the IFN signalling pathway, and demonstrated that it binds to the IFNAR2 receptor subunit blocking the interaction between the receptor and JAK1, consequently downregulating the JAK-STAT pathway described in Figure 1.1 (Malakhova *et al.*, 2006). The ISGylation/deISGylation process does not play a role in the negative regulation of the IFN pathway, as demonstrated by Kim *et al.* (2006) who using UBE1L$^{-/-}$ USP18$^{-/-}$ mice demonstrated that it was the absence of USP18 and not the accumulation of ISGylated proteins what caused the hypersensitisation to type I IFNs, prolonged STAT1 phosphorylation and increased expression of ISGs. However, Zhang *et al.* (2015) showed that ISG15 deficient patients also showed immunological and clinical signs of enhanced IFNα and β response, leading to the question of whether there was a deISGylating activity independent link between free ISG15 and USP18 that resulted in the negative regulation of the IFN pathway. Further experiments by Zhang *et al.* (2015) showed that the absence of intracellular free ISG15 prevented the accumulation of USP18, resulting in the enhanced IFN pathway in ISG15 deficient patient's cells and proving that ISG15 plays an important role in the negative regulation of IFN signalling stabilising USP18. On top of this, it has been proven that ISG15 prevents the S-phase kinase associated protein 2 (SKP2) mediated proteasomal degradation of USP18, further discussed in section 4.5 (Vuillier *et al.*, 2019), supporting its role as a USP18 stabiliser.

Vasou *et al.* (2021) determined recently that, although the ISG15-mediated stabilisation of USP18 is necessary for the regulation of the IFN pathway, it is not sufficient, showing that the non-covalent interaction between these two proteins also enhances the regulatory function of USP18 (Figure 1.14). To prove such claim, they used wild-type (^{152}LRLRGG) and mutated (^{152}LRLRAA or ^{152}LRLR) ISG15, placed under the control of the native ISG15 promoter, in ISG15$^{-/-}$ A549 lung carcinoma epithelial cells. By these means, they confirmed

that the diGly moiety essential for ISGylation is also crucial for the interaction between USP18 and ISG15 which, at the same time, is necessary for USP18 to act as a negative regulator of the IFN pathway. Although the mutated versions of ISG15 did inhibit ISGylation, they did not significantly reduce the levels of USP18. This proves that the teamwork of both ISG15 and USP18 is required for the regulation of the IFN signalling, crucial to avoid the overinduction of the pathway and its consequences, such as autoinflammatory disease, and that the C-terminal of ISG15 has a dual role that is independent of the ability of ISG15 to stabilise USP18.

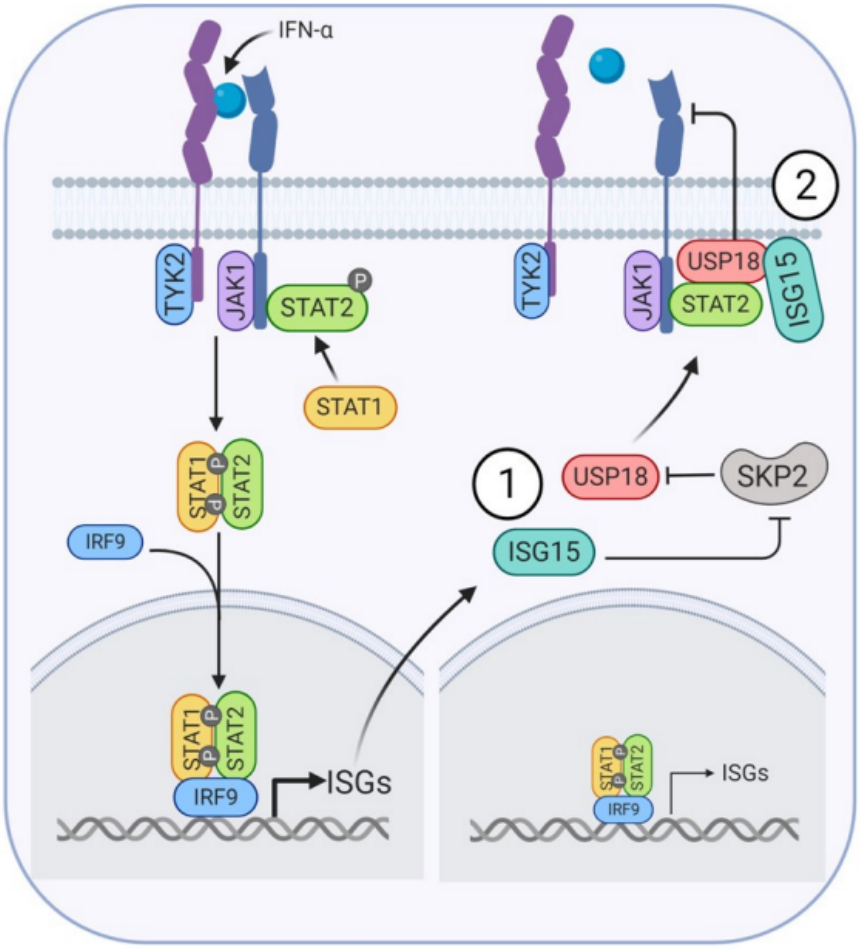

Figure 1.14: Model of the USP18/ISG15 interaction dependant negative regulation of the type I IFN pathway, by Vasou *et al.* (2021). Binding of IFNα to the IFNAR receptor results in the induction of ISGs, including ISG15 and USP18. ISG15 promotes the stabilisation of USP18 by preventing it from being degraded through SKP2 and by non-covalently interacting with it to promote its inhibitory function upon blocking INFAR2.

1.3.4 Other roles of ISG15

ISG15 in other diseases

In 2012, Bogunovic *et al.* (2012) found that patients with inherited ISG15 deficiency were more prone to mycobacterial infections, but not to viral infections. This was a surprising finding since ISG15 had been strongly linked with antiviral immunity (subsection 1.3.1). Their investigations in several ISG15 deficient human patients led to conclusion that the lack of secreted free ISG15 resulted in reduced production of IFNγ in immune cells and consequent increased susceptibility to these infections, leading to the inclusion of ISG15 to the list of genes known to cause MSMD. On the other hand, the absence of intracellular ISG15 or ISGylation did not lead to susceptibility to viral infections, neither at cellular nor at whole system level. This was later supported by Speer *et al.* (2016), who also reported cases of human ISG15 deficient patients that did not display the enhanced susceptibility to viruses observed in mice *in vivo*. Recently, other medical case studies have been published describing the effects of inherited ISG15 deficiency. Increased type I IFN signalling is linked to more SLE flares, more aggressive disease and tissue damage. Al-Mayouf *et al.* (2021) reported the case study of a female patient with autosomal recessive ISG15 deficiency presenting type I interferonopathy with SLE and inflammatory myositis, with history of encephalitis, ulcers, inflammatory skin lesions and autistic spectrum disorder features among others. Other cases have also been described with similar symptoms. Martin-Fernandez *et al.* (2020) reported the cases of five patients also presenting type I interferonopathy with skin lesions and inflammation, and Buda *et al.* (2020) reported the less severe auto-inflammatory case of a patient with recurrent ulcerative skin lesions, cerebral calcification and lung disease. Because the lack of ISG15 prevents accumulation of USP18 by stabilisation and consequent upregulation of the IFN type I pathway, the inflammatory and autoimmune symptoms described here are not surprising. However, skin lesions are not a common symptom of interferonopathy. Hayat Malik *et al.* (2022) also presented the cases of two ISG15 deficient siblings with chronic inflammation and skin ulcers, but they found that the cells lacking ISG15 downregulated expression of elements essential for epidermis integrity such as collagen and adhesion proteins, revealing a key role of ISG15 in skin and connective tissue homeostasis.

The overexpression of ISG15 has been found to cause detrimental effects in neurodegenerative disorders like Ataxia-telangiectasia (A-T) (Desai *et al.*, 2013), and ISGylation levels have also been found increased in the lumbar spinal cords of amyotrophic lateral sclerosis patients (Schwartzenburg *et al.*, 2019). Interestingly, this phenomenon was significantly higher in patients with a history of traumatic brain injury. Although the overexpression of ISG15 was not detected in the occipital lobe samples acquired from the same patients, they did find increased ISGylation levels in cerebral spinal fluid and derived lym-

phocytes. These results suggest that increased ISG15 expression is somehow linked to neurodegenerative conditions. ISG15 has also been related to vascular damage associated with hypertension through oxidative stress and inflammation (González-Amor *et al.*, 2022), colonic inflammation and malignant progression (Fan *et al.*, 2015b), and inflammation mediated maternal immune activation, which can lead to psychiatric disorders in offspring (Hu *et al.*, 2019). Some of the latest implications of the altered expression of ISG15 reported are the identification of downregulated ISG15 expression, among other altered genes, in blood samples of children with autism spectrum disorder compared to neurotypical children (Voinsky *et al.*, 2022) and the identification of ISG15 as a potential biomarker for sepsis (Ma *et al.*, 2023), although the latter is still pending peer review at the time of writing.

ISG15 in autophagy and proteosomal degradation

ISG15 also has a role in autophagy and the ubiquitin pathway, and it has been suggested that the former of these gets activated to compensate for the ISG15 dependent suppression of the proteasome mediated protein degradation, which leads to overinduction of autophagy and consequent aberrant autophagic flux. The silencing of ISG15 in A-T cells, a neurodegenerative neurological disorder, resulted in restoring of these functions (Desai *et al.*, 2013). Animal and cell models with enhanced ISGylation also showed enhanced increased basal and infection-induced autophagy following *Listeria monocytogenes* infection (Zhang *et al.*, 2019). Similarly, Bhushan *et al.* (2020) found ISG15 to be a link between the autophagy pathway and the defensive anti-parasitic properties of IFNγ following *Toxoplasma gondii* infection. In the contrary, Falvey *et al.* (2017) found ISG15 to be a negative regulator of the autophagy pathway in oesophageal cancer cells, and established that its knock down led to increased autophagic flux following treatment with cytotoxic drugs, which allowed cell recovery and treatment resistance. This seems to be a two-way regulation process, since Kong *et al.* (2020) found recently that knocking down ATG5 and ATG7 (essential proteins for the autophagy pathway) in mouse embryonic fibroblast resulted in the activation of type I IFN signals and increased ISG15 expression, this time promoting tumour associated phenotypes such as proliferation, migration and invasion. Altogether, it seems that ISG15 expression induces autophagy upon pathogenic attack to help clear the infection, but overexpression of ISG15 and consequent overinduction of this pathway can lead to aberrant autophagy flux. In a cancer background, ISG15 dependent autophagy can also be altered leading to different responses upon cytotoxic drug treatment and promotion of tumour-associated phenotypes. The effects of ISG15 in proteasomal degradation were first described by Desai *et al.* (2006), who showed that the increased levels of ISGylation in different tumours correlated with reduced levels of polyubiquitinated proteins. The silencing ISG15 or UbcH8 through targeted siRNA resulted in rescued levels of

polyubiquitinated proteins, suggesting that ISG15 antagonises ubiquitin mediated protein turnover. UbcH8 also works as an E2 enzyme for ubiquitin, as mentioned in section 1.3. This potentially overlaps the two pathways resulting in competition for E3 ligases, which could enhance the inhibition of the proteasome-mediated degradation pathway. Furthermore, as described in section 1.3, ubiquitin has been proved to be ISGylated, which can form ISG15-ubiquitin mixed chains that lock ubiquitin onto the substrate inhibiting its degradation (Fan *et al.*, 2015a). Even though there are studies reporting that ISGylation can promote specific substrate degradation (Im *et al.*, 2016; Yoo *et al.*, 2018), the broad image seems to suggest that ISG15 is capable of inhibiting proteasome-mediated protein degradation resulting in the stabilisation of tumorigenesis promoting proteins.

ISG15 in mitochondrial processes

ISGylation is also known to regulate basic mitochondrial functions, and its downregulation or overexpression can cause dysfunction of these mechanisms. Baldanta *et al.* (2017) analysed the proteome of ISG15 KO vs wild-type IFN treated bone marrow derived macrophages and found out that IFN treatment in the absence of ISG15 lead to disrupted oxidative phosphorylation and mitochondrial pathways. On the other hand, Juncker *et al.* (2021) proved that high expression of ISG15 alters mitochondrial distribution in A-T cells, increases the level of damaged mitochondria and disrupts its degradation process by attenuating polyubiquitylation, while the suppression of ISG15 restored these defects.

Conclusion

The evidence presented in this section proves the great variety of biological functions that somehow involve ISG15. Altogether, it can be concluded that although ISG15 plays a protective role in healthy individuals, the dysregulated ISG15 pathway plays an important role in disease by mediating inflammation, altering essential pathways such as autophagy, mitochondrial functions, epithelial integrity and protein degradation, and stabilising tumourgenic proteins. Nevertheless, there seems to be a lot of context and cell type variability, and further research is required to better elucidate in what conditions ISG15 targeting therapies could be beneficial.

Chapter 2

Materials and Methods

2.1 Chemicals and solutions

All chemicals used were purchased from Fisher Chemicals (ThermoFisher) or Sigma Aldrich unless stated otherwise in text.

2.2 Cell culture

2.2.1 Cell lines

The cell lines used throughout this project are listed in Table 2.1. Genetic modifications performed in each of them can be found in subsection 3.3.1. All the cell lines used in were regularly checked to ensure that they were not infected by mycoplasma infection.

Table 2.1: Different cell lines used throughout the project's development, indicating the their source, genetic edition if any, media required and supplementation.

Cell line	Source	Media	Supplementation
SiHa	Human cervical carcinoma	Gibco RPMI 1640 (#21875-034)	Removed 50 mL of media and added 50 mL of FBS (Gibco, #10437-028)
Caki-1	Human renal carcionoma	Lonza RPMI 1640 (#BE12-702F)	Removed 50 mL of media and added 50 mL of FBS (Gibco, #10437-028) 5 mL MEM NEAA (Sigma-Aldrich, #M7145) 2.5 mL ultra glutamine (Lonza, #BE17-605E)
GSC	Patient derived glioblastoma stem cells	Sigma DMEM F-12 Ham (#D8437)	7.25 mL Glucose (Sigma #G8644) 5 mL MEM NEAA 100x (Gibco, #11140-035) 5 mL Pen-Strep (Gibco, #15140-122) 800 μL BSA 7.5% (Gibco, #15260-037) 1 mL β-mercaptoethanol 50mM (Gibco, #31350-010) 5 mL B27 Supplement 50x (Gibco, #17504-044) 2.5mL N2 Supplement 100x (Gibco, #17502-048) 50 μL mouse EGF (Peprotech, #315-09) 50 μL human FGF (Peprotech,#100-18b) 1 mL laminin Cultrex Laminin, #3446-005-01)
NSC	Fetal neuronal stem cells	Sigma DMEM F-12 Ham liquid (#D8437)	Supplemented as for the GSC cell line

2.2.2 Cell line maintenance and subculture

Cells were cultured in the appropriate supplemented media as shown in Table 2.1. All cells were maintained in a humidified incubator at 37 °C and 5% (v/v) CO_2. SiHa and Caki-1 cells were kept in vented CELLSTAR® culture plates and flasks respectively (Greiner), while stem cells, both NSC and GSC, were kept in Corning® vented flasks.

Cells were regularly monitored using a bright-field inverted microscope and, when grown to a high confluence, they were passaged into new plates or flasks in a sterile lami-

nar flow cabinet and using single-use sterile plasticware. For this purpose, the media was first aspirated and the cells were gently washed with room temperature sterile phosphate-buffered saline (PBS). The appropriate dissociating reagent (0.05% or 0.25% (w/v) Trypsin-EDTA (Gibco) for SiHa and Caki-1 cells, incubating at 37 °C for 5 minutes, and StemPro™ Accutase (Gibco) for stem cells with incubation at 37°C for 3 minutes) was used to detach the cells from the plates or flasks. Cells were collected on fresh media and gently centrifuged either at 1000 rpm for 5 minutes (SiHa and Caki-1 cells) or at 1300 rpm for 3 minutes (stem cells) to remove any remains of dissociating reagent. When working with stem cells, DMEM F-12 supplemented only with pen-strep and BSA was used (henceforth F12 wash media) to collect the cells after dissociation to avoid wasting fully supplemented media. At this point, cells could be collected for assays and experiments or resuspended in clean fresh media to transfer a fraction of cell suspension to new sterile plates or flasks, usually at a 1:10 dilution.

2.2.3 Cell counting

Certain experiments require a consistent number of cells in each well/dish. To count them, cells were dissociated following the procedure detailed in subsection 2.2.2. After centrifugation, the supernatant was discarded and the pellet was resuspended in 1 mL of fresh media / F12 wash media and 10 μL of this were mixed with 10 μL 0.4% Trypan Blue stain (Labtech). 10 μL of the resultant mixture were loaded in each side of a Luna™ Cell Counting Slide (Labtech) and introduced on a Luna Automated Cell Counter (Labtech). An average of both reads was used to calculate the number of cells per mL of media and the volume of cell suspension required for each experiment.

2.2.4 Cryopreservation

For cell line storage, cells were prepared for cryopreservation and frozen at -80 °C. For this, cells were dissociated and centrifuged as described in subsection 2.2.2. Cell pellets were resuspended in cryopreservation media and 1 mL of the suspension was aliquoted in 1.8 mL Nunc® Cryotubes®. Cryovials were then inserted into a Cryo 1 °C Freezing Container (Nalgene™) and stored at -80 °C for at least two hours before taking them out of the container. For long-term preservation vials were transferred to liquid nitrogen, but they could be kept at the -80 °C freezers in appropriate boxes for short-term storage. The composition of the cryopreservation media depended on the cell line to be preserved. For SiHa and Caki-1 cells, a 50% (v/v), 40% (v/v), 10% (v/v) mixture of FBS, unsupplemented media and dimethyl sulfoxide (DMSO) respectively was prepared to the required volume, while stem cells required a 90% F12 wash media and 10% (v/v) DMSO mixture. Usually, one 10

cm plate or T75 flask gathered enough cells for three cryovials, but the exact amount could be decided upon observing the size of the cell pellet after centrifugation.

2.2.5 Cell recovery

To recover the cells from the liquid nitrogen storage, they were thawed quickly in a water bath at 37 °C and mixed gently with 9 mL of fresh media or F12 wash media and centrifuged as required by the cell-line to remove the DMSO, which can be toxic to cells. The cell pellet was resuspended in 1 mL of supplemented media and transferred to a new sterile plate or flask carefully integrating the suspension in the full media volume. The plates or flasks were then maintained at the humidified incubator at 37 °C and 5% (v/v) CO_2.

2.2.6 Cell treatment

Throughout the project, cells were treated with IFN as per the following guides:

- Commercial Human Recombinant Interferon α2 (Merck, #407294) purified from *E. coli* was used to a final concentration of 100 U/mL, unless otherwise stated in the text.
- Commercial Human Recombinant Interferon γ (Gibco, #PHC4031) purified from *E. coli* was used to a final concentration of 100 ng/mL.
- A series of secreted Recombinant Interferon α subtypes (1, 2, 4, 5, 6, 7, 8, 10, 14, 16, 17 and 21) were used at approximate final concentrations of 0.3 ng/mL, 0.9 ng/mL and 3 ng/mL. These IFNs were kindly provided by colleague Ashita Singh, who expressed them in HEK293 cells using a mammalian expression system and collected the secreted protein in DMEM media.

2.2.7 DNA transfection

For successful plasmid DNA transfection into SiHa cells, confluency had to be between 60% and 80% at the time of transfection. At the right time, DNA was mixed with Attractene Transfection Reagent (Qiagen) in fresh unsupplemented media following the volumes detailed in Table 2.2. Mixture was incubated for 15 minutes at room temperature before pipetting it onto the cells. Plates were then incubated at 37 °C and 5% (v/v) CO_2.

Table 2.2: Reactants and conditions for DNA transfection.

Plate type	DNA (μg)	Attractene (μL)	Media volume (μL)	Total well volume (μL)
92 well plate	0.2	0.75	50	100
24 well plate	0.4	1.5	60	500
12 well plate	0.8	3.0	80	1000
6 well plate	1.2	4.5	100	2000
1 well plate	4.0	15.0	300	10000

2.3 Microbiological techniques

All work involving living bacterial cells was carried out in sterile conditions.

2.3.1 Antibiotic concentration

All media used for microbiological techniques was prepared with either kanamycin or ampicillin depending on the resistance gene present in the plasmid of interest, allowing for positive selection. Ampicillin was used at a final concentration of 100 μg/mL while kanamycin was used at a final concentration of 50 μg/mL. If preparing LB-agar plates, the broth was heated until liquefied and the antibiotic was added only when the temperature dropped at 55 °C to avoid degradation.

2.3.2 Bacterial cultures

Bacterial cultures were grown in Lysogeny broth (LB, a.k.a. Luria-Bertani broth) in a shaking incubator at 37 °C and 220 rpm, the volume of the culture being 1/5 of the total volume of the flask to allowing proper oxygenation.

Compositions of the culture media used for bacterial growth are listed in Table 2.3. Liquid media was autoclaved after preparation, before adding the antibiotic. The agar was then poured into Sterilin™ Standard 90 mm Petri Dishes and left to solidify at room temperature. Once solid, plates could be either pre-warm for an hour at 37°C before use or stored upside down in the fridge for a couple of weeks. To avoid contamination and dehydration while stored, the plates were sealed with parafilm.

Table 2.3: Composition of the media used for bacterial culture growth. Liquid media was autoclaved after preparation, before adding the antibiotic. Agar plates were prepared with autoclaved agar broth before adding antibiotic and pouring into plates.

LB broth	LB agar plates	SOC
1% (w/v) Tryptone	1% (w/v) Tryptone	2% (w/v) Tryptone
0.5% (w/v) yeast extract	0.5% (w/v) yeast extract	0.5% (w/v) yeast extract
1% (w/v) NaCl	1% (w/v) NaCl	10 mM NaCl
	1.5% (w/v) granulated agar	2.5 mM KCl
		10 mM $MgCl_2$
		10 mM $MgSO_4$
		20 mM glucose

2.3.3 Glycerol stocks

For long-term storage, bacterial cultures could be frozen in glycerol stocks. For this, 10 mL of LB with antibiotic were inoculated with a single colony of bacteria and incubated over-night with gentle shaking. Cultures were centrifuged the following day at 3000 rpm using a table top centrifuge (Eppendorf) and the pellet was resuspended in filter-sterilised (0.22 μm Miller®GP sterile filter unit, Merck) solution composed of 0.5 mL of LB broth with antibiotic and 0.5 mL of 50% glycerol in Milli-Q water. Suspension was transferred to cryotubes, snap-frozen in liquid nitrogen and stored at -80 °C in appropriate boxes.

2.3.4 Preparation of competent cells

DH5α bacterial cells from commercial glycerol stocks (Invitrogen) were used to prepare small 5 mL cultures that were incubated with shaking at 37 °C over-night. The following day, 500 μL of this culture were transferred into 100 mL of fresh LB and incubated with shaking at 37 °C while monitoring the optical density measured at a wavelength of 600 nm (OD600) using a Lambda Bio UV/VIS spectrophotometer (Perkin Elmer). Once the right density was reached (0.4 - 0.6), the culture was centrifuged at 4000 rpm at 4 °C for 15 minutes. Keeping the tube on ice at all times, the supernatant was discarded and the pellet was resuspended in 32 mL of ice cold filter-sterilised (0.22 μm Miller®GP sterile filter unit, Merck) buffer I (see Table 2.4) and incubated on ice for 10 minutes. The suspension was then centrifuged again at 4000 rpm at 4 °C for 15 minutes. After discarding the supernatant, the pellet was resuspended in 4 mL of ice cold buffer II (see Table 2.4) and incubated on ice for another 10 minutes. Cells were aliquoted in pre-chilled sterile 1.5 mL Eppendorf tubes, each containing 50 μL of suspension, immediately snap frozen in liquid

nitrogen and stored in a -80 °C freezer.

Table 2.4: Composition of the buffers needed for the preparation of competent cells.

Buffer I	Buffer II
100 mM RbCl	10 mM RbCl
100 mM $CaCl_2 \cdot 2H_2O$	75 mM($CaCl_2 \cdot 2H_2O$
15% (v/v) glycerol	15% (v/v) glycerol
40 mM $MgCl_2 \cdot 6H_2O$	10 mM MOPS
60 nM CH_3COOK	pH 6.5 (adjusted with NaOH)
pH 5.8 (adjusted with HCl)	

2.3.5 Transformation of chemically competent cells

A frozen tube containing competent *E. coli* cells (see subsection 2.3.4) was thawed on ice. In the meantime, concentration of the plasmid DNA was measured using a NanoDrop 2000c spectrophotometer (Thermo Scientific). Once thawed, 100 - 200 ng DNA were added into the tube containing the competent cells. If using a pT-REX-Dest30, which contains a gene encoding a toxic protein (ccdB), commercial One Shot™ ccdB Survival™ (Invitrogen) competent cells were used instead. Once the DNA was added, the cells were incubated on ice for 30 minutes, heat shocked right after by placing the tubes in a heat-block at 42°C for 45 seconds, and immediately placed on ice for 5 minutes to recover. 500 μL of super optimised broth with catabolite repression (SOC, see Table 2.3) were then added to the tube to resuspend the cells, which were then incubated with shaking at 37°C for 1 hour. After the incubation time, 40 - 100 μL of bacterial culture were plated onto LB-agar plates with the appropriate selection antibiotic and incubated at 37°C over-night.

2.3.6 Amplification and purification of plasmid DNA

After transformation, single bacterial colonies were picked for inoculation of 10 mL LB cultures, which were incubated with shaking at 37°C. After over-night incubation, 1 mL of the culture was transferred to new 200 mL LB subcultures for over-night incubation as before. The bacterial pellet was collected the following day by centrifugation at 4000 rpm and the plasmid DNA was extracted and purified using a Qiagen® Plasmid Maxi-prep kit (#12163), following supplier's protocol. If smaller quantities were required quicker, an extraction and purification could be done straight from the 10 mL culture using a Qiagen® Plasmid Mini-prep kit (#12123).

2.4 Molecular and cellular biology techniques

2.4.1 DNA extraction and purification

Plasmid DNA extraction and purification from bacterial cells is described in subsection 2.3.6. To purify whole genome DNA from mammalian cultured cells, the Puregene® Core Kit B (Qiagen), collecting the amount of cells indicated and following the suppliers protocol.

2.4.2 Agarose gel electrophoresis of DNA

In order to separate the DNA fragments by size, samples were run in an agarose gel. To prepare the gels, electrophoresis-grade UltraPure™ Agarose (Invitrogen) was dissolved to 1 - 2% (w/v) (depending on the resolution required) in 1x TAE buffer (10 mM EDTA, 40 mM Tris-base, 20 mM glacial acetic acid, pH 8.5). Solution was heated up until full dissolution and left to cool down enough to safely add SYBR™ Safe DNA Gel Stain (Invitrogen, #S33102) to a 1: 10,000 dilution before pouring it into a gel mould. Once solidified, the required amount of sample was mixed with 6x DNA-loading dye (New England BioLabs, #B7024S) at a 5:1 dye-sample ratio and loaded into the gel. If DNA was to be purified by excision and gel extraction, the whole PCR reaction was loaded, but if bands were to be visualised before PCR product purification, loading 5-10 μL of the reaction was enough. Both these purification procedures were carried out with commercial kits from Qiagen (QIAquick® Gel Extraction kit (#28704) and QIAquick® PCR Purification kit (#28104)). Along with the samples, Quick-Load 100 bp DNA ladder, 1 kb DNA ladder or both (in different wells) were loaded as standards in order to help with the size identification of the fragments (both from New England BioLabs). The gel was run in 1x TAE buffer at 80 - 100 V until the bands were separated to the resolution required. The DNA bands were visualised by either placing the gel into a UV lamp (for gel excision) or into a Bio-Rad ChemiDoc MP imaging system with a built-in camera (for image capturing).

2.5 Biochemical techniques

2.5.1 Cell harvesting and pellet lysis

Cells were collected either by dissociation, as described in subsection 2.2.2, or by mechanical scraping. For the latter, plates or flasks were placed on ice, had the media aspirated and were washed three times with ice cold sterile PBS. 1-2 mL of PBS were used to

collect the cells with a disposable sterile plastic scraper and they were transferred to an appropriate collection tube to be centrifuged at 1000-1300 rpm for 3-5 minutes. The supernatant was discarded and the pellet was either frozen in liquid nitrogen for storage at -80°C or lysed for immediate use. To lyse, pellets were resuspended in 50 μL to 150 μL of lysis buffer (25 mM HEPES pH8, 7 M urea, 25 mM NaCl, 0.05% Triton x-100) depending on the pellet size and they were left on ice for 30 minutes. For mass spectrometry experiments, a compatible lysis buffer (50 mM HEPES pH8, 0.2% Triton-x, 150 mM NaCl, 10 mM NaF, 0.1 mM EDTA, 2 mM DTT, 1x protease inhibitor mix) was used. After 30 minutes, the tubes were centrifuged at 13,200 rpm for 30 minutes and the supernatant containing the soluble protein phase was transferred to new clean tubes.

2.5.2 Protein quantification

To quantify the protein in the lysate, two different techniques were used depending on the sensitivity required. For immunoblotting (see section 2.5.3, where the aim is a rough determination of protein content and the normalisation of the samples, a Bradford assay was carried out. When experiments required a higher precision, such as when preparing samples for mass spectrometry, a bicinchoninic (BCA) assay was used.

Bradford assay

First, a series of standards were prepared by dissolving bovine serum albumin (BSA) in Milli-Q water to a final concentration of 0.1 mg/mL, 0.2 mg/mL, 0.5 mg/mL, 1 mg/mL, 2.5 mg/mL, 5 mg/mL, 8 mg/mL and 10 mg/mL. 200 μL of diluted Bradford reagent were placed per well in a 96-well plate, prepared by dissolving the concentrated reagent (Protein Assay Dye Reagent Concentrate, Bio-Rad #5000006) in Milli-Q water at 1:4 ratio. 1 μL of each standard and sample were added to the reagent each in one well, leaving one for the blank where 1 μL of Milli-Q water was added as a control. The plate was gently shook at a low frequency to mix the reagent with the standard / sample and the absorbances were measured at 595 nm on a Spark® 20M Multimode Microplate Reader (TECAN). The readings were normalised with the reference reading and the values obtained from the standards were used to make a curve by plotting the concentration (x axis) vs the absorbance (y axis) on Excel (Microsoft). Finally, the concentration values of the unknown samples were extrapolated from the equation of the trend line of the standard curve.

BCA

When requiring a more sensitive protein quantification method, a Micro BCA^{TM} Protein Assay Kit (ThermoFisher) was used following the suppliers protocol unless otherwise stated in the text.

2.5.3 SDS-PAGE and immunoblotting

All gels set up for sodium dodecyl sulphate – polyacrylamide gel electrophoresis (SDS-PAGE) were 15% (w/v) acrylamide 1.5 mm gels. They were prepared by mixing the reagents and volumes stated in Table 2.5, adding the ammonium persulfate (APS) and the tetramethylethylenediamine (TEMED) before pouring the gel into the mould to crosslink. The resolving solution was added to the mould first, followed by a couple drops of isopropanol to get rid of any bubbles, and left to polymerase before adding the stacking solution. After adding the stacking solution, the 1.5 mm comb (either 10 or 15 well) was added and the gel was left to solidify completely. If the gel was not to be used immediately, it was wrapped in clean damp tissue and plastic film to keep it moist, and was stored in the fridge with the comb on for up to 10 days.

Table 2.5: Reagents and their volumes used to prepare 15% 1.5 mm acrylamide SDS-PAGE gels.

	Volumes (mL) for one gel		**Volumes (mL) for two gels**	
	Resolving gel	**Stacking gel**	**Resolving gel**	**Stacking gel**
Milli-Q H_2O	2.3	2.7	3.5	4.1
30% (w/v) acrylamide	5.0	0.67	7.5	1.0
1.5 M Tris (pH 8.8)	2.5	0.5	3.8	0.75
10% (w/v) SDS	0.1	0.04	0.15	0.06
10% (w/v) APS	0.1	0.04	0.15	0.06
TEMED	0.004	0.004	0.06	0.006

Having quantified the protein present in the samples of interest, the right volume of each sample was pipetted into a new clean tube so all samples would have the same protein amount. Unless otherwise stated in the text, 20 ng of protein were loaded per sample. The same volume (1:1 (v/v) ratio) of 2x sample loading buffer, which consists of 3 parts of protein buffer (5% SDS, 25% glycerol, 0.3M Tris-HCl pH6.8, a dash of Coomassie Brilliant Blue until electric blue coloured) and 1 part 1 M DTT, was added to each tube prior to loading. Samples were boiled at 85°C for 5 minutes and loaded into the gel along with 5 μL of Page Ruler Prestained Protein Ladder (ThermoFisher). The gel was submerged in a tank

with running buffer (14.4 g glycine, 3.02 Tris and 1 g SDS on Milli-Q water per litre) and run at 85 V for the first 15 minutes before increasing to 150 V until the standard marker of lowest molecular weight and the remains of loading buffer reached the bottom of the gel.

The protein, now vertically separated by size, was either stained with Coomassie Brilliant Blue R-250 Dye (Thermo Scientific™, #20278) for protein band visualisation or transferred from the gel into a piece of pure nitrocellulose blotting membranes (0.2 μm, Bio-Rad #1620112) for immunoblotting.

Gel staining

SDS-PAGE gels were stained to visualise the protein ladder formed after running the samples. For this, gels were fixed by submerging them in fixing buffer for 10 minutes at room temperature and were then stained with a Coomassie Brilliant Blue solution for 1 hour. Stained gels could be de-stained if necessary by leaving them on de-staining solution over-night. Composition of all the buffers used can be found in Table 2.6 and were prepared in distilled water. To visualise the gels, they were rinsed in Milli-Q water and placed in an Odyssey® Imaging System (LI-COR).

Table 2.6: Solutions used for SDS-PAGE gel staining.

Fixing solution	Staining solution	De-staining solution
50% (v/v) methanol 10% (v/v) glacial acetic acid	50% (v/v) methanol 10% (v/v) glacial acetic acid 0.2% (w/v) Coomassie Brilliant Blue	7.5% (v/v) methanol 10% (v/v) glacial acetic acid

Immunoblotting

For immunoblotting, a western-blot system was prepared. The tank was filled with transfer buffer (3.03 g Tris, 14.4 g glycine, and 200 mL methanol per litre in Milli-Q water) and the gel was transferred at 110 V for 70 - 90 minutes at room temperature or at 25 mA over-night at 4°C, with gentle stirring of the magnet.

The membranes were dyed with PBST (PBS + 1% Tween 20) and a couple drops of ink (Pelikan, black) for 15 minutes with gentle shaking and washed once with PBST for a couple of minutes to remove ink excess. They were then blocked with 5% (w/v) dried skimmed milk (Marvel Original) dissolved in PBST for 1 hour with gentle shaking to prevent the an-

tibodies from binding non-specifically. The selected antibodies were diluted in 5% (w/v) dried skimmed milk dissolved in PBST at the appropriate ratio (see Table 2.7) and poured over the membranes to incubate them for the required time. All primary antibodies were incubated over-night at 4°C except β-actin, which was incubated at room temperature for 1 hour.

Table 2.7: Antibody conditions for immunoblotting and fluorescence-activated cell sorting (FACS).

Protein target	Clonality	Species of origin	Dilution	Use	Company
ISG15	Polyclonal	Rabbit	1:500	WB	Cell Signaling Technology (#2743S)
ISG15	Monoclonal	Mouse	1:1000	WB	Santa Cruz Biotechnology (#166755)
V5	Monoclonal	Mouse	1:1000	WB	Abcam (#ab27671)
β-actin	Monoclonal	Mouse	1:1000	WB	Sigma (#A2228)
IFIT1	Polyclonal	Rabbit	1:2000	WB	ThermoFisher Scientific (#PA3-848)
MX1	Polyclonal	Rabbit	1:1000	WB	Abcam (#ab95926)
UBE2K	Monoclonal	Rabbit	1:10,000	WB	Abcam (#ab52930)
USP18	Polyclonal	Mouse	1:1000	WB	Abcam (#ab168478)
GAPDH	Monoclonal	Mouse	1:1000	WB	Abcam (#ab9484)
HLA-ABC	Monoclonal	Mouse	1:50	FACS	Invitrogen (#11-9983-42)
HRP anti-mouse	Polyclonal	Rabbit	1:1000	WB	Dako (PO260)
HRP anti-rabbit	Polyclonal	Swine	1:1000	WB	Dako (PO217)

After the incubation, membranes were washed in PBST with shaking three times for 5 - 10 minutes each time before adding the solution containing the secondary antibody. Membranes were washed again another three times in PBST with shaking before adding enough 1:1 mixture of Enhanced Chemiluminescence (ECL) solutions I and II prepared in Milli-Q water (see Table 2.8 to cover the membrane and incubate it for 1 minute. Finally membranes were gently tapped dry with clean tissue and visualised. During most of the project's duration, this was done by covering the membranes with X-Ray Film (SLS) or Hyperfilm ECL (Amersham) in a dark room, exposing them for different amonuts of time, before developing them on a Konica Medical Film Processor (SRX-101A). However, throughout the last year of this project immunoblots were visualised using a Amersham™ ImageQuant™ 800 biomolecular imager (Cytiva).

Table 2.8: Composition of the ECL I and ECL II solutions used in the immunoblotting procedure.

ECL I solution	**ECL II solution**
100 mM Tris-HCl pH 8.5	100 mM Tris-HCl pH 8.5
2.5 mM luminol from stock in DMSO	0.02% (v/v) H_2O_2
0.4 mM p-coumaric acid from stock in DMSO	

Chapter 3

Generation of isogenic ISG15 knock-out cell models

3.1 Introduction

The CRISPR genome-editing tool has revolutionised medical and biological research. This technology has its roots in an acquired immune mechanism found in many bacteria and archaea that protects the prokaryotic cell against invading foreign nucleic acids, such as bacteriophage and plasmid DNA. The base of this immune system is the **C**lustered **R**egularly-**I**nterspaced **S**hort **P**alindromic **R**epeat locus, whose defensive function was first described nearly simultaneously by three different groups in 2005 (Bolotin *et al.*, 2005; Mojica *et al.*, 2005; Pourcel *et al.*, 2005). These groups reported that the non-repetitive sequences, or spacers, found between the DNA repeats in the CRISPR locus derive from past invasions of extrachromosomal nucleic acids. Research conducted in this area in the following decade resolved the mechanistic process behind such immune response, consisting of three events defined as acquisition, expression and interference (Haft *et al.*, 2005; Barrangou *et al.*, 2007; Sontheimer & Barrangou, 2015; Marraffini, 2015). Once the foreign DNA or RNA enters the host prokaryotic cell, the acquisition process begins in order to obtain a piece of the invading sequence and insert it in the CRISPR locus (Figure 3.1). To this end, a group of Cas proteins encoded from a set of associated genes usually found adjacent to the CRISPR locus, cut the invading DNA by recognising characteristic target sequences known as protospacer adjacent motif (PAM) elements. Different organisms have different Cas genes, ranging from Cas1 to Cas13, that take part in different steps of the immune response, but Cas1 and Cas2, responsible for cleaving invading DNA in the acquisition event, are considered universal in genomes that contain the CRISPR loci (Makarova & Koonin, 2015; Butiuc-Keul *et al.*, 2022). The newly generated spacer sequence is inte-

grated into the locus flanked by two CRISPR repeat sequences, and this library of immune markers gathered from previous invaders allows for their recognition and targeting if the intrusion ever happens again. Upon a repeated infection, the expression of the locus takes place generating unique CRISPR RNAs (crRNAs) that specifically target the invading nucleic acid. The crRNA forms a complex with the Cas protein responsible of cleaving the foreign nucleic acid sequence during the interference event, usually Cas8, Cas9 or Cas13, and targets it by binding to the sequence complementary to the crRNA. When the target is DNA, the cleaving occurs specifically adjacent to the PAM sequence, whereas if it is RNA this specificity does not occur (Sontheimer & Barrangou, 2015).

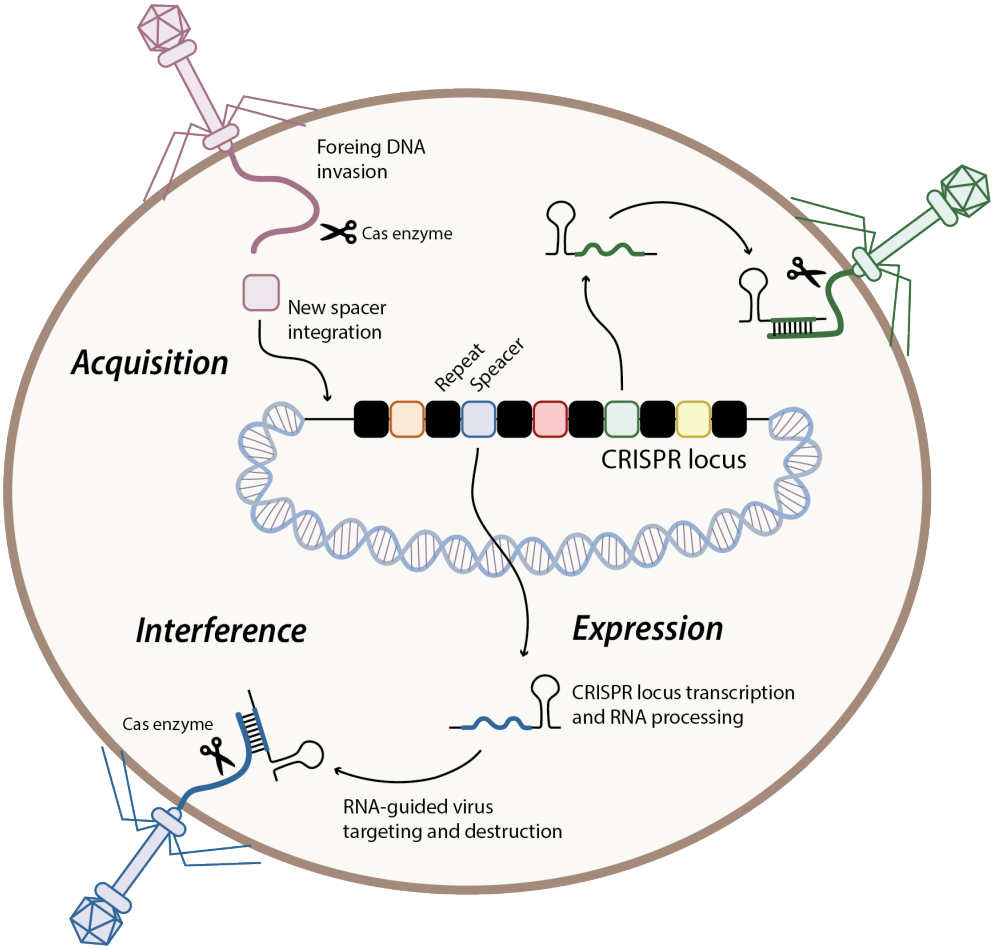

Figure 3.1: The CRISPR immune system. **a)** When invading nucleic acids enter the host prokaryotic cell, specific Cas enzymes cleave it to integrate a piece in the CRISPR locus, flanked by repeat sequences, in a process known as acquisition. **b)** Upon infection, the cell reaches to this library of immune markers gathered from previous invaders and expresses unique CRISPR RNAs (crRNAs, also known as single guide RNAs or sgRNAS) complementary to the sequences they came from. **c)** The crRNAs form a complex with another specific Cas enzyme and targets the intruder's sequence for its destruction by binding to the sequence complementary to the crRNA in a process known as interference.

Shortly after the molecular details of this prokaryotic immune response were unravelled, a race to prove that an engineered version of the system could be used in eukaryotic cells began. The collaboration between Emmanuelle Charpentier's group at the Laboratory for Molecular Infection Medicine of Sweden and Jennifer Doudna's group at University of California led to the first design of a programmable gene editing CRISPR/Cas9 system, published in 2012 (Jinek *et al.*, 2012). In January 2013, the Doudna group published the first paper proving that such system could be used to easily generate site-specific double-strand DNA breaks (DSBs) in human cells (Jinek *et al.*, 2013). This publication was closely followed by others that, independently, proved the same point (Mali *et al.*, 2013; Cong *et al.*, 2013; Hwang *et al.*, 2013; Cho *et al.*, 2013).

Since these studies were published, the CRISPR/Cas9 gene editing tool has been extensively used to edit genomes in a wide range of organisms. Upon insertion of Cas9 protein and a single gRNA complementary to the specific gene region of interest, the technique allows for gene knock-out (KO), gene knock-in (KI) and transcriptional activation/repression (Figure 3.2) (Graham & Root, 2015). Gene KO occurs when the indel mutations resulting from the non-homologous end-joining (NHEJ) endogenous DNA repair mechanism of the cell lead to frameshifts in the open reading frame, which at the same time result in gene loss of function. Gene KI can be achieved when using a DNA template with the desired sequence modification in the form of single-stranded oligodeoxynucleotide (ssODN). Once the Cas9 complex has nicked the DNA, the endogenous DNA repair machinery can use the provided DNA template for homology-directed repair (HDR), although this process is more complicated and usually results in a lower success rate than when trying to KO a gene. For gene transcriptional interference (CRISPRi) or activation (CRISPRa), a catalytically inactivated (D10A and H840A) or dead Cas9 enzyme (dCas9) fused with a transcriptional repressor or activator can be targeted to the promoter region of the gene of interest via sequence specific sgRNAs (see Figure 3.2c and d) (Gilbert *et al.*, 2013; Gilbert *et al.*, 2014).

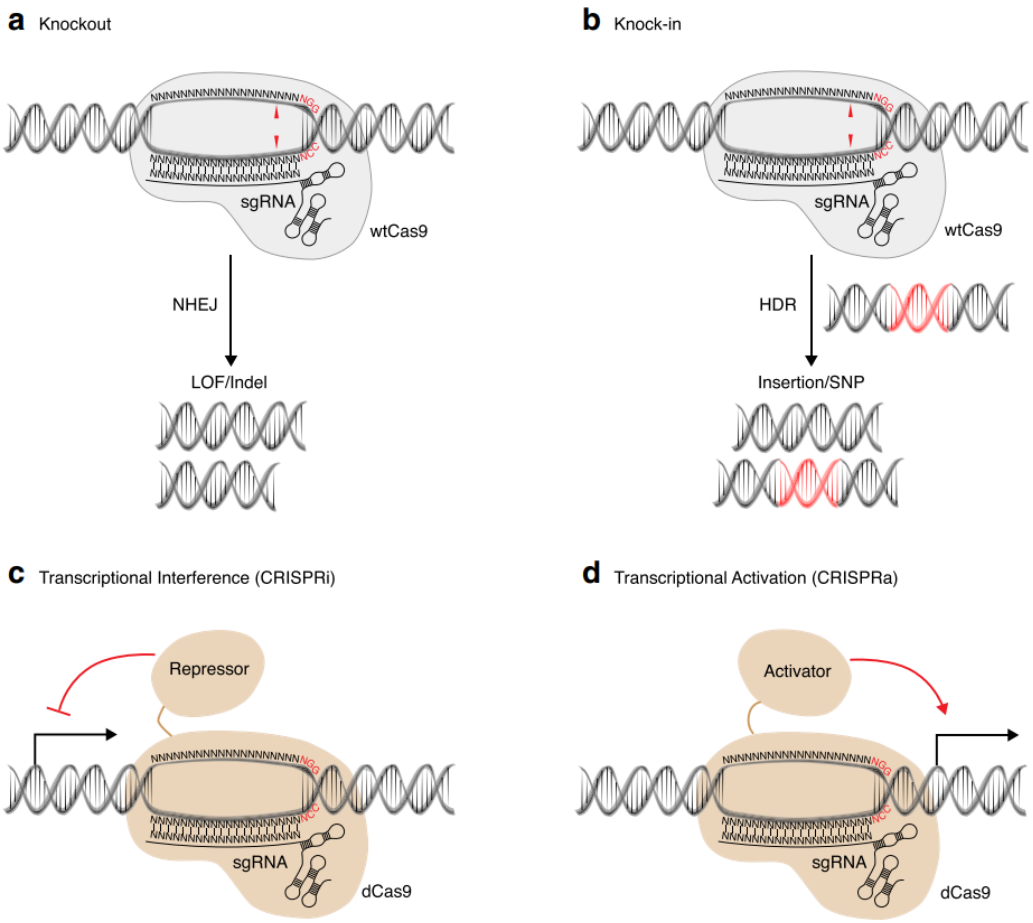

Figure 3.2: Different genetic alterations enabled by the CRISPR/Cas9 system, by Graham & Root (2015). **a)** Gene knock our or loss of function results from the indel mutations caused by the non-homologous end-joining (NHEJ) endogenous DNA repair mechanism of the cell trying to repair the double-strand DNA breaks (DSBs) caused by the sgRNA/Cas9 complex. **b)** Gene knock in can be achieved by using a single-stranded oligodeoxynucleotide (ssODN) sequence containing the modification of interest, so the endogenous DNA repair machinery can use it as a template for homology-directed repair (HDR). **c)** and **d)**. A catalytically inactivated or dead Cas9 enzyme (dCas9) fused to a transcriptional repressor or activator can be delivered to the promoter region of the gene of interest using sequence specific sgRNAs for transcriptional inhibition or activation (CRISPRi and CRISPRa respectively).

In the field of cancer research, CRISPR has been widely used to generate disease models both *in vivo* and *in vitro*, to perform genome-wide screens and to explore potential treatments by targeting genes in the cancer genome linked to disease progression and treatment resistance (Zhao *et al.*, 2021). In this chapter, different CRISPR approaches were used to knock-out ISG15 from the genome of different cell models in order to study the cellular behaviour of cancer cells lacking ISG15 upon different assays and treatments.

3.2 Aim and strategy

The aim of this work was to use CRISPR/Cas9 gene editing, a simplified protocol of which is shown in Figure 3.3, to study cellular behaviour in the absence of ISG15 and to perform immunofluorescence imaging experiments with V5 (MGKPIPNPLLGLDST) tagged cells. To this end, ISG15 was knocked out from several cancer cell models and V5 tag knock in was attempted at the N terminus of ISG15 in SiHa cells. crRNAs, Cas9 protein (Alt-R© S.p. Cas9 Nuclease V3, #1081058) and universal tracrRNA (Alt-R© CRISPR-Cas9 tracrRNA, #1072532) were ordered from IDT (https://www.idtdna.com) and an Amaxa™ 4D-Nucleofector™ was used for cellular nucleofection, providing an ssODN of the sequence containing the tag flanked by fractions of the ISG15 gene.

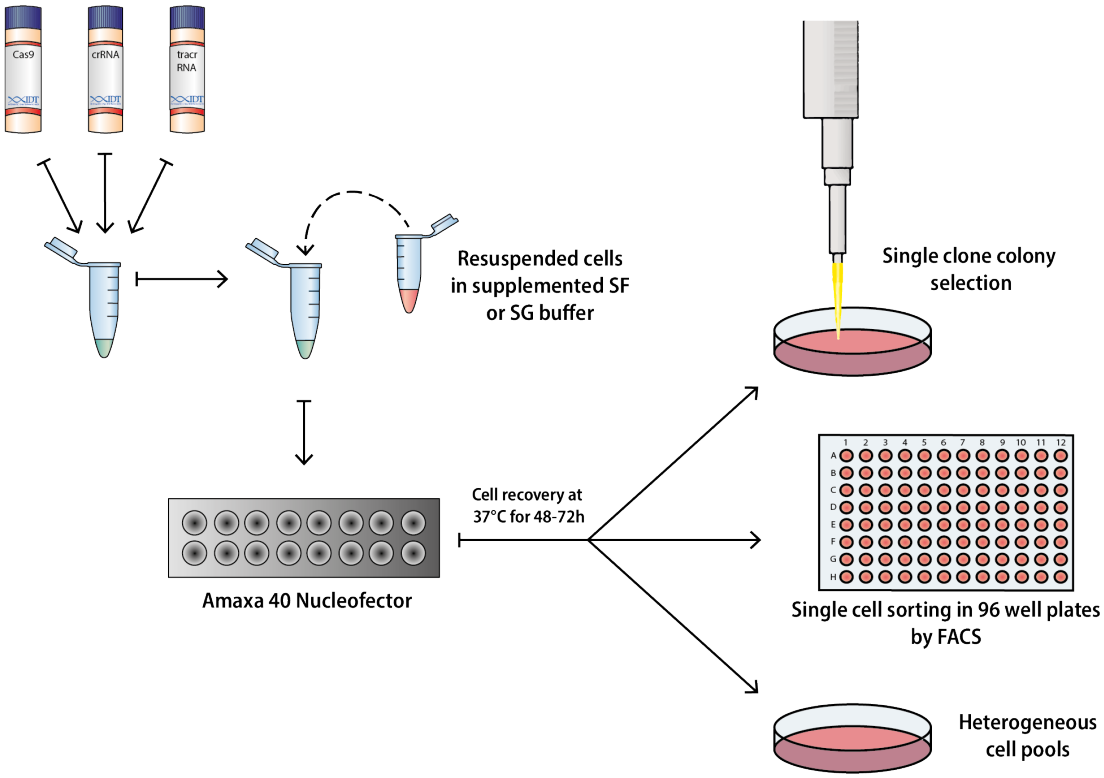

Figure 3.3: Simplified protocol for DNA nucleofection using Amaxa™ SG/SF Cell Line 4D-Nucleofactor™ Kit for CRISPR/Cas9 gene editing and clone sorting.

3.3 Methods

3.3.1 CRISPR gene editing

Design of crRNA and oligos for sequence repair

The gRNAs, shown in Table 3.1, were designed using a web tool for selecting target sites for CRISPR/Cas9 directed mutagenesis. This tool (https://chopchop.cbu.uib.no/) has been developed by the Computational Biology Unit of the University of Bergen (Labun *et al.*, 2019).

Table 3.1: gRNAs designed and used for CRISPR/Cas9 directed gene edition. The four of them were withing the open reading frame (ORF).

Name	Sequence 5'-3'	PAM	Location
Knock-in ISG15 gRNA	CACGGCACAAGCTCCTGTAC	TGG	Exon 5
1st ISG15 knock-out gRNA	GATGCTGGCGGGCAACGAAT	TCC	Exon 6
2nd ISG15 knock-out gRNA	CCTGACGGTGAAGATGCTGG	CGG	Exon 6
3rd ISG15 knock-out gRNA	TTCATGAACACGGTGCTCAG	GGG	Exon 6

The templates for Homology Directed Repair (HDR) for the insertion of the V5 tag was designed as a ssODN for repair following double strand break with the "knock-in ISG15 gRNA" (see Table 3.1). The ssODN sequence, shown below, has the start codon highlighted in light pink and the sequence for V5 highlighted in dark pink. The gRNA is underlined and highlighted in blue, with the mutated protospacer adjacent motif (PAM) sequence in a darker shade of blue, altered to avoid repeated cuts by Cas9 complex.

ssODN for V5 insertion on the ISG15 gene:

5' CAG GGA CAC CTG GAA TTC GTT GCC CGC CAG CAT CTT CAC CGT CAG GTC CCA GCC CGT AGA ATC GAG ACC GAG GAG AGG GTT AGG GAT AGG CTT ACC CAT GGC TGT GGG CTG TGG GCT GTG GGC CAC GGC ACA AGC TCC TGT ACT GCC AAA GAT GAG TTC GCT GCC TCT CAG CCG CCG GCT TCG GCA GGC AGC ACC GGC CC 3'

Ligation of tracrRNA-crRNA and nucleofection of cas9/gRNA

For the formation of the tracrRNA-crRNA-Cas9 complex, the crRNA and the tracrRNA were first mixed by pipetting 1.2 μL of each (from 0.1 mM stocks) in a sterile microcentrifuge tube. The mixture was heated up to 95°C in the thermocycler for 5 minutes to dena-

ture the oligos and left at room temperature for 30 minutes to anneal. Once cooled down, 10 μg of recombinant Cas9 protein were added to the mixture, which was incubated for 10 minutes at room temperature to form the cas9/gRNA ribonucleoprotein complex. The mixture was then kept on ice until transfection.

The cells to be edited were harvested as described in subsection 2.2.2, counted (see subsection 2.2.3) and 2x10^5 cells were transferred to a sterile Eppendorf tubes to be centrifuged at 1000 rpm for 3 minutes. The cell pellet was resuspended in 20 μL of supplemented P3 buffer from the Amaxa™ SG/SF Cell Line 4DNucleofactor™ X Kit S (Lonza) and gently added to the tubes containing the ribonucleoprotein complex, mixing very carefully to avoid the formation of bubbles that could negatively affect the transfection efficiency. When required, 30 pmol of ssODN were added at this point along with the 20 μL of cell suspension. The full mix was very gently combined by softly flicking the tubes and was then quickly dispensed into one of the micro cuvettes from the kit to be inserted in the Amaxa™ 4D-Nucleofector™, where the appropriate program was used for nucleofection. After the pulse, 200 μL of pre-warmed media were added to the well to collect the cells, mixing carefully and avoiding pipetting up and down. The full content of the well was transferred to a 6-well plate with pre-warmed fresh media for the cells to recover for three days.

3.3.2 Single cell sorting - FACS and manual sorting

Once the cells were recovered from nucleofection, they could be either left in heterogeneous cell pools or be single cell sorted to obtain isogenic cell lines from single clones. Two different methods could be used for single cell sorting depending on the needs and requirements of the cell line. Resistant cells like SiHa cells were automatically sorted through Fluorescence-Activated Cell Sorting (FACS) either on a BD FACSAria™ Cell Sorter or on a BD FACSJazz™ Cell Sorter. More delicate cells, like GSCs, did not withstand growing isolated as single cells, so small numbers of cells were seeded in Corning® vented 10 cm plates (i.e.: 500, 1000 and 1500 into three different plates) making sure to spread them properly over the plate. Once the cells grew enough to form colonies, healthy looking and properly isolated ones grown from single cells were selected to be transferred to 24 well plates. For this, the plates were gently washed with sterile PBS and 8-10 μL of warm media were used to pipette up and down right above the selected colony to aspirate it along with the media, without tilting the plate. If media was not enough to detach and collect the cells, the same volume of accutase could be used instead. This process was repeated as required until all or most of the cells in the colony were transferred to a new well, checking both the old and the new plate under the microscope to make sure the selected colony had been completely removed.

3.3.3 Validation of clones and mixed population pools

Immunoblotting was used as the first line of validation in both the heterogeneous cell pools and the isogenic clone cell lines (see subsection 2.5.3), using lysate from untreated and IFNα treated cells. For expression analysis, 100 U/mL of commercial recombinant IFNα2 (see subsection 2.2.6) were used for a 24h treatment unless otherwise stated in the text.

Polymerase Chain Reaction (PCR) was used as a second line of validation, for band size determination and to prepare samples for Sanger sequencing in some selected cell lines. To this end, a zero Blunt™ TOPO™ PCR Cloning Kit (ThermoFisher Scientific) was used to clone individual alleles into kanamycin resistant pCR™Blunt II-TOPO™ vectors. The plasmid DNA was used to transform DH5-Alpha *E. coli* competent cells, which were plated in LB agar plates with kanamycin (see subsection 2.3.1). Ten single colonies were picked the following day and grown in 10 mL LB cultures with kanamycin over-night before pelleting them for plasmid harvesting using a QIAprep Spin Miniprep Kit (Qiagen). The concentration of the obtained pure plasmids was determined using a NanoDrop 2000c spectrophotometer (Thermo Scientific). Samples to be sequenced were sent to either Source BioScience (https://www.sourcebioscience.com/sanger-sequencing/) or to the sequencing service available at the Institute of Genetics and Cancer (Edinburgh, UK), following sample concentration and volume requirements stated by the external service.

Primers designed to be used for PCR and sequencing purposes were ordered from Sigma-Aldrich (Table 3.2). PCR reactions were prepared by mixing the appropriate reagents (Table 3.3), keeping the tubes on ice at all times. Once ready, the reactions were transferred to a SureCycler 8800 thermocycler (Agilent Technologies) and the program described in Table 3.4 was run.

Table 3.2: Primers used for PCR / Sanger Sequencing and their features.

Oligo name	Sequence (5'-3')	GC %	T_m	Annealing T°
Forward ISG15	GTTTCTTCCGCTCACTCTGG	55	63.9°C	63.5°C
Reverse ISG15	GGGTTCTCCCTCCTGACTTC	60	64°C	

Table 3.3: Reagents and concentrations for Polymerase chain reaction (PCR).

Reagent	**Volume per 50 μL reaction**	**Final concentration**
2x Pfu Master Mix (R551, Rovalab)	25 μL	1x
Forward Primer (10 μM)	2.5 μL	0.5 μM
Reverse Primer (10 μM)	2.5 μL	0.5 μM
Template DNA	100 ng dsDNA	2 ng/μL
Nuclease free H_2O	Top up to 50 μL	

Table 3.4: PCR cycling conditions.

	PCR step	**Temperature**	**Time**
	Initial Denaturation	95°C	2 minutes
Cycle (x35)	Denaturation	95°C	20 seconds
	Annealing	Primer dependent*	45 seconds
	Elongation	72°C	1 minute
	Final Elongation	72°C	3 minutes

*See Table 3.2

3.4 Results

3.4.1 ISG15 null SiHa cells

The aim of this chapter was to obtain ISG15 knock-out cells in order to study the role of ISG15 in cancer. At the same time, the knock in of the V5 tag was also attempted for subsequent validation experiments. Even though the first attempt to generate knocked out clones using the 1st gRNA (Table 3.1) was unsuccessful and no V5 positive cells were recovered, the single cell sorted clones obtained from the V5 insertion protocol gave rise to an ISG15 negative cell line, as determined by the lack of ISG15 expression analysed by immunoblotting (Figure 3.4).

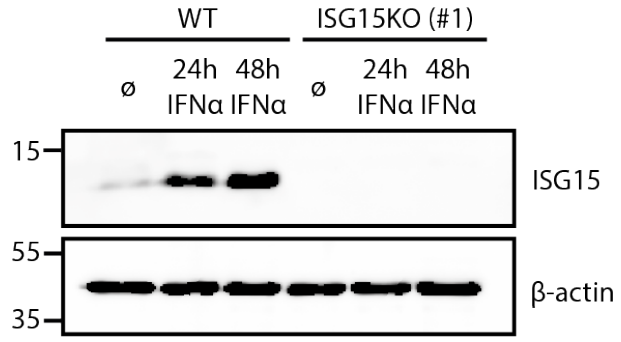

Figure 3.4: Immunoblotting for ISG15 on attempt to insert V5 on the N-terminus of ISG15 gene (clone #1). An equal amount of protein (40 μg) from whole cell lysate was loaded per lane in an 15% SDS-PAGE followed by immunoblotting. The membrane was developed using anti-ISG15 antibody (Santa Cruz Biotechnology (#166755) at 1:1000 in milk) followed by anti-β-actin antibody (Sigma (#A2228) at 1:1000 dilution). Lysate from untreated and 24 or 48 hour IFNα treated SiHa WT cells were used as controls. IFNα treatment concentration was 100 U/mL in both WT and clone #1 samples. These results are representative of at least two experiments.

The analysis of this clone, henceforth clone #1, and the identification of a phenotype of interest (chapter 4) lead to the decision of repeating the gene-editing procedure in order to identify additional ISG15 KO cells. Since clone #1 was obtained as the off-target result of a knocked-in attempt, a new strategy to obtain ISG15$^{-/-}$ clones to test the identified phenotype of interest was developed. Due to the low efficiency of the first attempt using a single gRNA, a double gRNA approach with newly designed gRNAs was chosen (2nd and 3rd gRNAs, seeTable 3.1). The two gRNAs were used independently to form tracrRNA-crRNA-Cas9 ribonucleoprotein complexes, and were mixed with the cell suspension prior to the nucleofection. Single cell sorting by FACS resulted in several putative ISG15$^{-/-}$ clones being identified by immunoblot analysis (see Figure 3.5).

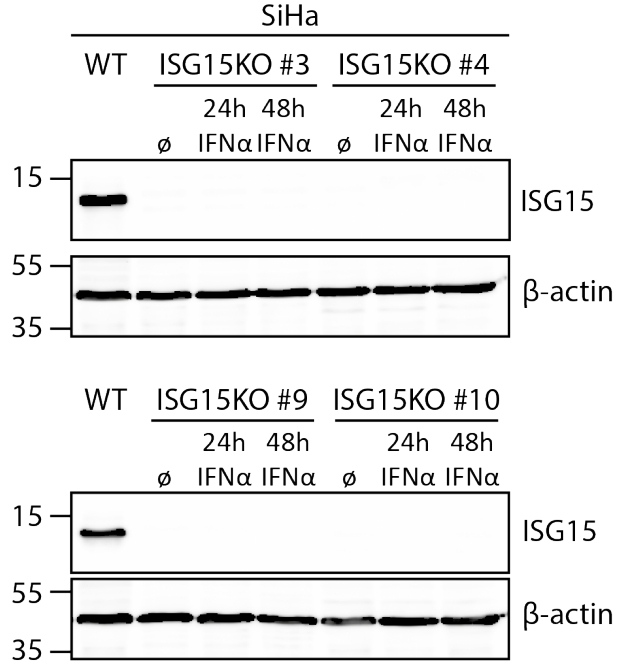

Figure 3.5: Immunoblots of four independent SiHa ISG15 KO clones (#3, 4, 9 and 10) obtained using a double gRNA approach. An equal amount of protein (50 μg) from whole cell lysate was loaded per lane in an 15% SDS-PAGE followed by immunoblotting. The membrane was developed using anti-ISG15 antibody (Santa Cruz Biotechnology (#166755) at 1:1000 in milk) followed by anti-β-actin antibody (Sigma (#A2228) at 1:1000 dilution). Lysate from SiHa WT cells treated with IFNα for 48 hours was used as a control. IFNα treatment concentration was 100 U/mL in both WT and clone #1 samples. These results are representative of at least two experiments.

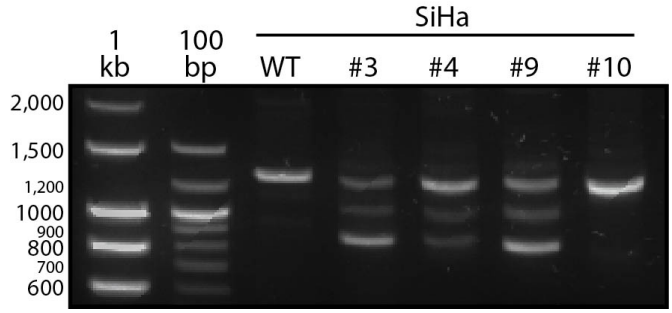

Figure 3.6: PCR product of ISG15 KO SiHa clones #3, 4, 9 and 10 amplifying the ISG15 region in a 1.5% agarose gel. The expected size for the WT reference is 1278 bp. These results are representative of at least two experiments.

In order to confirm that gene editing lead to the loss of ISG15 as determined by immunoblotting, PCR was used to amplify the edited section of the ISG15 gene (Table 3.2). The use of these primers in the unedited WT should amplify a sequence of 1278 bp. Comparing the size of the amplified band from the WT cells unedited DNA with the size of the band or bands obtained from amplifying DNA from the edited clones can help identify any significant insertions or deletions that could lead to loss of gene expression. At the same

time, the amplified PCR product can be sent for Sanger sequencing to characterise the exact editions occurred in each clone. After performing PCR, the resultant products were run on agarose gels (1-1.5%). As seen in Figure 3.6, several bands were detected in most of the clones. The band observed for the WT sample matches the 1278 bp expected size, and so does the single band observed in #clone 10. Samples run for clones #3, 4 and 9 on the other hand present three different bands each - the highest band matches the WT band size, the middle band is slightly above the 1000 bp size reference and the lower one is slightly above the 800 reference band. A very faint band can also be observed above the highest of the three main bands in clone #9, which could be unspecific. After several failed attempts to excise and purify the bands using QIAquick Gel Extraction Kit (Qiagen), a zero Blunt™ TOPO™ PCR Cloning Kit was used to clone single alleles of each clone into plasmid vectors. The plasmids were used to transform bacterial cells as described in the methods section to isolate, amplify and purify them before DNA sequencing. Using this method, several different edits were identified in each clone using the reverse primer, which is closer to the edited site. In a few cases, sequencing using the forward primer was used to complete the sequence. The sequence obtained from WT SiHa cells can be found below followed by the sequences obtained from each clone, showing the different edits identified. The gRNA sites are shown in blue, with the PAM sequence in a darker shade of blue. Insertions are shown in bright red, while deletions are shown with the number of bp deleted between bars, also in red. The ligation of an inverted sequence without loss of bp is expressed using double red bars. For easier illustration, the 395 bp found in between both gRNAs has been shortened, but the full sequences can be found in Appendix A.

SiHa WT

5'...GCAGATTCATGAACACGGTGCTCAGGGGCTTGAGGCCG...

375 bp

...AATTCGTTGCCCGCCAGCATCTTCACCGTCAGGTCCCA...3'

ISG15 KO clone #3

Edit 1

5'...GCAGATTCATGAACACGGTGCT|407 bp|GCATCTTCACCGTCAGGTCCCA...3'

Edit 2

5'...GCAGATTCATGAACACGGTGC|2 bp|AGGGGCTTGAGGCCG...

375 bp

...AATTCGTTGCCCG|4 bp|CATCTTCACCGTCAGGTCCCA...3'

Edit 3

5'...GCAGATTCATGAACACGGTGCTTCAGGGGCTTGAGGCCG...

368 bp

...CACCTGGAAT|26 bp|CAGGTCCCA...3'

ISG15 KO clone #4

Edit 1

5'...GCAGATTCATGAACACGGTGGTCAGGGGCTTGAGGCCG...

367 bp

...ACACCTGGAA|19 bp|TTCACCGTCAGGTCCCA...3'

Edit 2

5'...GCAGATTCATGAACACGGTGCTTCAGGGGCTTGAGGCCG...

375 bp

...AATTCGTTGCCCGCCAAGCATCTTCACCGTCAGGTCCCA...3'

Edit 3

5'...GCAGATTCATGAACACGGTG|2 bp|CAGGGGCTTGAGGCCG...

375 bp

...AATTCGTTGCCCGCCACGCATCTTCACCGTCAGGTCCCA...3'

Edit 4

5'...GCAGATTCATGAACACG|4 bp|TCAGGGGCTTGAGGCCGTACT
CCCCCAGCGGGAGCTGG|373 bp|TCTTCACCGTCAGGTCCCA...3'

ISG15 KO clone #9

Edit 1

5'...GCAGATTCATGAACACGGTGCTTCAGGGGCTTGAGGCCG...

375 bp

...AATTCGTTGCCCGCCAGGCATCTTCACCGTCAGGTCCCA...3'

Edit 2

5'...GCAGATTCATGAACACGGTGCTTCAGGGGCTTGAGGCCG...

375 bp

...AATTCGTTGCCCGCCA|3bp|TCTTCACCGTCAGGTCCCA...3'

Edit 3

5'...GCAGATTCATGAACACGGTGC|408 bp|CGCATCTTCACCGTCAGGTCCCA...3'

Edit 4

5'...GCAGATTCATGAACACGGTGCTTCAGGGGCTTGAGGCCG...

375 bp

...AATTCGTTGCCCGCCAG||TCAGGGGCTTGAGGCCG...

375 bp

...AATTCGTTGC|8bp|ATCTTCACCGTCAGGTCCCA...3/

ISG15 KO clone #10

Edit 1

5'...GCAGATTCATGAACAC|7bp|AGGGGCTTGAGGCCG...

375 bp

...AATTCGTTGCCCGCCAGGCATCTTCACCGTCAGGTCCCA...3'

Edit 2

5'...GCAGATTCATGAACACGGTGCT||TGGCGGGCAACGAATT...

375 bp

...CGGCCTCAAGCCCCT||GCATCTTCACCGTCAGGTCCCA...3'

Three different edits were found for clone #3. Edit 1 has a ligation of the two gRNAs, having lost the full sequence between them (- 407 bp). The amplification of this allele should result in a 871 bp band, which matches the lower band of the three observed in Figure 3.6. Edit 2 has a 2 bp deletion in the gRNA2 site and a 4 bp deletion in the gRNA1 site (-6 bp), which should result in a 1272 bp amplification matching the upper band of the three. The third edit should also match the highest band, having a 1 bp insertion in the gRNA2 site and a 26 bp deletion in the gRNA1 site (-25 bp), which should result in an amplification of 1253 bp.

The analysis of clone #4 revealed four different edits. Edits 1 to 3 should amplify bands of 1260, 1280 and 1277 bp (-18 bp, +2 bp and -1 bp) respectively, matching the highest of the three bands observed in Figure 3.6. Edit 4, on the other hand, has a 4 bp deletion in the gRNA2 site and a big 373 bp deletion in the gRNA1 site (-377 bp), resulting in most of the sequence between the gRNAs being absent. The band resultant from the amplification of this allele should be of 901 bp, matching the lowest of the three bands detected for this clone.

Four different edits were found for clone #9. Edit 1 (+ 2 bp) and 2 (- 2 bp) should result in an amplification of 1280 and 1276 bp respectively, matching the upper of the three main bands at the same level as the WT band. Edit 3 has a ligation of the two gRNAs, having lost all the sequence between them (- 407 bp), and should therefore have an amplification of 871 bp. This edit matches the lower of the three main bands. Edit 4 shows a duplication of all the sequence between the gRNAs, with a fusion of gRNAs in the middle (+ 402 bp). This should result in the amplification of 1680 bp. Interestingly, no band matching this

edit was detected on the agarose gel, since even the very light faint line above the highest of the three main bands would be too low for this edit.

Only two different edits were identified in clone #10, both matching the only band observed in the gel (Figure 3.6). The first one, with a 7 bp deletion in gRNA2 and 1 bp insertion in gRNA1 (- 6 bp) should results in an amplification of 1272 bp. The second one did not have any insertions or deletions, but the sequence between the two gRNAs had been inverted after the DSBs in both editing points, ligating the first half of one gRNA with the last half of the other and vice versa. This edition should result in an amplification of 1278 bp.

Table 3.5: Summary table of editions identified in ISG15$^{-/-}$ SiHa clones. Three edit types were identified: insertions and deletions either in the gRNA1 and gRNA2 separately or as one edition in between the gRNAs (indel), the inversion of the in between sequence upon incision (inversion) or a mix of both (mixed).

		Edition type	**Insertions (gRNA1/gRNA2)**	**Deletions (gRNA1/gRNA2)**	**Size***
WT		None	-	-	441 bp
#3	Edit 1	Indel	-	407 bp	34 bp
	Edit 2	Indel	-	2 bp/4 bp	435 bp
	Edit 3	Indel	1 bp/ -	- /26 bp	416 bp
#4	Edit 1	Indel	1 bp/ -	- /19 bp	423 bp
	Edit 2	Indel	1 bp/1 bp	-	443 bp
	Edit 3	Indel	- /1 bp	2 bp/ -	440 bp
	Edit 4	Indel	-	4 bp/373 bp	64 bp
#9	Edit 1	Indel	1 bp/1 bp	-	443 bp
	Edit 2	Indel	1 bp/ -	- /3 bp	439 bp
	Edit 3	Indel	1 bp	408 bp	34 bp
	Edit 4	Mixed	1 bp/ - 409 bp**	- /8 bp	843 bp
#10	Edit 1	Indel	- /1 bp	7 bp/ -	435 bp
	Edit 2	Inversion	-	-	441 bp

*Start of gRNA1 to end of gRNA2
**Insertion of a second copy of the sequence in between gRNAs

3.4.2 ISG15 null Glioblastoma cells

After successfully recovering several ISG15$^{-/-}$ SiHa clones using a double gRNA approach, the generation of a new ISG15 KO cancer cell model was attempted to validate and further research any phenotype of interest identified in the SiHa cells (see chapter 4). To this end, a patient-derived glioblastoma primary stem cell line (GSC) was selected, and the same two gRNA approach was used to obtain ISG15 KO GSC clones. Because of the delicate nature of these neural stem cells, the methodology to isolate clones grown from single cells had to be adapted. The few GSC cells that survived the process of mechanically single cell sorting would not withstand growing in isolation. To overcome this issue, small numbers of cells were seeded in 10 cm plates and the properly isolated colonies grown from single cells were collected by aspiration (subsection 3.3.2). Using this method, several ISG15 KO cell clones were identified by immunoblotting. Figure 3.7 shows the lack of detectable expression of ISG15 in the six clones. Again, to confirm that gene editing lead to the loss of ISG15 protein as suggested by immunoblotting, PCR was performed on whole DNA isolated from cell lysate. The resultant PCR products were run on an agarose gel (Figure 3.8). These results show a variety of edits, all of them with a very similar pattern to the one observed in the SiHa ISG15 KO clones. GSC clone #1 has a single lower band, matching the edit in which the sequence between the gRNAs is removed. GSC clones #2 and 3 have the three band pattern observed in SiHa ISG15 KO clones #3, 4 and 9, with the very faint band above the highest of the three also observed in #9. GSC clones #4, 5 and 6 have a single band around the size of the WT band, as observed in SiHa ISG15 KO clone #10.

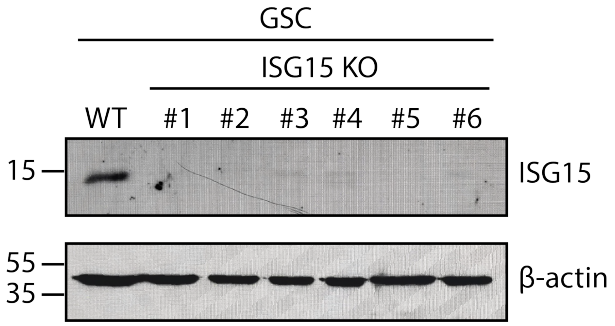

Figure 3.7: Immunoblotting for ISG15 on six different GSC ISG15 KO clones (#1-6) obtained through a double gRNA CRISPR approach after 24 hours of IFNα treatment. An equal amount of protein (40 μg) from whole cell lysate was loaded per lane in an 15% SDS-PAGE followed by immunoblotting. The membrane was developed using anti-ISG15 antibody (Cell Signaling Technology (#2743S) at 1:500 in milk) followed by anti-β-actin antibody (Sigma (#A2228) at 1:1000 dilution). Lysate from GSC WT cells treated with IFNα for 24 hours was used as a control. IFNα treatment concentration was 100 U/mL in both WT and clone #1 samples. These results are representative of at least two experiments.

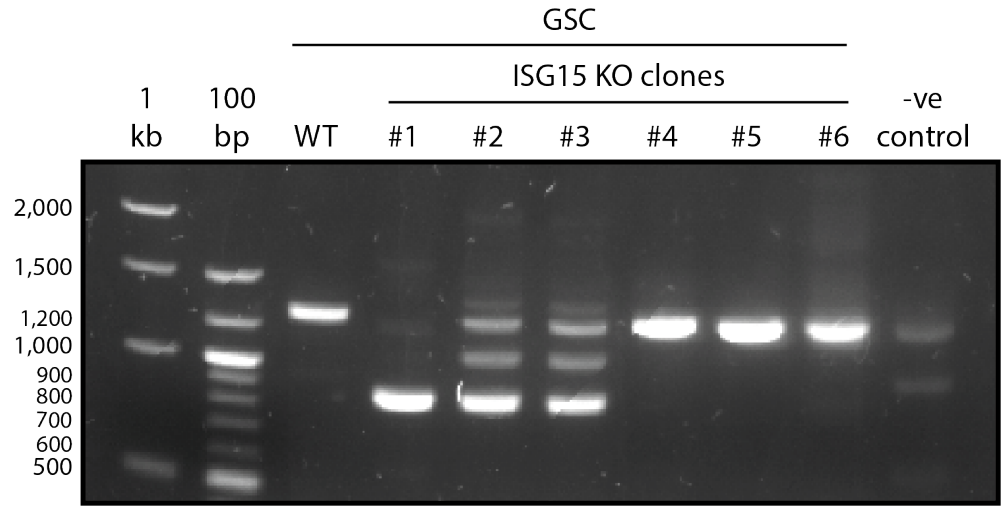

Figure 3.8: PCR product of ISG15 KO GSC clones #1-6 amplifying the ISG15 region in a 1.5% agarose gel. These results are representative of at least two experiments.

All these edits, except the band of around 1000 bp, had been characterised in the SiHa clones. In an effort to identify the uncharacterised band, GSC clone #2 was selected for TOPO cloning and sequencing along with GSC WT. Sequences obtained with the reverse primer are shown with the gRNA sites in blue, the PAM sequence coloured in a darker shade of blue. Insertions are shown in bright red and deletions are shown with the number of bp deleted between bars, also in red. The ligation of the two gRNAs is expressed using double red bars. Again, for easier illustration, the 395 bp found in between both gRNAs has been shortened, but the full sequences can be found in Appendix A.

GSC WT

5'...GCAGATTCATGAACACGGTGCTCAGGGGCTTGAGGCCG...

375 bp

...AATTCGTTGCCCGCCAGCATCTTCACCGTCAGGTCCCA...3'

GSC ISG15 KO clone #2

Edit 1

5'...GCAGATTCATGAACACGGTGCT||TGGCGGGCAACGAATT...

375 bp

...CGGCCTCAAGCCCCTG||AGCATCTTCACCGTCAGGTCCCA...3'

Edit 2

5'...GCAGATTCATGAACACGGTGCT||GCATCTTCACCGTCAGGTCCCA...3'

Edit 3

5'...GCAGATTCATGAACACGGTGC|2bp|AGGGGCTTGAGGCCGTA

CTCCCCCAGCGGGAGCT||GGTCTTCACCGTCAGGTCCCA...3'

Three different edits were identified in GSC clone #2 : edit 1 with the sequence between the two gRNAs inverted at the cut points (matching the highest of the three bands), edit 2 with the sequence between the two gRNAs removed (matching the lowest of the three bands), and edit 3 with a 2 bp deletion in gRNA2 and most of the sequence between the gRNAs removed, leaving gRNA1 incomplete and only 29 bp between them.

While the GSC colony sorted clones grew for validation, a sample of the edited mixed population pool was analysed by immunoblotting to get an idea of the efficiency level of the editing process. The level of expression of ISG15 right after the genome editing procedure is below the detection threshold, proving a very high efficiency of the double gRNA editing method (Figure 3.9).

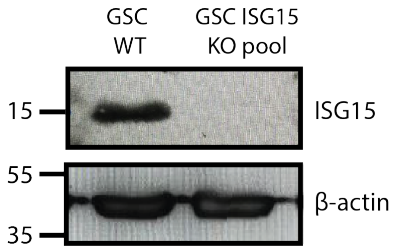

Figure 3.9: Immunoblot for ISG15 on GSC ISG15 KO mixed population pool. An equal amount of protein (40 μg) from whole cell lysate was loaded per lane in an 15% SDS-PAGE followed by immunoblotting. The membrane was developed using anti-ISG15 antibody (Cell Signaling Technology (#2743S) at 1:500 in milk) followed by anti-β-actin antibody (Sigma (#A2228) at 1:1000 dilution). Lysate from GSC WT cells treated with IFNα (100 U/mL) for 24 hours was used as a control. These results are representative of at least two experiments.

In order to edit different cell lines in a time efficient manner, and since no expression of ISG15 was detected, mixed population cell pools were used for some of the experiments (see chapter 4 and chapter 6).

3.4.3 ISG15 null Caki-1 cells

As part of a collaboration with Dr. Christine Tait-Burkard and Ms Alison Daniels at the The Roslin Institute (Edinburgh, UK), ISG15 KO Caki-1 cells were generated in order to test the response of these cells upon SARS-COVID-2 infection. After successfully obtaining a mixed population GSC cell pool with an ISG15 expression level below the detection threshold by immunoblotting, even when loading large amounts of protein (up to 50 μg), the whole pool of edited Caki-1 cells was also analysed before single cell sorting. Results in Figure 3.11 show that the level of ISG15 in the mixed population pool was again below detection threshold, suggesting that the efficiency of the method is indeed very high. PCR products of Caki-1 WT and ISG15 deficient heterogeneous cell pool were run on an agarose gel, a scan of which can be seen in Figure 3.10. Although two of them are very light, this figure shows the same three bands observed in SiHa ISG15$^{-/-}$ clones #3, #4 and #9 and in GSC ISG15$^{-/-}$ #2 and #3.

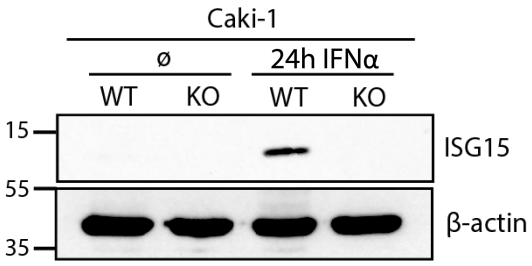

Figure 3.10: Immunoblotting for ISG15 on ISG15 KO Caki-1 mixed population cell pool obtained through a double gRNA CRISPR approach, untreated and treated with IFNα for 24 hours. 40 μg of protein were loaded in each line. Lysate from Caki-1 WT cells treated with IFNα for 24 hours and re-blotting of the membrane for β-actin were used as control.

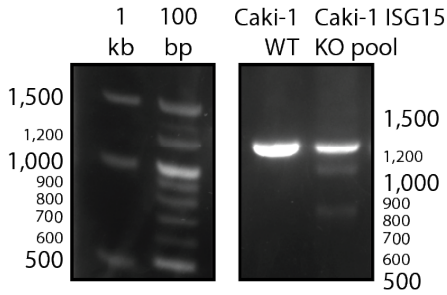

Figure 3.11: PCR product of ISG15 deficient Caki-1 mixed population pool amplifying the ISG15 region in a 1.5% agarose gel. Gel scan has been cropped to remove the non-relevant samples run between the ladder and the samples of interest. Because of the natural curve formed after running the gel, the sizes shown in the ladder are not representative of the sample band size, so the corrected numbers have been included at the right side of the sample columns. Full uncropped figure can be found in Appendix A. These results are representative of at least two experiments.

To make the most of the work performed as part of this collaboration, the obtained ISG15 KO Caki-1 cells were also used to test the phenotype of interest described in chapter 4, proving it is consistent in at least three different cancer cell models.

3.5 Discussion

ISG15 knocked-out cells and mice have been successfully generated before (Kim & Kim, 2019; Merkert *et al.*, 2020; Alcalá *et al.*, 2020; Martin-Fernandez *et al.*, 2020; Jurczyszak *et al.*, 2022). The immunoblots performed on the SiHa and GSC sorted clones show that the expression of ISG15 upon IFNα treatment is below the detection threshold. The characterisation by sequencing of all the editions identified showed that the generated mutations should result in truncated expression of ISG15. According to the multidisciplinary data base canSAR.ai, SiHa cells have a relative copy number of 1.05 (log2(copy number relative to ploidy + 1)) for chromosome 1 and the ISG15 gene (1p36.33), meaning they have two copies of this chromosome and gene. Therefore, a maximum of two different edits (one per allele) would be expected in SiHa cells edited for ISG15. Surprisingly, most of the clones presented more than two different edits, suggesting more than two copies of the ISG15 gene both in SiHa and GSC cell lines. Maintenance of cells in culture over a long period of time has been proven to lead to mutations that cause changes in cell behaviour, compared to the same cells at an early passage, resulting in extensive genomic variation between strains evolved from the same cell line (Ben-David *et al.*, 2019). A study by Ben-David *et al.* (2018) performed genetic analysis in 106 human cell lines to determine the consequences and the extent of the genetic and transcriptional heterogeneity found in cell lines that have evolved as a consequence of prolonged culture, grown in two independent laboratories in different countries. Their results exposed a significant genetic variation between strains that belonged to the same cell line, with around a 20% chance that a certain mutation would be found only in one of strains, and showed that even the cell culture maintenance under standard conditions lead to genomic evolution and diversification. Similarly, the research by Wenger *et al.* (2004) compared the karyotypic differences between two samples of a breast adenocarcinoma (MCF-7) and two samples of an endometrial adenocarcinoma cell line (Ishikawa), obtained from different places at different passages. One of the MCF-7 samples was obtained from the American Type Culture Collection (MCF-7-ATCC) at passage (p) 149 and they subcultured them another 16 times, while the other one (MCF-7-RIDC) was obtained from a partner laboratory at an unknown passage and it was subcultured 95 times. They also obtained a sample of Ishikawa cell line from the European Collection of Cell Cultures at p3, which they subcultured 130 times, and obtained another sample of the same cell line from another partner institution at an unknown passage before subculturing it for another 132 times. Their results showed that the

MCF-7-RIDC cell line had an extra chromosome 9 along with many chromosome arm duplications and other chromosomal abnormalities when compared to MCF-7-ATCC. With regard to the Ishikawa cell lines, the only similarity was a missing X chromosome. Again, an extra chromosome 2 and many chromosome arm duplications were identified when comparing the two samples.

Even in its natural microenvironment, chromosome instability is a near-universal feature of cancer, which can result in an unbalanced number of chromosomes, known as aneuploidy (Holland & Cleveland, 2009). The GSC primary cell line was obtained from patient-derived tissue after tumour excision surgery, which means that comparison with a database is impossible. Nevertheless, structural aberrations and aneuploidy in brain cancers are not uncommon events, and they have been characterised in human brain tumours for over 30 years. Griffin *et al.* (1988) analysed 21 primary paediatric brain tumours and found numerical abnormalities and structural aberrations in 6 and 12 tumours respectively. They identified indels and/or translocations in the p arm of chromosome 1 in five of the tumours, and most of them showed some form of aneuploidy, with some extreme cases being close to tetraploidy (Figure 3.12). Although the karyotypes of paediatric tumours often differ from the ones in adults tumours, a study published in the same year (Bigner *et al.*, 1988) showed that 42 of the 54 analysed tumours had abnormal karyotypes, and 6 out of the 38 cases that were fully characterised were near triploid or near tetraploid. The molecular heterogeneity of glioblastoma brain tumours was reviewed in 2014 by Eder & Kalman, and Keane *et al.* (2021) also reviewed brain tumour heterogeneity more recently.

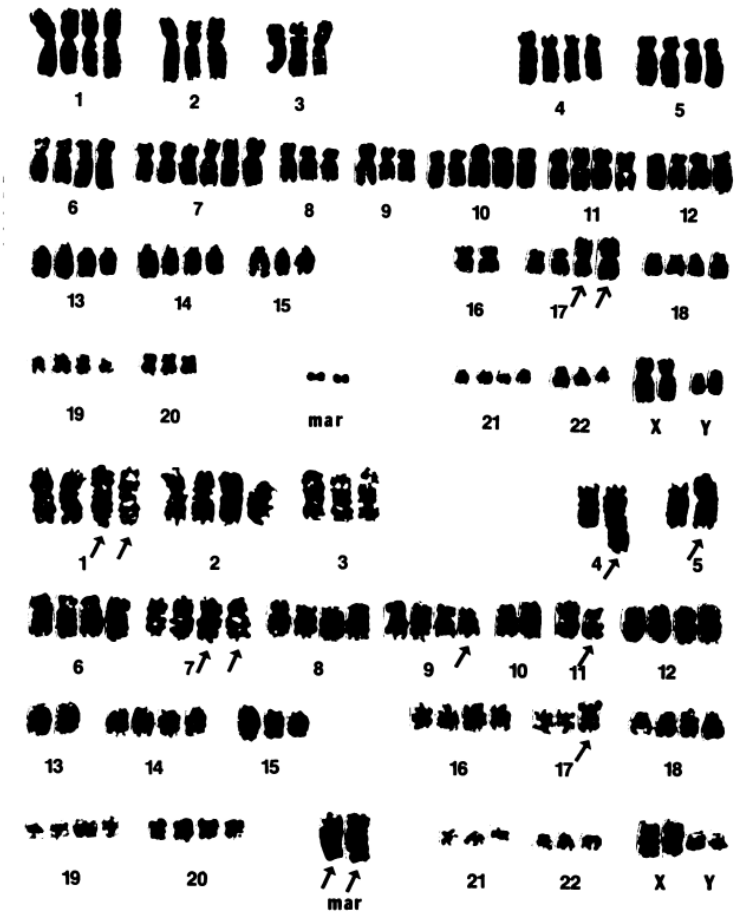

Figure 3.12: Karyotype of two paediatric brain tumours, by Griffin *et al.* (1988). Upper karyotype belongs to a newly diagnosed anaplastic astrocytoma from a 7 year old male, and the lower karyoptype belongs to recurring anaplastic astrocytoma from a 13 year old male. Arrows mark chromosomes with structural abnormalities, and markers are small fragments of chromosomes that could not be characterised.

It must also be borne in mind that, when a tumour is removed from its natural microenvironment to be cultured or implanted as xenografts, the cells undergo a radical change of environment and selective pressures, which can lead to adaptation and evolution resulting in a completely different karyotype than the one found in the primary tumour (Figure 3.13). In conclusion, although immortalised and patient-derived cell lines have been and are undeniably useful in the biomedical and cancer research field, these model systems might not always reflect the biology of actual human tumours. Therefore, new systems that reflect the right microenvironment should be used to avoid differences in selective pressures that lead to chromosome instability and variation.

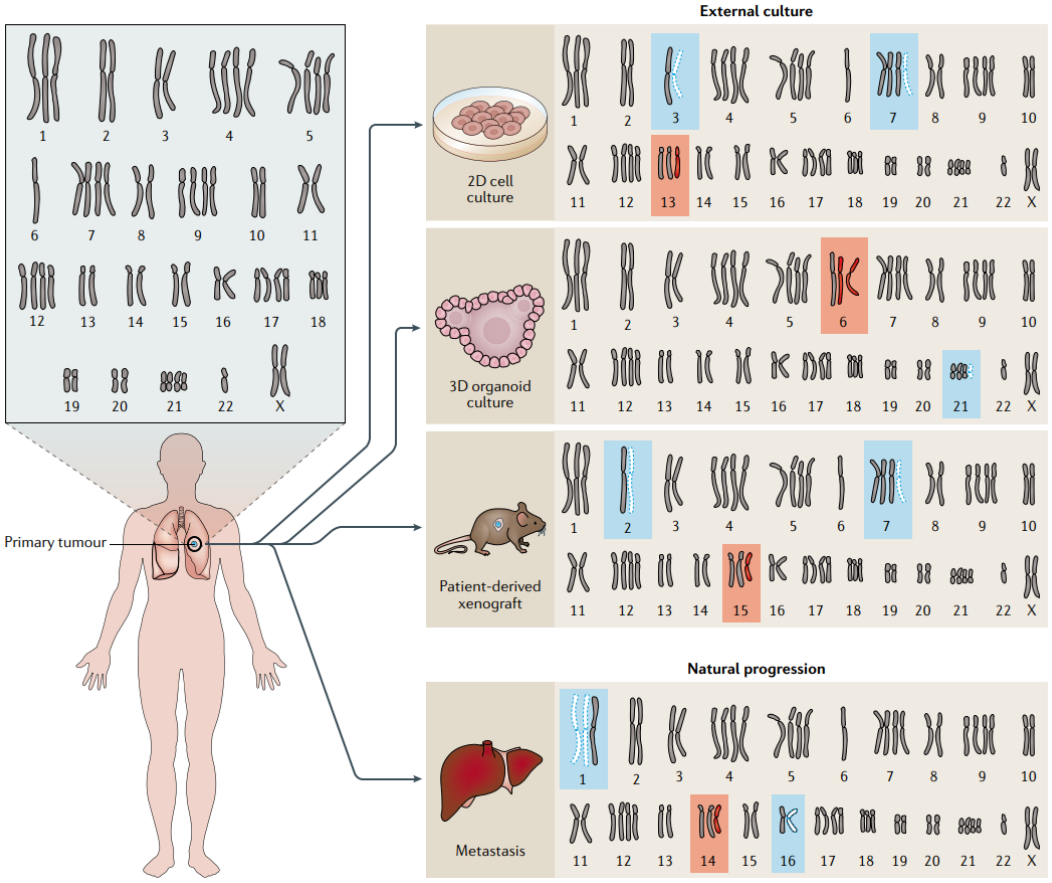

Figure 3.13: Karyotypic differences in cancer depending in the cellular microenvironment, by Ben-David & Amon (2020). Cancers that are removed from their natural microenvironment to be cultured as cell lines, organoids or patient-derived xenografts undergo selection pressure changes that can result in adaptation by gaining or losing chromosomes, shown in red and blue respectively. At the same time, cancer cells that travel to become metastatic also evolve to adapt to their new conditions and selection pressures, different to those found in the primary tumour environment.

The editions observed in the SiHa and GSCs clones can be categorised in three groups - edits with point mutations in the gRNA sites, cut an inversion of the sequence between the gRNAs and total or almost total deletion of the sequence between the gRNAs. Interestingly, no edition matching the middle band identified in SiHa ISG15 KO clones #3, #4 and #9 or GSC ISG15 KO clones #2 and #3 was characterised. This band could be a non specific target of the primers used, although they were checked using the "Primer-Blast" tool available on the National Library of Medicine web page (https://www.ncbi.nlm.nih.gov/tools/primer-blast/) and passed the multiple checks of the IDT primer designing tool (https://eu.idtdna.com/pages/tools/). Even if the band was specific, the significant decrease in bp found in this edition when compared to the WT (1278 bp against slightly above 1000 bp) would ensure the expression ablation of the WT protein.

It seems clear that the combined use of the two gRNAs selected results in a specific edition pattern, even in different cell lines, which results in a similar band arrangement when running the PCR products in agarose gels. The only exception seems to be the edit 4 in SiHa clone #9, where the sequence between the two gRNAs seems to have been duplicated. The hypothesis in this case is that the piece of DNA cut from another allele, such as the one sequenced in clone #9 edit 3, could have been inserted in the allele sequenced as clone #9 edit 4, since the cuts match perfectly. It would be of interest to find out exactly how many copies of chromosome 1 and ISG15 each of these clones and the parental WT cell line have - information that analysis of the edit patterns cannot provide. In order to find this out, Fluorescence In Situ Hybridization (FISH) could be performed. This technique uses fluorescent probes to allow for the detection and localisation of DNA sequences of interest. Selection of probes specific to a certain chromosome can provide information on the number of copies present in the sample (Cui *et al.*, 2016).

The high efficiency of the two gRNA editing approach lead to the decision of using ISG15 deficient mixed population cell pools, which was shown to have an ISG15 expression level below the detection threshold by immunoblotting, even when using high protein amounts for the validation. This technique has proved to have many advantages but also some disadvantages. On one hand, this approach is very time efficient since it does not require single cell sorting the edited pool. Growing and validating single cell sorted clones is very time consuming, and not having to do it on every edited cell line was much more time efficient. Using a variety of knock-out edits in the same pool can also be beneficial to avoid the effects of any potential unintentional off target. On the other hand, the heterogeneity of editions in the mixed population genes makes genetic characterisation by PCR very difficult, specially in the cell lines with high number of allele copies. This editing approach must be used with caution in these cell lines, as it can result only in partial knock-out. To counteract some of the more important disadvantages, the following measures were taken: 1) the edits in the single cell clones obtained were characterised to make sure all of them had open reading frame shifting mutations even with a high number of allele copies, which suggests high efficiency in the pool, 2) experiments were only performed in heterogeneous cells right after the cells recovered from nucleofection to avoid the potential overcoming of unedited WT cells over passages, 3) a sample of the pool was taken at the same time the experiment was set up for validation by immunoblotting to ensure sufficient reduction of protein expression.

Chapter 4

Identification of phenotypic differences between wild-type and ISG15$^{-/-}$ cells in cancer cell models

4.1 Introduction

IFNs have been shown to have potent antimitogenic and growth inhibiting properties. They have an important role in triggering and coordinating both the innate and adaptive immune responses. Because of this, recombinant IFNs have been used for decades in treatment of viral infections, some types of cancer and other diseases such as multiple sclerosis (Friedman, 2008). Research to understand such properties took off in the early 90s and still goes on today. In 1990, Salzberg *et al.* published a study focused in the role of IFN in cell growth and differentiation, in which they showed the growth inhibition caused by murine type I IFN in NIH 3T3 mice fibroblasts. They performed several experiments treating Moloney-murine sarcoma virus infected cells with different IFN concentrations for 72 hours, after which each sample was divided into two groups: one maintained at the same concentration of IFN and the other one IFN free. Their results showed a strong dose-dependent cell growth inhibition in IFN treated cells. When treating the cells with lower doses of IFN (90-450 IU/mL), cells fully recovered after treatment retirement, but when treating them with higher doses (1200-1800 IU/mL) treatment removal resulted in almost no recovery. Subramaniam & Johnson (1997) also investigated the role of IFNα and τ (not naturally produced in humans, but functionally and structurally homologous to type I IFNs capable of signalling through human IFNAR) in cellular growth arrest, examining the events that regulate cell cycle in Daudi cells (human Burkitt lymphoma). They observed that both IFNs repressed cell proliferation causing cell cycle arrest at G1 phase through p21

mediated inhibition of the cyclin-dependent kinase 2 (cdk2), IFNα being more active than τ. These results are consistent with the ones presented by Sangfelt *et al.* (1999), who studied the role of IFNα on cell cycle progression in three different lymphoid cell lines, including Daudi cells. They proved that IFNα treatment on Daudi and U-266 cells arrested at G0 and G1 phases respectively in a p21 and p15 mediated manner, while the third lymphoid cell line, H9, was completely resistant to IFNα. The continuous studies proving the anti-proliferative properties of IFNs in different cancer cell lines sparked the research on these cytokines as cancer treatments. A few examples include research by Zhang *et al.* (2010), who performed gene expression profiles on IFNα treated mice with metastatic hepatocellular carcinoma xenografts, and by Shi *et al.* (2016) that studied the effect of IFNα in HeLa cells as a model of cervical cancer. Both investigations concluded that the IFN treatment inhibited the growth of cancerous cells and increased apoptosis. Nevertheless, IFNs can also cause pro-tumour effects, as detailed in chapter 1. For instance, the intrinsic upregulation of the IFN pathway in tumours has been previously related with IFN and radiation treatment resistance (Khodarev *et al.*, 2007). Recent research by Abt *et al.* (2022) investigated the IFN response of pancreatic ductal adenocarcinoma, concluding that it caused the cells to arrest and survive by relying on stress-response signalling, and that interrupting this pathway by targeting a mediator (ATR) led to DNA damage and apoptosis.

Whether as anti-proliferative elements or as treatment resistance mediators, the understanding of ISGs and the IFN pathway in cancer seems crucial to develop more effective IFN-based therapies. ISG15 is a key element of the IFN pathway regulation and one of the first ISGs to be expressed upon IFN treatment. On top of this, hundreds of ISG15 targets have been identified by mass spectrometry, some of which are IFN response downstream effector ISGs, such as PKR, MxA, Hup56, and RIG-I (Zhao et al., 2005), and others are involved in the regulation of type I IFN signalling, like PLC1, JAK1, ERK1, and STAT1 (Malakhov et al., 2003). Although interferons are not the miraculous drug that was hoped for when they were first identified as anti-proliferative cytokines, its combination with novel therapies has proved to be helpful in the treatment of different cancers (Ferrantini *et al.*, 2007; Ningrum, 2014; Tarhini *et al.*, 2012), and the identification of new targets like ISG15 can help boost IFN treatments even in resistant cells. To this end, further researching the role of ISG15 beyond its implication in antiviral immunity in the cancer background is necessary.

4.2 Aim and strategy

The aim of this chapter was to identify any behavioural differences caused by the loss of ISG15 in terms of cell growth. For this, the clones obtained and validated in chapter 3 were tested versus the wild-type cells through several analysis, such as cell cycle and cell growth assays, with different IFN treatments in order to identify any phenotypic difference in the ISG15$^{-/-}$ cells.

4.3 Methods

4.3.1 Cell cycle analysis

For cell cycle analysis, $2{\cdot}10^5$ cells were grown in six well plates and, once at the right confluence, treated if required. 24 hours after treatment, if any, cells were collected appropriately and transferred to 1.5 mL Eppendorf tubes. Cell pellet was washed with 1 mL ice cold PBS and centrifuged for 5 minutes at 2000 rpm. After discarding the PBS, cells were fixed with very slow addition of ice cold 70% ethanol in PBS and tubes were very gently vortexed to avoid the formation of cell clumps. Fixed cells were left at 4°C for a minimum of two hours and preferably over-night before the analysis, although they could be stored for up to a week if necessary. When ready to analyse, cells were centrifuged again and washed with PBS twice. The cell pellet was resuspended in 500 μL of a 1:1000 solution of 4,6-diamidino-2-phenylindole (DAPI) in PBS, which binds to the DNA in the cells stoichiometrically. The cell suspension was then injected into a BD LSRFortessa™ Cell Analyser, where the cells were funneled through a nozzle that allowed only one cell at a time, guiding them to pass by a laser ray. In these kind of instruments, the individual cells are hit by the laser and sensors in the analyser detect the scattered light along with any fluorescence emitted by the stained DNA. The light scattered along the path of the laser, the forward scatter or FSC, allows for the discrimination of cells or particles by size as the light diffracts around the cell, as seen in Figure 4.1. The same figure illustrates the light scattered at 90° from the path of the laser, the side scatter or SSC, which allows for discrimination of cells by their intracellular structure or granularity. When analysing cell cycle phases in a homogeneous cell population, FSC and SSC are used to distinguish single cells from doublets, cell clumps or debris.

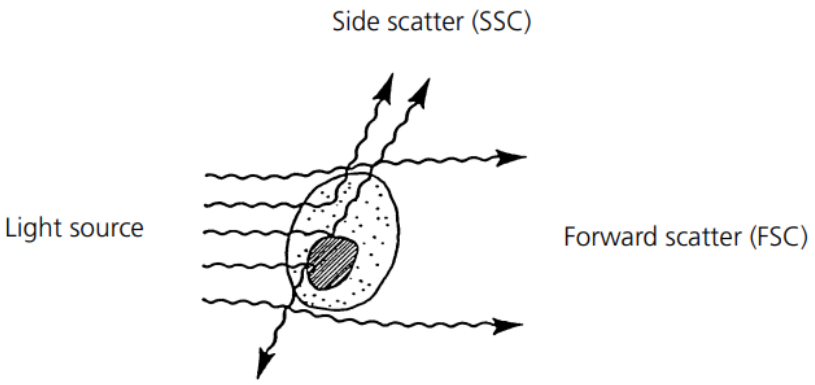

Figure 4.1: Forward scatter (FSC) measurement in cell cycle analysis allows for cell population discrimination by size as the light diffracts around the cell, while side scatter (SSC) can discern intracellular complexity or granularity. Figure by BD Biosciences.

The fluorescence emitted by the DAPI stain is also measured at 90° from the direction of the laser, which is directly proportional to the amount of stain and therefore proportional to the amount of DNA in the analysed cell. Since the DNA content and distribution changes as G_0 (non-cycling) cells enter and move through the cell cycle, the measurement of the DNA content on the cells allows for classification of the cell population across the three major phases of the cell cycle (G_0/G_1, S and G_2/M) at the moment of fixing (Figure 4.2a). Results are plotted in graphs representing the count of cells (events analysed) vs the fluorescence intensity (DNA amount). As shown in Figure 4.2b, cells with two full sets of chromosomes (DNA = 2N) are classified in G_0/G_1. As the cells enter the S phase and DNA replication begins (2n < DNA < 4n), the fluorescent intensity increases until the DNA content doubles (DNA = 4N) at phases G_2/M. During cell death, cells undergo chromatin fragmentation resulting in DNA loss (DNA < 2n), which can also be detected to determine the apoptotic population (phase subG1).

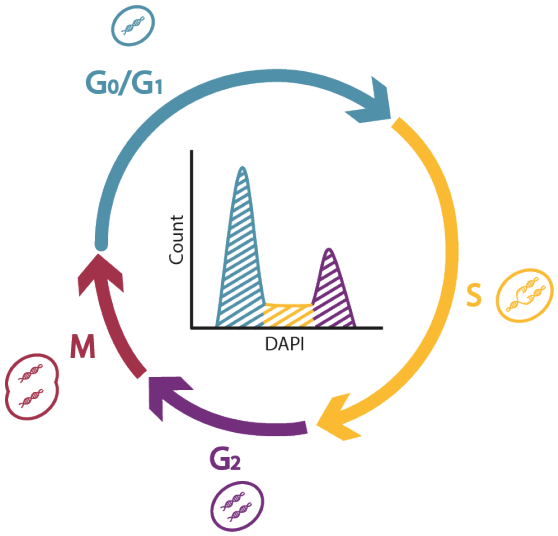

(a) DNA content and distribution changes as non-cycling cells (G_0) enter the cell cycle. The amount of DNA increases in each phase as the cycle begins at G_0/G_1, goes through DNA replication in phase S and reaches phases G_2/M when the replication is complete.

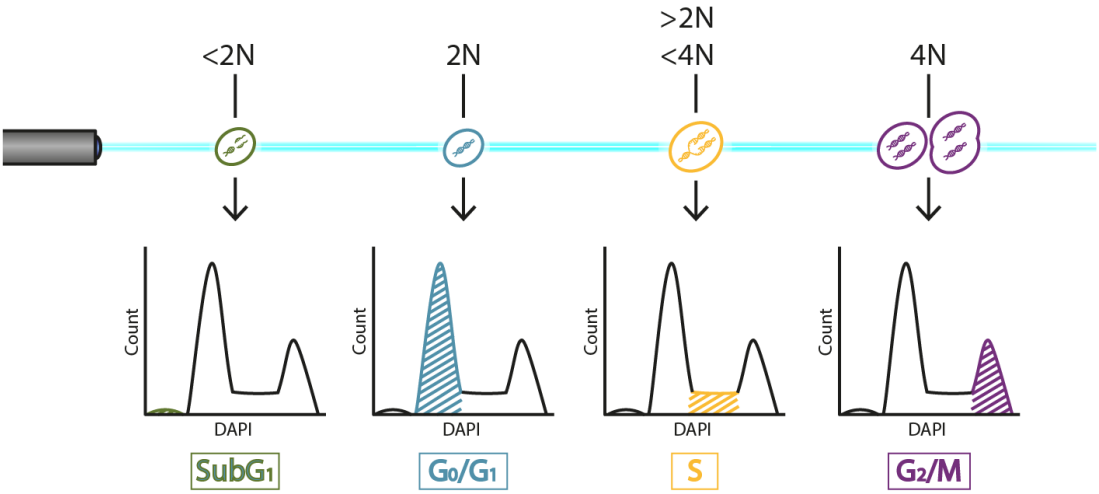

(b) The phase at which each cell is at the time of fixing can be determined by analysing the fluorescence intensity in each cell after DAPI staining. As the count of cells (events analysed, Y axis) are plotted against the fluorescence intensity (dependant on the stain amount in each cell and proportional to the DNA content, X axis) cells at phases G_0/G_1 (DNA = 2N) will peak at the left of the graph while the cells at phases G_2/M (DNA = 4N) will peak at the right of the graph. Those cells in the DNA replication process at the S phase (2n < DNA < 4n) will lie in between these two peaks. Cells undergoing DNA degradation (DNA <2N) will lie at the leftmost of the graph.

Figure 4.2: Cell cycle analysis by FACS

4.3.2 Live cell proliferation analysis

To measure real time cell proliferation, an Incucyte® Live-Cell Analysis System was used, consisting of a humidified incubator at 37°C and 5% CO_2 with an integrated camera capable of continuously monitoring the living cells for as long as required. The system enables detection and quantification of cells by automatically taking magnified pictures of the immobilised plates. The Incucyte software is capable of analysing the gathered images estimating the occupied area and thus determining the cell confluence over time. Unless otherwise stated in the text, 24 well plates were used for cell proliferation analysis, plating 30k cells per well in triplicates, and the system was programmed to take images every 2 to 3 hours for 5 days.

4.3.3 Colony formation assay

Clonogenic assays were performed by seeding 500 - 1000 cells per well in 24 well plates. 24 hours after seeding, cells were treated as required and left in the incubator for 10 to 14 days. If cells were to be treated in two different ways (i.e.: transfection and IFN treatment), 24 hours were also left between treatments to allow cells to recover. Media was then aspirated and wells were gently washed with room temperature PBS. The cells were fixed inside a fume hood by adding 400 μL of a 0.5% gluteraldehyde solution in PBS and the plates were incubated with gentle shaking for 20 minutes. The solution was discarded appropriately, also in the fume hood, and the wells were washed with water properly discarding at least the first wash. After shaking the plates to remove as much water as possible, they were left to dry upside down over clean paper tissue over-night. The following day, the colonies were stained with either a 1:20 Giemsa stain (GS500 Sigma-Aldrich) solution in PBS or a 0.2% Crystal Violet (C6158 Sigma-Aldrich) solution in PBS for one hour. The staining solution could be then collected and saved for future colony formation assays. The plates were washed again with water until the water ran clear, making sure to remove any residual dye, and were left to dry over-night. Quantitative measurement of the formed colonies could be achieved by destaining them on 1 mL of 10% acetic acid in water for 1 hour with gentle shaking and transferring 200 μL of each well into a 96 well plate to measure absorbance at 595 nm wavelength. Once destained, plates could be re-stained if necessary.

4.3.4 Generation of stable cell lines

Recovery of the expression of ISG15 in ISG15 knock-out isogenic cell lines obtained from single clones was attempted by transfection of the cell lines with pT-REX-Dest30 plasmids containing V5 tagged wild-type and mutated ISG15 (see section 4.3.4). Since this

plasmid contains a neomycin-resistance gene as a selectable marker, a neomycin analog called Geneticin™, also known as G418 Sulfate (Gibco, #10131035), was used for selective pressure to ensure proper insertion of the plasmid into the genome. The transfection of the pT-REX-Dest30 empty vector was used as a control.

Before transfecting the cells, a killing curve was prepared to find the optimal Geneticin concentration to use by treating untransfected SiHa cells with different concentrations of the selective marker (0, 150, 300, 450, 600, 750, 900, 1050, 1200, 1350, 1500 and 1650 μg/mL) and monitoring them over 10 days. The media with Geneticin was changed every 3 days approximately. Once ready to proceed with the transfections, cells were seeded in five wells of a 6 well plate. When 70 - 80% confluent, the cells in four of the wells were transfected each with either the pT-REX-Dest30 empty vector (henceforth EV), the plasmid containing the V5 tagged wild-type version of ISG15 (henceforth WT), the plasmid containing the V5 tagged mutated version of ISG15 (henceforth AA) or a pmaxGFP™ vector used as a transfection control. The fifth well was left untransfected as a control for the selective marker. 24 hours post-transfection, the cells in each one of the wells were transferred carefully to 10 cm plates with the appropriate media and Geneticin concentration and grown for 3 to 4 weeks. The expression of the new stable cell lines was validated by immunoblotting.

Plasmids used for ISG15 recovery

Two different versions of the pT-REx™-DEST30 plasmid (map shown in Figure 4.3) cloned to contain cDNA encoding for V5 tagged ISG15 were used for transfection and generation of stable cell lines. One contained the wild-type version of ISG15, while the other one contained a mutated version incapable of ISGylating. Such mutation consisted in the replacement of the last two amino acids of the mature carboxyl terminus ^{152}LRLRGG, which is essential for the ligation of ISG15 to the target proteins as described in section 1.3. These two glycines were replaced for two alanines, resulting in a ^{152}LRLRAA C-terminal. Both versions were tagged with V5 in the N-terminus, as shown in the sequences in Figure 4.4. These plasmids were prepared by me during my MScR project using the Gateway Cloning System, a diagram of which can be found in Appendix B (also originally prepared for my MScR thesis).

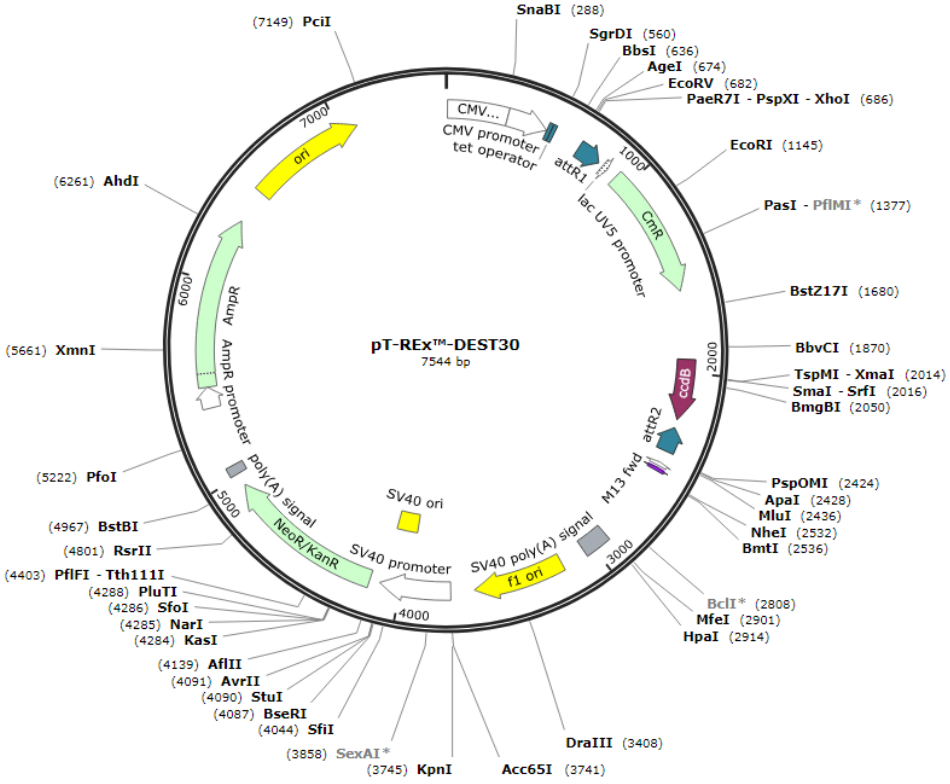

Figure 4.3: Map for the pT-REx-DEST30 plasmid, where the V5 tagged wild-type ISG15 and V5 tagged mutant ISG15 were cloned.

```
ACAAGTTTGTACAAAAAAGCAGGCTGCCGCCACCATGGGCAAGCCCATTCCTAATCCTCTGCTGGGCCTCGATAGCACC
GGCTGGGATCTGACAGTGAAGATGCTGGCCGGCAACGAGTTCCAGGTGTCCCTGTCTAGCAGCATGAGCGTGTCCGAG
CTGAAGGCCCAGATCACCCAGAAAATCGGAGTGCACGCCTTCCAGCAGAGACTGGCCGTTCATCCTAGCGGAGTGGCC
CTGCAGGATAGAGTGCCTCTGGCCTCTCAAGGACTCGGCCCTGGATCTACAGTGCTGCTGGTGGTGGATAAGTGCGAC
GAGCCTCTGTCTATCCTCGTGCGGAACAACAAGGGCCGCAGCAGCACATATGAAGTGCGGCTGACACAGACAGTGGCC
CACCTGAAGCAGCAAGTGTCTGGACTCGAGGGCGTGCAGGACGATCTGTTCTGGCTGACCTTTGAGGGCAAGCCTCTG
GAAGATCAGCTGCCCCTGGGAGAGTATGGCCTGAAGCCTCTGAGCACCGTGTTCATGAATCTGCGGCTGAGAGGCGGC
TGATGAACCCAGCTTTCTTGTACAAAGTGGG
```

```
ACAAGTTTGTACAAAAAAGCAGGCTGCCGCCACCATGGGCAAGCCCATTCCTAATCCTCTGCTGGGCCTCGATAGCACC
GGCTGGGATCTGACAGTGAAGATGCTGGCCGGCAACGAGTTCCAGGTGTCCCTGTCTAGCAGCATGAGCGTGTCCGAG
CTGAAGGCCCAGATCACCCAGAAAATCGGAGTGCACGCCTTCCAGCAGAGACTGGCCGTTCATCCTAGCGGAGTGGCC
CTGCAGGATAGAGTGCCTCTGGCCTCTCAAGGACTCGGCCCTGGATCTACAGTGCTGCTGGTGGTGGATAAGTGCGAC
GAGCCTCTGTCTATCCTCGTGCGGAACAACAAGGGCCGCAGCAGCACATATGAAGTGCGGCTGACACAGACAGTGGCC
CACCTGAAGCAGCAAGTGTCTGGACTCGAGGGCGTGCAGGACGATCTGTTCTGGCTGACCTTTGAGGGCAAGCCTCTG
GAAGATCAGCTGCCCCTGGGAGAGTATGGCCTGAAGCCTCTGAGCACCGTGTTCATGAATCTGCGGCTGAGAGCCGCC
TGATGAACCCAGCTTTCTTGTACAAAGTGGG
```

Figure 4.4: Designed sequences synthesised by GeneArt®(Invitrogen) encoding for V5 tagged wild-type (WT) and mutated (AA) ISG15, being the later incapable of ISGylating. Start and stop codons are highlighted in bright blue, while the V5 sequence and the ISG15 sequence are highlighted in green and muted yellow respectively. The nucleotides corresponding to the last two amino acids of the mature carboxyl terminus are highlighted in orange, showing where the mutation occurs. The Kozak sequence for the protein translation initiation is highlighted in grey and the attB1 and attB2 sequences for Gateway Cloning are highlighted in bright yellow.

4.4 Results

4.4.1 Cell cycle analysis

At the time this project started, most of the published studies focused on the effects of ISG15 on antiviral signalling and sensitivity to viral infection. In order to study the role of ISG15 in different cancer models, CRISPR gene editing technology was used to generate ISG15$^{-/-}$ clones, as detailed in chapter 3. Once the first ISG15$^{-/-}$ isogenic cell line was obtained (clone #1), a cell cycle analysis on IFN treated and untreated WT and clone #1 cells was performed to try to detect any difference caused by the deletion of ISG15. After fixing and staining the cells with DAPI as described in subsection 4.3.1, cells were sorted with FSC and SSC and the cells on the resultant population were allocated in the appropriate phase of the cell cycle (G1, S or G2/M) depending on their DNA content and distribution. The percentage of the analysed cells in each stage of the cycle was calculated for each sample and condition. Results revealed that the distribution of the cells across the three main cell cycle phases did indeed change when comparing the WT cell line with the ISG15 deficient cell line under different concentrations of IFNα treatment. A significant shift in phase G2/M is appreciated in Figure 4.5 when comparing clone #1 ISG15 KO cells to WT cells regardless of IFN treatment concentration. When plotting the percentage of cells in each condition and phase (see Figure 4.6), it can be observed that WT cells showed mostly consistent results across the different conditions, suggesting that the IFN treatment did not cause a significant change in the cell cycle profile in SiHa cells. On the other hand, ISG15 deficient cells showed a clear increase of cells in G1 phase, which seems to be an IFN dependent event with the percentage of cells in G1 increasing with the addition of IFN, suggesting the cells may be undergoing cell cycle arrest in G1 phase. At the same time, the amount of cells in S phase notably decreased as the concentration of IFN increased, which could explain the downturn in the amount of cells in G2/M. However, although there is a slight decrease in the percentage of cells in the G2/M phase as the IFN concentration increases, it is not as noticeable as in the other two phases, which could be the result of the cells not being able to bypass the S checkpoint and dying before entering G2/M phase. This could explain the increased amount of ISG15$^{-/-}$ cells in subG1 compared to WT cells in the same phase, although this increase is not steady and proportional as it would be expected from the results observed in the three major phases.

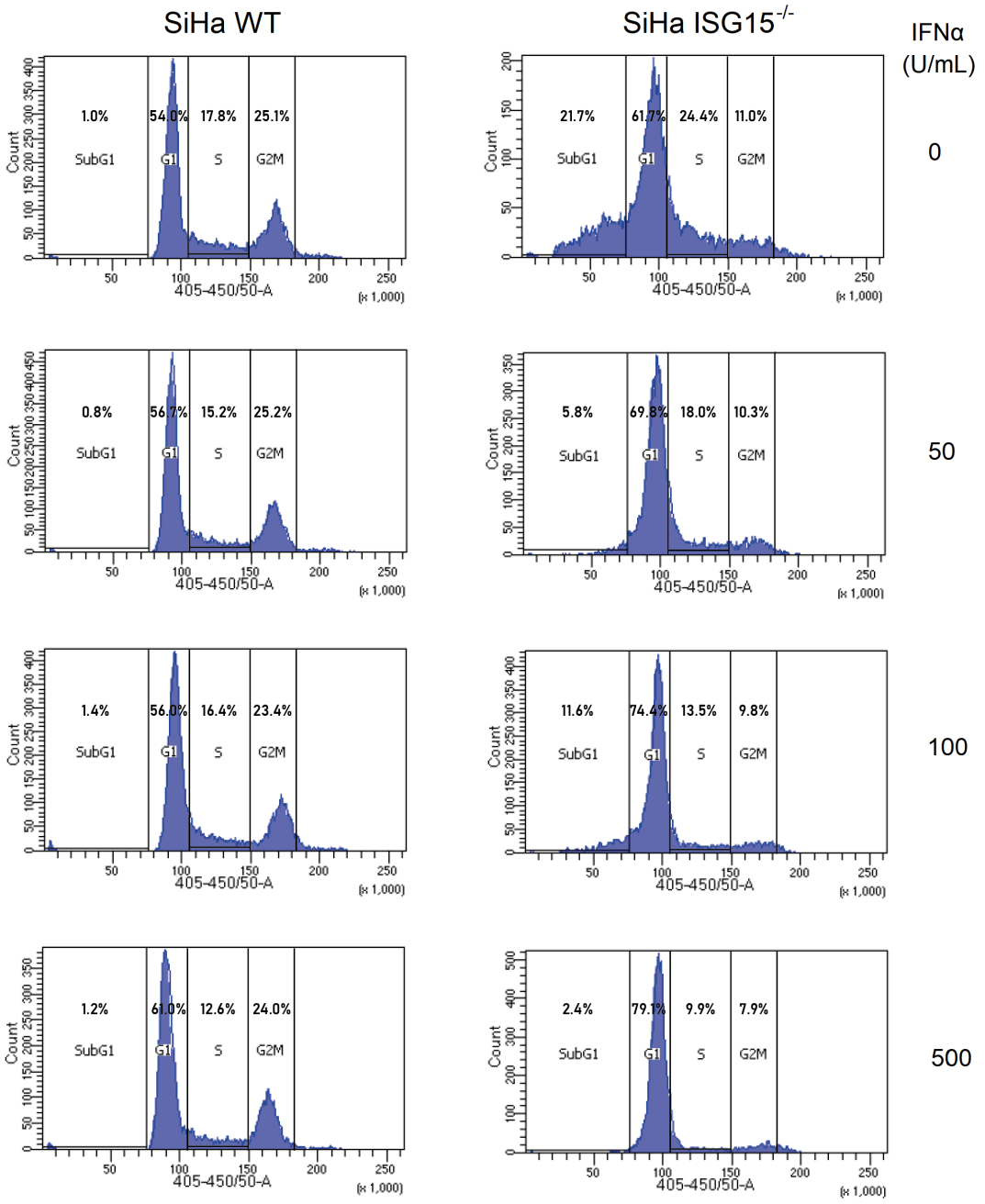

Figure 4.5: Cell cycle analysis on WT (left) and clone #1 isogenic ISG15$^{-/-}$ (right) SiHa cells stained with a 1:1000 DAPI solution. Histograms show single cell count (events analysed, Y axis) vs stain fluorescence (DNA content, x axis) at the time of fixing. The gates representing each cell cycle phase (G_0/G_1, S or G_2/M) are labelled and show the percentage of cells in each phase, including the subG_1 phase to determine the percentage of apoptotic cells. The top row of histograms belongs to the untreated WT and ISG15$^{-/-}$ samples, and the treatment increases (50 U/mL, 100 U/mL and 500 U/mL) from the second row to bottom row. These results are representative of at least two experiments.

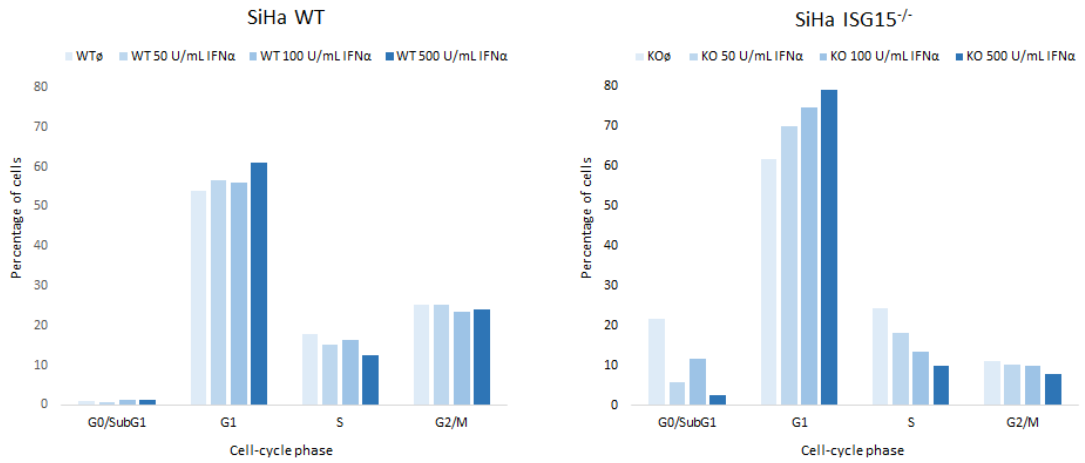

Figure 4.6: Clustered column graph showing the percentage of single cell events in each cell cycle phase (G_0/G_1, S or G_2/M) as the IFNα treatment increases (0 u/mL, 50 U/mL, 100 U/mL and 500 U/mL) in WT (left) and clone #1 isogenic ISG15$^{-/-}$ (right) samples.

In addition to the cell cycle assay, an analysis to detect activated apoptotic caspases 3 and 7 was carried out by FACS to explore if the amount of ISG15$^{-/-}$ cells gated in the subG1 phase were the result of an increase of apoptotic cells in ISG15 deficient cells. For this, the Vybrant™ FLICA Caspase Apoptosis Assay Kit for flow cytometry (Invitrogen, V35118) was used on WT and clone #1 ISG15 KO SiHa cells, untreated and treated with commercial IFNα, following the suppliers protocol. This assay uses a fluorescent inhibitor of the caspases that interacts with the enzymatic reactive centre of the activated caspases as an affinity label. The green fluorescent signal, detected by FACS at excitation-emission peaks of 488-525 nm, are a direct measure of the amount of active caspases present in the cells at the moment the reagent is added, while the unbound reagent diffuses out of the cells and is removed at the washing steps. Single particles were gated using the forward scatter (FSC) and living cells were gated using the side scatter (SSC) as explained in subsection 4.3.1, followed by determination of the percentage of fluorescent cells. Results presented in Figure 4.7 showed that the amount of apoptotic cells in the ISG15 deficient cells in clone #1 did not increase after the addition of IFNα, and neither it did as the concentration of IFN increased. Only 1.4% of the single living cells gated were positive for activated caspases in the untreated ISG15$^{-/-}$ sample, and 1.4%, 1.0% and 1.3% of the cells were positive in the IFNα treated samples, 50 U/mL, 100 U/mL and 500 U/mL respectively. WT cells did not reveal a significant difference between the samples either - 1.0% of the single living cells gated were positive in the untreated sample, and 0.9%, 1.2% and 1.5% were positive as the IFNα treatment increased.

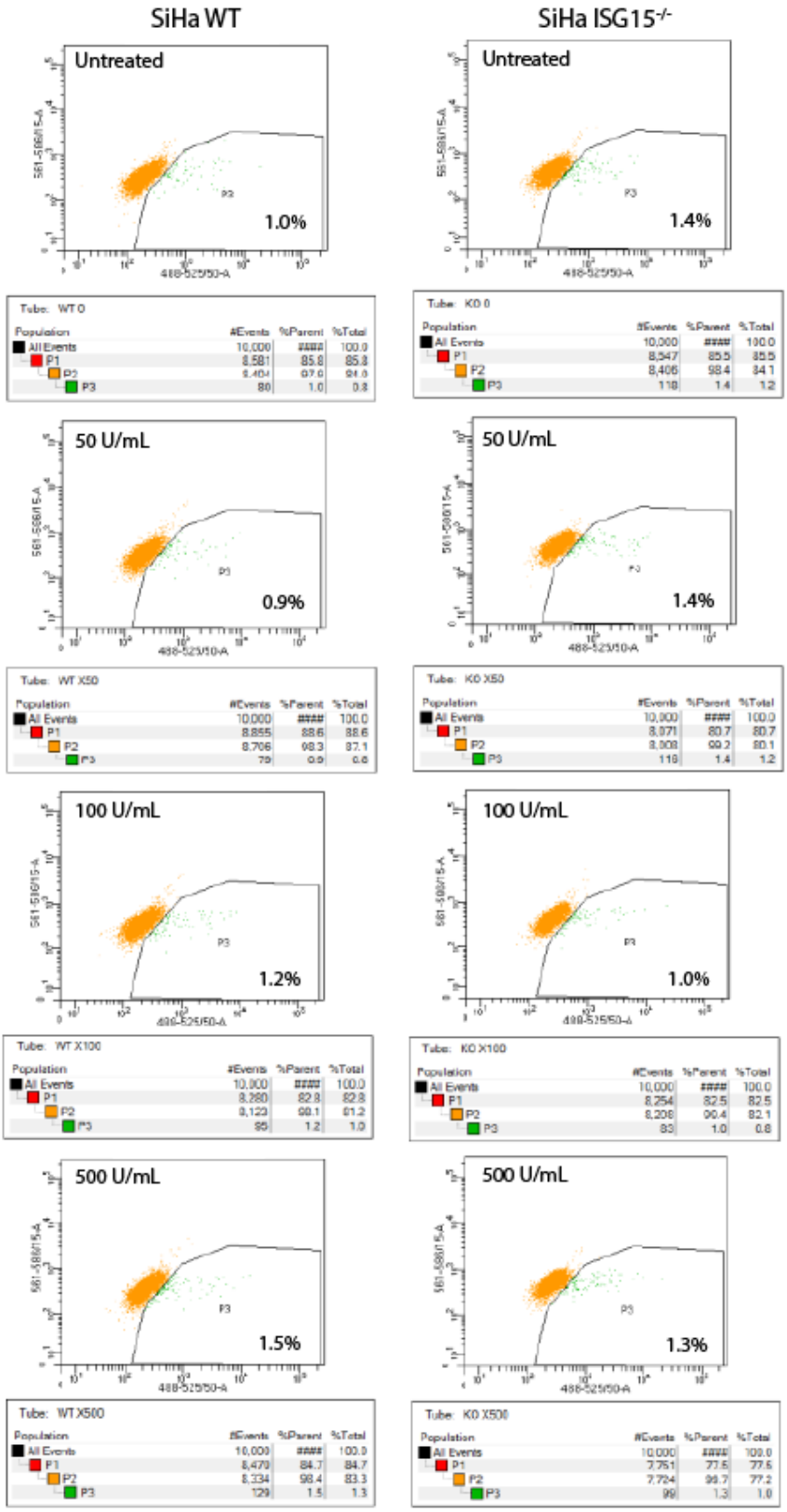

Figure 4.7: FACS analysis to detect activated apoptotic caspases 3 and 7 on IFNα treated and untreated WT and clone #1 ISG15 KO SiHa cells using the Vybrant™ FLICA Caspase Apoptosis Assay Kit for flow cytometry (Invitrogen, V35118). The FLICA fluorescent inhibitor interacts with the enzymatic reactive centre of the activated caspases as an affinity label, which is detected as a green fluorescent signal at excitation-emission peaks of 488-525 nm. No significant differences were observed on ISG15 KO vs WT cells upon addition of IFNα, nor as the treatment concentration increased.

4.4.2 Cell growth analysis

As part of the investigations of the detected IFN dependant G1 phase arrest, a real time cellular proliferation assay was carried out on wild-type and isogenic ISG15$^{-/-}$ SiHa cells with and without IFN. Cells were grown in an Incucyte® Live-Cell Analysis System as described in subsection 4.3.2. The same amount of cells were seeded per well, having triplicates per condition, and magnified images were captured every 3 hours for around 5 days (120 hours). Figure 4.8 shows a graph were each point reflects the average confluence value of each of the triplicates in each cell line (WT or clone #1 ISG15$^{-/-}$) and each condition (untreated or treated with 50 U/mL, 100 U/mL or 500 U/mL commercial IFNα). It can be observed that although the treatment did not make a difference in the growth rate of the wild-type cells, knocked out cells showed a treatment dependant decrease in cell proliferation over time. A significant difference starts getting noticeable after 40 hours, when ISG15 deficient cells show a greater proliferation reduction the higher the dose of IFN treatment. By the end of the experiment all wild-type cells grew to 85-90%, and while the untreated knocked out cells also grow to around 84%, proliferation in treated cells decreased approximately a 10% as the IFN concentration increased (around 70% for cells treated with 50 U/mL, 60% for those treated with 100 U/mL and 50% for the ones treated with 500 U/mL). Interpreting these results along with the ones obtained from the cell cycle analysis, the data suggests that the increase of cells observed in G1 phase could be due to cell cycle arrest.

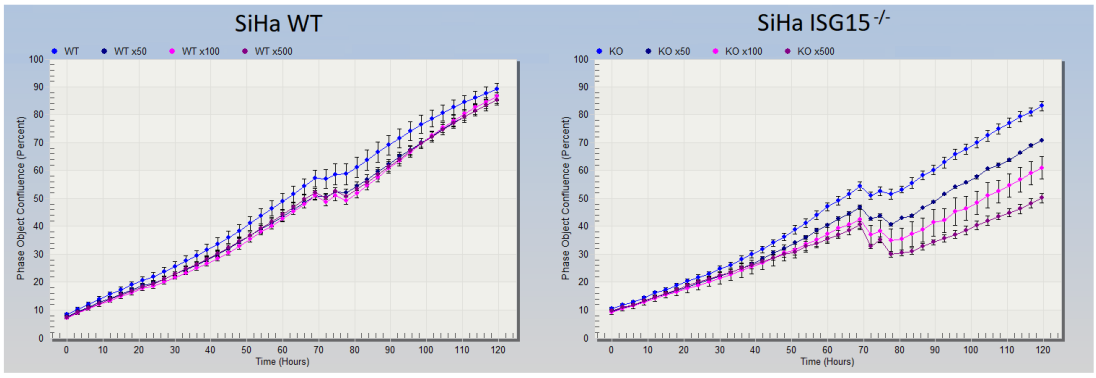

Figure 4.8: Real time cell proliferation assay in WT (left) and clone #1 isogenic ISG15$^{-/-}$ (right) samples as the IFNα treatment increases (0 U/mL in lighter blue, 50 U/mL in darker blue, 100 U/mL in pink and 500 U/mL in purple). Cells were grown in an Incucyte® Live-Cell Analysis System for 5 days, having triplicates per condition, and taking magnified every 3 hours. Each point represents the mean and standard deviation of the estimated cell confluency (measured in percentage, Y axis) of each of the triplicates at each time point (measured in hours, X axis). These results are representative of at least two experiments.

4.4.3 Colony formation assays

SiHa cells

To further research the IFNα dependent cell growth arrest detected via cell cycle and cell growth assays on clone #1 isogenic ISG15$^{-/-}$ cells, a clonogenic assay was performed to analyse the capability of single cells to grow into colonies. Only 500 cells were seeded per well, as described in subsection 4.3.3, and they were treated the following day before leaving them to grow for 10 to 14 days. In order to test if the cells also became sensitive to type II IFN, cells were also treated with IFNγ. Consistent with the results obtained in the cell cycle and cell growth experiments. Upon fixing and staining the colonies, a significant decrease in colony number as the IFNα treatment increased from x1 (1 U/ mL) to x500 (500 U/mL) was observed when compared to the WT cells, which seem not to be affected by the treatment (Figure 4.9). The effect of IFNγ on ISG15$^{-/-}$ cells, however, is not significantly different to that seen in the WT cells, suggesting that the depletion of ISG15 only causes sensitivity to IFNα and not IFNγ.

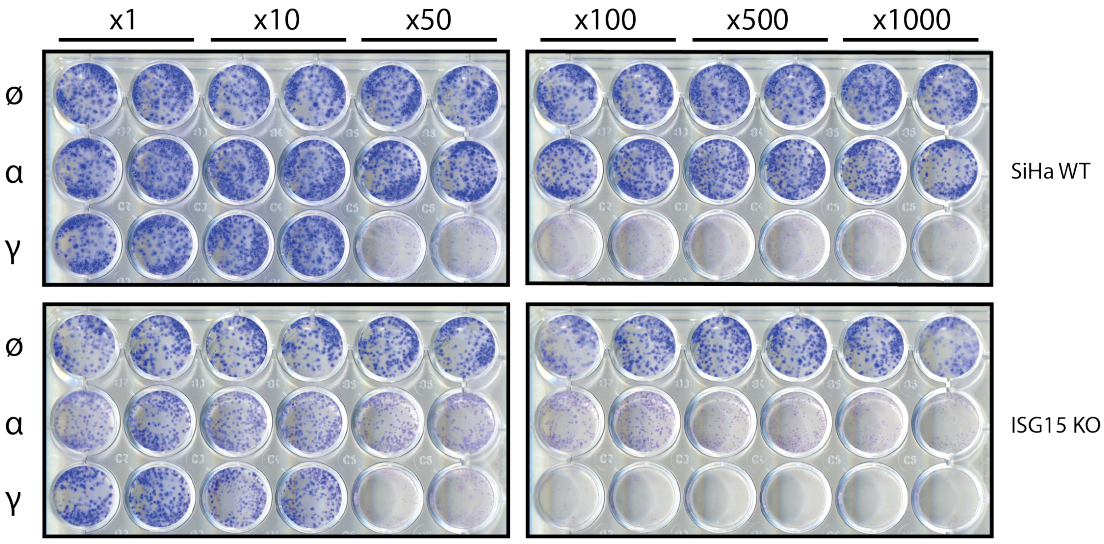

Figure 4.9: Colony formation assay on WT and clone #1 ISG15$^{-/-}$ SiHa cells, in duplicates for each condition - untreated (upper row), IFNα treated (middle row) and IFNγ treated (lower row). x1 of treatment equals to 1 U/mL commercial IFNα and 0.2 ng/mL commercial IFNγ. These results are representative of at least two experiments.

To verify these results and be able to quantify the colonies in each well, the experiment was repeated and the dye in each well was dissolved as described in subsection 4.3.3 in order to measure the absorbance, which directly correlates to the amount of dye in the well, representing the number/size of the colonies. The results of this replica (shown in

Appendix B) were consistent with the data from the first colony formation experiment and also showed a significant sensitivity to IFNα of ISG15$^{-/-}$ cells, but not to IFNγ. Quantitative measurement is shown in Figure 4.10, which confirms that the number of colonies formed in ISG15$^{-/-}$ cells decreased as the IFNα increased.

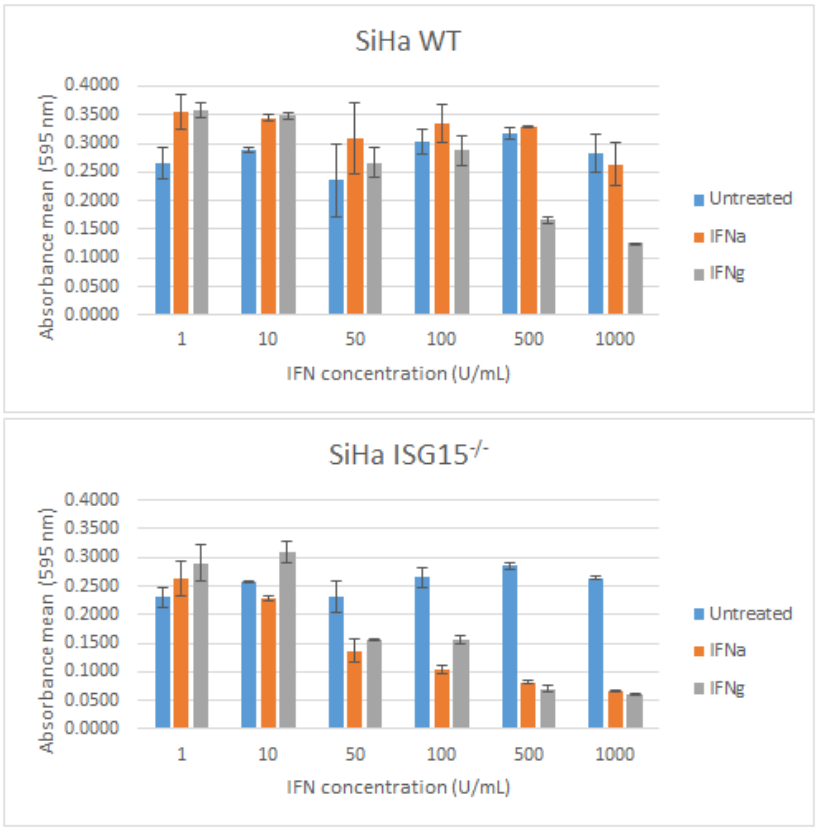

Figure 4.10: Quantitative measurement of formed colonies in IFNα and γ treated WT and clone #1 isogenic ISG15$^{-/-}$ SiHa cells. Colonies were destained with a 10% acetic acid solution and absorbance was read at 595 nm in each sample. The mean and standard deviation of each pair of duplicates are shown for each treatment condition and concentration, where x1 of treatment equals to 1 U/mL IFNα and 0.2 ng/mL IFNγ. Error bars equal to standard deviation. Linear regression statistical analysis performed on WT SiHa cells under different IFN treatments revealed no significant difference between untreated and IFNα treated samples (p-value $>$ 0.05), and a significant difference between WT and IFNγ treated samples (p-value $<$ 0.0001). Analysis on ISG15 KO SiHa cells revealed a significant difference between WT and IFNα (p-value $<$ 0.0001) and between WT and IFNγ treated samples (p-value $<$ 0.0001). Complete analysis results are available in Table B.1 and Table B.2.

To ensure that the observed phenotype occurred due to the lack of ISG15 and not due to off-target editions caused as a consequence of the failed insertion of the V5 tag in clone #1, colony formation assays were performed in another four successful ISG15$^{-/-}$ clones - #3, 4, 9, and 10. As seen in Figure 4.11 and Figure 4.12, all of the clones had an increased sensitivity to IFNα when compared to the WT, although clone #4 seems to be much more resistant than the other three. Interestingly, immunoblots for this clone showed ISG15

expression to be below the detection threshold and the allele screen by PCR described in chapter 3 did not detect silent mutations in any of the four edits identified, all of which should result in truncated expression.

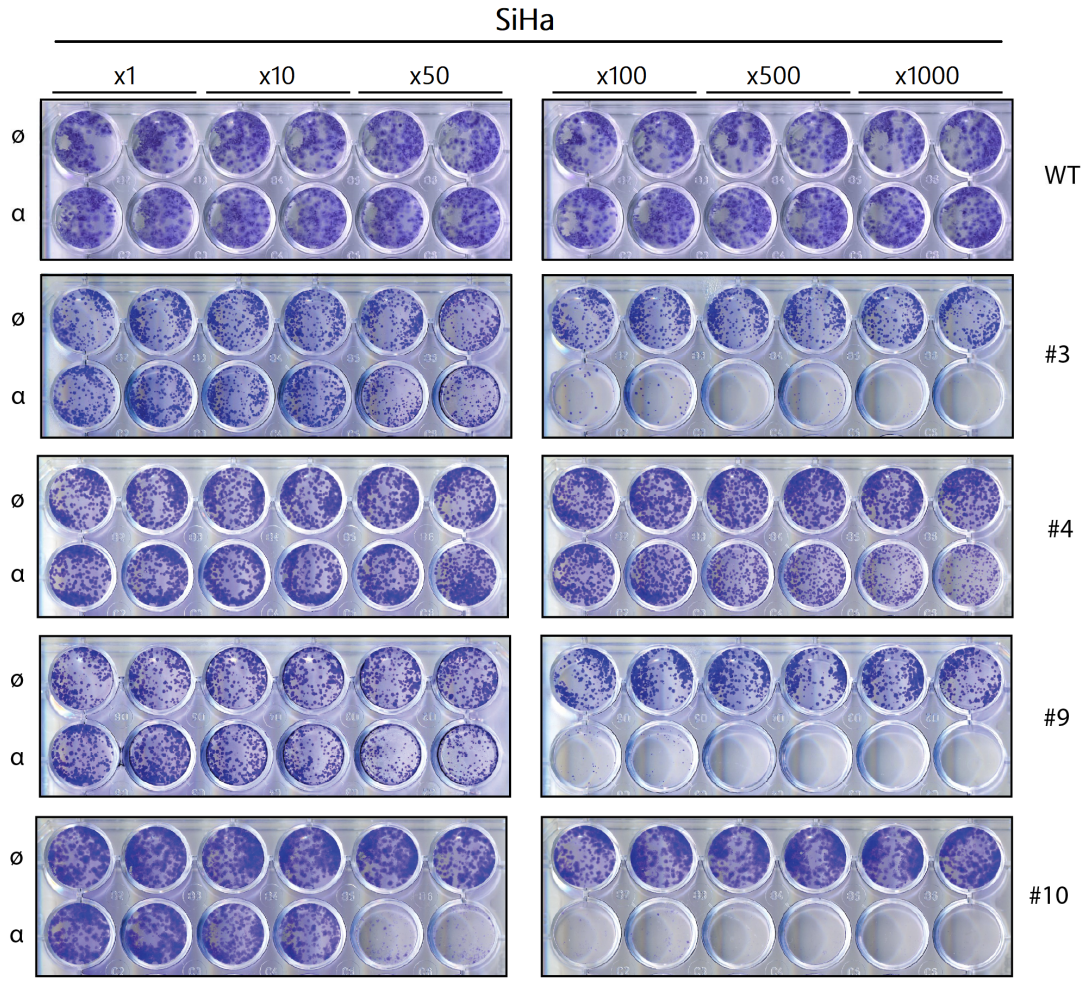

Figure 4.11: Colony formation assay on SiHa WT and ISG15KO clones #3, 4, 9, and 10 in duplicates for each condition. Upper row of each cell line is untreated, while the lower one is treated with increasing concentrations of commercial IFNα where x1 equals to 1 U/mL. These results are representative of at least two experiments.

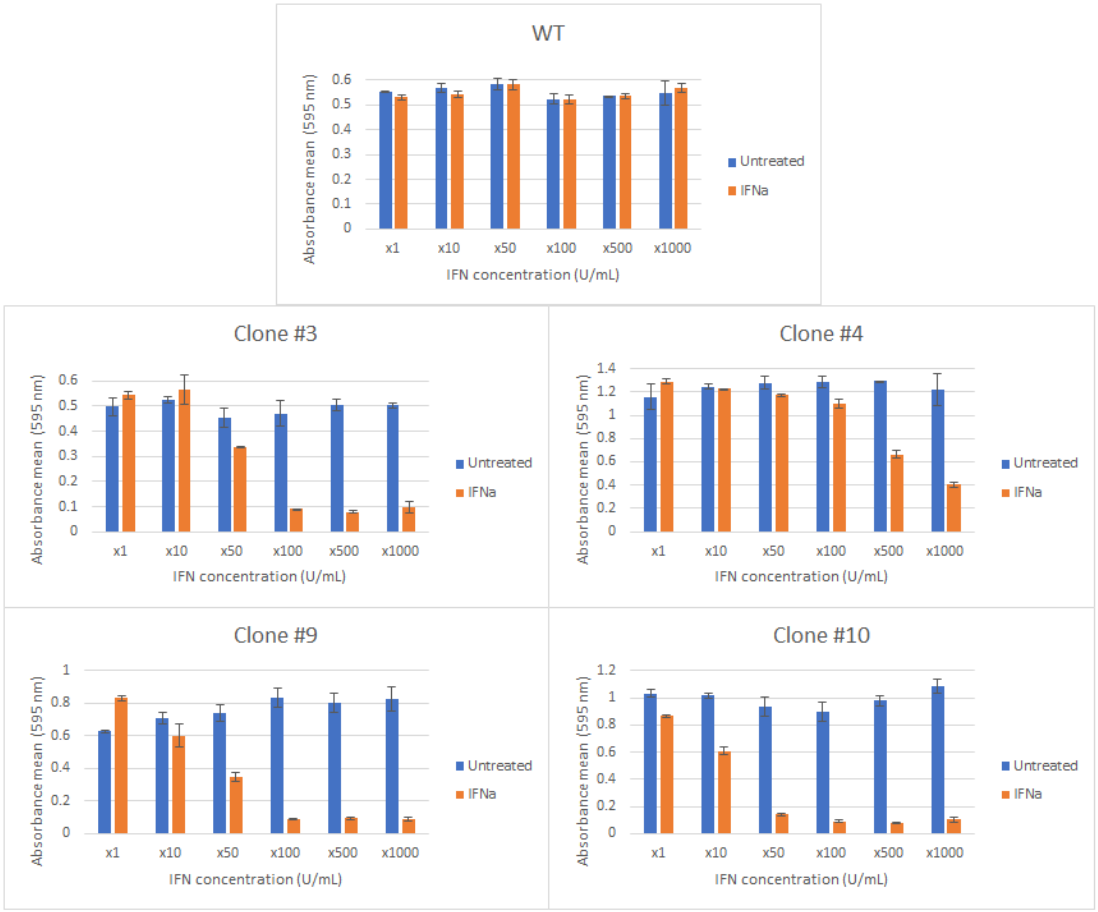

Figure 4.12: Quantitative measurement by absorbance reading of formed colonies in untreated and IFNα treated SiHa WT and ISG15 KO clones #3, 4, 9 and 10. Colonies were destained with a 10% acetic acid solution and absorbance was read at 595 nm in each sample. The mean and standard deviation of each pair of duplicates are shown for each treatment condition and concentration, where x1 of treatment equals to 1 U/mL IFNα. Linear regression statistical analysis performed on untreated and IFNα treated SiHa samples revealed no significant difference between untreated and IFNα treated WT samples (p-value = 0.2657), and a significant difference between untreated and IFNα treated samples in all clones (p-value < 0.0001). Complete analysis results are available in Table B.5, Table B.6, Table B.7, Table B.8 and Table B.9.

Altogether, the data presented here suggests that the lack of ISG15 in SiHa cells does indeed cause a significant dose dependent IFNα sensitivity that results in cell growth arrest at G1 phase.

GSC cells

To test if the sensitivity to IFN upon deletion of ISG15 was observed in SiHa cells is more generally applicable, GSC cells were selected since, as discussed in subsection 1.3.2, the IRDS has been shown to be upregulated in a high percentage of glioblastoma samples (see Figure 1.13) ISG15 being one of the top overexpressed genes, which is linked to treat-

ment resistance. Single cell sorted ISG15$^{-/-}$ GSC clones (obtained using the same double gRNA approach used to obtain ISG15 KO SiHa clones #3, 4, 9 and 10) were used for colony formation assays. As in the assays performed on SiHa cells, 500 cells were seeded per well, which turned out to be a too low confluence for GSC cells. Due to their morphology, these cells are harder to dye than the SiHa cells, and grow much slower especially at very low confluences. Even though results presented in Figure 4.13 show very few lightly stained colonies, it can be observed that the IFNα ISG15 KO clones #1, 2 and 3 are much more sensitive to the treatment than the WT GSC cells. In this case, quantification by dissolution with acetic acid was not successful due to the low number of colonies and the weak staining of the cells.

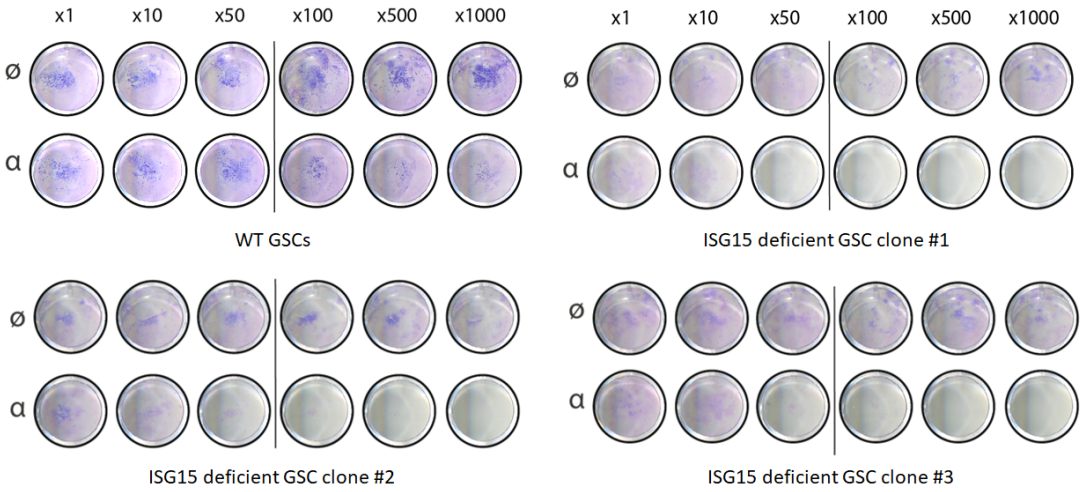

Figure 4.13: Colony formation assay on WT and ISG15 KO GSC clones #1, 2 and 3 untreated and treated with commercial IFNα in duplicates for each condition. Upper row of each cell line is untreated, while the lower one is treated with increasing concentrations of IFNα where x1 equals to 1 U/mL. GSC cells grow much slower than SiHa cells, specially when seeded at very low confluences, and are also harder to dye due to their morphology. Seeding only 500 cells per well resulted in a low amount of colonies with a very faint staining, but the sensitivity of the ISG15 KO clones can still be appreciated when compared to the WT cells. Quantification by dissolution with acetic acid was not successful due to the weak dying of the cells. This mistake was amended in subsequent clonogenic assays performed with GSCs.

While the GSC clones were expanded from single cells, the entire edited GSC pool was also tested by immunoblot. The editing efficiency of the double gRNA approach was good enough to ensure ISG15 expression levels below detection threshold by immunoblotting, even when loading large amounts of protein lysate (up to 50 μg). The ISG15 deficient heterogeneous cell pool was used to perform new clonogenic assays, this time seeding 1000 cells per well and monitoring cell growth on the microscope after 10 days. A series of secreted recombinant IFNα subtypes (1, 2, 4, 5, 6, 7, 8, 10, 14, 16, 17 and 21) were used in order to test if the ISG15 deficient cells were equally sensitive to each of the subtypes. These IFNs were kindly provided by my colleague Ashita Singh, who expressed them in HEK293 cells

using a mammalian expression system and collected the secreted protein in DMEM media. Final concentrations of 0.3 ng/mL, 0.9 ng/mL and 3 ng/mL were achieved by adding 1 μL, 3 μL and 10 μL of the media containing the secreted IFNs to each well containing 1 mL of standard media. As seen in Figure 4.14, the new seeding confluence led to much better colony formation rate and subsequent cellular staining than the ones obtained when seeding only 500 cells. This aided the appreciation in the subtle differences between the effects of the different IFNα subtypes. The higher concentrations of some of the most active ones greatly inhibited cell growth even in the WT cells, such as IFNα8, 10 and 14, while the least active ones turned out to be IFNα1 and 21.

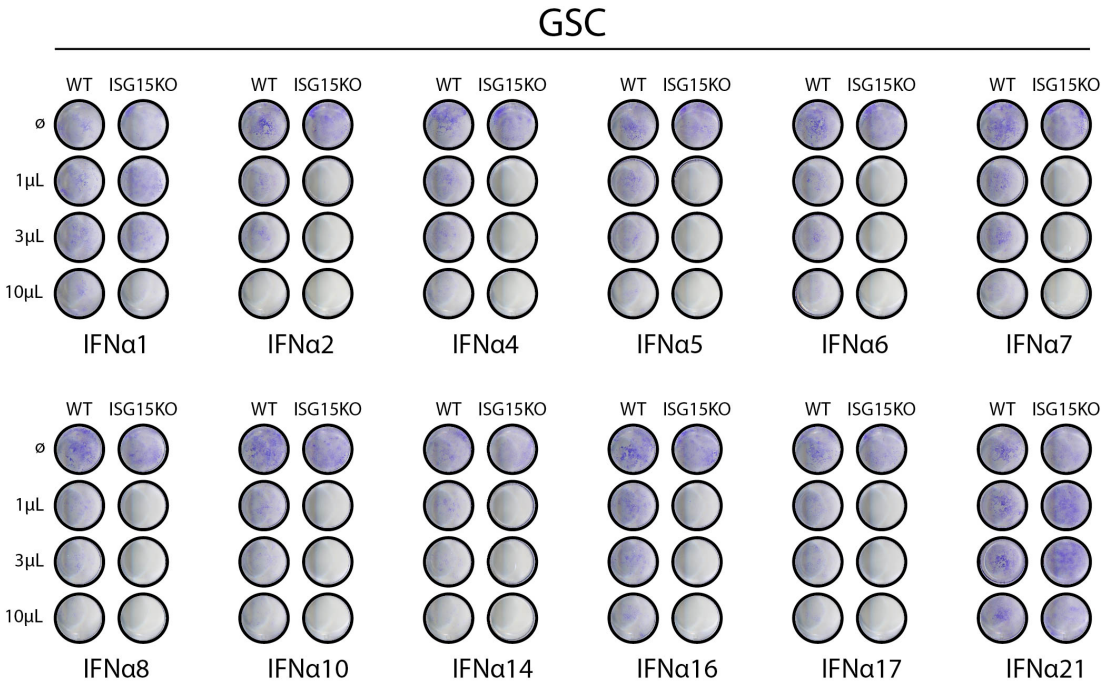

Figure 4.14: Colony formation assay on WT and ISG15$^{-/-}$ GSC mixed population pools untreated and treated with different secreted IFNα subtypes with triplicates of each condition. First row of each group represents an example well of the untreated samples, while second to fourth rows represent an example well of the treated wells. 1, 3 and 10 μL treatments translate to final concentrations of 0.3 ng/mL, 0.9 ng/mL and 3 ng/mL respectively.

Seeding inaccuracies and differences in cell growth rate could led to different densities even in untreated KO vs WT wells, making the comparison between the IFNα effect in WT vs KO more difficult specially on the samples treated with the most active subtypes. To overcome this issue, the mean absorbance of each triplicate treated sample (0.3, 0.9 and 3 ng/mL) was divided by the mean absorbance of the triplicate untreated sample. This way, a ratio between the untreated baseline and each treated sample was obtained in both WT and KO in each IFNα subtype group. Plotting these ratios together, when the untreated ratio of both cell lines is 1 (untreated baseline/untreated baseline) made the comparison of the effect of each different interferon in WT vs KO much easier (Figure 4.15).

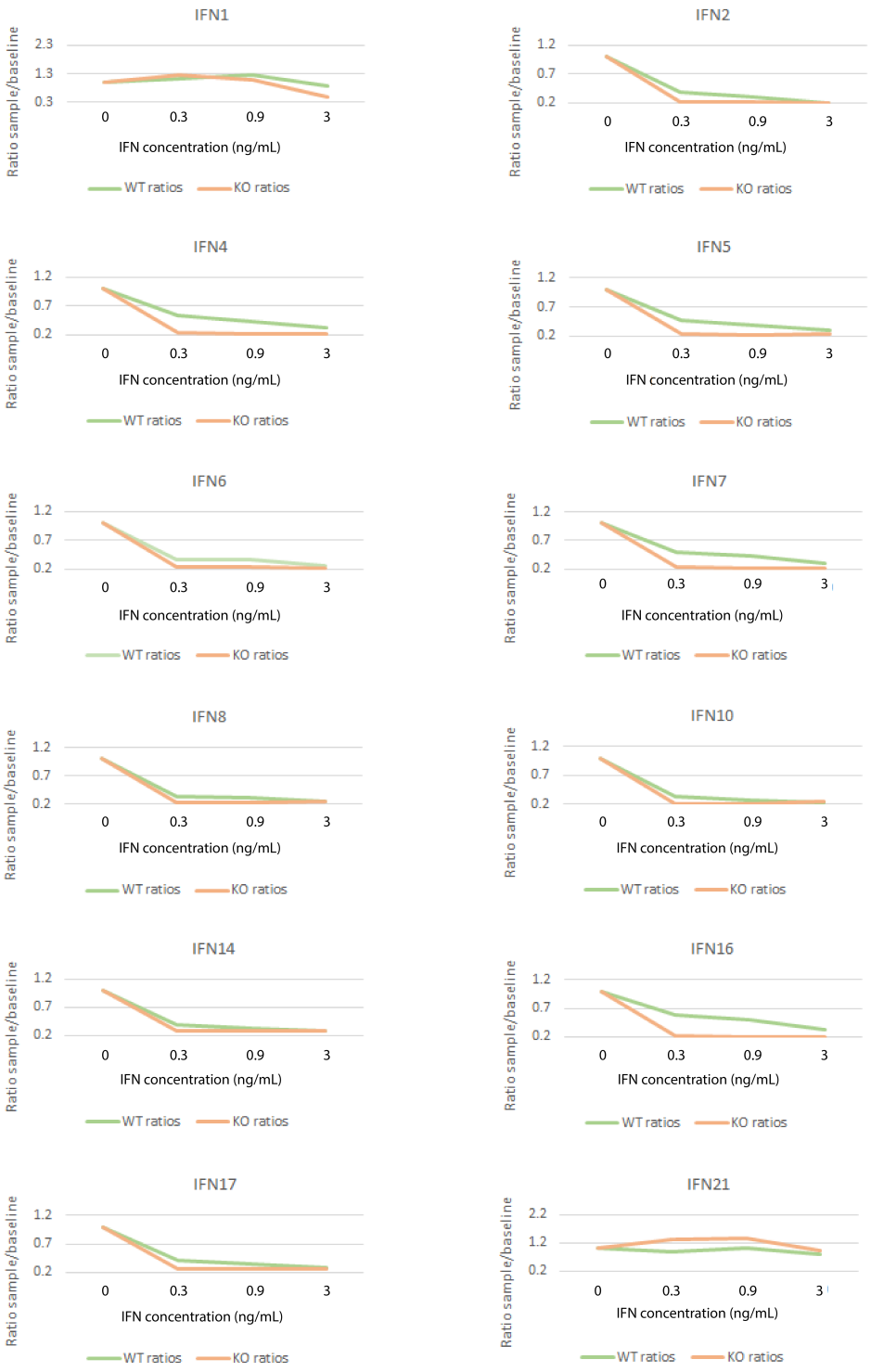

Figure 4.15: Treated sample to untreated baseline (triplicates') mean absorbance ratios for each treatment concentration on GSC ISG15 KO mixed population pools treated with IFNα subtypes. These absorbances were obtained at 595 nm after dissolving the colony formation assays shown in Figure 4.15. The untreated ratio in both WT and KO samples is 1 (the triplicate's mean absorbance of the untreated baseline divided by the triplicate's mean absorbance of the untreated baseline), making comparison between the effect of each IFNα subtype in the WT and ISG15 KO GSC cell lines easier.

Caki-1

In collaboration with Dr. Christine Tait-Burkard and Alison Daniels (see subsection 3.4.3), the generated ISG15 KO mixed population Caki-1 pool was also used to further test if the growth sensitivity to IFNα observed in ISG15 KO SiHa and GSC cells was consistent across other cancer model cell lines. The use of IFNα14, one of the most active IFNα subtypes (Figure 4.15), was requested by collaborators. Results seen in Figure 4.16a show that indeed, the ISG15 KO mixed population pool was more sensitive to IFNα than the WT Caki-1 cells. The absorbance readings after dissolving the stained colonies and the treated sample to untreated baseline ratios are shown in Figure 4.16b, quantitatively confirming the sensitivity of the ISG15 KO cells.

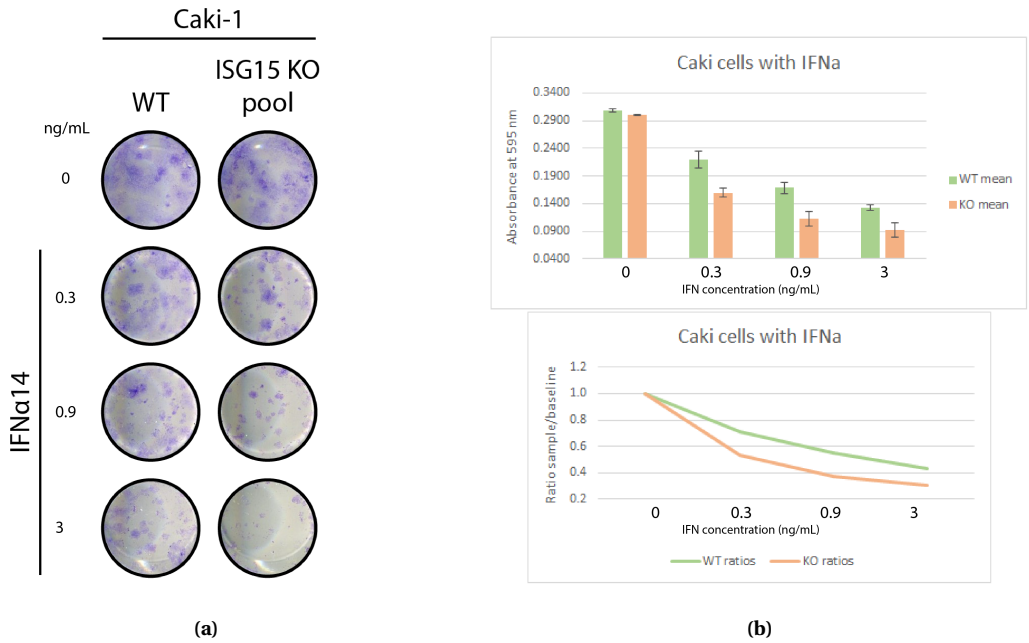

(a) **(b)**

Figure 4.16: a) Colony formation assay on the Caki-1 WT and ISG15 KO mixed population cells treated with 1, 3 or 10 μL secreted IFNα14, resulting in an approximate final concentration of 0.3 ng/mL, 0.9 ng/mL and 3 ng/mL. Each condition was plated in technical triplicates. **b)** Quantification of the colony formation assay by stain dissolution and absorbance reading at 595 nm. Upper graph shows the mean absorbance of each condition's triplicates. The error bars equal to standard deviation. The lower graph shows the absorbance ratios of each treated sample to the untreated baseline (using the mean absorbance of each triplicated condition).

4.4.4 Restoring the expression of ISG15 in isogenic cell lines

After confirming the sensitivity of ISG15 KO cells to IFNα in three different cancer model cell lines, the reinsertion of ISG15 in the genome of knocked out cells was attempted to test if the resistance to IFNα was rescued once the expression of ISG15 was restored. To

this end, ISG15 KO SiHa clone #1 was first selected for transfection with pT-REX-Dest30 plasmids containing V5 tagged wild-type (WT) and mutated ISG15 (AA), as described in subsection 4.3.4. Positively transfected cells that had integrated the plasmid in their genome were selected using Geneticin for 3 to 4 weeks, as described in subsection 4.3.4. The control plates containing the untransfected and GFP transfected cells died at day 6. An additional control was generated by transfecting the cells with the pT-REX-Dest30 empty vector (EV). Expression of the stable cell lines was validated by immunoblotting with and without IFNα treatment. For this, protein from the same samples was loaded in two different SDS-PAGE gels, resulting in two identical membranes. One of these was blotted for ISG15 and the other one was blotted for V5. Figure 4.17 shows that the cell lines generated with pT-REX-Dest30 WT and AA successfully expressed ISG15 even in the absence of IFN treatment. As expected, the cell lines generated with the empty vector did not show any ISG15 expression. Thanks to the higher affinity of the V5 antibody, a protein ladder can be seen in the line corresponding to the samples transfected with the wild-type version of ISG15, showing that it is capable of ISGylating. The absence of a protein ladder in the samples generated with the mutated cDNA proved that the expressed ISG15 was incapable of conjugating to other proteins. Although both the ISG15 variants were expressed regardless of treatment, it can be observed that the intensity of the ladder in the treated wild-type sample is slightly higher in the IFN treated samples.

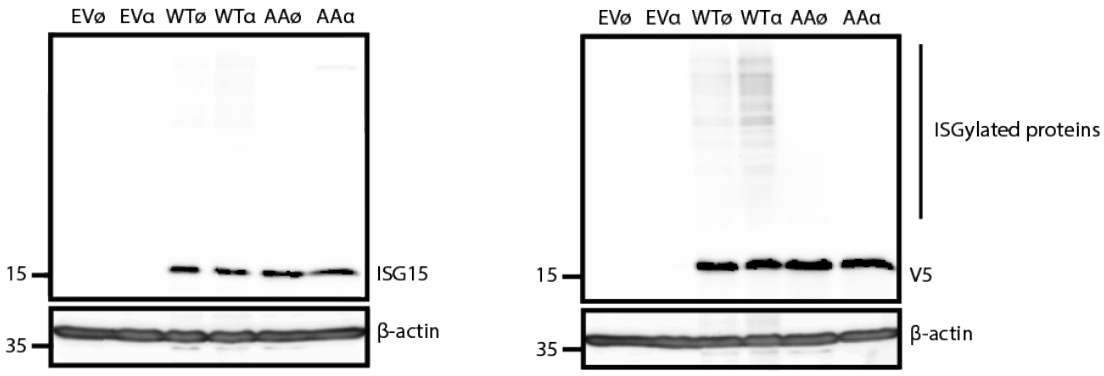

Figure 4.17: Immunoblots on stable cell line generated by transfecting pT-REX-Dest30 plasmids containing cDNA encoding ISG15 on isogenic ISG15$^{-/-}$ SiHa clone #1. Two different cell lines were generated by transfecting the cells with cDNA encoding wild-type ISG15 (WT) and a mutated version of ISG15 incapable of ISGylating (AA). An additional control cell line was generated by transfecting the cells with the pT-REX-Dest30 empty vector (EV). Equal amounts of protein (40 μg) from whole cell lysate were loaded per lane in two 15% SDS-PAGE gels followed by immunoblotting. One of the membranes (left) was developed using anti-ISG15 antibody (Santa Cruz Biotechnology (#166755) at 1:1000 in milk) followed by anti-β-actin antibody (Sigma (#A2228) at 1:1000 dilution) and the other one (right) was developed using anti-V5 antibody (Abcam (#ab27671) at 1:1000 dilution) followed by anti-β-actin antibody (Sigma (#A2228) at 1:1000 dilution). IFNα treatment concentration was 100 U/mL in all treated samples for 24 hours.

Once wild-type and mutated ISG15 expression was validated by immunoblotting in clone #1, the three stable cell lines (empty vector (EV), wild-type (WT) and mutated (AA)) were used for a colony formation assay in the presence of Geneticin (800 μg/mL), treating the cells with IFNα14. This subtype was selected for a preliminary study due to its higher activity level (Figure 4.15). Results in Figure 4.18 show that the recovery of ISG15 in the ISG15$^{-/-}$ did not rescue any resistance to IFNα14.

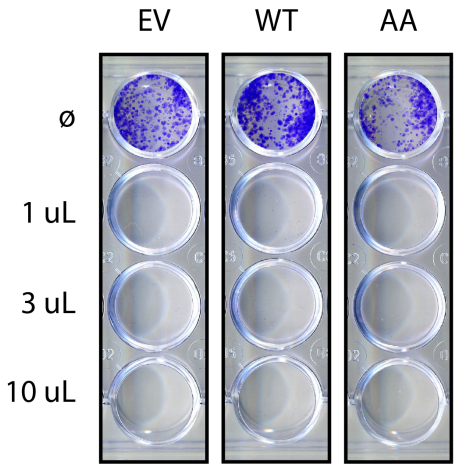

Figure 4.18: Colony formation assay on validated stable cell lines expressing wild-type and mutated ISG15. The stable cell lines were generated transfecting clone #1 with the pT-REX-Dest30 empty vector (EV), used as a control, and the same vector containing cDNA for a wild-type ISG15 (WT) and a mutated version of ISG15 (AA) incapable of ISGylating. Cells were grown in media containing 800 μg/mL Geneticin and treated with 1, 3 or 10 μL secreted IFNα14, resulting in an approximate final concentration of 0.3 ng/mL, 0.9 ng/mL and 3 ng/mL. Each condition was plated in technical triplicates.

Since the knocking out of ISG15 in clone #1 was the result of the off-target effect of a failed tag insertion, the generation of a new range of stable cell lines was attempted using an ISG15$^{-/-}$ clone whose edits had been characterised. For this, ISG15 KO clone #10 was selected. Following the same method described in subsection 4.3.4, three new cell lines (EV, WT and AA) were obtained from the transfection and selection of clone #10. Again, expression of ISG15 was confirmed by immunoblotting using anti-ISG15 and anti-V5 antibodies (see Figure 4.18), and the higher affinity of the V5 antibody allowed the detection of ISGylated proteins in the WT cell line regardless of IFN treatment.

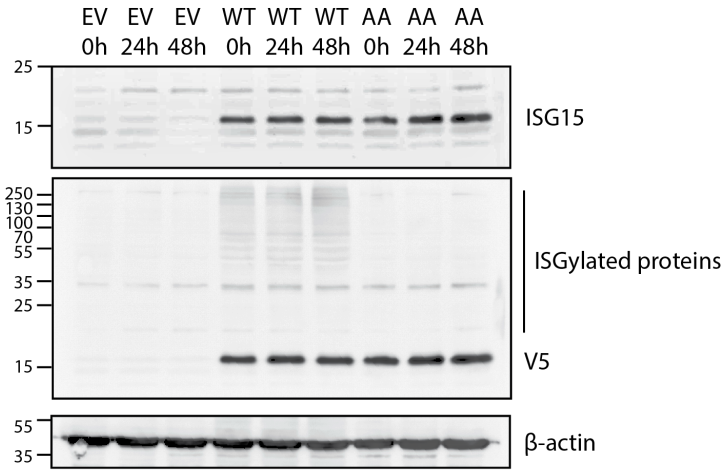

Figure 4.19: Immunoblots on stable cell line generated by transfecting pT-REX-Dest30 plasmids containing cDNA encoding ISG15 on isogenic ISG15$^{-/-}$ SiHa clone #10. Two different cell lines were generated by transfecting the cells with cDNA encoding wild-type ISG15 (WT) and a mutated version of ISG15 incapable of ISGylating (AA). An additional control cell line was generated by transfecting the cells with the pT-REX-Dest30 empty vector (EV). Equal amounts of protein (50 μg) from whole cell lysate were loaded per lane in two 15% SDS-PAGE followed by immunoblotting. The membranes was developed using anti-ISG15 antibody (Santa Cruz Biotechnology (#166755) at 1:1000 in milk) followed by anti-β-actin antibody (Sigma (#A2228) at 1:1000 dilution). IFNα treatment concentration was 100 U/mL in all treated samples.

Once wild-type and mutated ISG15 expression was validated by immunoblotting in clone #10, the three stable cell lines (empty vector (EV), wild-type (WT) and mutated (AA)) were used for colony formation assays. Although IFNα14 had been chosen before due to its high activity level, its potent growth inhibitory properties also affect the growth of wild-type cells fully expressing ISG15. In order to be able to better discern the effect caused in WT vs ISG15 KO cells, another two subtypes were selected to make sure that the results shown in Figure 4.18 were not just the effect of IFNα14 being excessively active. At the same time, SiHa WT and clone #10 cells were used as control. Results in Figure 4.20 show that indeed, the recovery of the ISG15 expression in the ISG15$^{-/-}$ clone #10 did not rescue the resistance to any of the three IFNα subtypes tested, regardless of the ability of ISG15 to conjugate. To compare the effect of each subtype on each of the stable cell lines and the controls, the stain in the colonies was dissolved using a 10% acetic acid solution and absorbance was measured at 595 nm. As before, the treated sample to untreated baseline ratios were calculated and plotted, using the mean absorbance of the triplicated samples (Figure 4.20b).

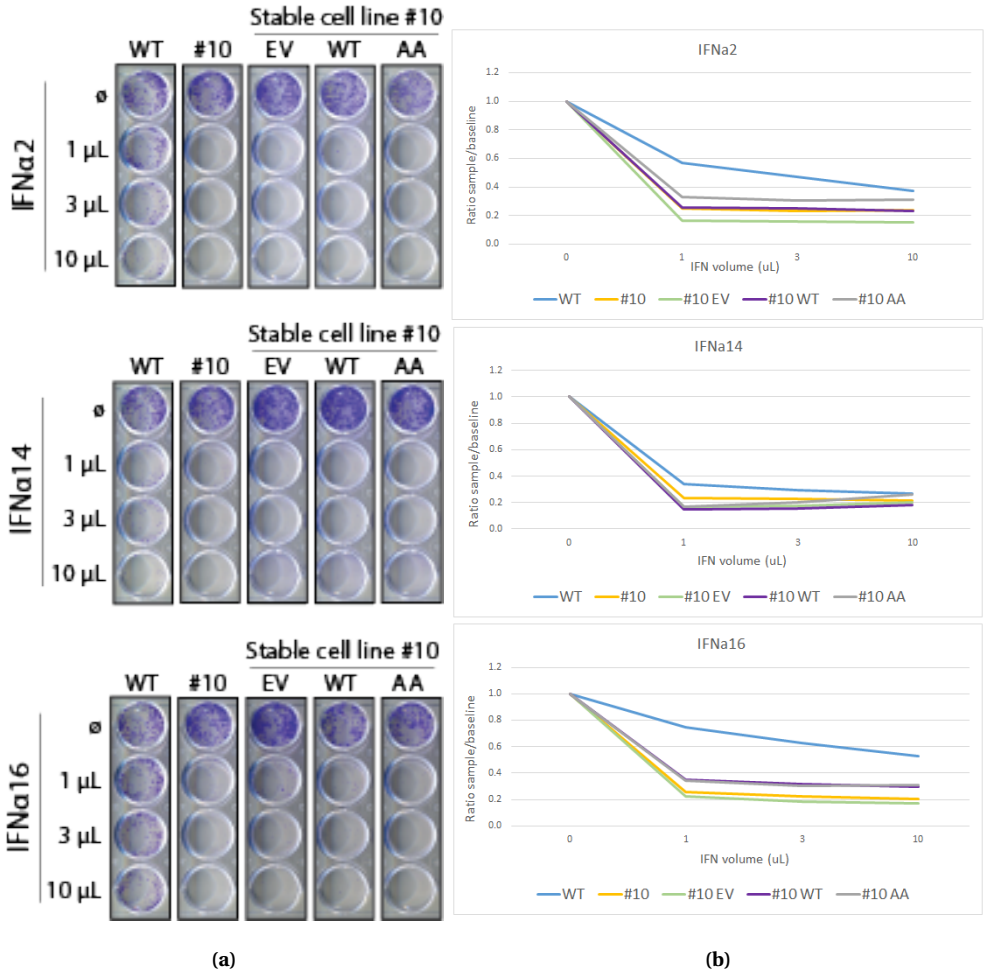

(a) **(b)**

Figure 4.20: Colony formation assay on stable cell lines generated on clone #10 expressing wild-type and mutated ISG15, treated with secreted IFNα2, 14 and 16. The stable cell lines were generated transfecting clone #10 with the pT-REX-Dest30 empty vector (EV), used as a control, and the same vector containing cDNA for a wild-type ISG15 (WT) and a mutated version of ISG15 (AA) incapable of ISGylating. **a)** Cells were grown in media containing 800 μg/mL Geneticin and treated with 1, 3 or 10 μL (final concentration of 0.3 ng/mL, 0.9 ng/mL and 3 ng/mL respectively) of either secreted IFNα2, IFNα14 or IFNα16. SiHa WT and untransfected clone #10 cells were used as controls. Each condition was plated in technical triplicates. **b)** The stained colonies were dissolved in a 10% acetic acid solution and the absorbance was read at 595 nm. The treated sample to untreated baseline ratios were calculated and plotted, using the mean absorbance of the triplicated samples, for easier comparison of the effect of each IFNα subtype in the controls vs the stables.

Finally, because most of the initial experiments and clonogenic assays were performed with commercial IFNα2, a last set of colony formation assays were performed in both stable cell line groups (generated from clone #1 and generated from clone #10) to confirm that the recovery of the expression of ISG15 does not rescue the resistance to IFNα. As seen in Figure 4.21 and Figure 4.22, the recovery of the expression of ISG15, both in its wild-type and mutated forms, does not rescue the resistance to IFNα observed in the SiHa WT cells (see Figure 4.9 and Figure 4.11).

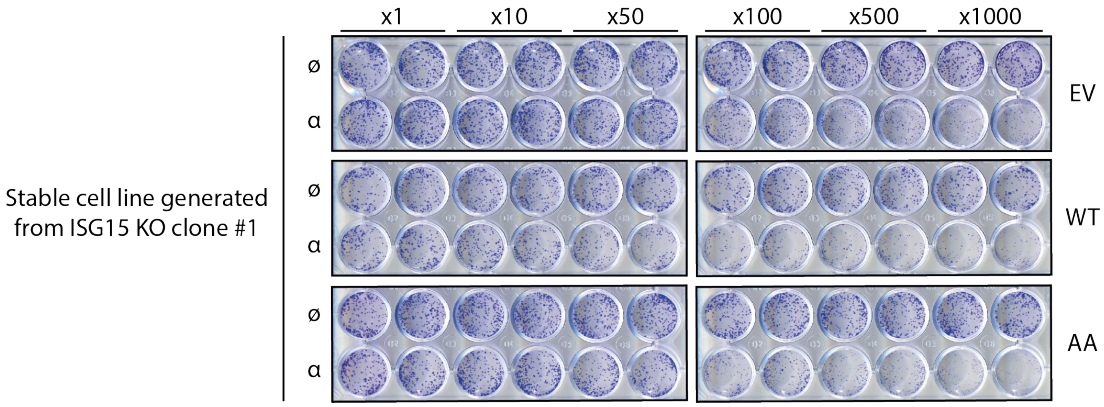

(a)

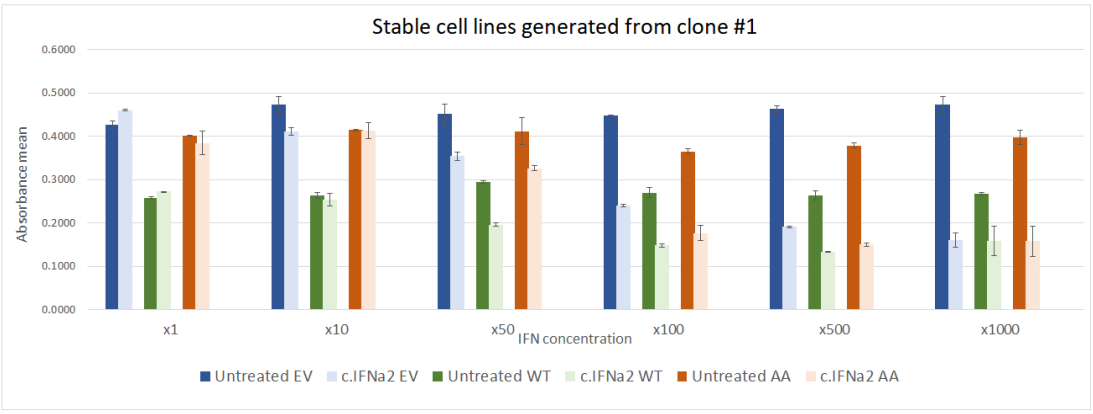

(b)

Figure 4.21: Colony formation assays on stable cell lines generated on clone #1 expressing wild-type and mutated ISG15 treated with commercial IFNα2. The stable cell lines were generated transfecting clone #1 with the pT-REX-Dest30 empty vector (EV), used as a control, and the same vector containing cDNA for a wild-type ISG15 (WT) and a mutated version of ISG15 (AA) incapable of ISGylating. **a)** Upper row of each cell line is untreated, while the lower one is treated with increasing concentrations of commercial IFNα where x1 equals to 1 U/mL, with each condition plated in duplicates. **b)** The stained colonies were dissolved in a 10% acetic acid solution and the absorbance was read at 595 nm. The mean and standard deviation of each pair of duplicates are shown for each treatment condition and concentration. Linear regression statistical analysis performed on untreated and c.IFNα2 treated EV, WT and AA stable cell lines in clone #1 showed highly significant differences between the samples (p-value < 0.0001). Complete analysis results are available in Table B.10, Table B.11 and Table B.12.

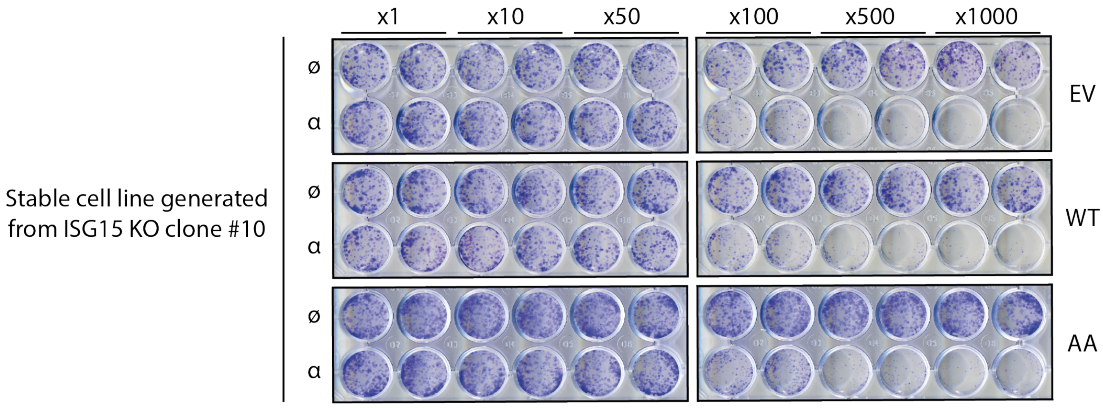

(a)

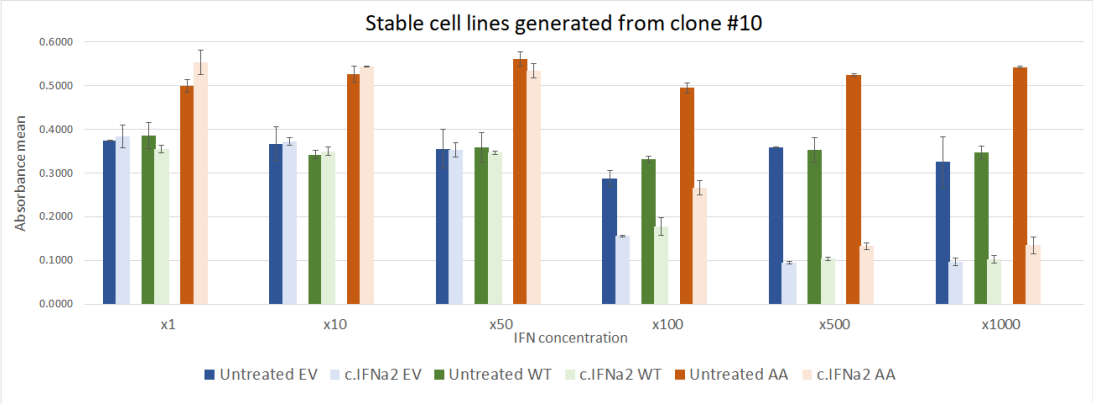

(b)

Figure 4.22: Colony formation assays on stable cell lines generated on clone #10 expressing wild-type and mutated ISG15 treated with commercial IFNα2. The stable cell lines were generated transfecting clone #10 with the pT-REX-Dest30 empty vector (EV), used as a control, and the same vector containing cDNA for a wild-type ISG15 (WT) and a mutated version of ISG15 (AA) incapable of ISGylating. **a)** Upper row of each cell line is untreated, while the lower one is treated with increasing concentrations of commercial IFNα where x1 equals to 1 U/mL, with each condition plated in duplicates. **b)** The stained colonies were dissolved in a 10% acetic acid solution and the absorbance was read at 595 nm. The mean and standard deviation of each pair of duplicates are shown for each treatment condition and concentration. Linear regression statistical analysis performed on untreated and c.IFNα2 treated EV, WT and AA stable cell lines in clone #10 showed highly significant differences across the samples (p-value < 0.0001). Complete analysis results are available in Table B.13, Table B.14 and Table B.15.

4.5 Discussion

The results presented in this chapter suggest that ISG15 is related with cellular resistance to the anti-proliferative properties of IFNα. The results of the cell cycle experiments combined with the real-time growth assays performed on SiHa WT and ISG15$^{-/-}$ cells show

that this is due to a significant IFNα dose dependant G1 cell cycle arrest, with a consequent inversely proportional decrease in the percentage of cells in S phase. Seeing these results (Figure 4.6), it would be expected that G2/M also showed the same escalated decrease as the concentration of the treatment increased, but this is not as noticeable as in G1 and S phases. It could be argued that some of the cells could not bypass the S checkpoint and died before entering G2/M, resulting in an increased number of cells in the subG1 phase. However, the increased amount of cells in subG1 phase in ISG15$^{-/-}$ cells when compared to WT cells does not follow the steady and directly/inversely proportional shift observed in the G1 and S phases respectively. Results of the detection of activated apoptotic caspases showed no significant increase or IFN dependent change on the number of apoptotic cells in ISG15 deficient cells compared to the WT cells, suggesting that the results observed in the subG1 gating of the ISG15$^{-/-}$ are not caused by the depletion of ISG15 or the increase of IFN concentration. The percentage of apoptotic cells in all the samples analysed for activated caspases 3 and 7, regardless of cell line or treatment, ranged between 0.9% and 1.5%. Although the WT cells showed a slight steady increase of apoptotic cells of 0.3% as the IFNα treatment increased, results from cell proliferation, cell cycle and colony formation assays suggest that this increase is not significant and more likely to be a casualty, since no difference was appreciated in the WT cells across treated samples in any of these assays. These results are consistent with the subG1 gating in the cell cycle assay, which showed similar percentages with 1% of the cells falling in this gate in the untreated WT sample, and 0.8%, 1.4% and 1.2% of the cells being in the subG1 gate as the treatment increased (50 U/mL, 100 U/mL and 500 U/mL respectively). Results by Rosewicz *et al.* (2004), who studied the effect of IFNα on the proliferation of WT human neuroendocrine tumour cell lines, show the same dose dependant cell growth inhibition seen in the experiments presented in this chapter. They treated WT QGP1 and BON cells with 100, 500 and 1000 U/mL IFNα, concentrations very similar to the ones used here (50, 100 and 500 U/mL). Similarly, Pinto-Fernandez *et al.* (2021) analysed cell growth rate of USP18$^{-/-}$ HAP1 cells (derived from human chronic myelogenous leukaemia cell line) with and without IFNα treatment (1000 u/mL) and described very similar results to the ones presented here. While both the WT and USP18$^{-/-}$ cells showed the same growth rate when untreated, IFN treatment resulted in a significant growth rate decrease in USP18$^{-/-}$ cells, but not in WT cells. This suggests that the responsible for the phenotypes described in this chapter is the loss of ISG15 and the subsequent instability of USP18, resulting in the amplification of the IFN pathway. Though the antiproliferative effects of IFNα have been widely described, the data presented here shows that IFN resistant cancer cell lines could benefit from ISG15 and USP18 targeting drugs to re-sensitise cells to treatment.

Effects of ISG15 in cellular proliferation were described by D'Cunha *et al.* in 1996, when they tested if the addition of ISG15 to B-depleted peripheral blood lymphocytes promoted proliferation. Their results suggested that addition of human ISG15 increased cell pro-

liferation in a dose dependant manner, while the use of antibodies specifically targeting ISG15 or heat denaturing the added ISG15 resulted in the proliferation level going back to the baseline levels. Further research showed that this increase was mainly the result of expansion of NK cell levels, recording no significant proliferation level in T cells, but they did not further research the mechanistic origin of these events and their relation with the cell cycle progression. More recent work by Vuillier *et al.* (2019) suggests that ISG15 and USP18 have an important role in regulating SKP2, the substrate recognising subunit of a larger E3 ligase complex (known as SCF^{SKP2}), responsible of promoting the entry of cells into S phase by targeting several elements that negatively regulate cell cycle progression. According to their results, these three proteins form a three way regulating pathway: SKP2 is capable of targeting USP18 for its degradation, free ISG15 is capable of interfering in this interaction binding to USP18, which destabilises SKP2 and accumulates USP18, and over-expressing ISG15 results in SKP2 (which they also proved can be weakly ISGylated) being more prone to proteasomal-mediated degradation. They showed that the levels of both ISG15 and USP18 were highest at G1 to S phase and decreased as cells progressed to G2/M, but when analysing USP18-silenced cells they arrested at G1, also had a reduced level of SKP2 and presented twice to three times the level of apoptotic cells compared to the controls. After rescuing USP18, expression of SKP2 increased again, showing that USP18 has a key role on cell cycle progression stabilising SKP2. Having shown that free ISG15 is capable of stabilising and accumulating USP18, they concluded that that the level of these two proteins in the cell are a key elements in the determination of the reduction of SKP2, and thus in cell cycle progression. Consistent with the results presented here, they reported that the silencing by siRNA of either ISG15 or USP18 (independently) lowered the expression of SKP2 under IFNβ treatment, which would result in G1 arrest. It would be interesting to check the levels of SKP2 on ISG15 deficient cells with and without IFN type I treatment to further research if it is involved in the mechanistic of the G1 arrest presented in ISG15$^{-/-}$ SiHa cells upon IFNα treatment.

G1 arrest resulting from the silencing of USP18 had been described before - Cai *et al.* (2017) observed that human hepatocellular carcinoma cells showed a significant proliferation reduction when transfected with shRNA targeting USP18, while overexpression promoted proliferation. Further investigation unveiled that the silencing of USP18 lead to cell cycle arrest at G1 and increased the number of apoptotic cells. The difference in the level of apoptotic cells following cell growth arrest in USP18$^{-/-}$ and ISG15$^{-/-}$ cells could be due to an ISG15-independent role for USP18. To check this, the levels of activated caspases could be analysed in WT and ISG15 KO cells with and without siRNA targeting USP18, or knocking out USP18 in already ISG15 knocked out cells. Upregulation of both ISG15 and USP18 in liver tissue samples has been repeatedly observed in patients with chronic hepatitis C virus (HCV) infections that do not respond to IFN based therapies (Chen *et al.*, 2011). Chen *et al.* (2005) used gene expression profiling to study liver biopsy samples,

taken before treatment, to be compared between responders and non-responders. Using this method, they were able to identify 18 genes whose expression significantly varied between the two groups, most of which were IFN responsive genes. Further analysis identified a subset of these that allowed treatment response prediction in 30 of 31 patients, regardless of their viral load, disease activity, or fibrosis state, which included ISG15 and USP18. Further studies of this team (Chen *et al.*, 2010; Li *et al.*, 2019) led to the conclusion that the upregulation of these two proteins results in non-responsiveness to IFNα treatment, with USP18 working in an isopeptidase-independent manner. Interestingly, cases in which the ISGylation of specific substrates enhances the tumour suppressive activity of type I IFN have been described. Yoo *et al.* (2018) demonstrated that ISG15 is capable of conjugating to the carboxyl terminus of Hsp70-interacting protein (CHIP) upon IFNα treatment, an E3 ligase with an important role in protein homeostasis. They proved that in A549 lung cancer cells the ISGylation of CHIP stimulates its activity, resulting in decreased levels of c-Myc due to increased ubiquitination and thus inhibiting tumour growth, which contrasts with the results shown in this chapter.

Human IFNα has 13 subtypes, all of which have similar sequences and structures and bind through the type I IFN receptor IFNAR. Nevertheless, the different subtypes have been shown to trigger different biological responses, which could be explained by the fact that each of them bind to the receptor subunits with different affinities and activating subtly different downstream signalling cascades (Gibbert *et al.*, 2013). Lavoie *et al.* (2011) analysed the binding affinities, antiviral and anti-proliferative activities of the human IFNα subtypes and compared them to the conventionally used IFNα2, revealing that IFNα7, -α6, -α17 and -α10 bind with higher affinity to IFNAR2 than IFNα2, and -α5 and -α21 bind with weaker. When analysing the affinities towards IFNAR1, all of them bind with higher affinity than IFNα2 except -α10 and -α17. They could not accurately determine the binding affinity of IFNα1 because of the affinity was weak, and unsurprisingly resulted in it being the one with weaker antiviral and anti-proliferative activities. They also showed that the binding affinity was related with the anti-proliferative activity of each subtype, concluding that IFNα1 had the weakest activity and IFNα14 the highest, but not with the antiviral activity. The difference in receptor binding affinity can be appreciated in the colony formation assays presented in Figure 4.14. Consequent with the results presented by Lavoie *et al.*, IFNα1 and -α21 are the subtypes with weakest anti-proliferative properties, while IFNα8, -α10 and -α14 have the highest. It must be born in mind that when very active IFN subtypes like these completely arrested cell growth in both WT and KO wells (especially in those treated with higher volumes of IFN), the ratio of these samples divided by the baseline absorbance would result in the same value. In these cases, the ratios of samples treated with lowest concentration are the most informative ones. Different type I IFNs can result in different ISG15 expression levels even though they signal through the same receptor, as demonstrated by Kunzi & Pitha who showed that the expression of ISG15 was

indeed higher after treating peripheral blood mononuclear cells with IFNω rather than with IFNα2. Thus, it would be of interest to analyse the expression level of ISG15 upon treatment with the different IFNα subtypes.

In order to confirm that the absence of ISG15 is indeed the cause of the sensitivity to IFNα observed in SiHa, GSC and Caki-1 cells, as suggested by the evidence provided in this chapter, the restoration of the ISG15 expression was attempted, and expression recovery was confirmed by immunoblot. The protein ladder observed in the stable cell lines generated by transfecting WT ISG15 cDNA (Figure 4.17 and Figure 4.19), which are absent in the EV and AA samples, suggest that the expressed WT ISG15 is able of successfully conjugate to other proteins, while the mutated version is not. Even though expression of WT ISG15 capable of ISGylating has been restored in two different ISG15$^{-/-}$ cell lines (clone #1 and #10), the resistance to IFNα presented in SiHa WT cells was not rescued. Figure 4.18, Figure 4.20, Figure 4.21 and Figure 4.22 all show that the stables cell lines generated transfecting WT ISG15 cDNA did not rescue the resistance to IFNα, nor did the ones generated by transfecting mutated ISG15 cDNA. Having proven that the restored ISG15 is indeed capable of conjugating to other proteins and the resistance to IFNα is still not rescued, it could be hypothesised that the ISGylating role of ISG15 is not involved in the resistance to IFNα, which is rather mediated by the free ISG15. Since the activity of the free ISG15 could not be confirmed in the experiments presented in subsection 4.4.4, it cannot be confirmed that this role is restored in the stable cell lines generated on clone #1 nor #10. Although the V5 tag is a very small peptide of only 14 residues, its presence in the N-terminus of the ISG15 cDNA could be sufficient to impair the proper folding of the protein or to interfere with the binding sites required to trigger the resistance phenotype. As detailed in section 1.3, Swaim *et al.* (2017) identified the key surface residues required for the free ISG15 to interact with NK cells to trigger the induction and secretion of IFNγ, all of which were on the C-terminal lobe of ISG15. However, later in 2020, the same group studied which residues were critical for the cellular secretion of ISG15, finding that at least L72, S83 and L85 are essential for this role (Swaim *et al.*, 2020). As seen in Figure 4.23a, S83 and L85 are located in the C terminal lobe of ISG15, while L72 is in the N-terminal lobe. The first 9 amino acids of the ISG15 sequence (MGWDLTVKM) are shown in blue to illustrate the proximity of the N-terminal, where the V5 tag would be, to one of the residues essential for the secretion of ISG15 - L72. Figure 4.23b shows a potential interaction between K8 on the first β-strand and L72. If the insertion of the V5 tag resulted in such missfolding or in the blockade of an important binding site in the N-terminal lobe that prevented its recognition by the binding proteins involved in translating the ISG15 signal, it could impair the function of the free ISG15 without affecting its ability to conjugate to other proteins. Technology to predict protein folding has come very far in the last couple of years. Artificial intelligence like the one found in neural network-based models such as AlphaFold can successfully predicting the three dimensional structure that a protein would take, based exclusively on

its amino acid sequence (Jumper *et al.*, 2021). AlphaFold includes over 360,000 predicted structures across the proteomes of many different model organisms, but it does not accept external sequences to predict their folding at the moment (Varadi *et al.*, 2022). Such technology could be used to predict if the insertion of the V5 tag in the N-terminus of the ISG15 sequence affects its folding, or if it blocks any particular site. Another possibility is that having removed the introns from the transfected cDNA, some essential regulatory elements had been altered, affecting the way free ISG15 works. At the same time, must be borne in mind that when the cDNA is transfected into the cells, the exact location in the genome where it gets reinserted cannot be predetermined, which could also have an effect in how this protein and its expression get regulated.

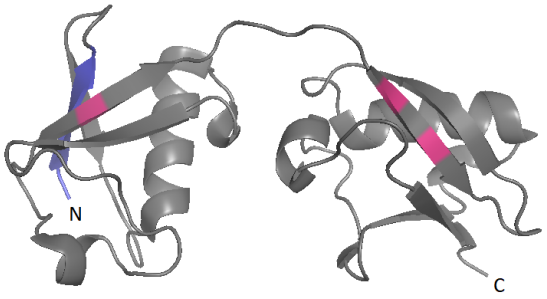

(a)

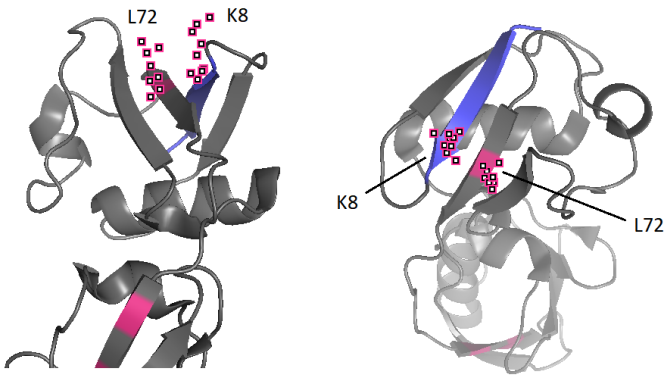

(b)

Figure 4.23: Identification of the surface residues of ISG15 required for its secretion and the potential interaction between K8 and L72 in ISG15 (PDB 1Z2M). **a)** ISG15 structure highlighting the surface residues required for its secretion identified by Swaim *et al.* (2020) (L72 in the N-terminal lobe and S83 and L85 in the C terminal lobe, shown in red), and the first 9 amino acids (shown in blue) to illustrate the proximity of the N-terminal (where the V5 tag is in the cDNA used for expression restoration) from one of the residues essential for secretion. **b)** Potential interaction between K8 in the N terminal and L72, a residue critical for ISG15 secretion, to demonstrate how the disruption of the correct folding of the N-terminal could potentially affect the secretion and role of free ISG15 without affecting its ISGylating capacity.

The inability to restore phenotypes observed in cell-lines expressing WT ISG15 in ISG15$^{-/-}$ has previously been described. As mentioned in subsection 1.3.2, Alcalá *et al.* (2020) knocked out ISG15 from pancreatic cancer stem cells after proving that ISG15 promotes self-renewal, migration, and tumorigenesis in these cells, properties that were mitigated in the KO cell line. However, treatment of the cells with free recombinant ISG15 did not rescue these phenotypes nor the ISGylation capacity, suggesting that conjugated and not free extracellular ISG15 was responsible for the phenotypes they were studying. They were able to support this hypothesis with partial restoration of the tumourgenic potential of one of the cell lines used through the overexpression of intracellular ISG15 transfecting a V5-tagged ISG15 construct. Although further research would be required to elucidate what is the reason for the failed phenotype recovery in the experiments presented in this chapter, the fact that it has been identified in multiple cell lines suggest that the loss of ISG15 is the responsible for the increased sensitivity to IFN.

Chapter 5

Analysis of the proteomic landscape of ISG15$^{-/-}$ cervical cancer cells employing isotopically labelled amino acids in cell culture (SILAC)

5.1 Introduction

Mass spectrometry (MS) is an analytical technique used to measure the mass to charge ratio of different ions, which allows for the identification of fragments of thousands of different proteins within a complex biological sample, thanks to genome sequence databases. This powerful technique, developed in the 1990s, revolutionised proteomic analysis in the field of biology. From analysing and identifying gel separated proteins (Lahm & Langen, 2000) to identifying protein-protein interactions (Ewing *et al.*, 2007), the coupling of mass spectrometry to different techniques opened a new era for the field.

First described in the early 2000s, stable isotope labelling by amino acids in cell culture (SILAC) is a MS-based technique in which growth medium containing specific stable isotope labelled amino acids is used to culture cells (Ong *et al.*, 2002; Ong & Mann, 2006). As shown in Figure 5.1, cells incorporate these amino acids into proteins during synthesis, leading to an ultimate protein-mass slightly higher to that in the same protein synthesised using common (light) medium containing natural isotopes. The complete labelling of the proteome is achieved after five cell doublings in labelled media. When these proteins get digested, the fragmented peptides can be precisely identified using MS, allowing separation of proteins synthesised exclusively with light media and proteins synthesised with la-

belled media. This allows for a comparative proteomic approach, in which one particular sample is grown with light media and another one is grown with labelled media and, after collecting the cells, the samples can be mixed and analysed together. Adaptations from the standard technique lead to different variants of SILAC, such as pulse SILAC (pSILAC) and dynamic SILAC (Figure 5.2). While the standard SILAC technique mixes the population of two samples, labelled and unlabelled, to analyse the relative changes in protein levels, pSILAC allows the comparison of the relative changes in protein synthesis by growing previously unlabelled cells in two different labelled medias (medium and heavy) before the analysis. Dynamic SILAC, on the other hand, collects samples at different timepoints after changing the media from unlabelled to labelled (or vice versa) to analyse the protein turnover by determining the degradation and synthesis times.

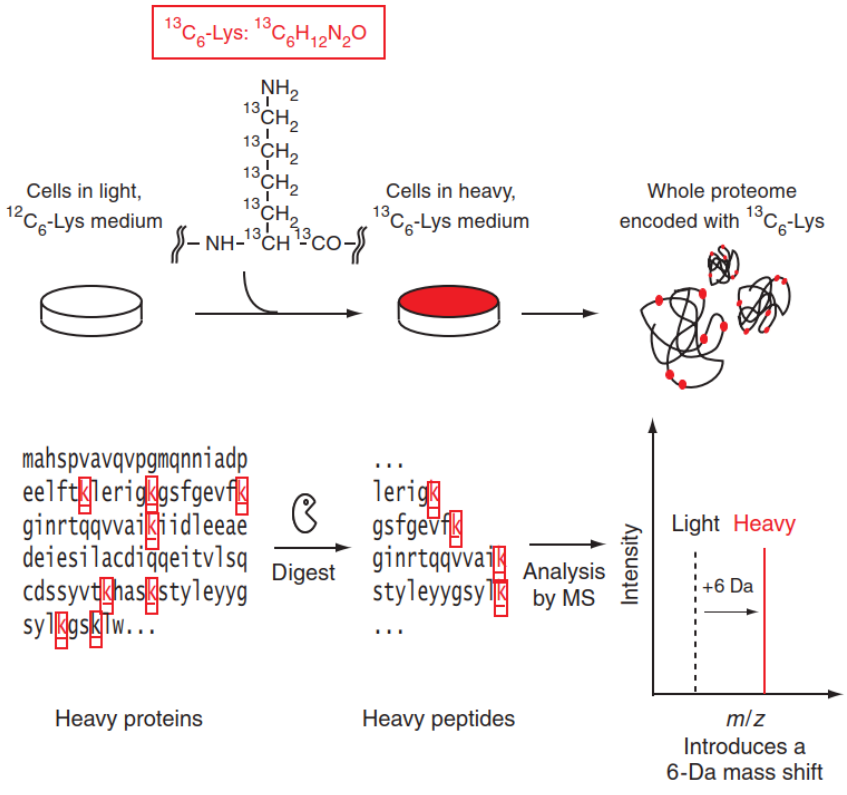

Figure 5.1: Protein labelling mechanism with SILAC, edited from Ong & Mann (2006). Cells growing in common light media containing natural isotopes are subcultured in heavy media containing stable isotope labelled lysine residues. As cellular reservoir of light lysine gets exhausted, heavy lysine is picked up from the media for metabolic incorporation into newly synthesised proteins, resulting in the spread of the heavy label throughout the proteome. The mass shift in the digested fragmented peptides can be precisely analysed my mass spectrometry, distinguishing and identifying the proteins with the isotope-labels.

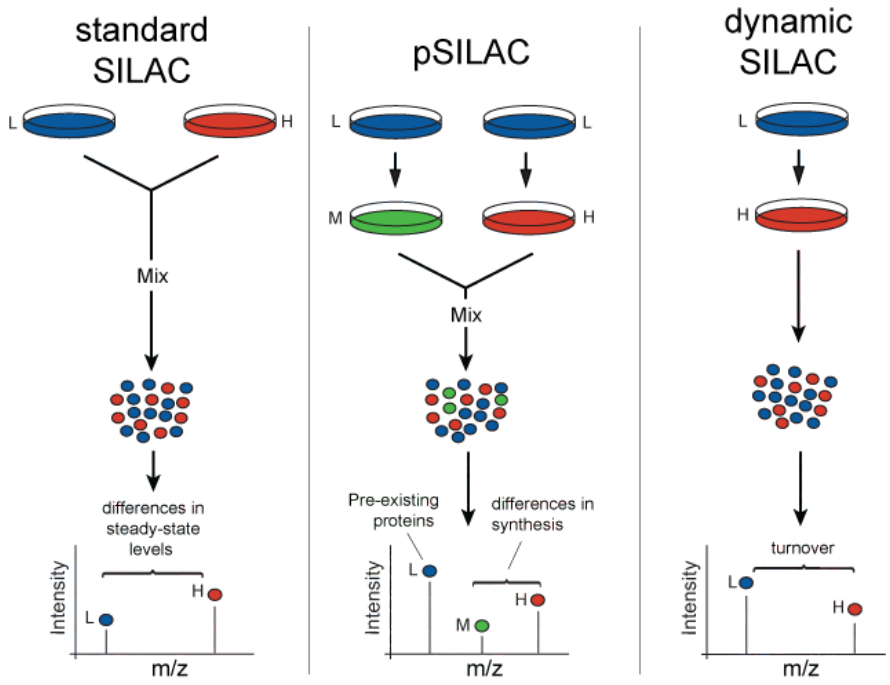

Figure 5.2: Different variants of the SILAC technique for cellular proteomic analysis, by Prof. Matthias Selbach (Max Delbrück Center for Molecular Medicine, Berlin). The standard SILAC technique mixes the population of two samples, labelled and unlabelled, to analyse the relative changes in protein levels. Pulse SILAC (pSILAC) allows the comparison of the relative changes in protein synthesis by growing previously unlabelled cells in two different labelled medias (medium and heavy) before the analysis. Dynamic SILAC collects samples at different timepoints after changing the media from unlabelled to labelled to analyse the protein turnover by determining the degradation and synthesis times.

One of the earliest examples of the application of this powerful technique can be found in the work published by Everley *et al.* (2004), in which they used standard SILAC to compare the protein expression levels of a prostate cancer cell line with high metastatic potential (PC3M-LN4) and another one with low metastatic potential (PC3M). Out of the nearly 1000 proteins they identified, they were able to confidently compare the expression levels of 440 proteins across the two cell lines, 60 of which were overexpressed in PC3M-LN4 by over three-fold compared to PC3M, and 22 were significantly downregulated. Further analysis along with technique and software optimisations resulted in a much higher quantification rate of proteins distinctly expressed between the cell lines (Everley *et al.*, 2006). One explanation for this significant increase between the first and second study is the use of a double labelling approach. While only heavy labelled lysate amino acids were used in the first study, they decided to use both arginine and lysine isotopic variants for the second study, resulting in a much greater number of identified and quantified proteins. This approach allowed them not only to identify possible biomarkers for metastasis and progression but also potential metastasis suppressor candidates (absent proteins in PC3M-LN4).

Schwanhäusser *et al.* (2009) developed the pSILAC variant to measure and compare protein translation rates between samples. To test the technique, they compared it against the firefly luciferase reporter assay commonly used to analyse gene expression at the transcriptional level. For this, they used cervical cancer Hela cells with a luciferase gene under control of tetracycline responsive promoter, heavy media (containing $^{13}C_6{}^{15}N_4$ L-arginine and $^{13}C_6{}^{15}N_2$ L-lysine) and medium media (containing $^{13}C_6$ L-arginine and D_4 (deuterium) L-lysine). While one set of cells in medium media was treated with a tetracycline derivative to induce luciferase for different timepoints, another set of control cells was equally treated in heavy media for 10 hours. At the same time, they used a third set to measure the expression of luciferase using the standard assay approach for the same time points as in the first set. The value determined at 10 hours through the heavy control peptides being 100% expression, the relative expression of luciferase in the medium labelled samples was determined at each time point. Comparison of these results with the ones obtained from the luminescence quantification in the assay, shown in Figure 5.3, demonstrate the efficacy of the pSILAC method to determine differences in translation rates in complex protein mixtures.

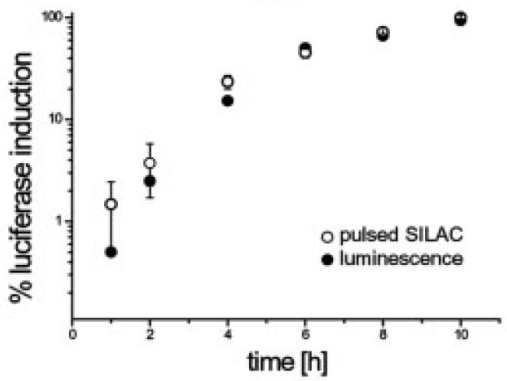

Figure 5.3: To evaluate the efficacy of the pSILAC approach to measure the relative changes in protein synthesis on two different samples, Schwanhäusser *et al.* (2009) compared it against the firefly luciferase reporter assay. The time course of the induction of luciferase relative to the reference in the control sample measured by pSILAC are shown along with the luminescence readouts from the assay.

Finally, an example of the use of dynamic SILAC to measure protein turnover (explained in more detail in Figure 5.4) is the work published by Doherty *et al.* (2009), in which they used this technique to determine the degradation rate of proteins in human adenocarcinoma A549 cells. To this end, they grew the cells into heavy medium containing $^{13}C_6$ L-arginine for 13 days before changing the medium to light unlabelled media and collected samples over a period of 8 h (0, 0.25, 0.5, 1, 2, 4 and 8 hours). By comparing the ratio of peptides belonging to the same protein containing heavy or light peptides in each sample, they were able to calculate the turnover rate of nearly 600 different proteins.

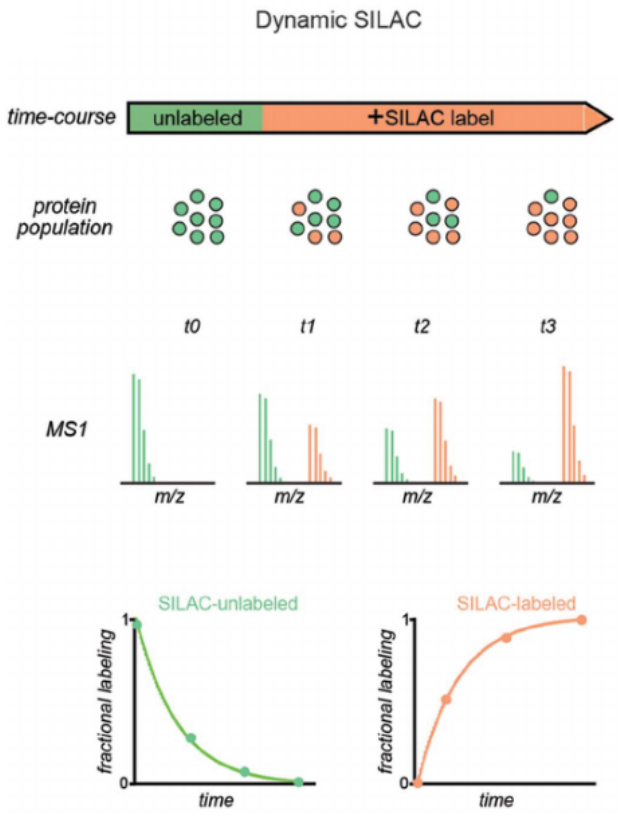

Figure 5.4: Dynamic SILAC, by Welle *et al.* (2016). Cells grown in light media are moved to labelled media and, as the proteins are isotopically labelled through the incorporation of heavy amino acids (in orange), unlabelled proteins (in green) are cleared and replaced. Samples are collected at different time points after the media change for mass spectrometry analysis and posterior comparison. This process can also be carried out growing the cells in labelled media first for enough doublings to ensure the whole proteome is isotopically labelled before putting the cells back into light media, as in the experiment carried out by Doherty *et al.* (2009).

SILAC has also been used to study the expression of ISGs. In 2015, Li *et al.* used standard SILAC to study the induction of type I IFNs by HIV RNAs in U937 human myeloid leukaemia cell line monocytic cells. For this, they grew one set of cells in light media (containing $^{12}C_6{}^{14}N_4$ arginine) and another one in heavy media (containing $^{13}C_6{}^{15}N_4$ arginine) for six passages to make sure the proteome was labelled (or unlabelled) as appropriate and they transfected the cells with HIV RNA and GAPDH RNA respectively. Cells were collected at different time points post-transfection and analysed with MS. This allowed them to identify 281 proteins with high confidence in the cells transfected with HIV-RNA when compared with cells transfected with control RNA. A variety of ISGs turned out to be upregulated in all the time points in viral RNA transfected cells, including IFITs, IFITM1/3, ISG15, MX1, GBP1 and PKR. In the same year, the first study using SILAC to study ISG15 was published. Radoshevich *et al.* (2015), who focused their research in *Listeria monocytogenes* infected human cells, performed a SILAC analysis in transduced cells expressing Flag-His tagged mature ISG15 cultivated in either medium (containing $^{13}C_6$ L-arginine and D_4 L-

lysine) or heavy media (containing $^{13}C_6{}^{15}N_4$ L-arginine and $^{13}C_6{}^{15}N_2$ L-lysine). Control cells expressing the empty vector were grown in unlabelled light media. After treating the cells grown in heavy media with 1000 U/mL IFNα2 for 40 hours and leaving the medium labelled and control cells untreated, they lysed the cells and performed a nickel affinity purification. After ruling out the peptides identified in the unlabelled light samples, resultant of non-specific binding, they identified 30 proteins resultant of the overexpression of ISG15, and 12 additional proteins resultant of the overexpression plus IFN treatment. A gene ontology analysis of these 30 targets revealed that 80% of the proteins targeted upon overexpression of ISG15 were integral membrane proteins, most of them belonging to the endoplasmic reticulum and Golgi apparatus, which was related to an increased cytokine secretion upon infection.

5.2 Aim and strategy

The aim of this chapter was to determine the proteomic changes in the absence of ISG15 in both the basal and IFN treated states to try to elucidate what proteins and biological processes could be ISG15 modulated and which might drive IFN resistance. As discussed in chapter 1, ISG15 has been reported to regulate the degradation and stabilisation of many proteins, taking part in the dynamic remodelling of the proteome. Moreover, ISG15 has also been reported to be involved in the modification of newly synthesised proteins, and HERC5 has been reported to be physically associated with the 60s ribosomal subunit near the channel of exit of the nascent polypeptides (Durfee *et al.*, 2010). In order identify newly synthesised proteins whose expression is altered in the absence of ISG15, a combination between pulse and dynamic SILAC was used in SiHa WT and ISG15$^{-/-}$ cells. Comparison of the peptides found in KO vs WT cells allows for the identification of differently expressed proteins in ISG15 KO cells. At the same time, comparing the proteins identified upon IFN treatment with those identified in the absence of IFN treatment can help elucidate the role of ISG15 under basal conditions and in IFN resistance.

Two time points were selected to try to differentiate the roles of ISG15 as a free protein and as a conjugated protein. ISG15 is induced within 30 minutes upon IFN treatment and is detectable by immunoblot from as early as 6 hours, peaking at around 24 hours and, once free ISG15 starts building up in the cell, the process of ISGylation starts and peaks from around 48 hours (Loeb & Haas, 1992; Radoshevich *et al.*, 2015; Wong *et al.*, 2006; Bade *et al.*, 2012). Although the exact time points at which free and ISGylated proteins peak differ from cell line to cell line, based on the literature and the analysis by immunoblotting of the cell lines used 24 and 48 hour time points were selected as a standard for the experiments in this thesis.

Two sets of cells were seeded in light unlabelled media and, once at the right confluence, both sets were changed to heavy media for 24 hours. One of the sets was then collected (henceforth 24h samples), while the other one was changed to medium media for another 24 hours before collecting them (henceforth 48h samples). This system, described in Figure 5.5 (a), was repeated for each cell line and treatment condition - untreated WT, untreated ISG15 KO, treated WT and treated ISG15 KO. Each sample was set in biological triplicates and the treated samples had 100 U/mL added at the time of changing media from light to heavy (time point 0h). The full setup is illustrated in Figure 5.5 (b).

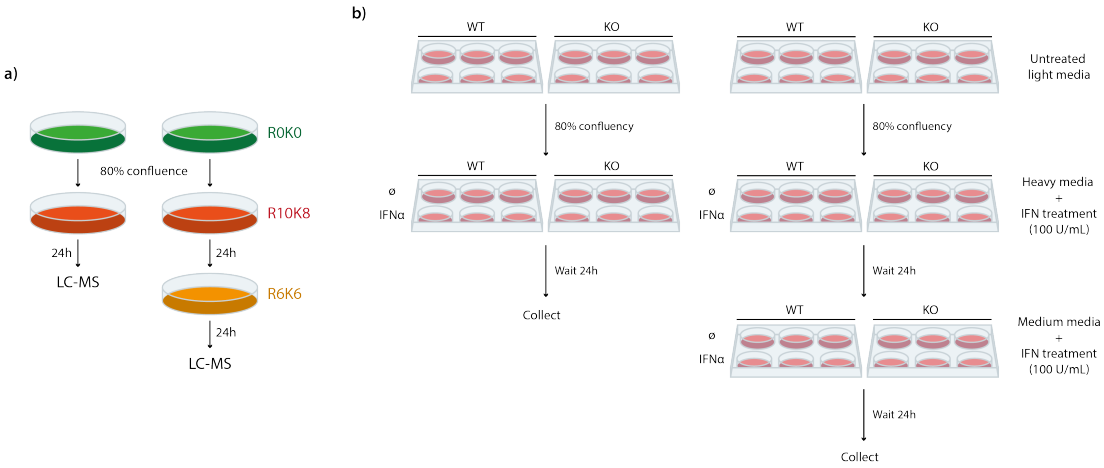

Figure 5.5: SILAC experiment setup to determine the proteomic changes in ISG15$^{-/-}$ cells. **a)** Media changes in each time point. **b)** Full experiment setup.

5.3 Methods

5.3.1 Sample preparation

For the SILAC labelling, $2{\cdot}10^5$ SiHa cells were seeded per well in 6 well plates with unlabelled light media (SILAC RPMI 1640 R0K0, GeminiBio SM019). Wild-type and ISG15 knock-out cells grown from a single clone were used, in triplicates per condition. Two identical sets were prepared to be collected at two different time points, as explained in section 5.2, and media was changed as appropriate to either heavy media containing ^{13}C and ^{15}N labelled arginine and ^{13}C and ^{15}N labelled lysine (SILAC RPMI 1640 R10K8, GeminiBio SM021) or to medium media containing ^{13}C labelled arginine and ^{13}C labelled lysine (SILAC RPMI 1640 R6K6, GeminiBio SM018), with 100 U/mL commercial human recombinant IFNα2 if appropriate.

5.3.2 Sample processing for mass spectrometry analysis

Cells were collected by scraping and the pellets lysed with a mass spectrometry compatible lysis buffer (50 mM HEPES pH8, 0.2% Triton-x, 150 mM NaCl, 10 mM NaF, 0.1 mM EDTA, 2 mM DTT, 1x protease inhibitor mix). The samples were sent to the Masaryk Memorial Cancer Institute (Masaryk University, Brno, Czechia), where Professor Ted Hupp from the University of Edinburgh processed the cells through filter aided sample preparation (FASP) and desalting C18 columns. Due to an unforeseen issue, only duplicates could be processed. The peptides in the samples were separated and analysed through liquid chromatography and mass spectrometry, run by Professor Lenka Hernychová.

Liquid chromatography (LC) and sample ionisation

Once the sample is ready for the analysis, a predetermined amount is injected into the LC system (UltiMate^{TM} 3000 HPLC by Thermo Fisher), and a pump-circulated loading buffer pushes the sample onto the trap column of the liquid chromatography system with a steady flow, in this case of 0.3 μL/min. The sample gets caught in the column while the buffer keeps circulating for a couple minutes for a final washing step, getting rid of any salts that could have remained in the sample. Then, the switch of a valve connects the trap column to the analytical column and the sample is quickly pushed by a mobile phase composed of 98% solution A (99.9% LC-MS grade water and 0.1% formic acid) and 2% solution B (80% acetonitrile, 19.92% LC-MS grade water and 0.08% formic acid) into the analytical column. At first, the low volume of acetonitrile causes the sample to get stuck into the analytical column without separation. Then, the composition of the mobile phase slowly changes increasing the amount of organic compound. The gradual increase of organic solvent results in the decrease of the polarity of the mobile phase, reducing the hydrophobic interaction between the stationary phase in the column and the peptides, which causes their gradual mobilisation. This allows the groups of the same peptides to move together gradually, resulting in a sample entering the mass spectrometer in a manageable flow. As shown in Figure 5.6, once the gradual increase of solution B reaches the 40% and all the peptides should have been mobilised, the percentage of solution B is increased to 98% in order to wash all the peptides that could have been stuck in the column. Finally, the composition is shifted to 98% water so the column is equilibrated, washing the large amounts of organic solvent.

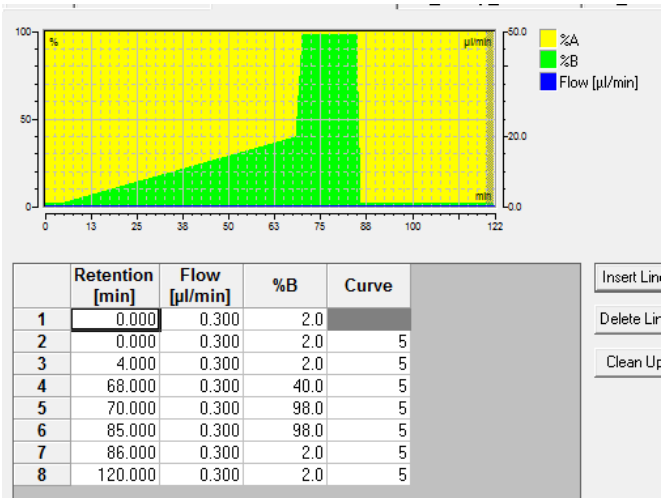

	Retention [min]	Flow [µl/min]	%B	Curve
1	0.000	0.300	2.0	
2	0.000	0.300	2.0	5
3	4.000	0.300	2.0	5
4	68.000	0.300	40.0	5
5	70.000	0.300	98.0	5
6	85.000	0.300	98.0	5
7	86.000	0.300	2.0	5
8	120.000	0.300	2.0	5

Figure 5.6: Gradual peptide mobilisation in liquid chromatography. A mobile phase composed of 2% acetonitrile and 98% water pushes the samples into the analytical column. The composition of the mobile phase changes to slowly increase the volume of the organic solvent, resulting in the gradual mobilisation of the peptides. All the peptides should be mobilised once the increase of acetonitrile reaches the 40%. Then, the percentage of organic compound is increased to 98% in order to wash any stuck peptides before the composition is shifted to 98% water to equilibrate and wash the column from organic solvent.

The separated sample travels to the emitter located in the entrance of the mass spectrometer for electrospray ionisation, with the small percentage of formic acid in the mobile phases aiding the process by supplying free ions. The potential difference of 1.8 kV between the nozzle and the spectrometer inlet pushes ions from the solution to the tip of the emitter and, as the amount of ions increases, they build-up forming a cone known as "Taylor Cone" (Figure 5.8). This process reaches a point where the tip becomes unstable causing the droplets to break off repelling each other, which results in a fine charged spray (Figure 5.7).

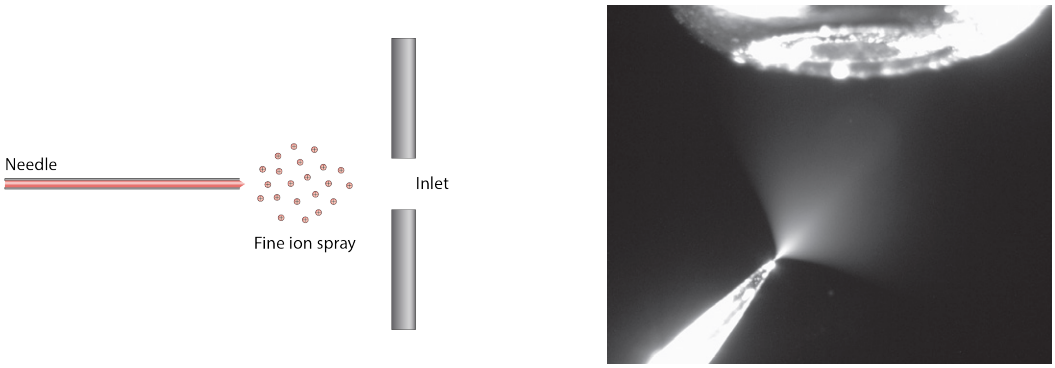

Figure 5.7: Electrospray ionisation (ESI) caused by the potential difference between the sample nozzle and the spectrometer inlet. **a)** The high voltage causes the droplets in the nozzle tip to break off repelling each other, resulting in a fine charged spray. **b)** Real photo of a sample being ionised and directed to the mass spectrometer inlet.

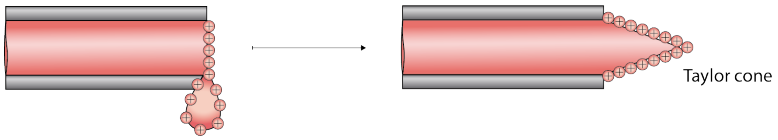

Figure 5.8: Taylor cone formed in the electron ionisation process as a result of the potential difference between the sample nozzle and the spectrometer inlet.

The destabilisation process of the Taylor cone does not occur as a result of the sample's flow rate, but because of the electric field that pushes the charged droplets towards the spectrometer inlet. Once the droplets are on the way to the inlet, the ions become free of the solvent. In some cases, the solvent evaporates leaving one ion per droplet (Figure 5.9a). In other cases, droplets containing several ions start to evaporate bringing the chargers close to each other. When the repulsion force between charges is greater than the surface tension (Rayleigh limit) the droplet explodes generating smaller charged droplets (Coulomb explosion) (Figure 5.9b). In both cases, ions get free of the solvent eventually resulting in the sample moving to a gas phase composed of charged molecules. This allows the molecules to be manipulated through electrical fields, getting rid of any uncharged particles that would not be guided inside the analyser.

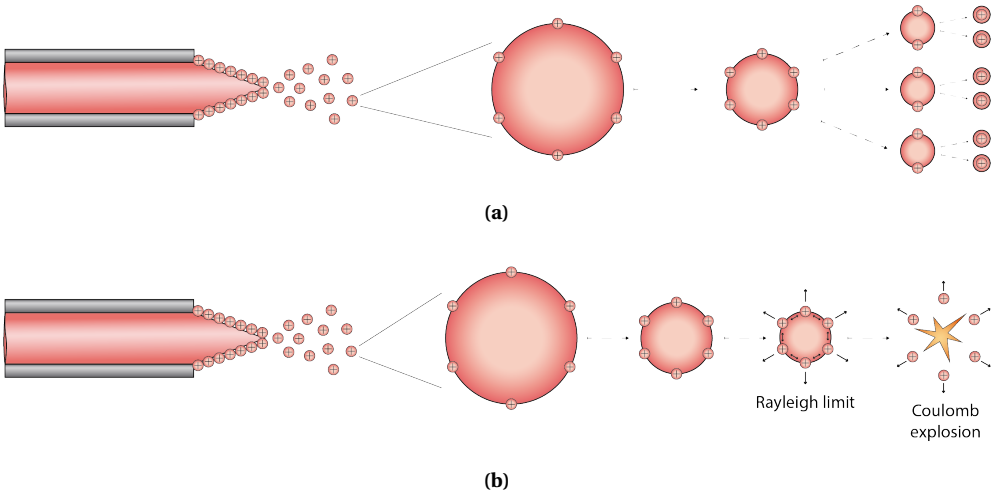

Figure 5.9: Solvent evaporation processes in electrospray ionisation. The droplets on the way to the inlet evaporate leaving the ions free of the solvent. **a)** In some cases, the solvent evaporates until there is only one ion per droplet. **b)** In other cases, droplets evaporate until the ions are too close to each other. When the repulsion force between charges is greater than the surface tension (Rayleigh limit) the droplet explodes generating smaller charged droplets (Coulomb explosion). In both cases, the sample becomes an aerosol composed of charged molecules, which allows the molecules to be manipulated through electrical fields.

The mass spectrometer and its components

A mass spectrometer is a system used to measure the mass to charge ratio (m/z) of the molecules that compose a sample. These accurate measurements can be used to quantify and identify such molecules. The three essential components of a mass spectrometer are an ionisation source, a mass analyser and an ion detection system. On top of this, each spectrometer may have additional components to optimise and boost the process and results of the analysis. For this experiment, a Thermo Scientific Orbitrap Elite Hybrid Mass Spectrometer was used. For illustrative purposes, a figure of a Thermo Fusion Orbitrap Mass Spectrometer (Figure 5.10) has been used to point out some of the key features of these type of machines. The features described here are also present and function the same way in the system used to analyse the samples of this experiment.

- **Ion source**: Described in previous section, it creates a fine charged aerosol as the result of the potential difference between the sample nozzle and the mass spectrometer inlet.
- **Active Beam guide**: Guides the charged molecules into the system getting rid of any uncharged particles.
- **Quadrupole mass filter**: Consistent of four cylindrical rods, this mass filter uses both alternating and direct voltage to filter ions based on m/z to select the appropriate sized ions to be analysed and getting rid of unsuitable sized ions. In this experiment, selected ions had a m/z of 400-2000.
- **C-trap**: Once the ions have been filtered, the C-trap gathers and confines them before injecting them into the Orbitrap. During this process, the ions move freely along the length of the trap. Collisions with N_2 in the trap result in the ions losing kinetic energy, "cooling" them. Once the ions have low kinetic energies, parameters are altered so the ions are not trapped anymore, being shot into the Orbitrap.
- **Orbitrap**: When the ions enter the orbitrap, they spin around the central core moving back and forth the pole. Ions of the same m/z oscillate with the same frequency along the axis, resulting in grouped rings moving around and along the pole. The outer shell of the orbitrap detects the current induced by the ions moving charge and so, as the rings of ions move along the axis of the core, they produce sine oscillating waves of this induced current. The amplitude of such waves determines the amount of ions and, as mentioned above, the frequency determines the m/z. Fourier transformation is later used to separate and discern the readings of the superimposed waves, allowing for the data to be translated to accurate mass to charge ratios and abundances. The accuracy of the Orbitrap allows for the differentiation of

isotopes between otherwise identical peptides. This first analysis of the sample is referred to as MS1. As peptides go through the orbitrap and m/z peaks are determined, equivalent peptides get selected for fragmentation. The peaks are recorded and remembered by the system as they are detected and selected for fragmentation and, if the same peak is detected again within a set time, it is not selected again. Once the set time has passed, if the same peak is identified again, it is sent for fragmentation and the time count is set again. This is called dynamic exclusion, and allows for the identification of less abundant peptides without "distracting" the system with the most abundant ones that could dominate the spectrum through the analysis. This is a parameter that can be altered and optimised. In this experiment, the dynamic exclusion was set to 30 seconds.

- **Ion-routing multipole**: Once the peptides have been analysed in the orbitrap, the ion-routing multipole (a multipurpose quadrupole) gathers the ions to guide them into the next detector.

- **Dual-pressure linear ion trap**: As per its name, the dual-pressure linear ion trap is composed of two parts - the high-pressure cell and the low-pressure cell. When the samples enter the high-pressure cell, the high-speed collisions of the ions with Helium (He) gas fragments the peptides into smaller pieces. Identical peptides can get fragmented in different points, resulting in different fragment length and amount. The fragments then enter the low-pressure cells, which in a similar way to the quadrupole mass filter, it is able to manipulate the electric field so very specific masses over charges get gradually ejected from the analyser to get caught by the large-surface-area detectors, identifying the peptide fragments using protein data bases. As this analysis requires the data obtained from the MS1, is referred to as MS2.

- **Peptide identification**: The peptides detected in MS1 and MS2 spectra are matched against reference protein sequence databases to identify what proteins do they derive from, allowing for the identification of the proteins that compose a complex biological sample. Different softwares such as Proteome Discoverer and MaxQuant include search engines that are capable of analysing the obtained datasets, as well as statistical tools. Settings in these search engines, such as mass tolerances or the search of post-translational modifications, can be adjusted as required by the experiment. Because a given peptide can belong to different protein isoforms and subtypes, sometimes a peptide will be matched to a group of proteins rather than to a specific protein. The identification of unique peptides can help discern the protein of origin from the rest of proteins.

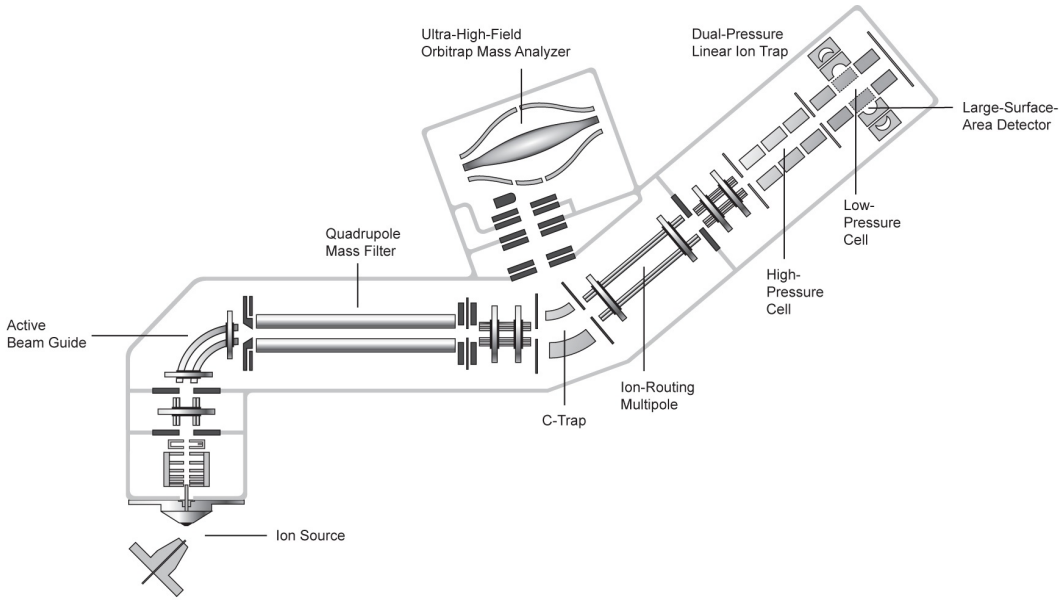

Figure 5.10: The mass spectrometer and its components. Orbitrap IQ-X Tribrid MS, by ThermoFisher Scientific.

5.3.3 Analysis and validation of mass spectrometry data

Once the data was acquired, it was selected, sorted and filtered by Professor Lenka Hernychová and Tomáš Henek using the Proteome Discoverer Software by Thermo Fisher Scientific. Results were used to generate volcano plots using the web tool VolcaNoseR, developed by Goedhart & Luijsterburg (2020) (https://huygens.science.uva.nl/VolcaNoseR2/), using equal or below 0.5 and equal or above 2 as fold change (ISG15 KO vs WT) cut-offs (x-axis) and $p \leq 0.05$ as significance cut-off (y-axis). The web tool STRING (https://string-db.org) was also used to perform functional protein association network analysis. After this, the data was further sorted for gene set enrichment analysis. Although the criteria was set to a fold change equal or above 1.5 and equal or below 0.67, all the upregulated proteins had a fold change >2 or were only found in ISG15 KO samples, while all the downregulated samples had a fold change <0.3 or were only found in WT samples. The gene names were inserted into g:Profiler (https://biit.cs.ut.ee/gprofiler/gost) and the Gene Ontology terms (GO terms) compiling genes by their biological process along with their assigned p-values were acquired from the uncapped results and fed into Revigo, a web tool based on a clustering algorithm used to visualise and summarise long lists of GO terms by removing the redundant ones (Supek *et al.* (2011), http://revigo.irb.hr/). The settings were adjusted to obtain a medium list (0.7) with associated p-value, and to work with the default semantic similarity metric (SimRel) and the human UniProt protein database (9606). For the final two-directional bar graphs, the final list obtained from Revigo was further refined to combine some terms

into one, since the software did not remove all the repetitive and redundant terms. When such combination occurred, the start of a change in pattern in the bar (from solid to white-striped) represents the lowest p-value of the terms combined, and the end of the bar matches the highest p-value of those combined. The unaltered full lists obtained from g:profiler can be found in Appendix C. A flow chart showing the summarised data analysis process can be found in Figure 5.11.

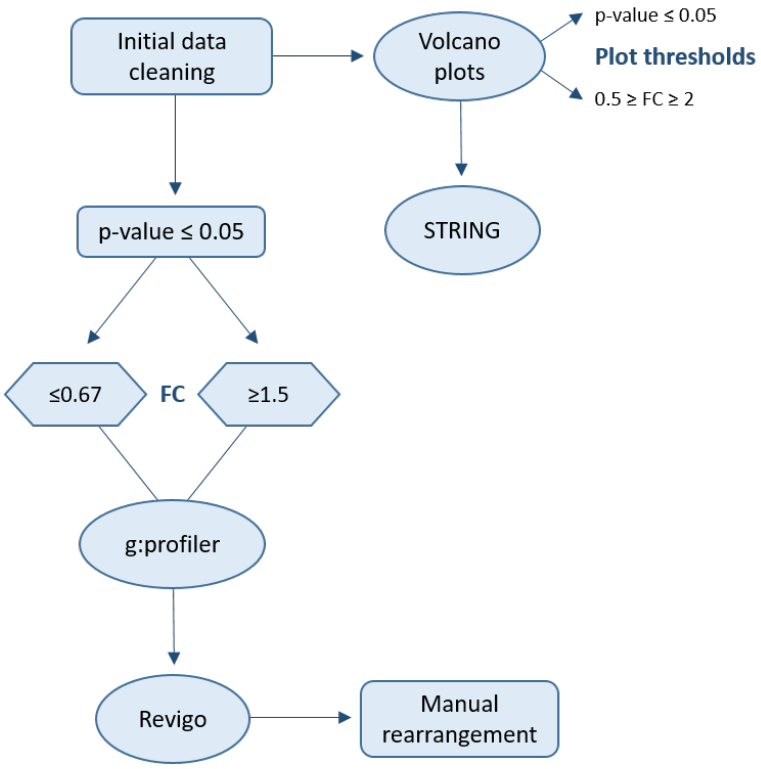

Figure 5.11: Flow diagram of the data analysis methodology used in the SILAC mass spectrometry analysis.

A number of proteins identified through mass spectrometry were selected for preliminary validation of the results by immunoblotting.

5.4 Results

5.4.1 Identification of *de novo* synthesised proteins in ISG15$^{-/-}$ SiHa cells upon IFNα treatment

In order to determine what proteins were differently synthesised in the absence of ISG15 right after IFNα treatment, cells were grown in isotopically labelled media for 48 hours with and without treatment, and untreated samples were used as controls. As described in section 5.2, the cells were grown in heavy media (R10K8) for the first 24 hours,

moment in which one treated and one untreated set of samples were collected and the media in the other two was changed to medium media (R6K6) for another 24h. After MS analysis, the proteome discoverer software was used to identify only those proteins with heavy and medium modifications, independently, and these were plotted by abundance ratio (ISG15 KO vs WT) and significance (p-value). Thresholds for the volcano plots generated were set at >2 and <0.5 for abundance and <0.05 for p-value. The proteins synthesised *de novo* during the first 24 hours, untreated and treated with IFNα, are shown in Figure 5.12. The ones synthesised 24 to 48 hours after IFN treatment and the corresponding untreated control are shown in Figure 5.13.

Results show that MX1 and FGB are synthesised throughout the treatment, both during the first and the last 24 hours of IFNα treatment. Neither of these proteins were upregulated in the untreated controls, suggesting their overexpression is IFN dependant. MT1G is also upregulated during the two treatment time ranges, but its upregulation in untreated samples collected at 48 hours show that this upregulation is not IFNα dependant. The untreated controls also prove that proteins like NQO1 and ACTR3 are upregulated in the absence of ISG15 regardless of treatment.

Filtering the data to detect proteins labelled with heavy media (R10K8) in samples collected 48 hours after IFN treatment allowed to inspect the state of those proteins synthesised only during the first half of the treatment time as this progressed, providing more information. As seen in Figure 5.14, ATM, IFIT1 and PABPC1 were identified when searching for proteins modified with heavy labels, providing evidence that these proteins were also synthesised during the first 24 hours. The fact that they were not identified in the samples collected at 24 hours would suggest that the abundance ratio in ISG15 KO vs WT samples during the first 24 hours upon IFN treatment was not significant, but as the treatment progressed the proteins got degraded in WT but not in ISG15 KO samples, causing them to be identified as upregulated 48 hours after treatment. To confirm or disprove this, these three proteins were searched among the proteins identified in the samples collected 24 hours after IFN treatment to inspect their fold change expression. While ATM could not be detected in these samples, IFIT1 and PABPC1 was shown to be overexpressed in ISG15 KO vs WT samples (fold change of 3.349 and 2.408 respectively), but they did not make it through the filtering process of the volcano plots due to poor p-values. This discards the hypothesis that ISG15 could be mediating the degradation of these proteins in WT cells, but expression during the first 24 hours after IFN treatment and their sustained upregulation should be further confirmed by other means such as immunoblotting. The detection of MX1 confirms that this protein is continuously synthesised throughout the treatment, and that the protein synthesised during the first 24 hours of treatment remains undegraded 48 hours after. MT1F was also detected in this screening, confirming it was also synthesised during the first 24 hours, as seen in Figure 5.12b. The *de novo* synthesis-

ing of this protein was not detected 24 to 48 hours after treatment, but the R10K8 labelled protein synthesised during the first 24 hours remained upregulated even after 48 hours after treatment. Nevertheless, the search of this hit in the data revealed that it was found only in ISG15 KO cells and not in WT cells in untreated samples collected at 48h, showing that, as with MT1G, its upregulation is not IFN dependant.

WARS is the only protein found to be synthesised only 24 to 48 hours after treatment in an IFN dependant manner (not upregulated in the absence of IFN). To see if this protein presented a delayed expression following treatment or if it was also expressed/upregulated in samples collected at 24 hours, its fold change values were searched among the proteins synthesised during the first 24 hours (R10K8). These revealed downregulation in untreated samples (0.526 and 0.511 at 24 and 48 hours respectively) and upregulation in the treated samples (1.661 and 2.052), but with poor p-values.

Regarding the downregulated proteins, ISG15 was found to be downregulated in both the treated categories, suggesting peptides belonging to this protein were identified probably due to transcribed non-functional or protein fragments. Nonetheless, the very low ratio of ISG15 derived peptides in the knock out cell line vs the WT cells validates the results observed by immunoblotting and sequencing. The expression of UBE2K and CNN2 was found to be downregulated in an IFN dependant manner only during the first 24 hours of treatment, but not in the following 24 hours. Again, in an attempt to clarify the expression state of these proteins, their fold change values were searched in the samples collected 48 hours after treatment. UBEK2 was found downregulated in all the categories, treated and untreated, but only data obtained from samples treated for 24h had a significance value low enough to pass the threshold. CNN2 was also found downregulated in all conditions, except in the samples treated for 48h where it had a fold change of 1.182, but in all cases had very poor p-values. In both cases, it seems that these proteins are downregulated in the absence of ISG15 regardless of treatment, but more experiments need to be carried out to confirm this assumption.

EIF1 and DAB2 were found to be downregulated regardless of treatment in all conditions, although downregulated expression was confirmed by a significant p-value only in treated samples collected after 48 hours, the protein having been synthesised during the first 24 hours after treatment (R10K8). The expression of ATAD2 was found downregulated only 24 to 48 hours after IFN treatment. This could be again due to poor p-values in the other conditions or suggest that the expression of this protein is delayed with respect to treatment and that the absence of ISG15 somehow abates its expression. A search through the data shows that ATAD2 was also found in untreated WT cells but not in untreated ISG15 KO cells collected at 48 hours. Because the proteins that were found only in one of the two conditions do not have a fold change ratio, they were not included in the volcano plots. However, this finding discards the hypothesis that the downregulation of ATAD2 is IFN

dependant. Finally, the expression of proteins like EXT and MTERF were downregulated regardless of treatment, as seen by the untreated controls.

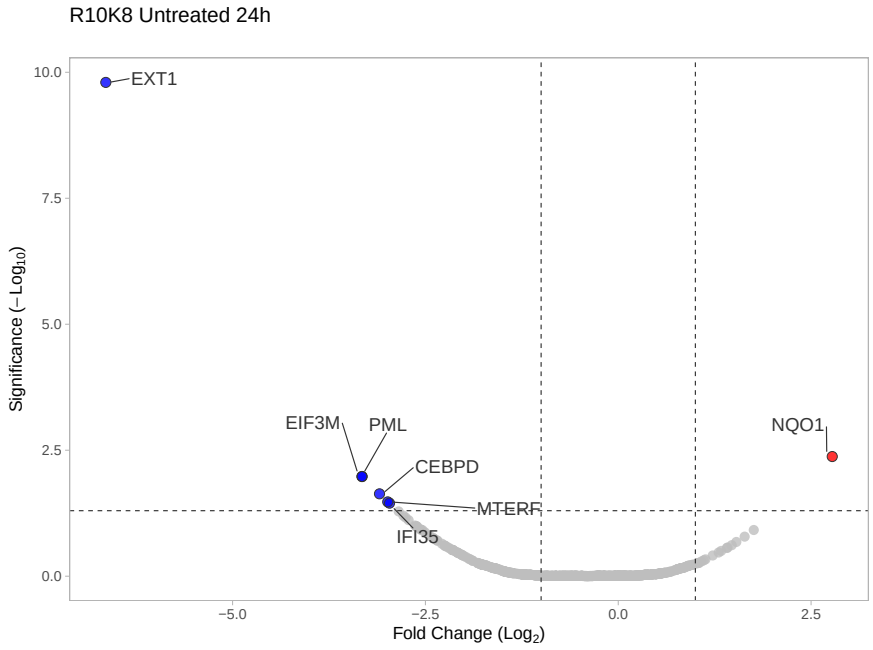

(a)

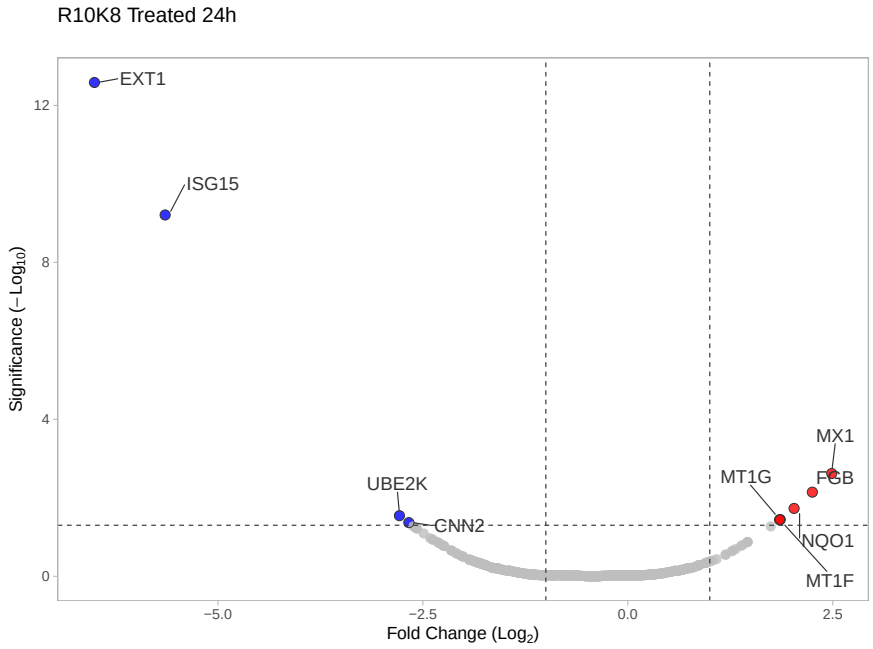

(b)

Figure 5.12: Volcano plots showing the proteins synthesised *de novo* in untreate ISG15$^{-/-}$ vs WT SiHa cells (**a**) and during the first 24 hours after IFNα treatment (**b**). The fold change ratios of each protein found were plotted against the -log$_{10}$ of the adjusted p-value using VolcaNoseR. The most significant hits (fold change above 2 and below 0.5 with a p-value below 0.05) were highlighted in red (upregulated) and blue (downregulated), with the top ten proteins labelled. ISG15 KO and WT samples were analysed in duplicates.

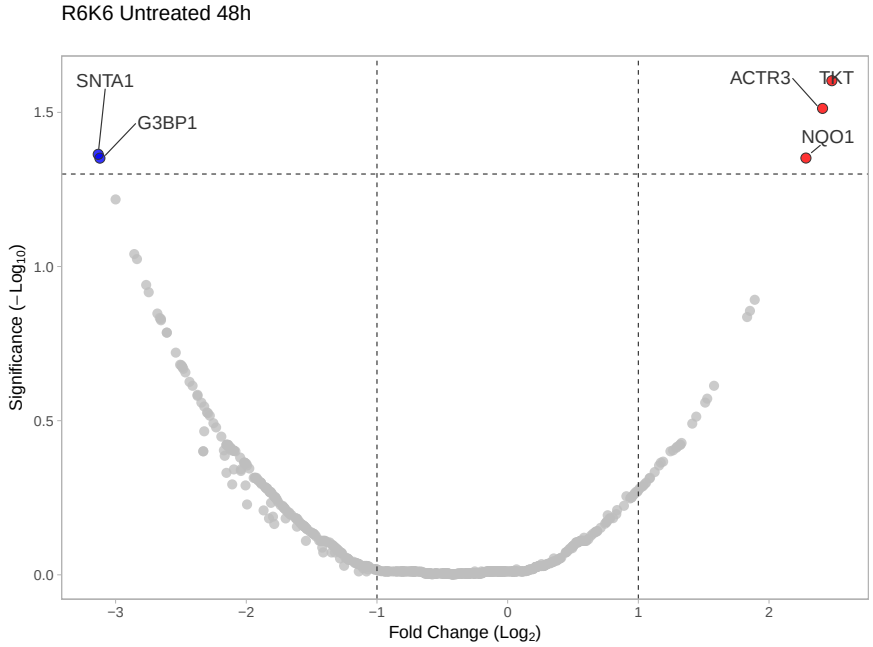

(a)

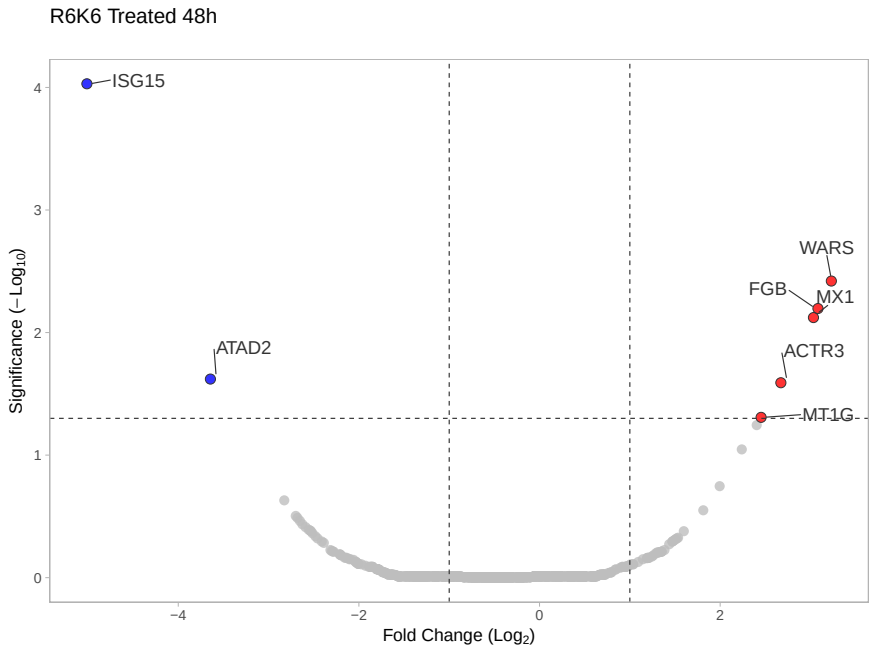

(b)

Figure 5.13: Volcano plots showing the proteins synthesised *de novo* in untreated ISG15$^{-/-}$ vs WT SiHa cells (**a**) and 24 to 48 hours after IFNα treatment (**b**). The fold change ratios of each protein found were plotted against the -log$_{10}$ of the adjusted p-value using VolcaNoseR. The most significant hits (fold change above 2 and below 0.5 with a p-value below 0.05) were highlighted in red (upregulated) and blue (downregulated), with the top ten proteins labelled. ISG15 KO and WT samples were analysed in duplicates.

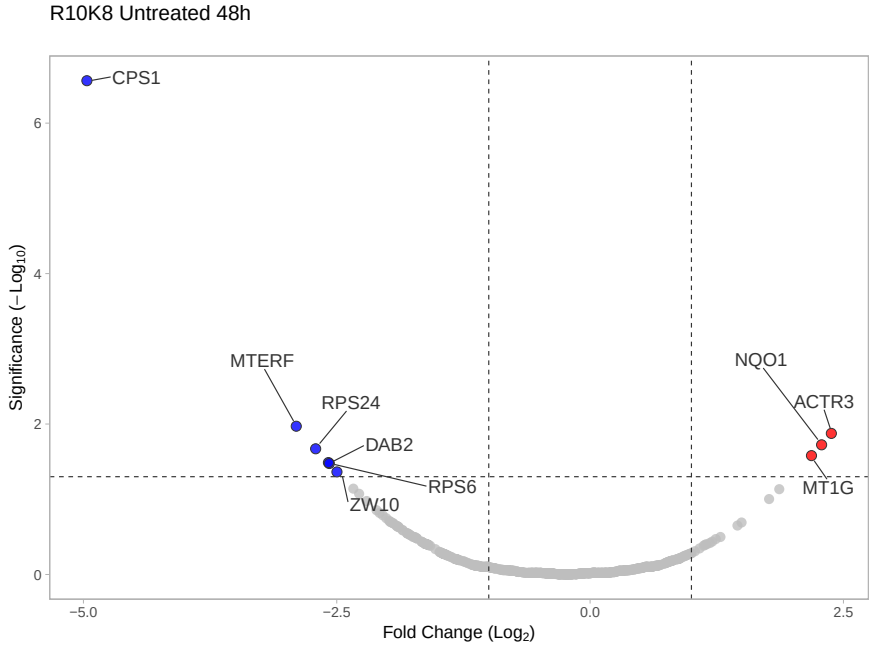

(a)

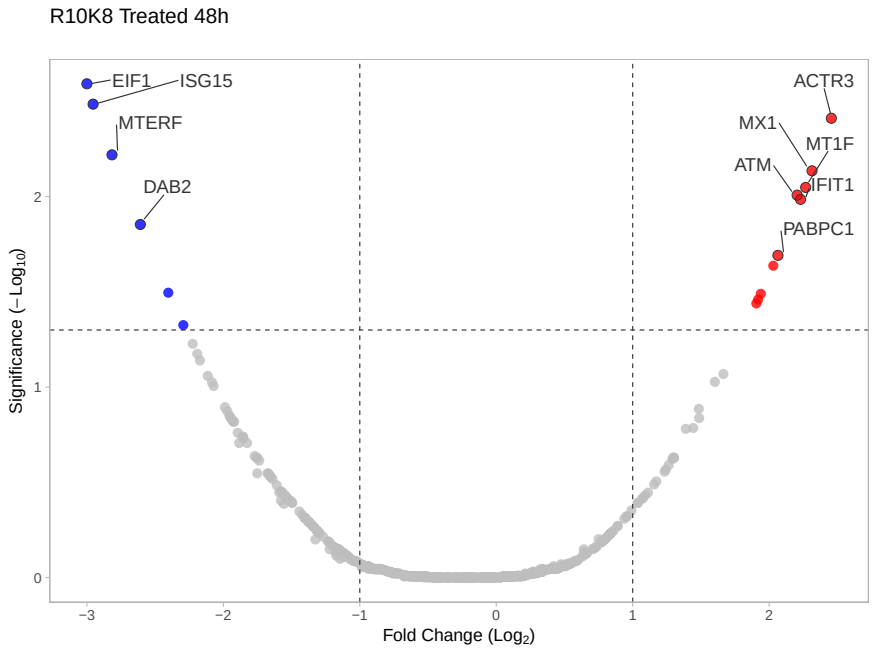

(b)

Figure 5.14: Volcano plots showing the proteins synthesised *de novo* in untreated ISG15$^{-/-}$ vs WT SiHa cells (**a**) and during the first 24 hours after IFNα treatment only (R10K8) (**b**) identified in samples collected 48 hours after. The fold change ratios of each protein found were plotted against the -log$_{10}$ of the adjusted p-value using VolcaNoseR. The most significant hits (fold change above 2 and below 0.5 with a p-value below 0.05) were highlighted in red (upregulated) and blue (downregulated), with the top ten proteins labelled. ISG15 KO and WT samples were analysed in duplicates.

5.4.2 Analysis of the expression of selected targets in ISG15$^{-/-}$ SiHa cells upon IFNα treatment

Three different proteins were selected to verify the results observed in the volcano plots by immunoblot (Figure 5.15). MX1, not detected in the absence of IFN, presented increased expression in ISG15 KO samples compared to WT once treated, consistently with the results observed in the volcano plots. Similarly, IFIT1 was mainly detected upon IFN treatment with increased expression in ISG15 KO samples. It was detected both in samples treated for 24 and for 48 hours, which suggests that the ISG15 KO vs WT fold change obtained in samples treated for 24 hours was representative of the biological effect observed by immunoblotting despite the poor p-value. UBE2K, on the other hand, was only detected downregulated in the volcano plot representing samples treated for 24 hours and collected after 24 hours (R10K8), but the immunoblot shows downregulated expression in both ISG15 KO samples, regardless of treatment. These results are again consistent with the data obtained prior filtering by significance value, showing that caution is needed before discarding data solely based on p-value, and that validation of the observed biological effect is required by other experimental means.

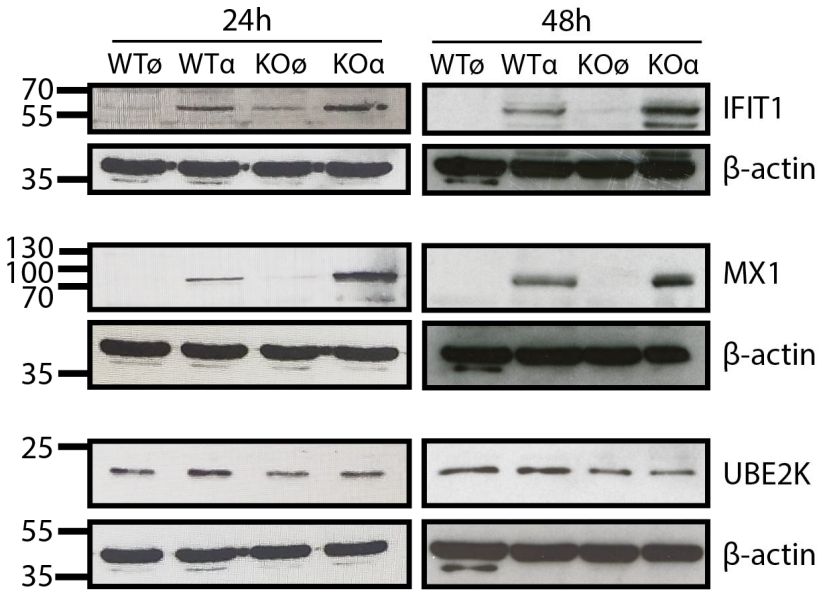

Figure 5.15: Immunoblotting for IFIT1, MX1 and UBE2K in untreated and IFNα treated SiHa ISG15$^{-/-}$ clone #1. An equal amount of protein (20 μg) from whole cell lysate was loaded per lane in an 15% SDS-PAGE followed by immunoblotting. The membranes were developed using either anti-IFIT1 (ThermoFisher Scientific (#PA3-848) at 1:2000 dilution), anti-MX1 (Abcam (#ab95926) at 1:1000 dilution) or anti-UBE2K (Abcam (#ab52930) at 1:10000 dilution) antibody, followed by anti-β-actin antibody (Sigma (#A2228) at 1:1000 dilution). IFNα treatment concentration was 100 U/mL. These results are representative of at least two experiments.

The ISG15 mediated stabilisation of USP18 and the interaction between them is required for USP18 to perform as negative regulator of the IFN pathway. An analysis by immunoblot was carried out to determine if the loss of ISG15 resulted in degradation of USP18, but no significant change was appreciated in the band intensity when compared to the SiHa WT sample.

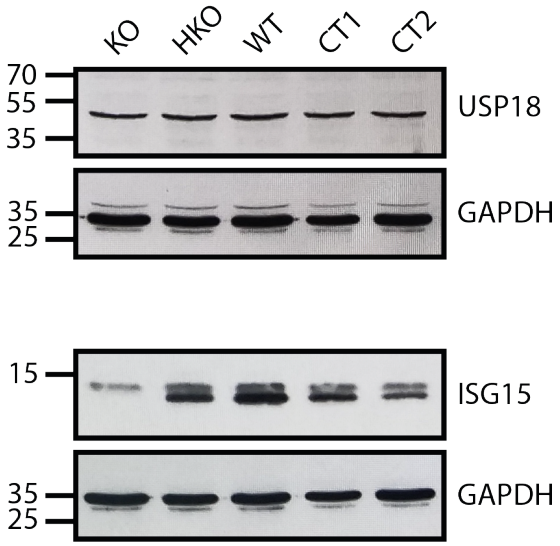

Figure 5.16: Immunoblotting for ISG15 and USP18 in IFNα treated WT SiHa, ISG15$^{-/-}$ clone #1 (KO) and a suspected heterogenic ISG15 KO (HKO) SiHa clone. Two clones that underwent the CRISPR editing procedure but were unsuccessful to generate the desired edition were used as controls. An equal amount of protein (20 μg) from whole cell lysate was loaded per lane in an 15% SDS-PAGE followed by immunoblotting. The membranes were developed using either anti-ISG15 (Cell Signaling Technology (#2743S) at 1:500 in milk) or anti-USP18 (Abcam (#ab168478) at 1:1000 dilution) antibody, followed by anti-GAPDH antibody (Abcam (#ab9484) at 1:1000 dilution). IFNα treatment concentration was 100 U/mL. These results are representative of at least two experiments.

5.4.3 Analysis of functional protein association networks

In order to better understand the role and impact of the significantly altered identified proteins, an analysis of the known and predicted protein-protein interactions was performed using the STRING web tool on a selection of the top hits. The most complete and meaningful network identified is the one involving MX1 and IFIT1, a well known IFN induced immune and antiviral system that includes ISG15 and USP18 as key members, shown in Figure 5.17. The network also includes another member of the IFIT family (IFIT3), three of the four members of the antiviral OAS family (OASL, OAS1 and OAS3), the interferon regulatory transcription factor IRF7, and IFI6 and RSAD2, another two interferon inducible antiviral proteins.

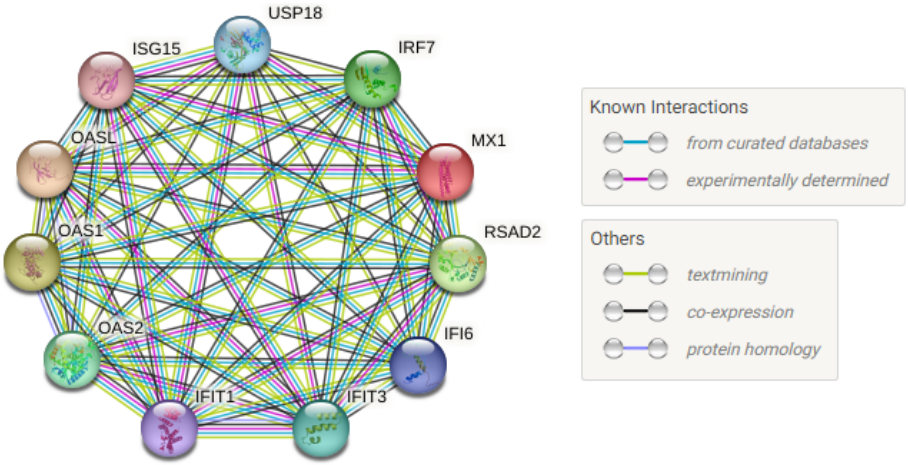

Figure 5.17: Analysis of the functional protein association network of MX1 and IFIT1, using the STRING web tool, to identify their protein-protein interactions and associations.

Other interesting networks identified include the closest interactions of NQO1, a two-electron oxidoreductase enzyme known to activate several anti-tumour quinones and stabilise p53 (Figure 5.18(a)) and of the two metallothionein MT1G and MT1F (Figure 5.18(b)).

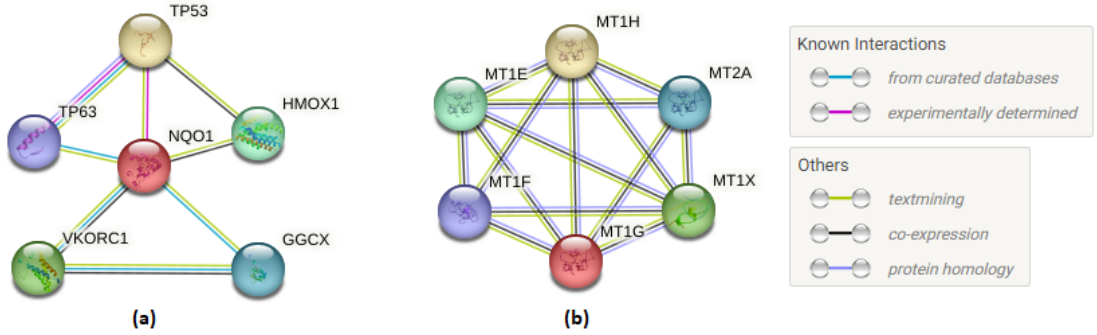

Figure 5.18: Analysis of the functional protein association network of MT1G and MT1F (**a**) and NQO1 (**b**), using the STRING web tool, to identify their protein-protein interactions and associations.

5.4.4 Determination of the significantly altered biological processes in IFNα treated ISG15$^{-/-}$ SiHa cells through gene set enrichment analysis

As seen by the volcano plots, the absence of ISG15 causes the upregulation and down-regulation of a cohort of proteins. To obtain a better perspective of what pathways might be dysregulated in ISG15 KO vs WT cells, a gene set enrichment analysis was carried out by entering the names of the significantly down- and upregulated genes (p-value<0.05, FC <0.3 and >2) into g:Profiler to group them by biological process. For this purpose, both

R10K8 and R6K6 modified proteins were searched in each of the four conditions (treated or untreated and collected at 24 or at 48 hours). The GO terms obtained were fed into Revigo to summarise and filter the terms. However, the obtained lists still had many repetitive and redundant terms, so, in order to create two-directional bar graphs, these were further refined by combining them into a single bar when applicable. When such combination occurred, the start of a change in pattern in the bar (from solid to white-stripped) represents the lowest p-value of the terms combined, and the end of the bar matches the highest p-value of those combined.

The biological processes identified to be down- and upregulated in untreated ISG15$^{-/-}$ vs WT are shown in Figure 5.19. Because these samples were not treated with IFN, there is no change in condition to discern the samples collected at 24 hours and the samples collected at 48 hours. Therefore, some of the identified biological processes are similar between the two time course samples. In the absence of IFN, the lack of ISG15 leads to various upregulated metabolic and catabolic processes, including aldehyde and nitrogen compound metabolism and protein catabolic processes. Additionally, mRNA related processes were found upregulated in the untreated samples collected at 48 hours. Interestingly, the absence of ISG15 also resulted in the downregulation of metabolic and catabolic processes including organic and organonitrogen compound metabolism and protein metabolism. On top of this, other processes such as defence response to viruses and viral processes, cellular response to cytokine stimulus and peptide biosynthetic processes are also downregulated in ISG15$^{-/-}$ cells even in the absence of IFN.

The changes in the biological processes resultant from the IFN treatment in ISG15$^{-/-}$ vs WT cells are presented in Figure 5.20. Although the processes dysregulated in the samples treated only for 24 hours did not differ much from the ones dysregulated in untreated cells (mRNA and aldehyde metabolic processes and macromolecule catabolic processes), treatment prolonged past 24 hours resulted in the dysregulation of pathways not seen altered in the absence of IFN. These include upregulation of the antigen processing and presentation pathway, and downregulation of processed related to response to wounding and wound healing.

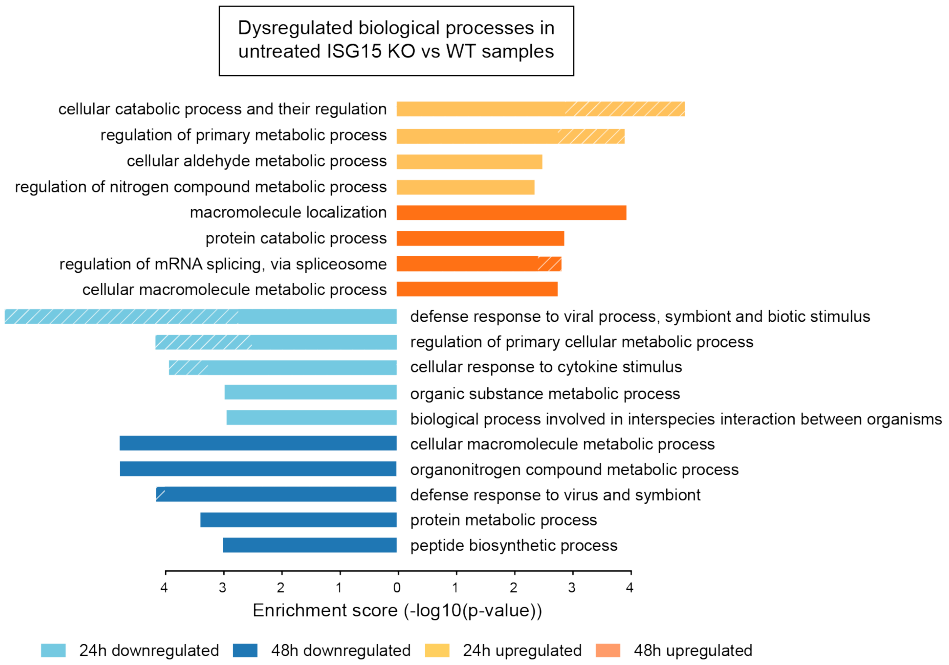

Figure 5.19: Two directional bar graph showing the dysregulated biological processes identified untreated ISG15$^{-/-}$ vs WT samples monitored for 48 hours. The downregulated processes (left) are shown in blue colours, and the upregulated processes (right) are shown in yellow and orange. When terms were combined to reduce the number of repetitive or redundant terms, the start of a change in pattern in the bar (from solid to white-stripped) represents the lowest p-value of the terms combined, and the end of the bar matches the highest p-value of those combined.

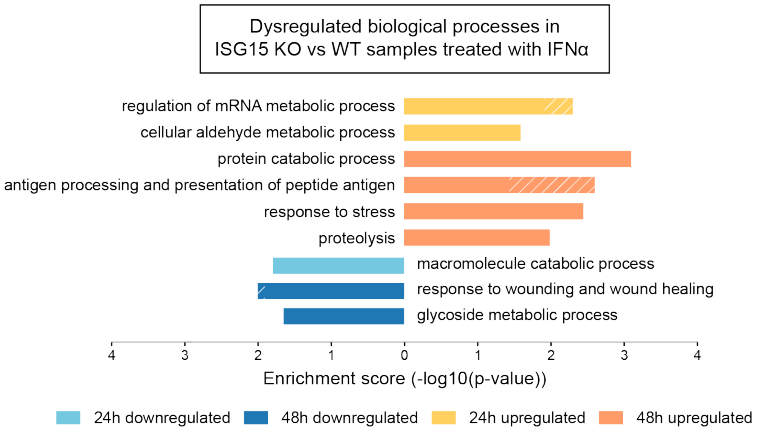

Figure 5.20: Two directional bar graph showing the dysregulated biological processes identified ISG15$^{-/-}$ vs WT samples treated with IFNα for 48 hours. The downregulated processes (left) are shown in blue colours, and the upregulated processes (right) are shown in yellow and orange. When terms were combined to reduce the number of repetitive or redundant terms, the start of a change in pattern in the bar (from solid to white-stripped) represents the lowest p-value of the terms combined, and the end of the bar matches the highest p-value of those combined.

5.5 Discussion

The volcano plots presented here identified several interesting targets to further investigate. Nevertheless, caution is required when interpreting these results, especially regarding the expression levels in the two different time-points, as some of the proteins identified were not included in the analysis due to statistical significance factors, which does not mean they were not present or altered in the sample. Many hypothesis and potential conclusions had to be discarded or questioned after double-checking the data, individually searching proteins only found in one of the two conditions (meaning no fold change was available) and targets excluded from the filtering process due to not being identified with enough confidence. For instance, many of the fold change values of the expression of IFIT1 and UBE2K in ISG15 KO vs WT samples were not included in the analysis after the data was filtered by significance, and although the exact values cannot be determined by immunoblotting the overall biological effect (down- or upregulation) matched that seen in the data despite the poor p-values. Although for many years the weight of the p-value in biological analysis has been undisputed, even if it meant leading to important reproducibility issues or discarding biologically relevant data, its role is now being questioned in favour of using it as a decision-making guide for the scientists to interpret and select what targets to validate experimentally (Nuzzo, 2014; Halsey *et al.*, 2015; Wasserstein & Lazar, 2016; Colquhoun, 2017; Halsey, 2019; Amrhein *et al.*, 2019). The targets identified here provide valuable information on the proteins whose levels dysregulated by ISG15 in an IFN dependant manner or regardless of treatment, but further experiments would be required before making any assumptions on the expression pattern throughout the IFNα treatment.

ISG15 was detected among the significantly downregulated proteins. Even though the knock-out of ISG15 was confirmed several times by immunoblotting and sequencing, the identification of ISG15 in a genetically knocked out cells line could indicate the partial expression of a defective protein, whose peptides after degradation were detected. A relatively recent publication by Smits *et al.* (2019) studied the frequency in which genes knocked out with frameshift mutations generated by CRISPR held residual protein expression. Their results revealed that around a third of the knock-outs studied retained partial expression, even though most of them presented reduced protein levels. A more in depth analysis of three of the knock-outs revealed that the protein expressed was somehow truncated, but retained some of its function. Although the cellular phenotype and response to IFN of this cell-line (clone #1) resembled those in other cell lines whose ISG15 expression knock-out had also been confirmed via immunoblotting and sequencing (clones #3, #4, #9 and #10), further determining the level of expression reduction via RNA-sequencing could be useful to confirm the knock-out state of the gene.

As described in chapter 1, free ISG15 plays a key role as a negative regulator of the IFN pathway by interacting and stabilising USP18, which binds to the IFNAR2 receptor blocking its interaction with JAK1, in an ISGylation independent process (Malakhova *et al.*, 2003; Malakhova *et al.*, 2006; Kim *et al.*, 2006; Zhang *et al.*, 2015). Hence, the sustained upregulation of IFN driven pathways like the immune antiviral system showed in Figure 5.17 is expected in the treated ISG15 KO samples. However, a decrease in USP18 protein level would also be expected upon loss of ISG15 (Espada *et al.*, 2019; Vasou *et al.*, 2021), but no significant decrease was detected in ISG15 knocked-out SiHa clone #1 (Figure 5.16). This result should be validated through other means such as immunofluorescence and, since this immunoblot was performed in a clone obtained as the off-target result of a knocked-in attempt, the experiment should be repeated in other cell lines. If a different expression level in WT and ISG15 KO cells is confirmed by other means, the immunoblot protocol for the extraction of this protein should be optimised (denaturing conditions, extraction buffer, etc.). If the results are confirmed, although further research would still be required to investigate the state of USP18 upon loss of ISG15, this cell line could potentially be an interesting model to study ISG15 roles uncoupled from USP18 in humans.

NQO1 (NAD(P)H quinone oxidoreductase-1) was one of the most upregulated proteins regardless of treatment. This reductase enzyme plays an important role in fighting oxidative stress by promoting the reduction of quinones, which are important elements in diverse functions such as cellular respiration and by-products of the metabolism of aromatic compounds, in order to avoid oxidative cell damage (Dinkova-Kostova & Talalay, 2010). The direct catalysis of quinones to hydroquinones through its two-electron reduction ability avoids the formation of intermediate reactive semiquinones, and prevents electrophilic quinones from taking part in other reactions that could also lead to reactive oxygen species (Rashid *et al.*, 2021). By this means, NQO1 plays a key role in stress responses by protecting the cells from the accumulation of damaging species. However, NQO1 has also been described to have other roles. Asher *et al.* (2002) report that NQO1 can stabilise p53, an interaction represented in the protein association network presented in this chapter. More recently, Wang *et al.* (2022) linked the upregulation of NQO1 with malignancy progression, invasion and bad prognosis in hepatocellular carcinoma, and showed that the NQO1/p53 interaction could enhance the activity of the sterol regulatory element-binding protein 1 (SREBP1), a transcription factor that regulates lipogenesis, which at the same time promoted tumour progression through abnormal lipid metabolism in the liver.

Interestingly, p53 has been shown to induce ISG15 (Liu *et al.*, 2004), and ISG15 has also been reported to target misfolded p53 via HERC5 for its ISGylation and consequent degradation (Huang *et al.*, 2014). The fact that p53 induces ISG15, which at the same time degrades p53, could be part of a negative regulatory control system. At the same time, NQO1 stabilises p53, and the lack of ISG15 promotes accumulation of NQO1, as seen in

the results presented here. Nonetheless, if ISG15 inhibits or represses NQO1 has part of the hypothetical IFN independent negative regulatory pathway of p53 has not been described. According to the database canSAR.ai, SiHa cells present overexpression of p53 (6.283366), with no mutations at a genomic level. A possible explanation, analysing the data presented here, is that the lack of ISG15, and ISG15 dependant overexpression of stabilising NQO1 could be involved in the accumulation of p53. Although p53 was not detected in the analysis presented here, which only determined the *de novo* synthesised proteins in a short period of time, it would be of interest to determine the p53 status of the cell line in the presence and absence of ISG15. There is, however, contradictory publications that refute this hypothesis. As described in subsection 1.3.2, Park *et al.* (2016) declared that, under DNA-damaging conditions, the ISGylation of p53 enhances its anti-tumour properties by promoting its binding activity. In their study, they stated p53 to be ISGylated through TRIM25 and not HERC5, and showed that silencing of TRIM25 prevented this modification, while the silencing of HERC5 did not. This information contrasts with that presented by Huang *et al.*, who reported p53 to be ISGylated by HERC5 but not TRIM25. In support of the data presented by Huang *et al.*, another study by Wang *et al.* (2017) reported that overexpression of HERC5 decreased p53 levels, while its downregulation resulted in p53 accumulation. In any case, further research is required to determine the consequences of the ISGylation of p53 and the role of NQO1 in its accumulation in SiHa cells.

The overexpression of MT1G and MT1F brought attention to the family of MT metallothionein proteins. These antioxidant metal ion binding small proteins are involved in several biological processes including response to oxidative stress, cell damage, inflammation and, as suggested by their name, metal homeostasis among others (Laukens *et al.*, 2009). There are 11 functional MT genes in humans (MT1A, MT1B, MT1E, MT1F, MT1G, MT1H, MT1M, MT1X, MT2A, MT3 and MT4), but there are also seven pseudogenes and four MT-like genes, many of which have very similar amino acid sequences (Laukens *et al.*, 2009). The wide range of very similar small proteins has hindered the study of their individual roles in health and disease.

Even though MTs are involved in protective processes under physiological conditions, they have also been found overexpressed in several diseases such as inflammatory (Dai *et al.*, 2021) or neurodegenerative conditions (Mocchegiani *et al.*, 2005). In cancer, particularly, MTs have been described to play a role in tumour growth, differentiation, drug resistance, immunomodulation, angiogenesis and metastasis, although the levels of the different subtypes vary in different cancers (Cherian *et al.*, 2003; Pedersen *et al.*, 2009; Si & Lang, 2008). This is also the case for the two MT1 members identified upregulated in the absence of ISG15 in SiHa cells, MT1F and MT1G. Nguyen *et al.* (2000) proved that eight out of eleven patient-derived renal cell carcinoma samples presented both nuclear and cytoplasmic MT staining. A deeper analysis revealed that some of the subtypes remained

unaltered when compared to the controls (MT-1E, MT-1F and MT-1X), while others were downregulated (MT-1A and MT-1G) or upregulated (MT-2A), suggesting function specificity. Jin *et al.* (2001) also described a general upregulation of MTs in patient-derived primary invasive ductal breast cancer samples, significantly higher in the higher grade tumours, but reported the expression of MT-1F to be significantly elevated in the highest graded tumours, unlike in the samples analysed by Nguyen *et al.* In contrast, results by Lu *et al.* (2003) showed downregulated MT1F levels in hepatocellular carcinoma tumours compared to healthy and para-cancerous tissue, and noted that exogenously added MT1F resulted in growth inhibition in HepG2 cells. This inconsistent up- and down regulation in different cancer types has also been observed in the other MT subtypes and isoforms. Figure 5.21, created from databases by Si & Lang (2008) for their review on the involvement of these proteins in cancer, shows the mRNA transcript level state of the different MT types and isoforms found in different cancers compared to those found in normal samples, counting in how many datasets a specific isoform was found up- or downregulated (shown in red or blue respectively).

Analysis Type by Cancer	Cancer vs. Normal *MT1A*		Cancer vs. Normal *MT1B*		Cancer vs. Normal *MT1E*		Cancer vs. Normal *MT1F*		Cancer vs. Normal *MT1G*		Cancer vs. Normal *MT1H*		Cancer vs. Normal *MT1M*		Cancer vs. Normal *MT1X*		Cancer vs. Normal *MT2A*		Cancer vs. Normal *MT3*		Cancer vs. Normal *MT4*	
Bladder Cancer		1	1			1		2		1	1	1		2	1	1		2				
Brain and CNS Cancer		1	1		1	1	1		1	2	1	2	1	1	3		1		1	6		
Breast Cancer	1	2		2		6	1		1	3		4		18		15		2		2		
Cervical Cancer																						
Colorectal Cancer		7		9		20		20		25		24		21		21		20		4		
Esophageal Cancer					1		1			1				1		2						
Gastric Cancer		3		3		7		10		11		8		10		9		4		3		1
Head and Neck Cancer					1	2		3		4		2		2		3	1					
Kidney Cancer						6		9		11		11		2		6		5				
Leukemia							1	2	1	3	1	1			1	1		2				
Liver Cancer				1		5		7		8		6		6		5		3				
Lung Cancer		2		4		5		3		2		3		6		5		5		2		
Lymphoma	3				4		5		3		6				8		8	1				
Melanoma																2						
Myeloma	1							1						1								
Other Cancer	2		1		4	1	6	1	5	1	5		2		4		5	1		1		1
Ovarian Cancer				1			2		5		1				1			1				
Pancreatic Cancer				1		2		3		4		4		1		1		1				
Prostate Cancer						3		1		2		2		4		5		1				
Sarcoma		1				9		10		12		9		9		8		7		3		
Significant Unique Analyses	7	17	3	21	11	68	17	71	16	89	15	77	3	84	18	84	15	55	1	21		2
Total Unique Analyses	199		254		419		441		449		448		354		434		416		410		205	

Figure 5.21: Expression of different MT isoforms in different cancers, by Si & Lang (2008). The numbers indicate how many datasets with significant upregulated (red) or downregulated (blue) MT mRNA transcripts were identified in a specific type of cancer.

As seen in MT1G and MT1F's proteins interaction maps, these proteins work in close relation with the other members of the MT1 and MT2 family. However, MT1G and MT1F were the only two isoforms identified in the analysis presented in this chapter. Like NQO1, both of them were upregulated in an IFN independent manner. To date no interaction between ISG15 and these proteins has been described in a cancer background. Nevertheless,

ISG15 has been identified to play a role in oxidative stress. Juncker *et al.* (2021) described ISG15 to mediate mitophagic failure following mitochondrial degradation, downregulation of which resulted in restored mitophagy and reduced oxidative stress, and a recent study has described ISG15 to mediate induction of ROS production, resulting in cardiovascular damage (González-Amor *et al.*, 2022). Also, many ISGylation targets have been described to be involved with oxidative stress (Zhao *et al.*, 2005; Giannakopoulos *et al.*, 2005), including TRXR1, which is strongly co-expressed with NQO1 upon *mycobacterium tuberculosis* infection (Singh *et al.*, 2017). On the other hand, FOXO3α, a transcription factor found to interact with other proteins to mediate the activation of a NQO1 containing complex that promotes an anti-inflammatory M2 macrophage mediated response (Singh *et al.*, 2017), has been shown to degrade upon ISGylation (Wang *et al.*, 2020a). Therefore, it could be conjectured that the downregulation of ISG15 allows for the accumulation of FOXO3 and subsequent activation of anti-inflammatory properties of NQO1. Contradictory, a very recent publication by Fakhar-Ul-Hassnain Waqas *et al.* (2022) reported that the knock-out of ISG15 in macrophages resulted in increased oxidative stress and downregulation of NQO1, suggesting further research is required to elucidate if there are other factors affecting this pathway, such as cell-type dependant regulation.

Most of the biological processes altered in untreated ISG15$^{-/-}$ are some form of metabolic or catabolic mechanism. These were found to be both up- and downregulated when comparing ISG15 KO vs WT cells. Type I IFNs have been proven to have the ability to alter metabolic pathways as part of their anti-viral activity, such as downregulation of lipid metabolism (Blanc *et al.*, 2011; York *et al.*, 2015; O'Neill, 2015) and upregulation of oxidative phosphorylation (Wu *et al.*, 2016), which could explain the results presented here. Nonetheless, caution is advised when assessing these results. Re-evaluation of the methods used to interpret gene enrichment analysis have brought up interesting points for discussion. In this type of analysis, once a list of genes of interest has been identified (e.g., genes found overexpressed in ISG15 KO vs WT samples), it is inserted into gene enrichment analysis tools such as g:profiler. The analyser groups the genes in functional categories such as biological processes, cellular component or molecular function, and determines if these are down- or upregulated compared to what would be expected to obtain in a list of the same size of randomly selected genes within the organism of interest (Timmons *et al.*, 2015). For example, suppose that a list of 60 genes is analysed (query = 60) and that 30% of them turn out to be listed in the term designated as "lipid metabolism" (intersection size = 18). If in the human genome (effective domain size = 20000), this particular term has 1300 genes listed (term size = 1300), setting a gene enrichment analysis tool to search within the human database would come back with what percentage of genes would be expected to belong to this biological process given a random list of 60 genes within the human genome, providing a statistical value representing the likelihood that this under- or over-representation occurred by chance. Since the term size is 6,5% of the effective do-

main size, 3.9 genes would be expected to be found in the query list analysed, meaning a significant over-representation of this term. However, as recently discussed by Wijesooriya *et al.* (2022), this methodology can lead to a very significant amount of false discoveries. This group challenged the current methodology used in hundreds if not thousands of published papers, arguing that the use of the whole genome as a background can lead to false discoveries if used incorrectly, since different cells derived from different tissues do not constantly express the entire genome. The data obtained from the experiment presented in this chapter was sorted by significance and fold-change, separating significantly upregulated and downregulated proteins in ISG15 KO cells when compared to WT, which means the proteins expressed in WT cells were used as a control or background to list only the significant differentially expressed proteins. These lists were independently fed into a gene enrichment analysis tool, which identified to which biological processes each of them belong and compared the representation level of each process with the representation level each would have if the genes in the list were uniformly distributed using the whole genome as a reference. It is reasonable to assume that using the particular expression pattern of a cell-line as a background will produce different results to those obtained when using the whole genome, specially in the hits with lower scores. Therefore, when possible and/or appropriate, a specific list of genes can be used as a background list to limit the number of false over- and down- representations found based on the whole genome instead of in the basal expression of the model used. However, as discussed in section 3.5, the genetic variation arisen from the maintenance of cells in culture as well as expression regulatory changes resultant from the adaptation of cells to the environment must be borne in mind. It is likely that the basal expression from cells in different labs are significantly different from each other and from the one gathered in data bases, making the selection of the appropriate background list challenging.

Accordingly, the information gathered thorough this analysis was cautiously used as a tool to identify possible pathways to further explore, more than to make assumptions on what pathways are dysregulated upon the silencing of ISG15. According to the results, the biological processes of the proteins whose expression was significantly altered in ISG15 KO vs WT cells during the first 24 hours of IFN treatment did not differ much from those observed in untreated cells (mRNA and aldehyde metabolic processes and macromolecule catabolic processes). Nevertheless, as treatment prolonged past 24 hours other interesting processes were identified. ISG15 KO cells treated for 48 hours downregulated the expression of proteins involved in response to wounding and wound healing. If confirmed by other means, this would be particularly interesting considering that a common symptom in ISG15 deficient patients is the appearance of recurrent skin lesions. Hayat Malik *et al.* (2022) studied these lesions in two ISG15$^{-/-}$ patients and found that the expression of elements essential for epidermis integrity, such as collagen and adhesion proteins, were downregulated these cells. Finally, the expression of proteins related to the antigen pro-

cessing and presentation pathway were detected to be significantly upregulated in ISG15 KO cells treated for 48 hours when compared to WT cells under the same treatment. However, not much has been described in the possible role of ISG15 in the MHC I pathway.

In conclusion, the upregulation of antioxidant proteins such as NQO1, MT1G and MT1F upon loss of ISG15 suggest new interesting targets to further research in the context of cancer. On the other hand, and bearing in mind the limitations of this methodology, it seems that the lack of ISG15 could result in metabolic dysregulation regardless of IFN treatment. Similarly, the downregulation of wound response and healing elements is consistent with the patient reports published to date, all of which described ISG15$^{-/-}$ patients to present ulcerative skin lesions (Buda *et al.*, 2020; Martin-Fernandez *et al.*, 2020; Al-Mayouf *et al.*, 2021; Hayat Malik *et al.*, 2022). Using the findings in this chapter as a base, the possible involvement of ISG15 in the regulation of antigen processing and presentation is investigated and described in the following chapter.

Chapter 6

Whole proteomic and immunopeptidomic analysis on ISG15 deficient patient-derived glioblastoma stem cells upon IFNα2 treatment

6.1 Introduction

The major histocompatibility complexes (MHC) are polymorphic membrane glycoproteins responsible for binding foreign and self protein fragments to present them at the cell surface, where T cells recognise them to activate the appropriate immune response. There are two types of MHCs - class I and II. While MHC class I is present in almost every cell of the organism and its peptides are recognised by $CD8^+$ T cells, MHC class II are mainly found in macrophages and lymphocytes and its peptides are recognised by $CD4^+$ T cells (Rock *et al.*, 2016). By presenting these peptides to T-cells, the immune cells help eliminate pathogens or damaged cells they belong to, while also aiding adaptive response development. Figure 6.1 shows the simplified pathway that leads to peptide presentation on MHC-I molecules (Neefjes *et al.*, 2011), where proteins synthesised inside the cells are degraded by the proteosome, resulting in peptide fragments. These fragments are translocated through the Transporter associated with Antigen Presentation (TAP) into the endoplasmic reticulum (ER), where they are loaded into the peptide-binding groove of MHC-I molecules. The resultant complexes are transported through the Golgi apparatus to the cell membrane for presentation to $CD8^+$ T cells. Alternative MHC-I peptide sources in-

clude rapidly degrading proteins from defective ribosome products (DRiPs) (Bourdetsky *et al.*, 2014), introns of non-spliced quickly translated newly synthesised mRNAs, known as pioneer translation products (PTPs) (Apcher & Fåhraeus, 2015), and spliced peptides composed of fragments distant in the sequence of the protein of origin, instead of being linear fragments of proteins (Vigneron *et al.*, 2017).

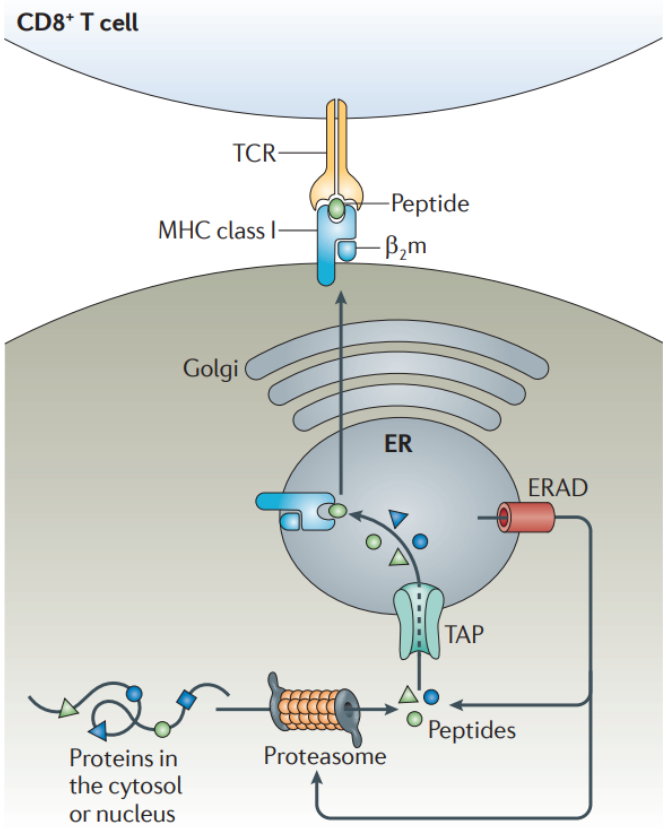

Figure 6.1: Simplified MHC-I antigen presentation pathway, by Neefjes *et al.* (2011). Proteins synthesised inside the cells are degraded by the proteosome, resulting in peptides that are translocated though the transporter associated with antigen presentation (TAP) into the endoplasmic reticulum (ER). Here, peptides are loaded into MHC-I molecules and the resultant complexes are transported through the Golgi apparatus to the cell membrane, where the peptides are presented to $CD8^+$ T cells.

Different cancer types are known to have different somatic mutations at different levels, called mutation signatures. Figure 6.2 (Alexandrov *et al.*, 2013), shows the prevalence of 4,938,362 somatic substitutions and small insertions/ deletions (indels) across 30 distinct human cancer types, each dot representing a different sample and the red line marking the median number of mutation events. In every case, the normal DNA of each patient was also sequenced to determine the origin of the mutation. These DNA mutations found in cancer can result in peptides specific to these cells, called tumour specific antigens (TSAs). While different cancer types share common mutations whose identification could be used for general patient treatment, each patient will have an unique combina-

tion of somatic mutations creating a specific personal signature (Figure 6.3). Identifying this patient-specific signature would open the door to personalised immunotherapy treatments when more general treatments fail.

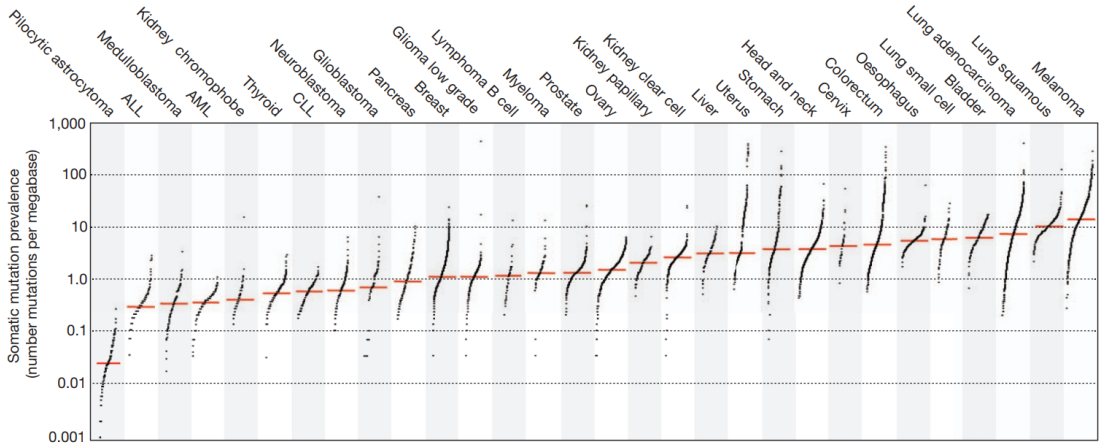

Figure 6.2: Prevalence of somatic mutations across different human cancer types, by Alexandrov *et al.* (2013). Each dot represents a different sample in the respective cancer type, while the red line marks the median number of mutations in each category. In every case, the normal DNA from each patient was also sequenced to determine the origin of the mutation.

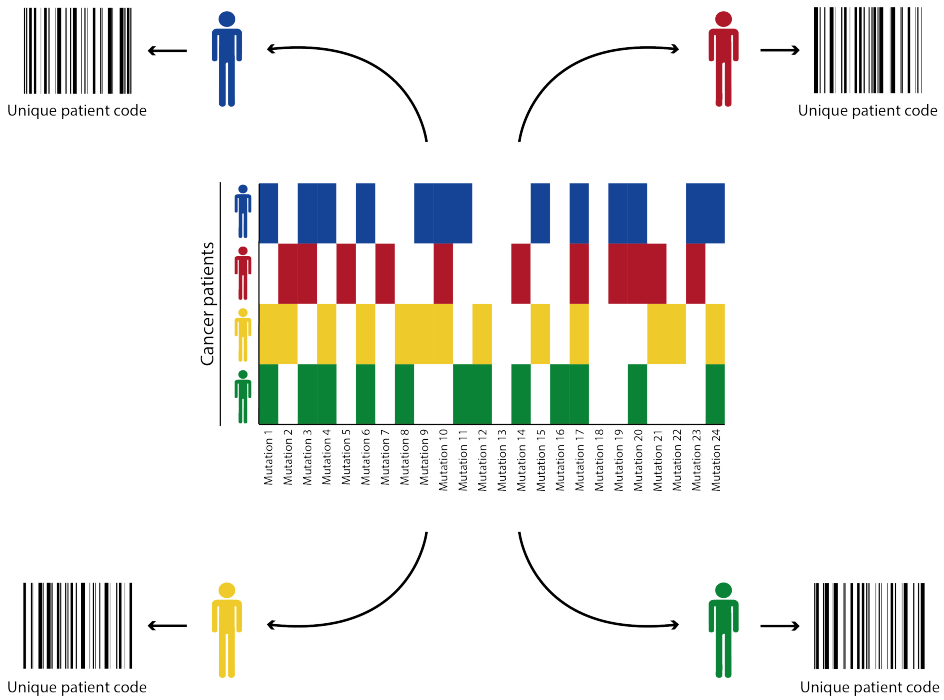

Figure 6.3: Patient specific cancer barcode, adapted from figure by Urionabarrenetxea *et al.* (2019). Although a group of patients with a certain cancer type will likely share many of the mutations belonging to the signature of such cancer, the unique combination of somatic mutations in patient creates a specific personal signature which could be used for personalised immunotherapy treatments.

The neoantigen landscape of patient-derived tumour samples has been analysed with therapeutic purposes before. A report by Rooij *et al.* (2013) described the case of a stage IV melanoma, ipilimumab-responsive patient whose tumour and non-tumour samples were used for sequencing to identify tumour-specific mutations. After filtering the 1,657 identified mutations, they selected 448 potential $CD8^+$ T cell epitopes with a significant binding affinity for HLA-A and B. These peptides were used for T-cell reactivity analysis, which revealed two different promising patient specific neoantigens that caused significant T-cell response. To ensure that the response observed was specific to the peptide, they further tested one of them by analysing the T-cell response with both the mutated peptide and the wild-type epitope, with the latter not causing any response. The following year, Snyder *et al.* (2014) published a study in which they also analysed melanoma samples from patients treated with anti-CTLA-4 drugs (ipilimumab and tremelimumab), which aids the activation of T-cells allowing them to destroy the cancer cells from which the TSAs came from. The neoantigen peptides identified were tested for their ability to activate T-cells against the cancer cells, determining a peptide signature capable of doing so specifically present in tumours reactive to CTLA-4 blocking therapy. As the authors admit, the variety of previous treatments the patients had received prior to the genomic analysis and the different progression points at which the samples were collected could have limited the results. However, this study proves the potential of analysing the immunopeptidomic landscape of tumour samples and provides proof of principle that such analysis can be used to predict which patients could benefit the most from immunotherapy.

A case study reported by Tran *et al.* (2014), on a patient with a metastatic cholangiocarcinoma, described that whole-exomic sequencing from resected lung metastasis revealed 26 mutations. Minigene constructs encoding for these mutated peptides were tested against the patient's tumour infiltrated lymphocytes (TILs), and found that the $CD4^+$ cells in the patients TILs were capable of recognising and beneficially reacting to a peptide belonging to a mutated version of the erbb2 interacting protein (ERBB2IP) expressed by the tumours. In a similar manner, Segal *et al.* (2008) used *in silico* approaches to identify new potential TSAs in cancer. To this end, they used the data published by Sjöblom *et al.* (2006), who analysed 13,023 genes in breast and colorectal cancers. Using cell lines or xenografts, they analysed 11 samples of each type, identifying 189 different mutated genes that contributed to carcinogenesis. Further analysing all mutated genes identified by Sjöblom *et al.*, Segal *et al.* selected 1,152 mutated peptides, identifying an average of 10 and 7 previously unknown unique MHC class I TSAs in breast and colorectal cancer respectively, some of which were included in the neoplastic subset identified by Sjöblom *et al.* More information of the use of neoantigens as a tool to target cancer cells through immunotherapy can be found in the many reviews published over the last years (Bobisse *et al.*, 2016; Schumacher *et al.*, 2019; Smith *et al.*, 2019; Zhang *et al.*, 2021c; Chong *et al.*, 2022).

While patient sample sequencing and analysis is a straightforward method for mutation and potential TSA identification in patient personalised treatment, mass spectrometry is a more convenient approach when trying to identify neoantigens in complex biological samples compared at a large scale. For example, Nelde *et al.* (2021) analysed the immunopeptidome of primary chronic lymphocytic leukaemia (CLL) samples by MS in order to identify non-mutated CLL-associated antigens recognised by patient-derived T-cells for the construction of peptide vaccines in a clinical trial at the University Hospital Tuebingen (NCT04688385). Optimised mass spectrometry protocols for the identification of peptides that lead to an effective adaptive immune response have been published in the last couple of years (Kote *et al.*, 2020). Purcell *et al.* (2019) described their protocol to collect the naturally MHC-I bound immunopeptides through immunoaffinity from a variety of cell types, which are then eluted with acid denaturation. Peptide separation by nano-ultra-performance liquid chromatography and subsequent high-resolution mass spectrometry leads to the identification of thousands of peptides.

This chapter aims to identify, through mass spectrometry, any potential differences in the peptides bound to MHC-I in wild-type and ISG15 knocked out patient-derived glioblastoma stem cells. Not much has been described regarding a potential role of ISG15 in the antigen presentation pathway of MHC-I. In 2015, Burks *et al.* studied the role of free ISG15 in breast cancer cells *in vitro* and *in vivo*, and showed that free ISG15 had a tumour suppressor role and enhanced MHC-I membrane expression, while ISGylation did not. Recently, Held *et al.* (2020) investigated the role of ISG15 and ISGylation in protein degradation and antigen presentation on transfected HEK293T cells, IFNβ treated murine embryonic fibroblasts (MEFs) and wild-type, ISG15$^{-/-}$ and USP18 mutated mice derived lymphocytes. Their results showed that, unlike ubiquitination, the ISGylation pathway did not induce bulk protein degradation and that cells derived from mice lacking either ISG15 or USP18 did not express MHC-I differently to cells derived from WT mice. However, the fusion of ISG15 to the lymphocytic choriomeningitis virus (LCMV) nucleoprotein (NP) did enhance the MHC-I bound presentation of two NP derived peptides. Results obtained in the SILAC analysis of SiHa cells, which identified antigen processing and presentation related biological processes to be upregulated in IFNα treated ISG15$^{-/-}$ cells (chapter 5), along with the conclusions of Held *et al.* (2020) suggesting that ISG15 could have a role in antigen presentation lead me to test the expression of MHC-I in ISG15 deficient cancer models.

One of the challenges for the development of targeted immunotherapies in malignancies with a lower mutational burden is the lack of known tumour specific neoantigens. As seen in (Figure 6.2), glioblastoma, which is the most common malignant primary brain tumour, is on the lower end in the ranking of cancers with most somatic mutations. Identifying and exploiting the potential neoantigens arising from these mutations is key to design

effective immunotherapies against this kind of tumour. Relatively novel peptide-based vaccines have been already tested in clinical trials with glioblastoma suffering patients. An example of this is the study by Keskin *et al.* (2018), in which they used a multi-epitope strategy to treat newly diagnosed glioblastoma patients with personalised vaccines. After surgical tumour resection, malignant and matched healthy cells were analysed to identify neoantigens for vaccine production, which was administered after surgery recovery and conventional radiotherapy treatment to eight patients. They detected increased amounts of tumour infiltrating T cells among the patients that reacted to the vaccines generating a neoepitope-specific immune response, which were the ones that had not received dexamethasone treatment during the study. A subset of these, found within post-vaccination intracranial resected tumours, was specific for the neoantigens targeted by the vaccine, demonstrating that the specific T cells generated as response to the vaccine can travel from the peripheral blood into an intracranial glioblastoma tumour. The eight patients taking part in the study eventually died after tumour recurrence, showing that further research is required to progress in the development of effective neoantigen vaccines. However, this study poses proof of concept that such vaccines can be a viable therapy for glioblastoma tumours even though they have a relatively low mutational burden and tend to be immunologically cold.

6.2 Aim and strategy

ISG15 has been found upregulated in glioblastoma tumours and has been related with cancer stemness. Weichselbaum *et al.* (2008), who identified the IRDS to be overexpressed in several human tumours, described ISG15 to be one of the signature members showing higher expression levels across the studied cancer types, including glioma (Figure 1.13). As mentioned above, the aim of this chapter was to determine if the loss of ISG15 led to differences in the immune peptides presented by MHC-I that could be further studied in the context of anti-cancerous treatments. Long term, the data obtained through this experiment could be combined with genomic and RNA-seq data to try to identify potential neoantigens for these therapies. To this end, WT and ISG15 deficient patient-derived glioblastoma stem cells were used. Before proceeding with the experiment, the expression of MHC-I was measured in the cells. Once expression was confirmed, two corning flasks were used per sample and condition (in triplicates), as seen in Figure 6.4, and cells were either treated with commercial human recombinant interferon α2 for 24 and 48 hours or left untreated. At the same time of seeding these flasks, remaining cells were used to perform a colony formation assay to confirm the phenotype described in chapter 4. When at the right confluence, the MHC-I bound peptides were eluted from the cells with an acid wash and analysed by mass spectrometry. These same cells were collected and sent for

whole proteomics analysis.

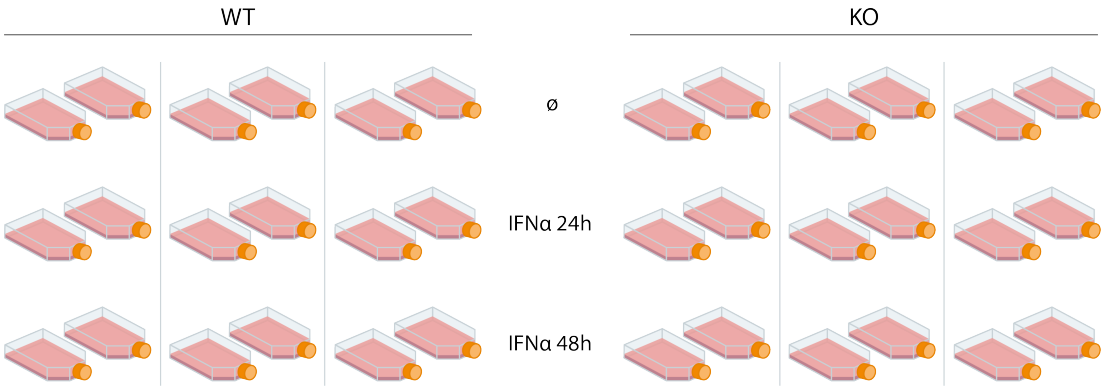

Figure 6.4: Experiment setup of the immunopeptidome and whole proteomics analysis of WT and ISG15 deficient GSC cells. Two T75 corning flask were used per sample in triplicates. Cells were either left untreated or treated with commercial Human Recombinant Interferon α2 for 24 or 48 hours.

6.3 Methods

6.3.1 Analysis of the expression of MHC-I through immunofluorescence staining and FACS

In order to find out if the GSC cells had enough MHC-I expression to perform an immunopeptidome analysis, quantification was carried out through FACS in wild-type and ISG15 deficient GSC cells. Cells were grown at two different levels of confluency, each in duplicate, seeding 100,000 cells for the lower confluence samples and 275,000 for the higher confluence samples. Half of the samples were treated with 100 U/mL commercial human recombinant interferon α2 for 0, 24 or 48 hours before being lifted and counted so the same amount of them could be stained with a fluorescein isothiocyanate-conjugated (FITC) HLA-ABC antibody (Invitrogen, #11-9983-42). Cell pellets were resuspended in 200 μL of PBS with 4 μL of antibody and they were left to incubate for 30 minutes in the dark. After the incubation, 2 mL of PBS were added to each tube and centrifuged before the pellets were reconstituted in 400 μL of PBS and transferred to FACS tubes. Cells were injected into a BD LSRFortessa™ Cell Analyser, where the fluorescent cells were detected and sorted by intensity across the different samples and conditions.

6.3.2 Peptide elution sample preparation

For the collection of peptides via acid elution for mass spectrometry analysis, two T75 flasks of wild-type and ISG15 deficient pooled GSCs were used in triplicates per condition

(see section 6.2). Once the cells reached around 70% confluency, two thirds of the plates were treated with commercial IFNα2 to a final concentration of 100 U/mL. After 24 hours, the untreated cells and half of the treated flasks were collected, leaving the other half in the incubator for another 24 hours before collecting them (48 hour treatment in total).

6.3.3 Peptide collection and processing for mass spectrometry analysis

To collect the samples, the flasks were placed and kept on ice during the whole procedure. The media was discarded and the flasks were washed quickly but gently with ice-cold PBS, freshly prepared with LC-MS water, by tilting the flasks to the PBS. Then, 3 mL of freshly prepared citrate-phosphate buffer (131 mM citric acid, 66 mM Na_2HPO_4, NaCl 150 mM) adjusted at pH 3.3 with NaOH and prepared with LC-MS grade water were pipetted into the flasks, making sure that the solution completely covered all flask surface. Once fully covered, the flasks were incubated on ice for 3 minutes gently shaking them manually time to time, front to back and left to right, to favour elution. After the incubation, the supernatant containing the immunopeptides was collected on 15 mL falcon tubes. The tubes were centrifuged at 1000 rpm and 4°C for 5 minutes in order to remove cell debris. The clean supernatant was then transferred to new 15 mL falcon tubes, being very careful not to take any debris. Since each sample was composed by two flasks, the supernatant of these were mixed together resulting in one tube per sample and biological replica. The samples were snap frozen in liquid nitrogen and stored before further purification steps. The cells on the flasks were collected by scraping and, mixing the pellets that belonged to the same sample, the tubes were also snap frozen and stored at -80°C.

Peptide desalting

Once ready to process the peptide samples, these were thawed on ice and Oasis HLB filtering cartridges (Waters, #WT186000382) were assembled on 15 mL falcons to desalt them. The columns were conditioned with 1 mL condition buffer (0.2% v/v formic acid (FA) in methanol) per cartridge and it was left to flow by gravity, without applying any force or centrifuging. The collection tubes were emptied (as after each following step) and 1 mL of equilibration buffer (0.2% v/v FA in LS-MS water) was added per cartridge, again letting it flow by gravity. The samples were then loaded into the columns and left to flow. To wash the samples, 1 mL of washing buffer (5% methanol and 0.2% FA in LS-MS water v/v) was added to each cartridge and, after passing by gravity, the wash was repeated two more times. Finally, cartridges were transferred to low affinity, low binding 2 mL collection tubes and the samples were eluted by adding 1 mL of elution buffer (80% methanol and 0.2% FA in LS-MS grade water v/v) to each cartridge and letting it flow by gravity. The

recovered volume in each sample, around 0.9 mL, was mixed with 0.9 mL equilibration buffer to dilute the methanol in the sample to 40%.

Peptide purification

After the samples had been desalted, the samples were passed through 3kDa Amicon Ultra-2 Centrifugal Filters (Millipore, #UFC200324) for further purification. For this, columns were first washed by adding 1 mL LS-MS grade water to each and were centrifuged at 4°C and 4000 xg for 30 minutes. The collection tubes were emptied along with any water that had not passed the filter after the centrifugation, making sure there was none left in the column. The 1.8 mL that composed each sample were added to each column and they were centrifuged at 4°C and 4000 xg for 135 minutes. The filtered samples were transferred into low affinity, low transfer 2 mL tubes. A CentriVap centrifugal concentrator (Labconco$_{®}$) was used to evaporate the elution supernatant and dry the peptides. Dried peptides were snap frozen and sent to the International Centre for Cancer Vaccine Science (Gdansk, Poland) along with the cell pellets harvested after collecting the peptides. Samples were sent in a big polystyrene box with 10 kg dried ice to ensure they arrived in the adequate condition for further processing.

6.3.4 Sample preparation for whole proteomic mass spectrometry analysis

Pellet lysis

The frozen GSC cell pellets, from which the immunopeptides were eluted, were thawed on ice and 300 μL of freshly prepared urea buffer (8M urea in 0.1M Tris-HCl pH 8.5) were added to each sample. Tubes were left on ice for 30 minutes with occasional mid-speed vortexing. After making a small hole in the lid of each sample with a needle to avoid pressure contrast, tubes were snap frozen by dipping them in liquid nitrogen. Samples were thawed and the process was repeated two more times. The tubes were then placed in a floating holder and in a tray full of ice-cold water, which was left in an ultrasonic bath for 5 minutes making sure that the waves transferred to the cold water through the tray. Samples were centrifuged at full speed (17,000 xg / 13,300 rpm) for 15 minutes at 11°C to avoid urea precipitation at lower temperatures. The supernatant of each sample was transferred to new clean low binding tube and a BCA assay was performed (ThermoFisher Scientific, #23225) to determine protein concentration in the samples. Before proceeding, an aliquot of each sample was diluted into a final concentration of 3M of urea, since higher concentrations interfere with the assay. The standards were created with a solution of urea in Tris-HCl to match the concentration in the samples and the protocol provided by the

supplier was followed.

Sample filter aided sample preparation (FASP)

For FASP, 200 μL of urea buffer were added to each Microcon-10kDa Centrifugal Filter Units with Ultracel-10 membrane (Merck, #MRCPRT010), followed by 75 μg of protein mixed by gently pipetting up and down into the urea buffer. The rest of each sample was frozen immediately at -80°C. Samples were centrifuged at full speed at room temperature for 30 minutes to pass them through and adhere the protein to the column membrane. To reduce the samples, 100 μL of urea and 20 μL of 100 mM Tris (2-carboxyethyl) phosphine hydrochloride (TCEP) in LC-MS water were added to each column. Tubes were incubated at 37°C and 600 rpm in a shaking thermoblock for 30 minutes and centrifuged at full speed and room temperature for 30 minutes. Next, 100 μL urea with 20 μL of 300 mM iodoacetamide in LC-MS H_2O were added to each column for protein alkylation. Tubes were placed in the shaking thermoblock again for a minute to mix the reagents well (37°C and 600 rpm) and, because iodoacetamide is light sensitive, they were left on a dark clean cabinet at room temperature for 20 minutes for the reaction to take place. Samples were centrifuged at full speed at room temperature for 30 minutes. Columns were washed with 100 μL of 100 mM ammonium bicarbonate (NH_4HCO_3, aka ABC) in LC-MS water to dissolve any remaining precipitated urea, because this interacts with trypsin inhibiting its proteolytic activity, and at the same times provides an optimum environment for trypsin to work if maintained at 37°C and pH 7.8. Samples were centrifuged at full speed and room temperature until all the solution passed through the membrane before washing another three times each with 100 μL of NH_4HCO_3, slightly vortexing after each addition to properly wash the walls of the columns. Collection tubes were then changed for new clean ones to proceed to sample elution. For this, 21 μL of LC-MS water were added to a vial containing 20 μg of lyophilized sequencing grade modified porcine trypsin (Promega, #V511A). This trypsin is modified to be resistant to autolytic digestion that would result in additional fragments that would interfere with the peptide detection by mass spectrometry. The vial was briefly centrifuged to collect all the trypsin into the added water, resulting in a final concentration of 0.9524 μg/μL. 100 μL of 50 mM NH_4HCO_3 in LC-MS water and 1 μL of trypsin were added to each sample. The ideal ratio trypsin:protein for a column digestion over-night is between 1:33 and 1:100 - in this case the ratio is 0.95:75, which translates to approximately 1:79. Samples were wrapped with parafilm to ensure sealing of the column's lid as well as the joining between the column and the collection tube. They were placed in a lidded big rack with the adjacent empty wells filled with water to avoid sample evaporation, and the rack was left in the incubator at 37°C over-night. The following day, the parafilm on each tube was carefully removed before centrifuging the samples at full speed and room temperature for fifty minutes to collect all of the elution. In order to increase

the recovery yield, columns were washed with 50 μL of 0.5 M NaCl in LC-MS water and centrifuged at full speed and room temperature for forty minutes.

Sample desalting

Before proceeding with the desalting protocol and to ensure there was peptides in the samples after the issue with precipitation, a BCA test was carried out by pooling 2 μL of each sample in a tube and placing 25 μL of the pool in a 96 well plate well. 25 μL of 50 mM NH_4HCO_3 in LC-MS H_2O were placed in the adjacent well and 200 μL of BCA working reagent were added to each well. A strong purple colour in the sample well showed a high contrast with the pale greenish colour in the blank well, suggesting a good concentration of peptides. For desalting, columns were washed with 200 μL of acetonitrile (ACN) + 0.1% FA and centrifuged at 0.3 rpm for 2 minutes at room temperature. All following centrifugations were carried out at room temperature unless stated otherwise. This process was repeated two more times. Columns were then equilibrated with 200 μL 0.1% FA on LC-MS water and centrifuged at 0.5 rpm for 2 minutes. A second round was added, this time leaving the solution for 15 minutes before centrifuging to hydrate the slurry phase of the column. The eluted peptides were transferred into the C18 columns and centrifuged at 0.7 rpm for 2 minutes. Samples were desalted with 200 μL 0.1% FA on LC-MS water and centrifuged at 0.7 rpm for 2 minutes. This step was repeated another two times, emptying the collection tube after each centrifugation. Collection tubes were then changed for new clean ones to proceed to sample elution. Peptides were eluted by adding 200 μL of 50% ACN, 0.1% FA in LC-MS water and centrifuging at 0.7 rpm for 2 minutes. To ensure full extraction of the peptides, 200 μL of 80% ACN, 0.1% FA in LC-MS water were added to each column, followed by centrifugation at 0.7 rpm for 2 minutes. A last elution step was performed in new clean tubes with 200 μL of 80% ACN, 0.1% FA in LC-MS water. The collected elutions were combined resulting in a total of 600 μL. Desalted peptides were kept at 4°C over-night and dried in a evaporator centrifuge Concentrator Plus (Eppendorf) before freezing them at -80°C for posting alongside the purified peptides.

6.3.5 Mass spectrometry analysis

30 μL of loading buffer composed of 0.08% trifluoroacetic acid (TFA) and 2.5% ACN in MS-LC grade water were used to reconstitute the vacuum dried peptides before Dr. Sachin Kote and Dr. Jakub Faktor analysed them at the e International Centre for Cancer Vaccine Science using a Ultimate 3000 nanoLC system coupled to an Orbitrap Exploris 480 mass spectrometer (Thermo Fisher Scientific). Upon sample injection, peptides were separated by liquid chromatography as previously described in section 5.3.2 using 0.1% FA in LS-MS

water as solvent A and 0.1% FA and 80% ACN in LS-MS water as solvent B. Samples were analysed with the following settings: applied normalized collision energy at 30%, MS/MS resolution at 60,000 (at 200 m/z), AGC target value of 100% and a maximum injection time of 100 ms. Details on the key components of an Orbitrap mass spectrometer can be found in section 5.3.2.

6.3.6 Data analysis

Data analysis was performed with the quantitative proteomics software MaxQuant using the UniProt database (https://www.uniprot.org/) by Dr. Sachin Kote and Dr. Jakub Faktor. Following the same protocol described in subsection 5.3.3, the obtained results were used to generate volcano plots using the web tool VolcaNoseR (https://huygens.science.uva.nl/VolcaNoseR2/), using below 0.5 and above 2 as fold change cut-offs (x-axis) and $p<0.05$ as significance cut-off (y-axis). Data was further sorted for gene set enrichment analysis ($p<0.05$ and fold change above 1.5 and below 0.67) and the gene names were inserted into g:Profiler (https://biit.cs.ut.ee/gprofiler/gost). For this analysis, the proteins found only in ISG15 KO samples and only found in WT were also included as upregulated and downregulated respectively. The Gene Ontology terms (GO terms) compiling genes by their biological process and cellular component location along with their assigned p-values were acquired from the uncapped results and fed into Revigo (http://revigo.irb.hr/). The settings were adjusted to obtain a medium list (0.7) with associated p-value, and to work with the default semantic similarity metric (SimRel) and the human UniProt protein database (9606). To display the cellular location of the significant upregulated and downregulated proteins, the data was exported from Revigo in a tree map format to create pie charts using the Circular Gene Ontology (CirGO) web tool (https://bio.tools/cirgo). A flow chart showing the summarised data analysis process can be found in Figure 6.5.

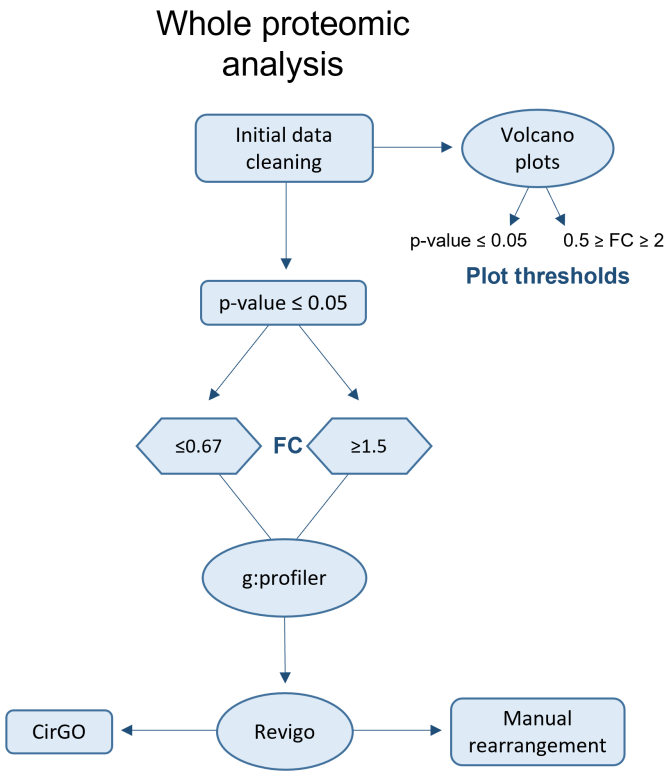

Figure 6.5: Flow diagram of the data analysis methodology used in the whole proteomic mass spectrometry analysis.

The analysis of the immunopeptidome of ISG15 KO vs WT GSC samples identified thousands of peptides, each of them with its own p-value. All the peptides with a p-value over 0.05 were discarded for the analysis. A flow diagram summarising the methodology used for the analysis of the data of this section is shown in Figure 6.6.

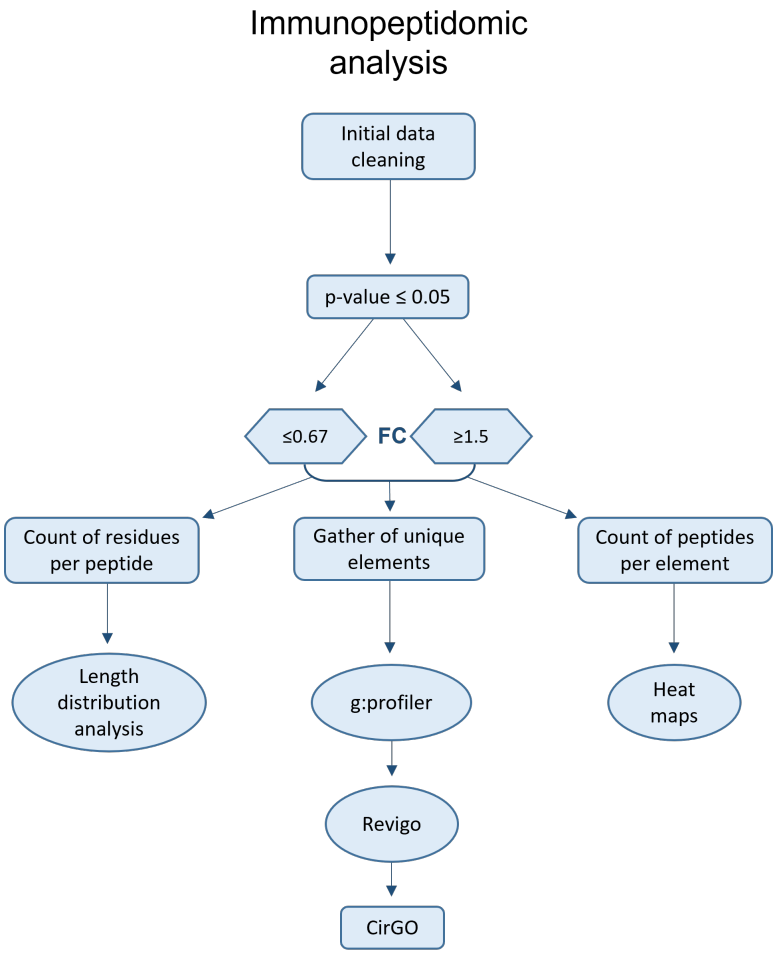

Figure 6.6: Flow diagram of the data analysis methodology used in the immunopeptidomic mass spectrometry analysis.

6.4 Results

6.4.1 Analysis of the expression of MHC-I in ISG15 deficient GSC cells

The identification of upregulated antigen processing and presentation related biological processes in ISG15$^{-/-}$ SiHa cells lead to the decision of further analysing the possible involvement of ISG15 in the regulation of the MHC class I system. Before proceeding with the elution of the MHC class I bound peptides for their analysis by mass spectrometry, the expression level of MHC in ISG15 KO cells had to be confirmed. FACS analysis of GSC WT and ISG15 KO cells incubated with a FITC conjugated HLA antibody resulted in the 100% of the analysed single cells being gated as fluorescent, regardless of treatment condition. The mean fluorescence intensity (488-525/50-A) of each sample, directly correlated to the amount of fluorophores in the sample and therefore to the expression of HLA, was com-

pared between samples to identify any differences between the cell lines and treatment conditions. Figure 6.7a shows that the average of the duplicates in both untreated cell lines (ISG15 KO and WT) presented very similar intensity means but, once treated, HLA expression was significantly higher in ISG15 deficient cells. The mean intensity increase was directly proportional to duration of the treatment, being the highest at 48 hours, and the confluency level of the cells did not make a difference in the level of HLA expression. To determine if the increased fluorescence intensity was due to a higher number of events analysed, the total number cells recorded and analysed in each sample was plotted along with the average mean fluorescence intensity of the duplicates in each sample. Figure 6.7b shows that, even if the number of events analysed was higher in most of the untreated samples, the fluorescence intensity was lower than in the treated samples. These results suggest that the increase in HLA expression was the result of treating the cells in the absence of ISG15, while its absence alone did not make a difference in the expression of HLA.

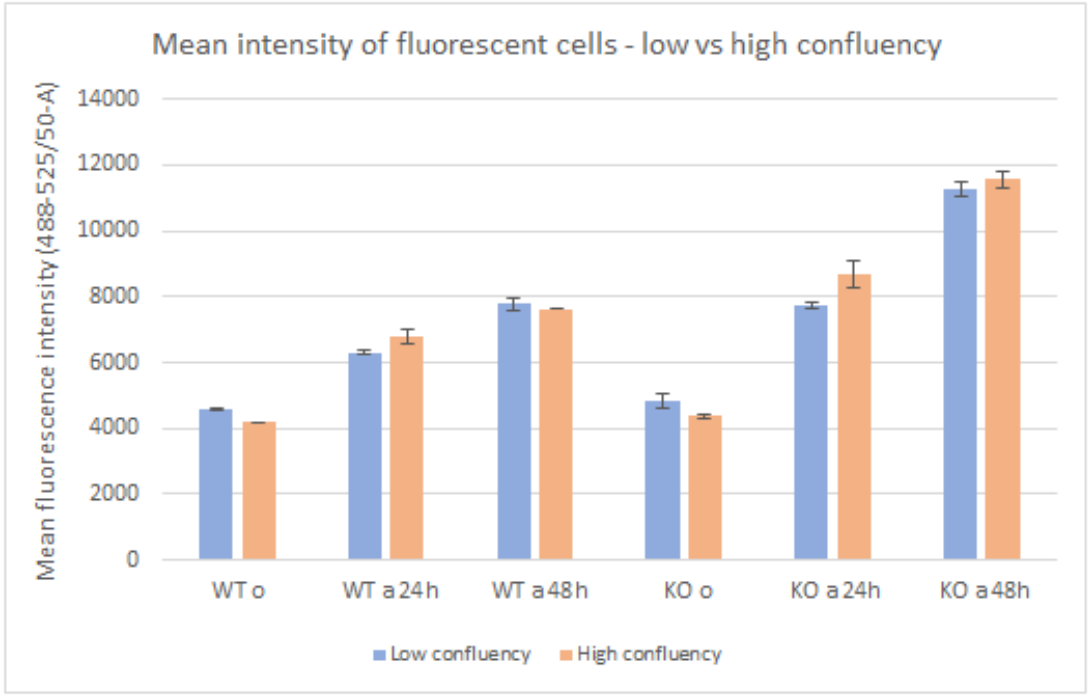

(a)

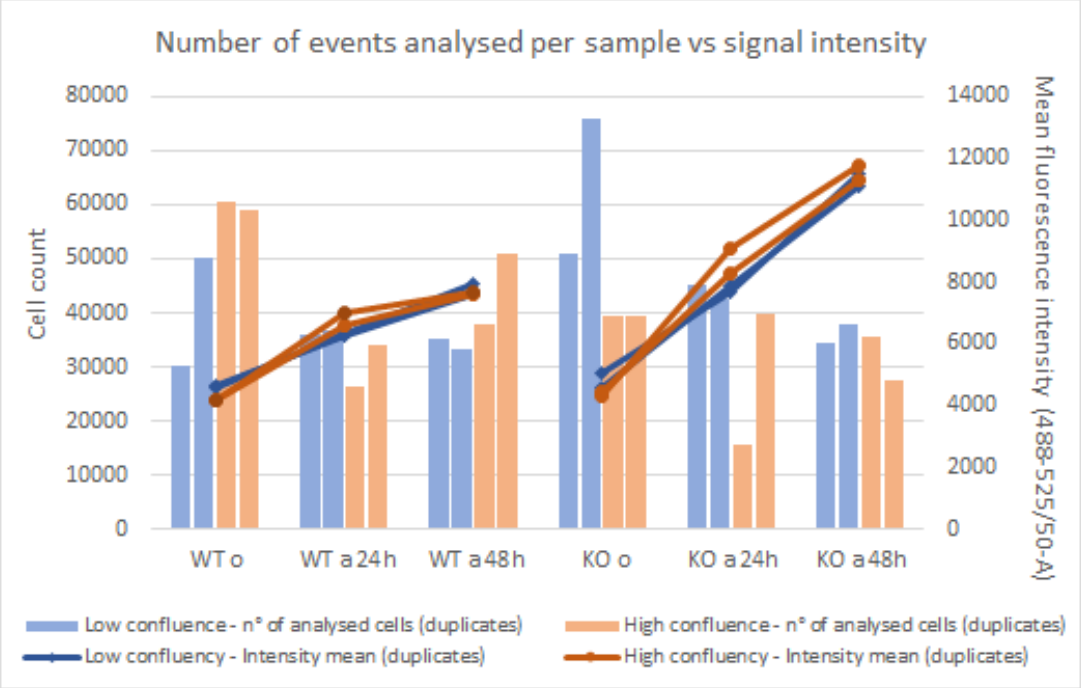

(b)

Figure 6.7: Quantification of MHC-I expression in GSC WT and ISG15 KO cells through FACS. Untreated and 24 and 48 hour IFNα treated (100 U/mL) cells incubated with an anti HLA-ABC FITC conjugated antibody were analysed by flow cytometry. **a)** Fluorescence intensity mean (duplicate's average) in higher (275,000 cells seeded) and lower (100,000 cells seeded) confluence samples of GSC WT and ISG15 KO treated and untreated cells. **b)** Count of analysed events in each sample (columns), in duplicate, versus their average intensity mean (lines). Error bars represent ±SD. Linear regression analysis run on same group samples showed no significant differences in HLA expression (p-value WT = 0.6361 & p-value KO = 0.2523). However, significant differences were found comparing WT and KO samples for both confluences (p-value low confluence < 0.0001 & p-value high confluence = 0.001). Statistical results are available in Table D.13, Table D.14, Table D.15 and Table D.16.

6.4.2 Immunoblot and colony formation assay on GSC cells

In order to confirm the phenotype described in chapter 4 in the same batch of cells used for the immunopeptidomic and whole proteomic experiment, an immunoblot for ISG15 and a colony formation assay were performed using the cells left after plating all the necessary flasks for the experiment. As seen in Figure 6.8, IFNα treated WT cells show a high level of ISGylated proteins and a band matching the size of free ISG15, which are absent in the untreated WT and both treated and untreated ISG15 KO samples, proving the lack of ISG15 expression in the KO cell line.

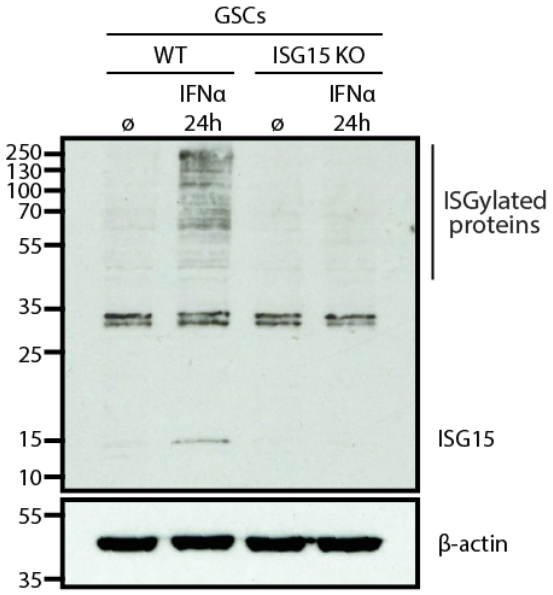

Figure 6.8: Immunoblot for ISG15 on GSC WT and ISG15 KO IFNα2 treated and untreated samples. The samples were collected from plates seeded with the cells remaining after seeding the flasks for the whole proteomics and immunopeptidomics experiment, meaning they reflect the ISG15 expression state of the samples used for both the mass spectrometry analyses. An equal amount of protein (50 μg) from whole cell lysate was loaded per lane in an 15% SDS-PAGE followed by immunoblotting. The membrane was developed using anti-ISG15 antibody (Santa Cruz Biotechnology (#166755) at 1:2000 in milk) followed by anti-β-actin antibody (Sigma (#A2228) at 1:1000 dilution). IFNα treatment concentration was 100 U/mL in all treated samples.

Regarding the colony formation assays, the morphology of GSC cells does not allow for a strong staining process, which results in a faint colour after staining as described in subsection 4.4.3. However, it can be observed in Figure 6.9a that the ISG15 deficient cells are more sensitive to IFNα than the WT cells, which is most noticeable in the last row corresponding to the higher treatment concentration. To confirm this quantitatively, the stain was dissolved in 1 mL of acetic acid as described in subsection 4.4.3, and the absorbance ratios were calculated from the mean of the triplicates using the untreated control as a reference. Absorbance readings and ratios shown in Figure 6.9b confirm the IFN sensitivity acquired upon deletion of ISG15.

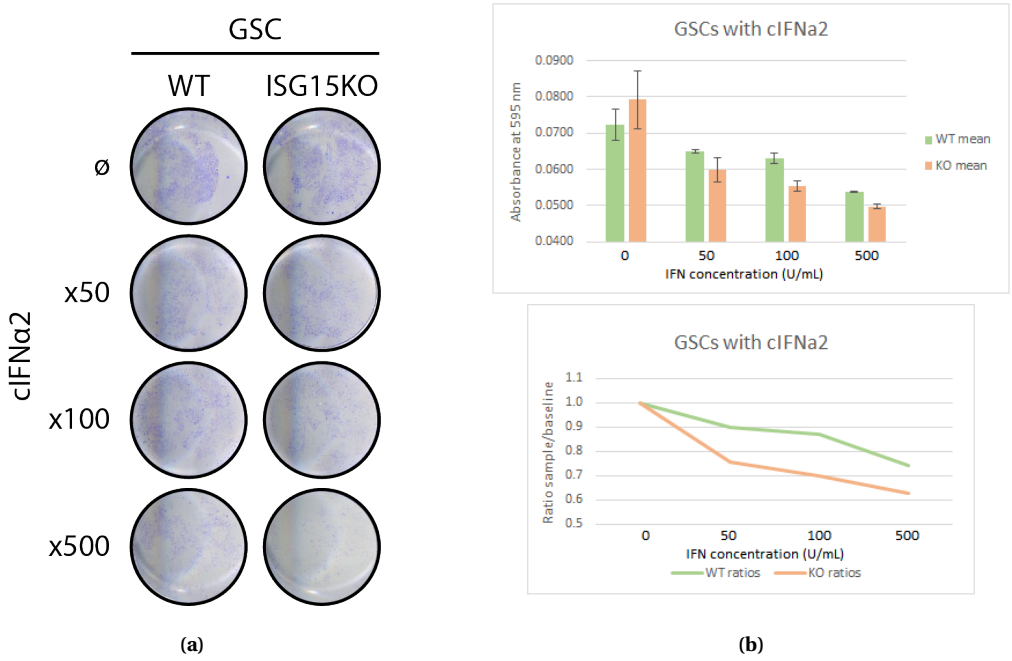

(a) **(b)**

Figure 6.9: Confirmation of the IFN sensitive phenotype on the same GSC cell batch edited for the mass spectrometry analysis. **a)** Colony formation assay treating cells with commercial IFNα2 at final concentrations of 50, 100 and 500 U/mL. Each condition was plated in technical triplicates. **b)** Quantification of the colony formation assay by stain dissolution and absorbance reading at 595 nm. The upper graph shows the mean absorbance of each condition's triplicates. Error bars equal ±SD. The lower graph shows the absorbance ratios of each treated sample to the untreated baseline obtained using the mean absorbance of each triplicated condition.

6.4.3 Whole proteomic analysis on ISG15 deficient GSC cells

As the IFNα sensitivity phenotype and the expression of ISG15 were analysed, the MHC class I bound peptides were collected with a gentle acid solution. The cells from which the peptides had been eluted were then collected by scrapping, lysed and sent to the International Centre for Cancer Vaccine Science in Gdansk, where I later travelled to process the samples before mass spectrometry analysis. Data obtained from the quantitative proteomics software MaxQuant were further filtered by p-value for the generation of volcano plots and for gene set enrichment analysis.

Volcano plots

For the generation of volcano plots the $\log_2$ of the fold change ratios of each protein found in KO vs WT obtained from MaxQuant were plotted against the -$\log_{10}$ of the adjusted p-value for each treatment condition (untreated or treated with IFNα for 24 or 48

hours) using VolcaNoseR. To select the most significant hits, those proteins with a fold change above 2 (red) and below 0.5 (blue) with a p-value below 0.05 were highlighted, labelling the top ten proteins. As seen in Figure 6.10, the comparison of protein expression in untreated ISG15 KO vs WT results in more proteins being downregulated that upregulated. Eight of the top ten most significantly altered proteins are downregulated, one of them being ISG15. Within the range of biological functions of the remaining seven hits, a commonality can be observed. NFIC (a transcription factor), ROA0 (a ribonucleoprotein) and HMGA1 (chromatin-associated protein) are DNA and RNA related proteins, and ADA is a DNA methyltransferase involved in the purine catabolic pathway. While ADPPT is a poorly described metabolic enzyme, PPHLN seems to play an important role in epithelial differentiation and TM41B is a regulator of autophagy and lipid mobilisation. On the other hand, NDUA4 and CATD (cathepsin D) were identified as the two top upregulated proteins in ISG15 KO cells vs WT cells in the absence of treatment, the first being a component of the electron transport chain complex I subunit and the second an key protease found in lysosomes.

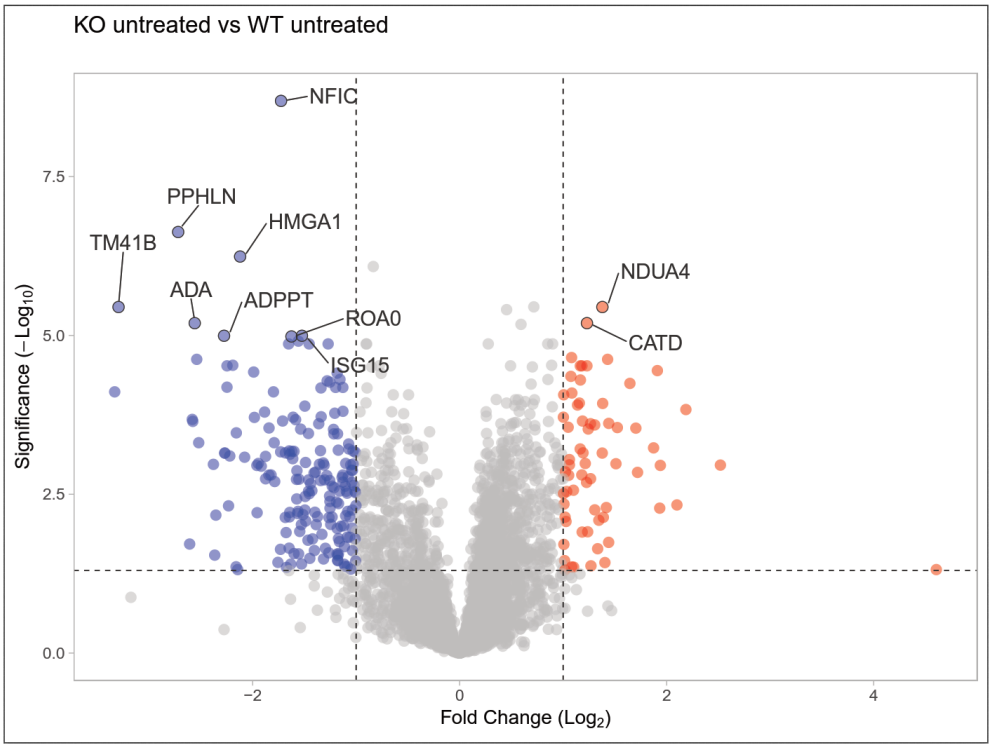

Figure 6.10: Volcano plot generated with the untreated ISG15 KO vs WT data obtained from the whole proteomic analysis performed on GSC cells. The fold change ratios of each protein found were plotted against the -$\log_{10}$ of the adjusted p-value of the untreated samples using VolcaNoseR. The most significant hits (fold change above 2 and below 0.5 with a p-value below 0.05) were highlighted in red (upregulated) and blue (downregulated), with the top ten proteins labelled. ISG15 KO and WT samples were analysed in triplicates.

The volcano plots generated with data from IFNα treated samples (see Figure 6.11) show that nine out of the top ten hits are upregulated proteins, with the only very significantly downregulated protein being ISG15. DHX58, IFIH1 (also known as MDA5), CMPK2, CD151, IFIT1, IFIT2 and IFIT3 are commonly upregulated in both IFNα treated KO vs WT comparisons regardless of the treatment time course. DHX58 and MDA5 are DExH-Box helicases, proteins with important roles in RNA metabolism and regulation of antiviral signalling. The IFIT members are also well known IFN induced proteins involved in viral immune response, while CMPK2 and CD151 are a mitochondrial kinase and a transmembrane protein from the tetraspanins family, respectively. The two uniquely significantly upregulated proteins in the KO vs WT samples treated for 24 hours were SYWC (an aminoacyl-tRNA synthetase) and 5NTD (a membrane protein involved in the conversion of extracellular nucleotides to membrane permeable nucleosides), while MX2 (an IFN induced antiviral protein) and LG3BP (a secreted glycoprotein member of the β-galactoside binding protein family) were the two most significant uniquely upregulated proteins in the KO vs WT samples treated for 48 hours.

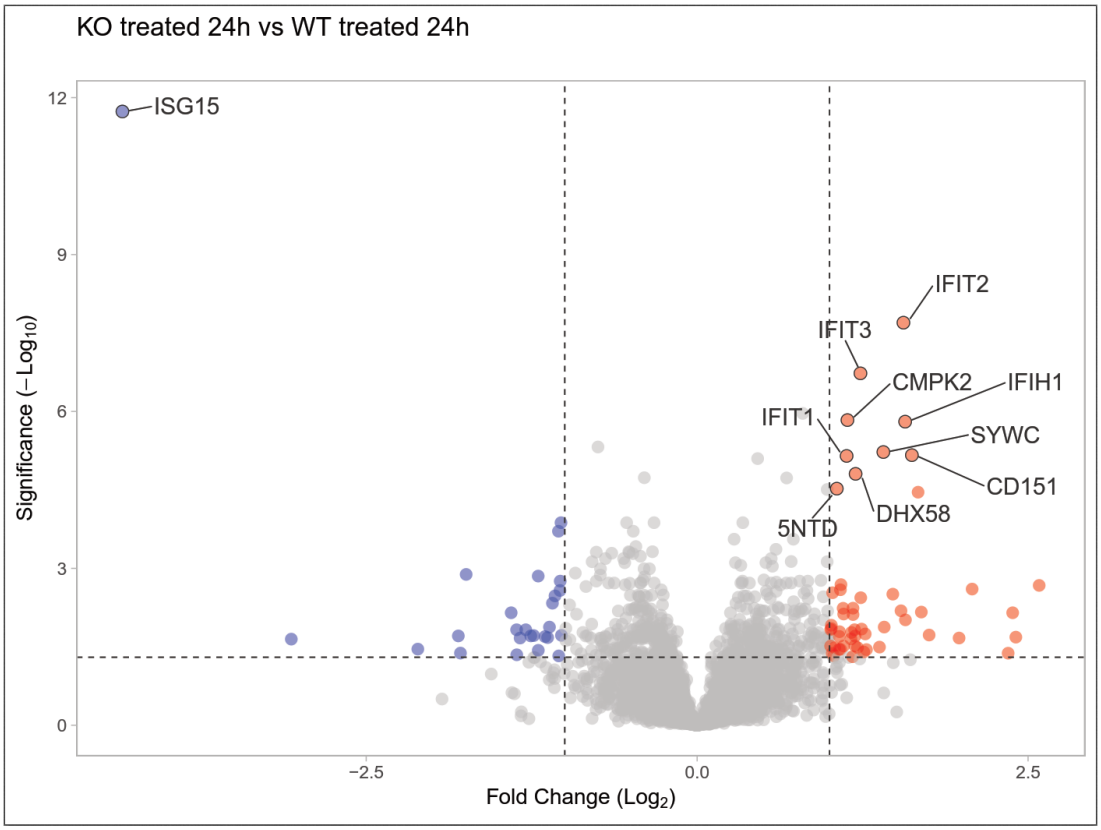

(a)

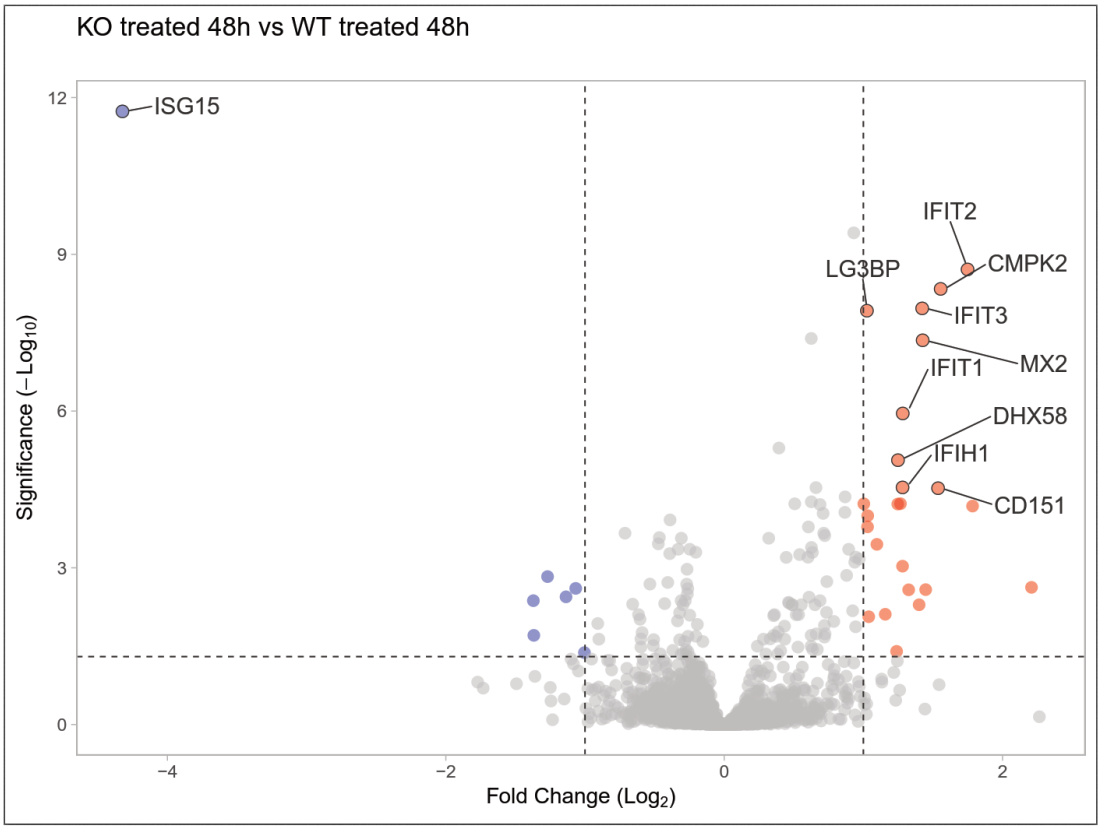

(b)

Figure 6.11: Volcano plots generated with the 24 (**a**) and 48 (**b**) hour IFNAα treated ISG15 KO vs WT data, obtained from the whole proteomic analysis performed on GSC cells. The fold change ratios of each protein found were plotted against the -$\log_{10}$ of the adjusted p-value for each treatment condition (treated with IFNα for 24 or 48 hours) using VolcaNoseR. The most significant hits (fold change above 2 and below 0.5 with a p-value below 0.05) were highlighted in red (upregulated) and blue (downregulated), with the top ten proteins labelled. ISG15 KO and WT samples were analysed in triplicates.

Gene set enrichment analysis - Analysis of biological processes

The data was further sorted for gene set enrichment analysis ($p<0.05$ and fold change above 1.5 and below 0.67) and the gene names were inserted into g:Profiler. Those proteins that were identified only in ISG15 KO or WT samples and therefore did not have a p-value or ratio were also included in the analysis. The acquired Gene Ontology terms (GO terms) compiling genes by their biological process were then inserted into Revigo. Even though Revigo designed to remove redundant GO terms, the full lists of results (available in Appendix D) showed some highly overlapping terms. The most significant ones were selected and in some cases, two or more were combined in one term in order to make bar graphs that represented the results. When such combination occurred, the start of a change in pattern in the bar (from solid blue to white and blue) represents the lowest p-value of the terms combined, and the end of the bar matches the highest p-value of those com-

bined. Figure 6.12 shows the biological processes upregulated in KO vs WT samples treated with IFNα for 24 hours, the two most significant ones being organonitrogen compound metabolic and catabolic processes. Other interesting hits are nucleobase-containing small molecule metabolic processes, positive regulation of type I IFN production, MDA-5 signalling pathway, response to stress, regulation of cell death and programmed cell death, proteolysis and protein and peptide metabolic processes. Only three downregulated biological processes were identified, but all of them are related with mitochondrial processes: protein localisation to mitochondrion (-$\log_{10}$ p-value 2.89), respiratory electron transport chain (-$\log_{10}$ p-value 1.95) and establishment of protein localisation to mitochondrion (-$\log_{10}$ p-value 1.92).

The biological processes found to be upregulated in KO vs WT samples treated with IFNα for 48 hours are shown in Figure 6.13. Although the most significant process is, unsurprisingly, negative regulation of viral processes and defence response to virus / symbiont / biotic stimulus, the second most significant process is related to antigen processing and presentation of endogenous peptide antigen. Other upregulated processes to consider are: immune system process and response, negative regulation of innate immune response, response and regulation of cytokine stimulus and production, IL-27 mediated signalling pathway, T cell mediated immunity and cytotoxicity, regulation of nuclease and ribonuclease activity, response to IFNβ, positive regulation of cell killing, positive regulation of tumour necrosis factor production, positive regulation of macromolecule metabolic processes, production of molecular mediator of immune response and regulation of immune effector processes. Common processes with the ones identified in ISG15 KO samples vs WT treated for 24 hours were also found, such as response and regulation of type I IFN, response to stress and response to organic substances. No significant downregulated biological processes were identified in KO vs WT samples treated with IFNα for 48 hours.

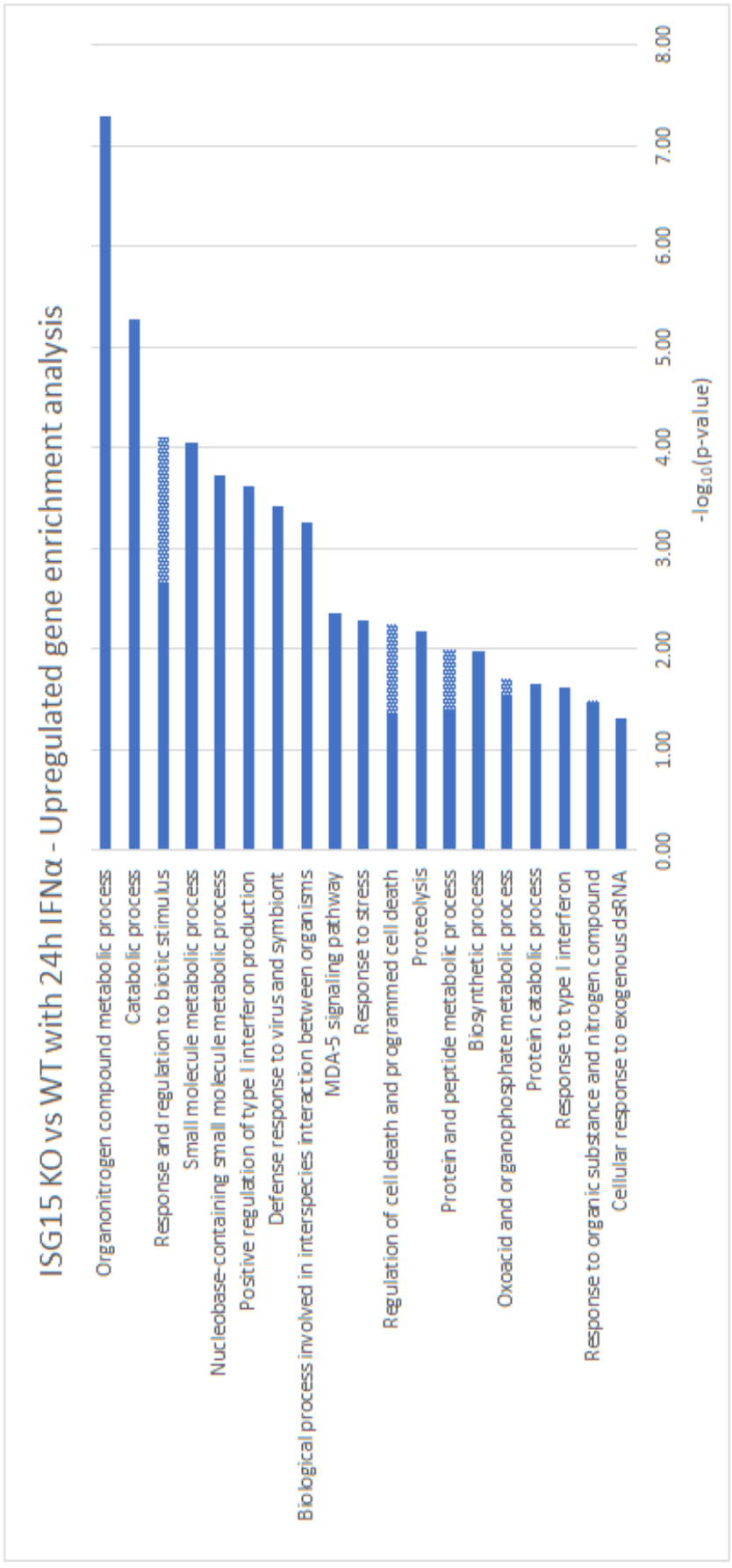

Figure 6.12: Upregulated biological processes in ISG15 KO vs WT GSC samples treated with IFNα for 24 hours identified as part of the whole proteome analysis. The ratios and p-values obtained from MaxQuant were sorted ($p<0.05$ and fold change above 1.5 and below 0.67) and selected protein names were inserted into G:Profiler to obtain the GO terms that grouped the proteins by their biological process, which were filtered to remove redundant terms using Revigo. Those proteins that were identified only in ISG15 KO or WT samples and therefore did not have a p-value or ratio were also included in the analysis. The final list was further refined to combine some terms into one and to remove repetitive terms. When such combination occurred, the start of a change in pattern in the bar (from solid blue to white and blue) represents the lowest p-value of the terms combined, and the end of the bar matches the highest p-value of those combined.

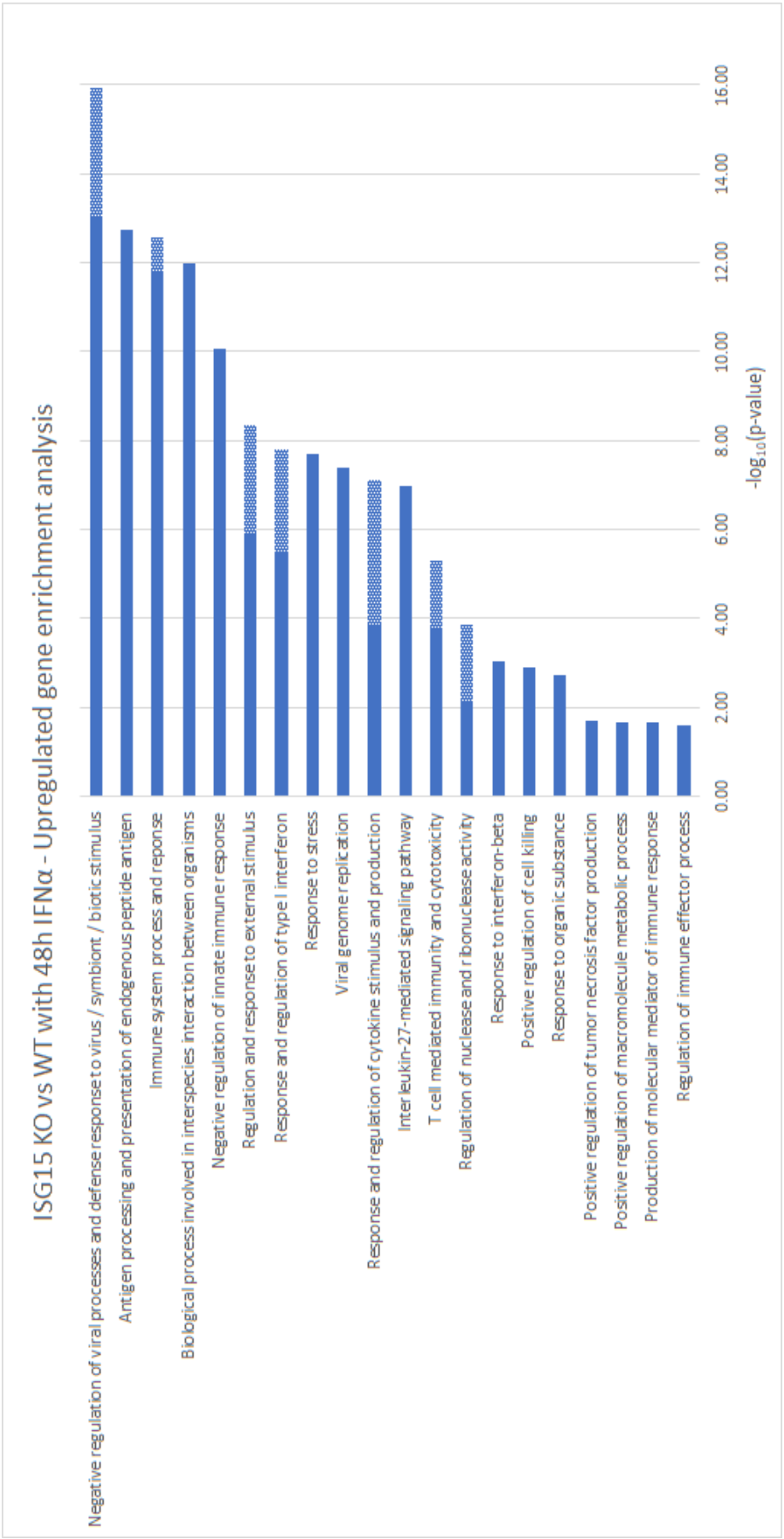

Figure 6.13: Upregulated biological processes in ISG15 KO vs WT GSC samples treated with IFNα for 48 hours identified as part of the whole proteome analysis. The ratios and p-values obtained from MaxQuant were sorted ($p<0.05$ and fold change above 1.5 and below 0.67) and selected protein names were inserted into G:Profiler to obtain the GO terms that grouped the proteins by their biological process, which were filtered to remove redundant terms using Revigo. Those proteins that were identified only in ISG15 KO or WT samples and therefore did not have a p-value or ratio were also included in the analysis. The final list was further refined to combine some terms into one and to remove repetitive terms. When such combination occurred, the start of a change in pattern in the bar (from solid blue to white and blue) represents the lowest p-value of the terms combined, and the end of the bar matches the highest p-value of those combined.

Gene set enrichment analysis - Analysis of cellular compartments

To determine the cellular origin of the significant upregulated and downregulated proteins identified in ISG15 KO vs WT GSC cells upon whole proteomic analysis, the filtered data ($p<0.05$ and fold change above 1.5 and below 0.67) was inserted in g:Profiler and the obtained GO terms compiling genes by their cellular compartment location were then introduced into Revigo. Those proteins that were identified only in ISG15 KO or WT samples and therefore did not have a p-value or ratio were also included in the analysis. The Circular Gene Ontology (CirGO) web tool was used to create pie charts that display the data obtained from Revigo. Figure 6.14 shows that 33,7% and 13.7% of the significant downregulated proteins in untreated KO vs WT GSC samples belong to the cytoplasmic vesicle lumen and cytosol respectively. The next most significant categories are cytosolic ribosome (9.3%), membrane-bound organelle (8.4%), cytoplasm (7.9%) and vesicle (5.6%). On the other hand, 32.1% of the significant upregulated proteins in untreated KO vs WT GSC samples belong to the mitochondrial protein containing complex. Secretory granule (13.7%), cytoplasm (13.4%) and vacuolar lumen (12.7%) are the following more important groups.

IFNα caused a shift in the proteins upregulated in ISG15 KO vs WT cells treated for 24 hours (Figure 6.15), moving from the biggest group of proteins belonging to the mitochondrial protein complex in the untreated samples to 34.2% of the proteins belonging to the nuclear envelope. Regarding the downregulated proteins in these samples, 28.4% of them belong to the mitochondrial-bounded organelle and 24.2% to the membrane-bounded organelle. Other significant categories include envelope (9.7%), mitochondrion (8.1%), and a quite specific category also related to the mitochondria - the respirasome (4.2%). Interestingly, proteins located in the mitochondrial complex were significantly upregulated in ISG15 KO cells prior IFN treatment.

Increasing the treatment time from 24 hours to 48 also caused a considerable change in the origin of the upregulated proteins (Figure 6.16), with a significant 50.1% of the proteins belonging to the lumenal side of the endoplasmic reticulum membrane, followed by a 14.1% belonging to the MHC class I protein complex. Only two common cellular compartments could be identified from the list of significant downregulated proteins in ISG15 KO vs WT samples treated for 24 hours: cell body (53.9%) and astrocyte end-foot (46.1%).

A summarising graph showing the three top downregulated and upregulated cellular compartments of each treatment condition can be found in Figure 6.21, condensing Figure 6.14, Figure 6.15 and Figure 6.16.

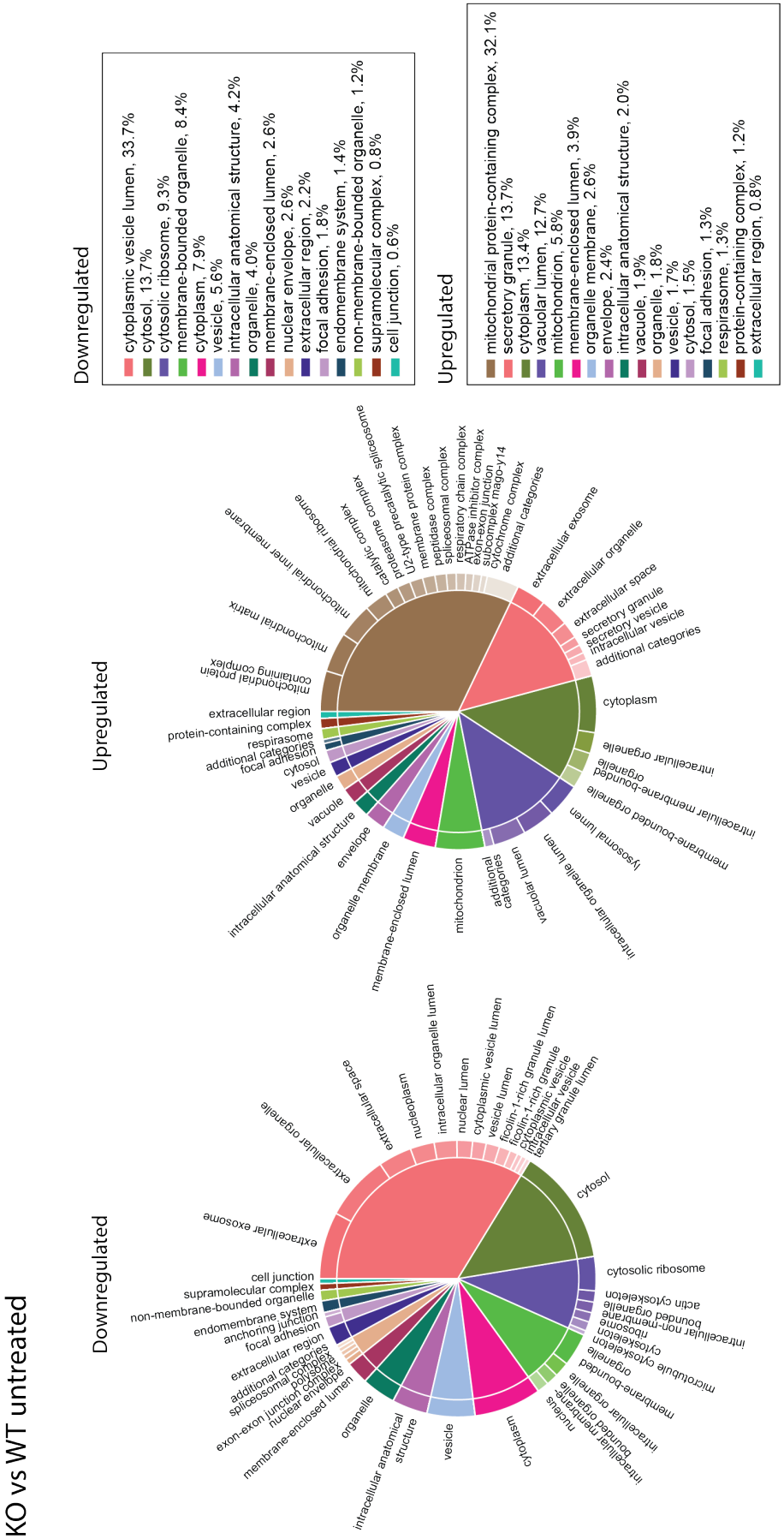

Figure 6.14: Pie charts showing the cellular origin of the significantly upregulated and downregulated proteins in untreated ISG15 KO samples vs WT. The ratios and p-values obtained from MaxQuant were sorted ($p<0.05$ and fold change above 1.5 and below 0.67) and selected protein names were inserted into G:Profiler to obtain the GO terms that grouped the proteins by their cellular compartment, which were filtered to remove redundant terms using Revigo. Those proteins that were identified only in ISG15 KO or WT samples and therefore did not have a p-value or ratio were also included in the analysis. The data was arranged in pie charts using the CirGO web tool.

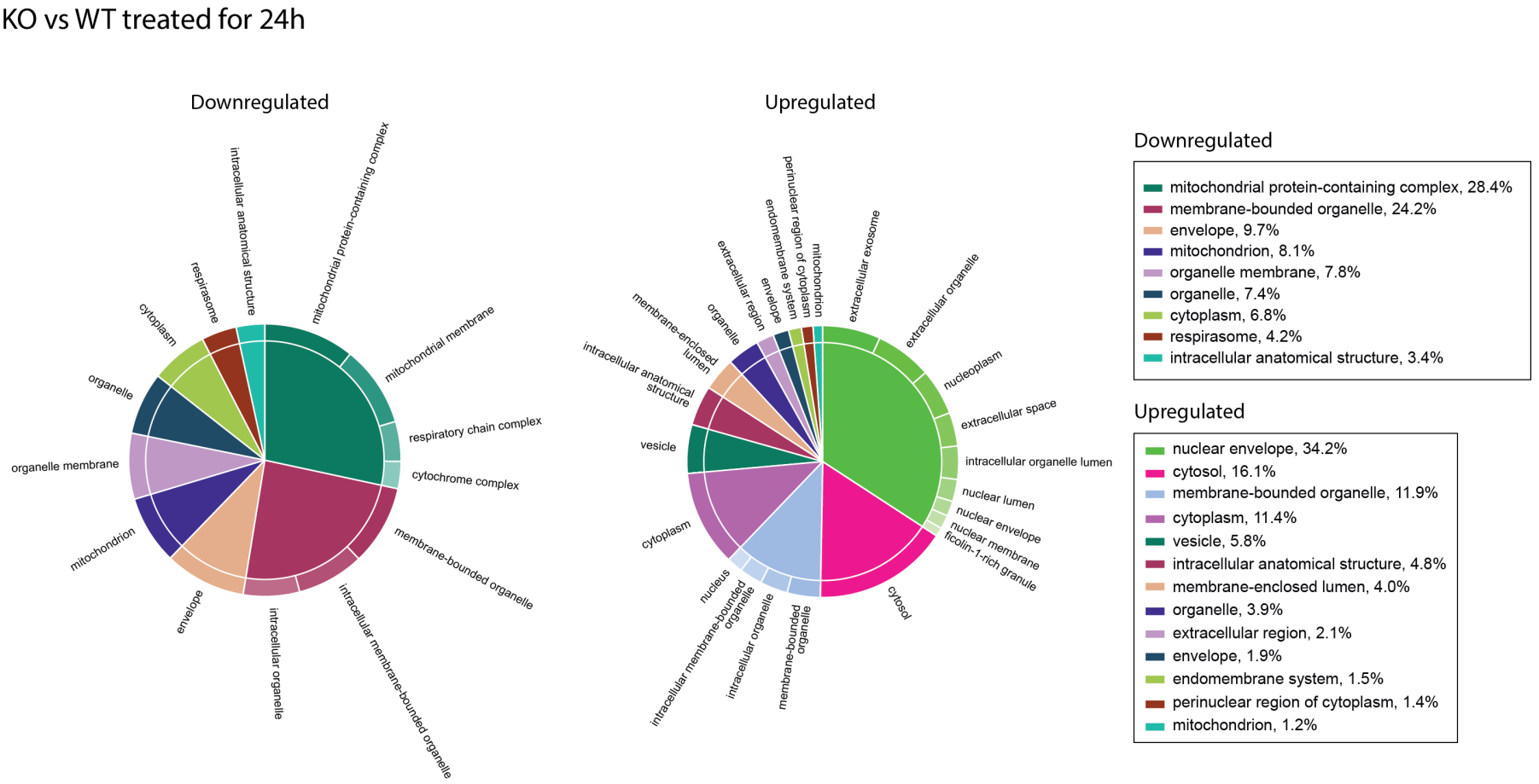

Figure 6.15: Pie charts showing the cellular origin of the significantly upregulated and downregulated proteins in ISG15 KO samples vs WT treated with IFNα for 24 hours. The ratios and p-values obtained from MaxQuant were sorted ($p<0.05$ and fold change above 1.5 and below 0.67) and selected protein names were inserted into G:Profiler to obtain the GO terms that grouped the proteins by their cellular compartment, which were filtered to remove redundant terms using Revigo. Those proteins that were identified only in ISG15 KO or WT samples and therefore did not have a p-value or ratio were also included in the analysis. The data was arranged in pie charts using the CirGO web tool.

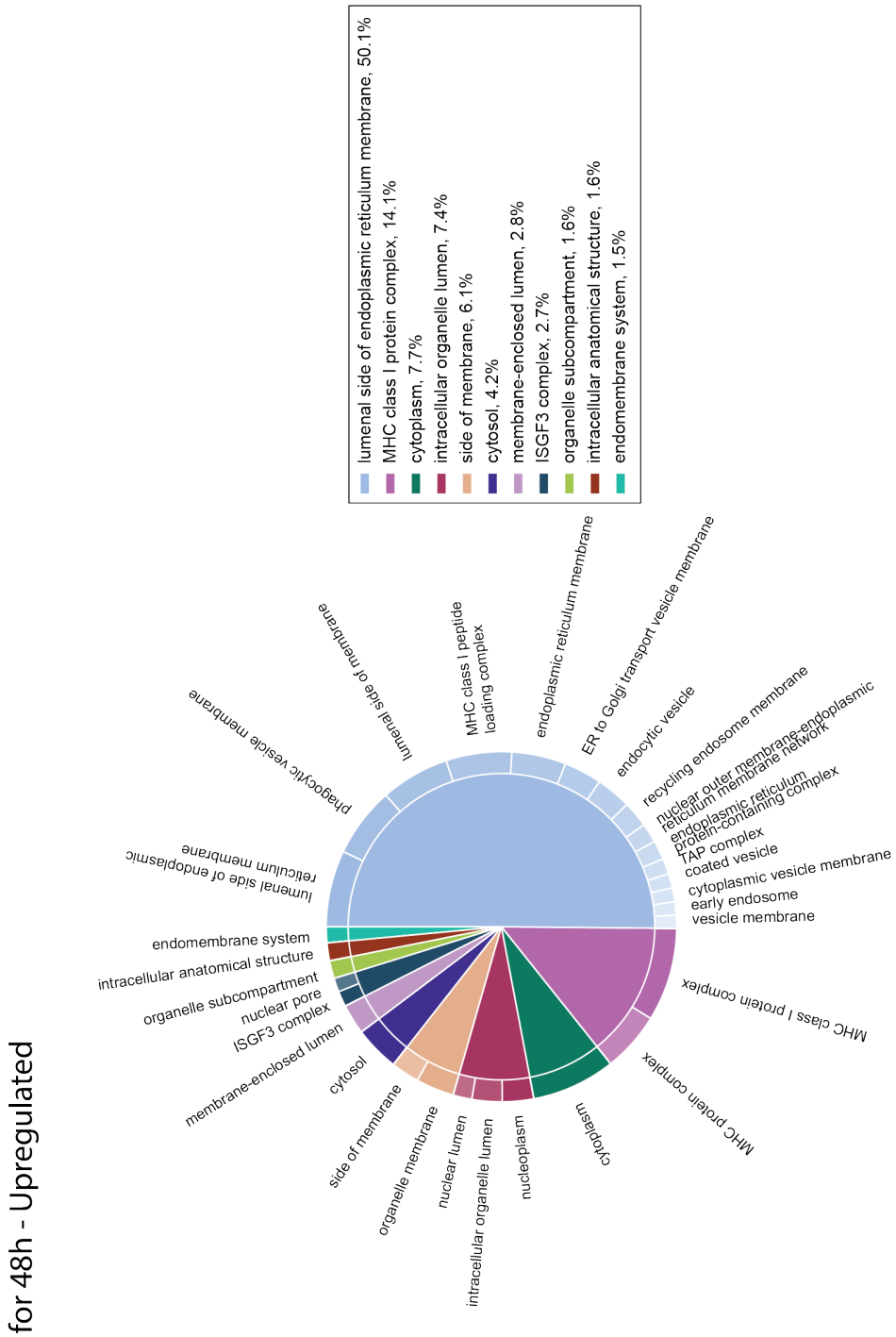

Figure 6.16: Pie charts showing the cellular origin of the significantly upregulated proteins in ISG15 KO samples vs WT treated with IFNα for 48 hours. The ratios and p-values obtained from MaxQuant were sorted ($p<0.05$ and fold change above 1.5 and below 0.67) and selected protein names were inserted into G:Profiler to obtain the GO terms that grouped the proteins by their cellular compartment, which were filtered to remove redundant terms using Revigo. Those proteins that were identified only in ISG15 KO or WT samples and therefore did not have a p-value or ratio were also included in the analysis. The data was arranged in pie charts using the CirGO web tool.

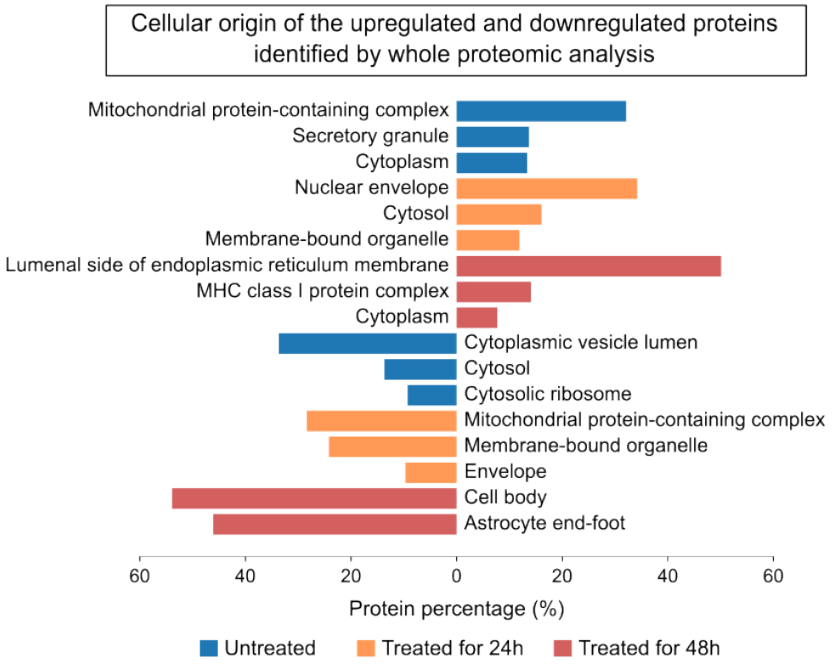

Figure 6.17: Two directional bar graph showing the top three downregulated (left) and upregulated (right) cellular compartments in each of the three treatment conditions (untreated, treated with IFNα for 24h and treated with IFNα for 48h) following whole proteomic analysis on KO vs WT GSC cells. The x axis represents what percentage of the upregulated and downregulated proteins belonged to the cellular localisation presented in the y axis.

Gene set enrichment analysis - Analysis of cellular compartments

In order to identify the cellular origin of the proteins to which the significantly enriched and underrepresented peptides identified in untreated ISG15 KO vs WT samples belonged, the filtered data ($p<0.05$ and fold change above 1.5 and below 0.67) was inserted in g:Profiler and the obtained GO terms compiling genes by their cellular compartment location were then introduced into Revigo. The proteins that were identified only in ISG15 KO or WT samples and therefore did not have a p-value or ratio were also included in the analysis. The Circular Gene Ontology (CirGO) web tool was used to create pie charts that display the data obtained from Revigo.

Figure 6.18 shows that 37.2% and 12.1% of the significant downregulated proteins in untreated KO vs WT GSC samples belong to secretory granule lumen and mitochondrial protein-containing complex respectively, followed by membrane-bounded organelle (7.5%) and cytosolic ribosome (6.8%). Interestingly, 41.9% of the enriched peptides identified in untreated KO vs WT GSC samples also originated from proteins belonging to the secretory granule lumen, followed by CENP-A containing nucleosome (29.4%) and membrane enclosed lumen (5.8%).

When analysing the peptides identified in KO vs WT GSC samples treated with IFNα for 24h (Figure 6.19), the secretory granule lumen is once again the top protein origin both in the enriched and underrepresented categories, with 38.1% and 41.4% respectively belonging to this cellular location. Peptides originated from proteins belonging to the CENP-A containing nucleosome, which were enriched in KO vs WT untreated cells, show to be underrepresented once treated with IFNα, with 19.4% of the protein origins belonging to this location. The next most underrepresented location is the membrane-bounded organelle (7.2%), also underrepresented in the untreated cells. The second most enriched protein origin is the cytoplasm (20.3%) followed by the cytosol (%10.3).

Finally, when analysing the origin of the underrepresented peptides upon IFNα treatment for 48h, 47.4% of the proteins belonged to nuclear periphery, followed by 11.8% belonging to the cytoplasm and 6.8% to the vesicle. The enriched peptides belonged to proteins originated from the melanosome (23.3%), polysome (11.9%) and nuclear body (11.9%).

To summarise these results, the top three cellular compartments of the proteins from which the enriched and underrepresented peptides originated in each treatment condition were plotted together in Figure 6.22. For easier analysis, Figure 6.21 has been copied again next to Figure 6.22 to allow for better comparison of the origin of the proteins detected through whole proteomic analysis and the origin of the peptides detected via immunopeptidomic analysis.

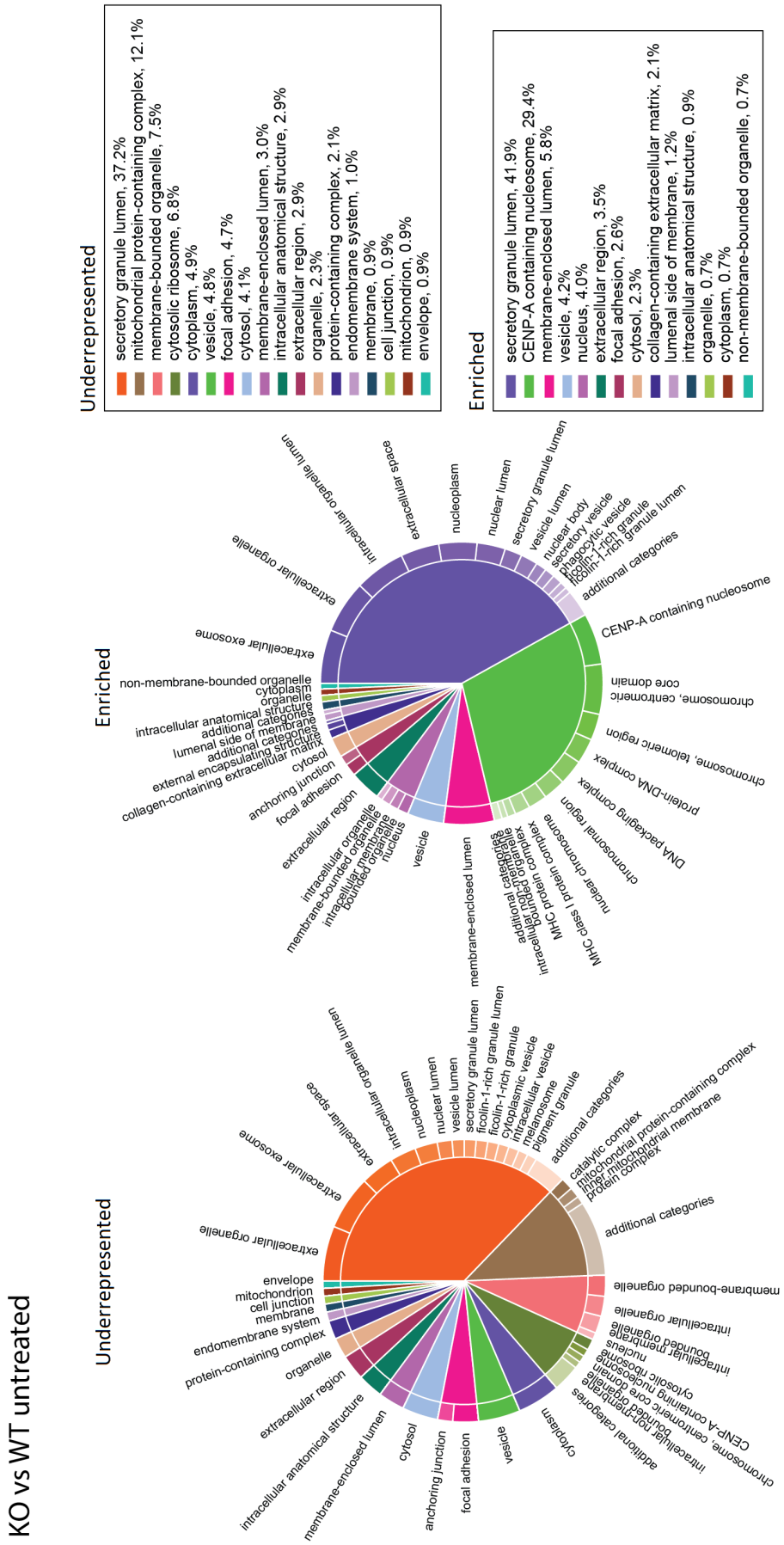

Figure 6.18: Pie charts showing the cellular origin of the proteins to which the significantly enriched and underrepresented peptides identified in untreated ISG15 KO vs WT samples belong. The names of the proteins that had at least one peptide identified with a p-value below 0.05 and and fold change above 1.5 and below 0.67 were inserted into G:Profiler to obtain the GO terms that grouped the proteins by their cellular compartment, which were filtered to remove redundant terms using Revigo. Those peptides that were identified only in ISG15 KO or WT samples and therefore did not have a p-value or ratio were also included in the analysis. The data was arranged in pie charts using the CirGO web tool.

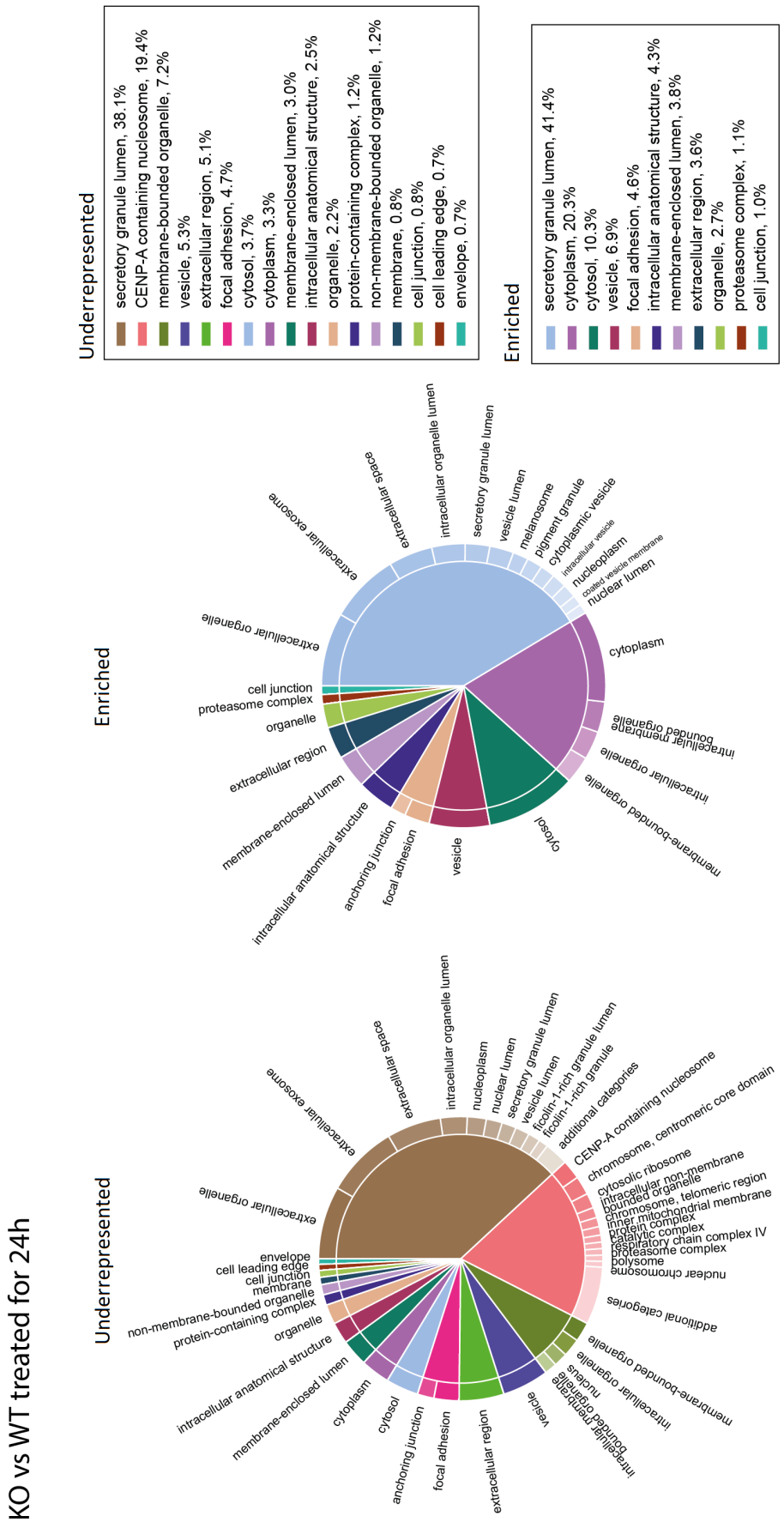

Figure 6.19: Pie charts showing the cellular origin of the proteins to which the significantly enriched and underrepresented peptides identified in ISG15 KO vs WT samples treated with IFNα for 24 hours belong. The names of the proteins that had at least one peptide identified with a p-value below 0.05 and and fold change above 1.5 and below 0.67 were inserted into G:Profiler to obtain the GO terms that grouped the proteins by their cellular compartment, which were filtered to remove redundant terms using Revigo. Those peptides that were identified only in ISG15 KO or WT samples and therefore did not have a p-value or ratio were also included in the analysis. The data was arranged in pie charts using the CirGO web tool.

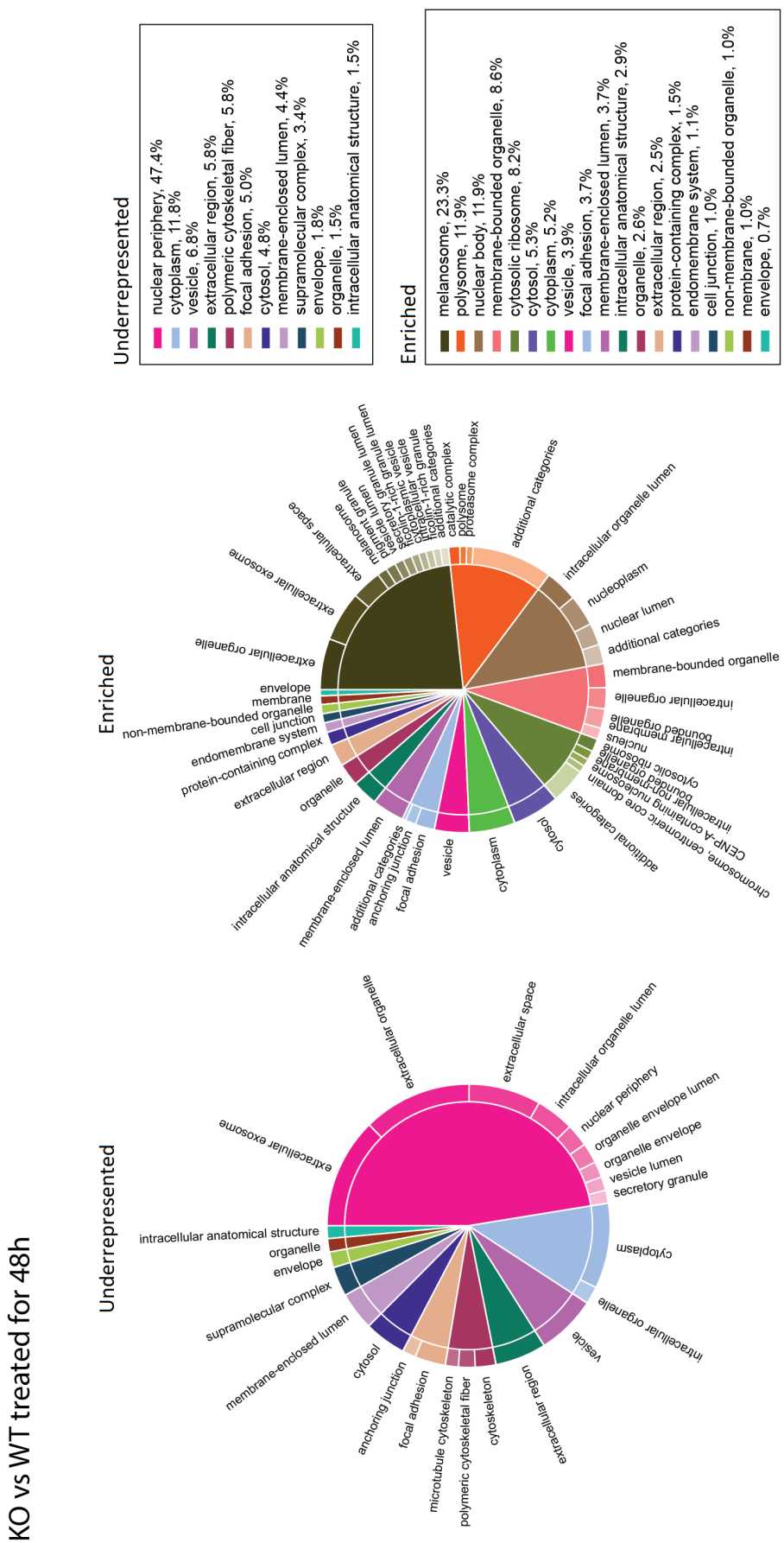

Figure 6.20: Pie charts showing the cellular origin of the proteins to which the significantly enriched and underrepresented peptides identified in ISG15 KO vs WT samples treated with IFNα for 48 hours belong. The names of the proteins that had at least one peptide identified with a p-value below 0.05 and and fold change above 1.5 and below 0.67 were inserted into G:Profiler to obtain the GO terms that grouped the proteins by their cellular compartment, which were filtered to remove redundant terms using Revigo. Those peptides that were identified only in ISG15 KO or WT samples and therefore did not have a p-value or ratio were also included in the analysis. The data was arranged in pie charts using the CirGO web tool.

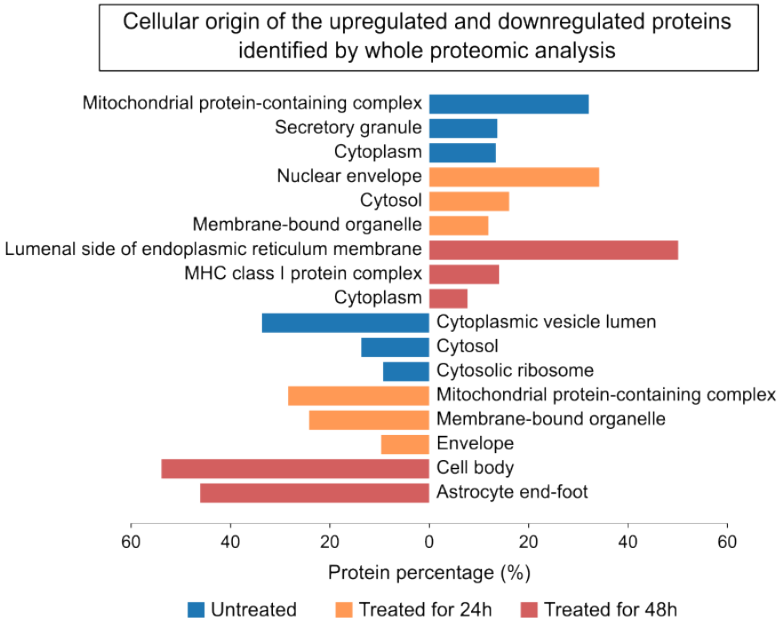

Figure 6.21: Two directional bar graph showing the top three downregulated (left) and upregulated (right) cellular compartments in each of the three treatment conditions (untreated, treated with IFNα for 24h and treated with IFNα for 48h) following whole proteomic analysis on KO vs WT GSC cells. The x axis represents what percentage of the upregulated and downregulated proteins belonged to the cellular localisation presented in the y axis.

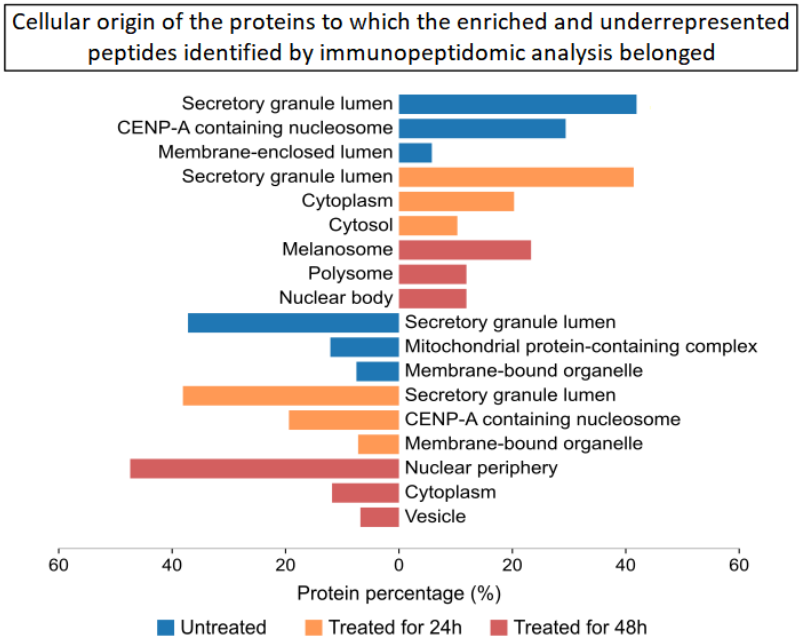

Figure 6.22: Two directional bar graph showing the top three underrepresented (left) and enriched (right) cellular compartments in each of the three treatment conditions (untreated, treated with IFNα for 24h and treated with IFNα for 48h) following immunopeptidomic analysis on KO vs WT GSC cells. The x axis represents what percentage of proteins found to be the origin of the enriched and underrepresented peptides belonged to the cellular localisation presented in the y axis.

The comparison of the cellular origin of the proteins identified by whole proteomic analysis and the origin of the proteins to which the peptides identified by immunopeptidomic analysis belonged revealed interesting results. Proteins belonging to the mitochondrial protein-containing complex were found upregulated in untreated ISG15 KO vs WT GSC cells, and yet peptides originated from these proteins were underrepresented in the cellular membrane under the same conditions. As an example of this phenomenon, any significantly altered NDUA4 peptides were searched in the data belonging to untreated ISG15 deficient vs WT samples. As seen in Table 6.1, the four peptides identified in untreated ISG15 KO samples were underrepresented when compared to WT samples - two of them were only found in WT cells and the other two had fold changes of 0.08 and 0.16.

Table 6.1: NDUA4 peptides identified in untreated ISG15 deficient vs WT GSC cells (p-value<0.05). Even though the results of the whole proteomic analysis show that NDUA4 was upregulated in untreated ISG15 deficient cells when compared to WT cells, immunopeptidomic analysis found that peptides belonging to NDUA were underrepresented.

Peptide	FC
SKLKKERPDF	Only found in WT
YSVNVDYSKLKKERPDF	Only found in WT
SVNVDYSKLKKERPDF	0.083018184
YSKLKKERPDF	0.160460891

Another seemingly dysregulated pathway according to these results is the secretory granule pathway. Proteins belonging to this cellular compartment were found upregulated in untreated ISG15 KO vs WT cells, and they were not detected to be significantly downregulated or upregulated at a protein expression level upon IFN treatment. In spite of that, peptides originated from proteins belonging to the secretory granule lumen were found both underrepresented and enriched in untreated and treated for 24h ISG15 KO cells when compared to WT cells.

Peptide length distribution analysis

In order to determine if there was a particular peptide length distribution among the peptides differently enriched in ISG15 deficient vs WT cells, the number of residues per peptide with a p-value below 0.05 were counted, and they were separated by fold change. All significant enriched peptides had a fold change above 1.5 and all significant underrepresented peptides had a fold change below 0.67, so no peptides were discarded by this requirement. Figure 6.23 is composed of three subfigures showing the peptide length dis-

tribution of peptides identified in ISG15 KO vs WT GSC samples under different conditions: untreated (a), treated for 24h (b) and treated for 48h (c). No peptides with less than 7 residues were identified, and the longest peptides identified had 45 amino acids. For plotting purposes, peptides with 7 to 23 residues were selected, as very few peptides with more than 23 amino acids were identified, but a full table with the length distribution of all the peptides can be found in Appendix D. Results show a significant number of peptides being underrepresented in untreated ISG15 KO vs WT samples, and a very high number of enriched peptides in samples treated for 48 hours.

These distributions were obtained using only the peptides found in ISG15 KO samples relative to those found in WT samples. In an effort to analyse the changes within WT and KO samples independently, peptides found in 24h treated WT and KO samples relative to the untreated correspondents and peptides found in 48h treated WT and KO samples relative to the correspondent samples treated for 24h were sorted. This way, the peptides enriched during the first 24h upon IFNα treatment and the peptides enriched 24 to 48h after treatment were evaluated. Because the data obtained was exported as pairwise comparisons, the state of the enriched peptides in WT untreated and ISG15 KO untreated samples could not be determined independently. Figure 6.24 shows the length distribution of peptides presented in the first 24 hours (a) and 24 to 48 hours after IFNα treatment (b) in ISG15 KO (right, red) and WT (left, blue) GSC cells. Again, all significant enriched peptides had a fold change above 1.5 and below 0.67, so no peptides were discarded according to fold change requirements.

Overall, the results presented suggest a significant increase in peptides being enriched in the absence of ISG15 48 hours after IFNα treatment, which seem to maintain the standard peptide distribution with ninemers being the most abundant.

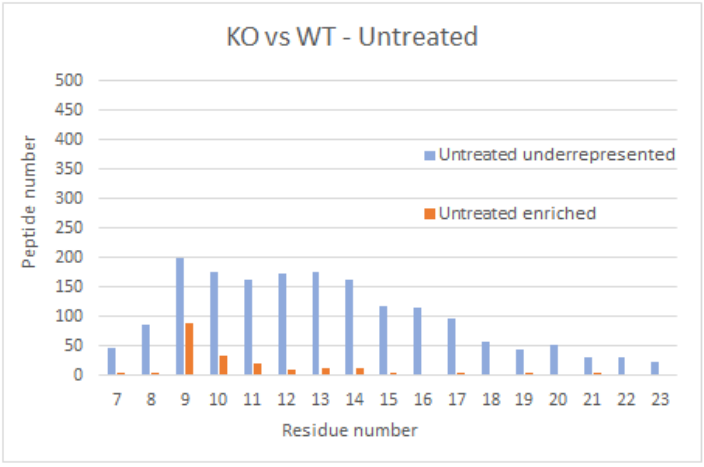

(a)

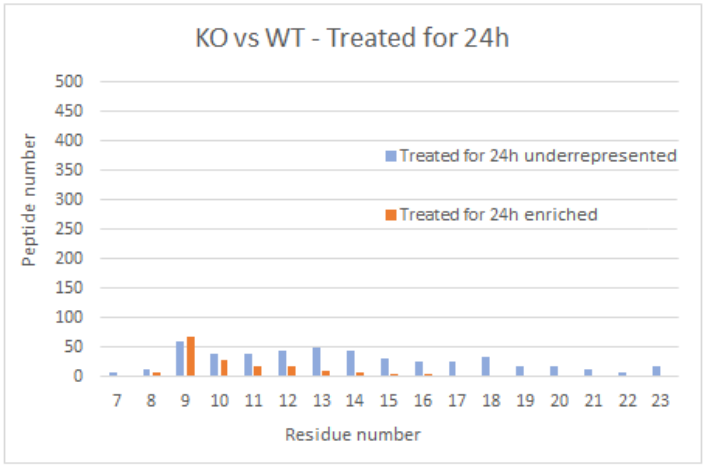

(b)

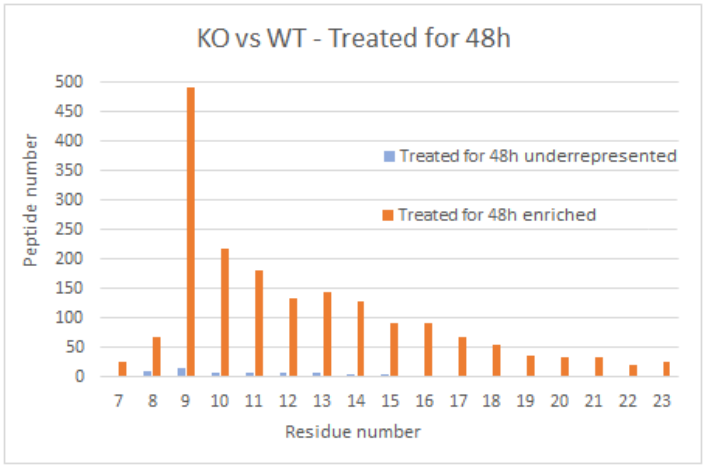

(c)

Figure 6.23: MHC-I presented peptide length distribution in ISG15 KO vs WT GSC cells untreated **(a)**, treated with IFNα for 24h **(b)** and treated with IFNα for 48h **(c)**. The peptides identified were sorted by significance (p-value<0.05) and separated by fold change as enriched (above 1.5) or underrepresented (below 0.67). The graph represents the number of peptides (y axis) that have certain number of residues (x axis). No peptides with less than 7 residues were identified. Columns 24 to 45 were neglected for this figure due to extremely low number of peptides having this amount of residues.

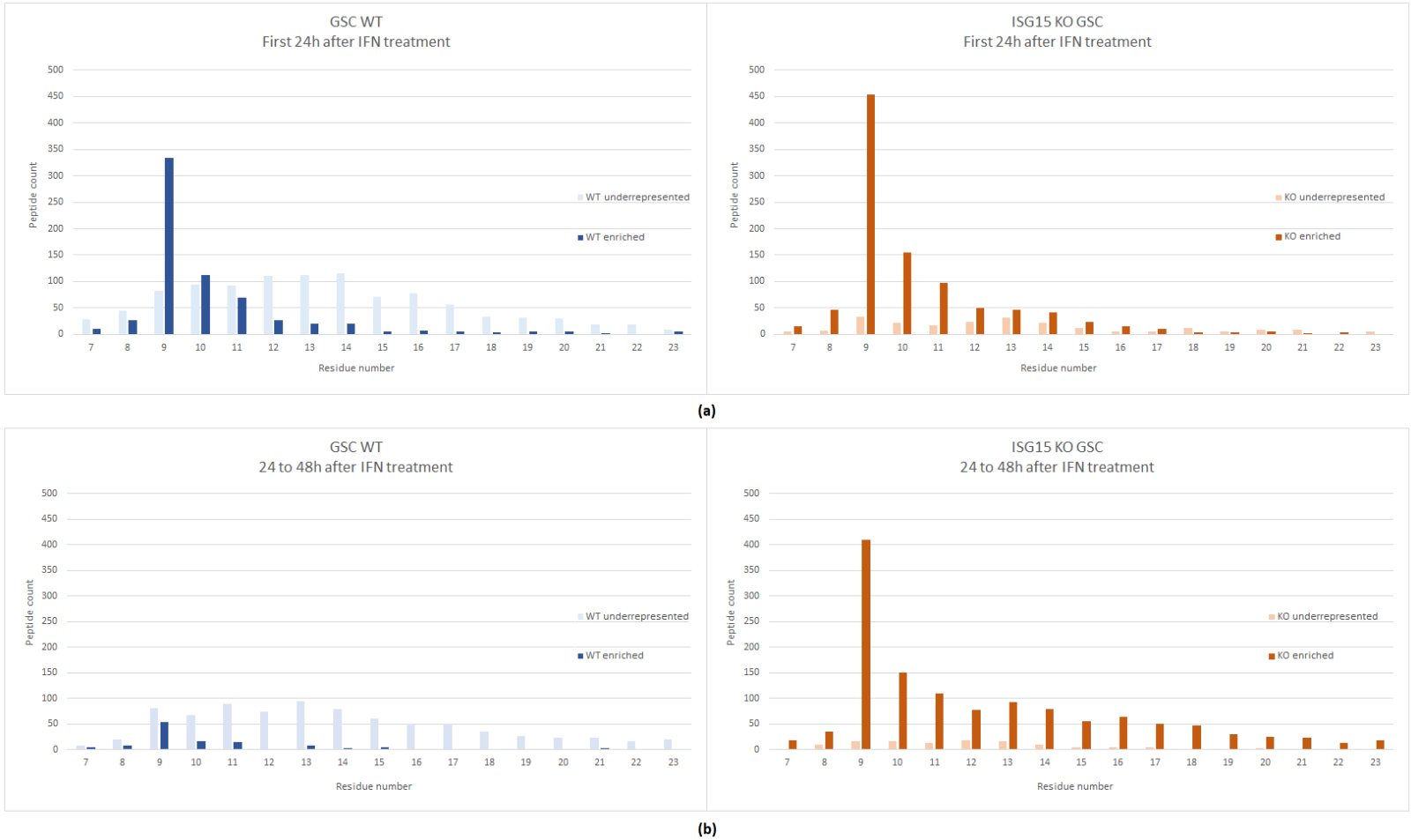

Figure 6.24: Length distribution of peptides presented in the first 24 hours **(a)** and 24 to 48 hours after IFNα treatment **(b)** in ISG15 KO (right) and WT (left) GSC cells. The peptides identified were sorted by significance (p-value<0.05) and separated by fold change as enriched (above 1.5) or underrepresented (below 0.67). The graph represents the number of peptides (y axis) that have certain number of residues (x axis). No peptides with less than 7 residues were identified. Columns 24 to 45 were neglected for this figure due to extremely low number of peptides having this amount of residues.

Identification of Peptide distribution analysis

In an effort to identify potential protein targets constituting sources of peptides differently in ISG15 deficient vs WT cells, the number of significant peptides per protein were counted. The top 47 and 44 proteins with most underrepresented or enriched peptides respectively were selected to be plotted into three column heat maps, one per treatment condition (untreated, treated for 24h and treated for 48h), as seen in Figure 6.25.

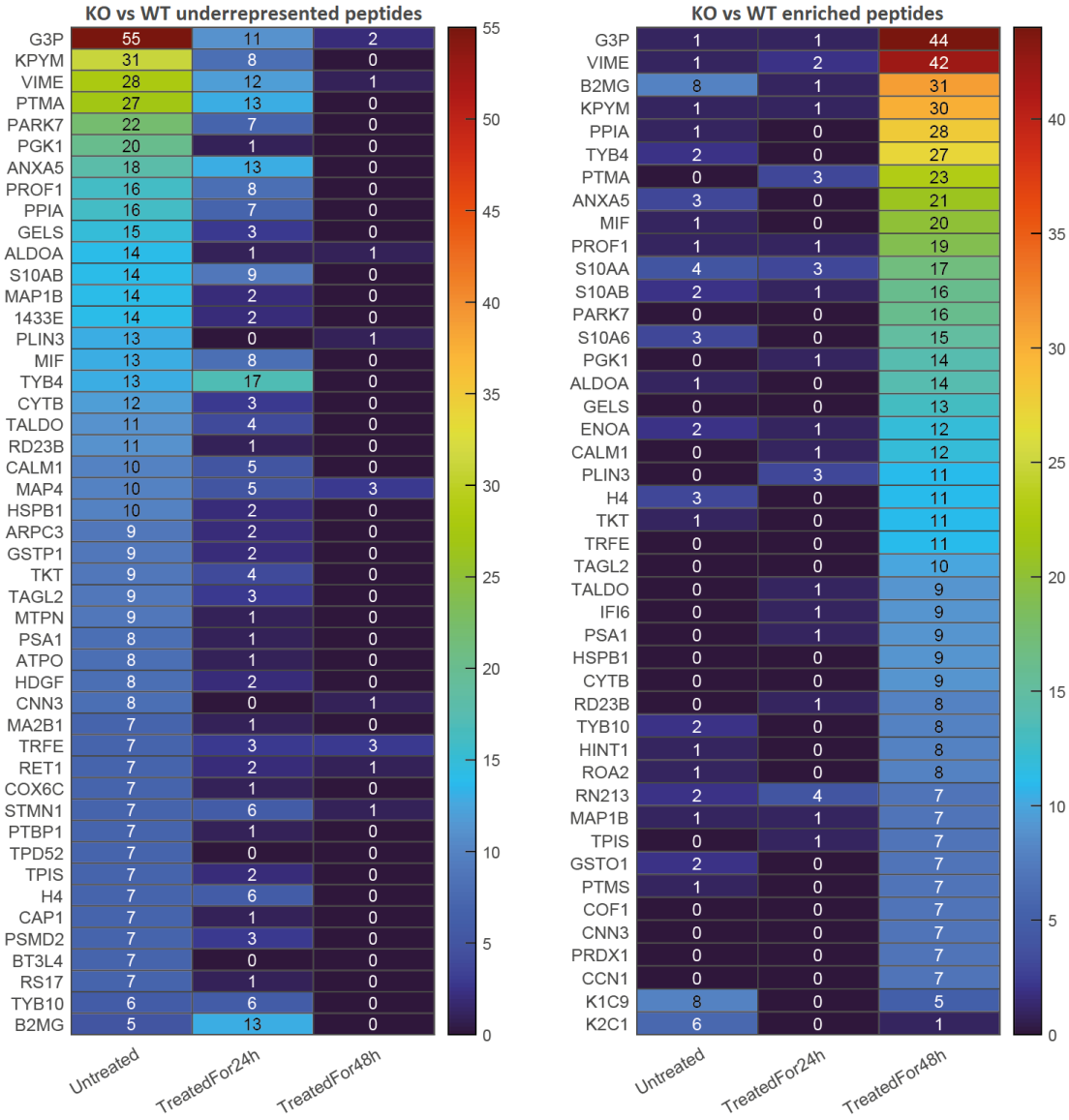

Figure 6.25: Heat map displaying the proteins with the most differentially enriched and underrepresented peptides in the absence of ISG15 in GSC cells (KO vs WT). The map showing the proteins with the most underrepresented peptides is located in the left, showing the number identified in each treatment condition, and the one showing the proteins with the most enriched peptides is located in the right.

The top proteins with the most differentially enriched peptides were selected to compare their peptide expression with the protein expression determined by the whole proteomic analysis. Although the p-values of most of them were not low enough to be considered significant, the correlation between the protein and peptide expression could be confirmed in some of the cases. As seen in Table 6.2, the protein expression of G3P in untreated ISG15 KO GSC cells was 0.29 times that expressed in untreated WT GSC cells (p-value 0.0001), consistent with the large amount of underrepresented peptides detected in KO vs WT cells on this condition (55 peptides). Interestingly, the over 2 fold change expression of this protein (p-value 0.0058) in ISG15 KO cells compared to WT upon IFN treatment for 24h is not reflected in the number of enriched peptides detected in this condition, since only 1 peptide was detected to be enriched. Upon treatment for 48h, on the other hand, 44 enriched peptides were identified in ISG15 deficient cells compared to WT, but unfortunately the protein expression fold change could not be confirmed due to a poor p-value. Out of the 55 peptides found underrepresented in untreated ISG15 KO samples vs WT samples, 28 had fold change values ranging 0.02 to 0.26, while the other 27 were only found in WT samples and not in KO samples. On the other hand, from the 44 peptides found enriched following treatment for 48h, 12 had fold change values ranging between 3.00 and 156.10. B2M also showed to have a great number of highly enriched peptides in the absence of ISG15 following IFNα treatment for 48h (31), but its protein expression fold change is only 1.54 (p-value 0.0196). This is interesting since 14 of the 31 peptides detected were found to be enriched with fold changes ranging 2.08 to 100.51, while the other 17 were only detected in ISG15 KO samples and not in WT samples. However, since B2M is a component of the HLA class I moleculaes, the enrichment of peptides detected at 48 hours after IFNα treatment could not be the result of the elution of peptides cleaved from B2M proteins and bound to HLA molecules, but of HLA molecules being eluted and digested with the samples prior analysis by mass spectrometry. This would be consistent with the results observed in the analysis of HLA expression performed by flow cytometry, which showed that IFNα treatment induced HLA overexpression in ISG15 KO samples when compared to WT samples, with the highest expression being at 48 hours. Therefore, experimental validation and further investigation would be required to discern these two options.The fold change values of the peptides identified for G3P and B2M can be found in Appendix D.

Table 6.2: The steady state expression level determined by whole proteomic analysis of targets of interest identified in immunopeptidomic analysis, showing the fold change in ISG15 KO vs WT and the p-value of each protein in each treatment condition.

	Untreated		**Treated for 24h**		**Treated for 48h**	
Name	**FC**	**p-value**	**FC**	**p-value**	**FC**	**p-value**
G3P	0.2874	0.0001	2.2619	0.0058	1.3279	0.5859
KPYM	0.4195	0.0041	1.8563	0.0508	1.1418	0.9224
VIME	1.1006	0.3840	1.0617	0.6718	0.9113	0.7668
PTMA	0.8761	0.5122	1.0203	0.9465	1.1205	0.8765
PARK7	0.9790	0.9616	0.9539	0.9329	1.0207	0.9952
PGK1	0.5768	0.0080	1.3524	0.1670	1.1257	0.8783
ANXA5	1.1946	0.3720	1.1554	0.5460	1.1230	0.8849
PROF1	0.6381	0.0380	1.2754	0.3206	1.1689	0.8298
PPIA	1.0423	0.8933	1.3986	0.2691	1.0407	0.9886
GELS	0.6825	0.0117	1.1699	0.3474	0.8892	0.7881
ALDOA	0.3938	0.0007	1.5888	0.0716	1.2308	0.7430
B2MG	1.1173	0.4434	1.0905	0.6313	1.5421	0.0196
TYB4	0.8361	0.6188	1.0314	0.9510	1.1949	0.9131
MIF	1.6206	0.0998	0.8553	0.6829	1.2370	0.8313
S10AA	2.8745	0.0003	1.0133	0.9687	1.2718	0.6752
S10AB	2.2377	0.0568	0.8189	0.7186	1.1358	0.9580
S10A6	0.4426	0.0292	1.7229	0.1851	1.2842	0.8456
ENOA	1.2174	0.2409	1.3758	0.0885	1.2484	0.5050

6.5 Discussion

The aim of this chapter was to determine if the lack of ISG15 altered the MHC-I mediated peptide presentation pathway, and to detect any significant differences that could potentially lead to the identification of targets for treatment in glioblastoma cells. To this end, the first step was to identify any differences in the membrane expression of HLA in the patient-derived WT and ISG15 deficient cell lines and ensure sufficient expression for the immunopeptidome analysis. All the single cells analysed in both WT and ISG15 cells expressed detectable HLA. The determination of the mean fluorescence intensity of each sample revealed an increased IFN treatment dependent expression of HLA in ISG15 deficient cells compared to WT, even though the basal expression in untreated cells was very similar in both cell lines. As described in section 6.1, Held *et al.* (2020) analysed the expression of HLA in lymphocytes of WT, ISG15$^{-/-}$ and USP18$^{-/-}$ mice, and their results showed

that, after the induction of the IFN pathway in these mice, there was no difference in the expression of MHC class I (H2K and H2B). They concluded that neither ISG15 nor protein ISGylation altered MHC class I expression in mice. Ir must be borne in mind that ISG15 seems to have different roles in humans and in mice. Over the last two decades, extensive research on the role of ISG15 in virology has been published (see subsection 1.3.1), most of it performed in mice and *in vitro*, and although some studies have proved ISG15 to have antiviral properties in human samples, ISG15 deficient patients do not exhibit the viral susceptibility observed in ISG15 deficient mice (Bogunovic *et al.*, 2012; Speer *et al.*, 2016). On top of this, the role of ISG15 as a negative regulator of the IFN pathway seems to be human exclusive. Speer *et al.* (2016) demonstrated that the stabilising between ISG15:USP18 which happens in humans does not occur in mice, who seem to be able to regulate the IFN response in the absence of ISG15. An analysis of the USP18 dependant ISGylome in USP18$^{-/-}$ vs WT HAP1 (a cell line derived from human chronic myelogenous leukemia) revealed upregulation of components from the antigen presentation pathway, and proved better antigenicity of USP18$^{-/-}$ cells by measuring their T cell response. On the other hand, Burks *et al.* (2015) reported that free ISG15 in breast cancer cells had a tumour suppressor role and enhanced MHC-I membrane expression in experiments performed both in human and mice, but ISGylation did not. Free ISG15 has been proved to promote the expression of IFNγ (Recht *et al.*, 1991; Bogunovic *et al.*, 2012; Swaim *et al.*, 2017) in a role that is independent of its ability to negatively regulate the IFN pathway, which at the same time upregulates MHC-I expression (Lefebvre *et al.*, 2001; Elsen *et al.*, 2004; Carey *et al.*, 2019). Therefore, the results presented in this chapter concerning the expression of MHC in ISG15 deficient cells are consistent with the evidence that HLA is induced by IFN and that ISG15 is a negative regulator of the IFN response in humans, and suggest it could also play a role as a negative regulator of immunogenicity. Whether USP18 is affected by the loss of ISG15 in GSCs remains to be determined. However, the analysis by immunoblot performed in SiHa cells showed that USP18 levels did not increase when ISG15 was silenced (section 5.4).

The determination of the changes at whole proteomic level in ISG15 deficient vs WT GSC cells in the absence and presence of IFNα treatment (24h or 48h) allowed for several data analyses. These included the identification of the most differentially expressed proteins, which identified many interesting targets for validation and further research, and gene pathway analysis, which shed light into the broader picture of the roles of ISG15 in the cells studied. The volcano plots generated showed that upon IFNα treatment and in the absence of ISG15, the most significantly differently expressed proteins were upregulated, and only one significantly downregulated protein was identified - ISG15. Again, this seems to be as a result of the lack of ISG15 as a negative regulator of the IFN pathway, since the unregulated exacerbated IFN response would result in the overexpression of many ISGs. Overall, the upregulated elements are proteins involved in IFN triggered immune and vi-

ral response. Bearing in mind that these cells were ISG15 KO mixed population cells, it is expected to find a very small abundance of ISG15 when analysing with a technique as precise and accurate as mass spectrometry, but the fact that ISG15 was found to be so significantly downregulated in treated ISG15 KO vs WT samples validates the expression analysis performed by immunoblot and proves that the deficiency of ISG15 in these cells. When comparing the proteins found differentially expressed in ISG15 deficient vs WT untreated cells, there are many more significantly downregulated than upregulated proteins. Although ISG15 is one of these, it is not the top downregulated protein due to the lack of IFN to create the major difference between the ISG15 levels observed in the volcano plots generated from the data of the treated samples. Only two significantly upregulated proteins were detected, one of which was a mitochondrial protein - NDUA4. When looking back at the IFN related upregulated proteins in the treated samples, CMPK2 can be found upregulated in both treated conditions, which is another mitochondrial protein. The upregulation of two different mitochondrial related proteins, one in untreated and other one in the both treated ISG15 KO samples, suggests a potential upregulation of this biological process. Regarding the downregulated proteins in ISG15 deficient vs WT untreated cells, there seems to be a common pattern in the function of these proteins, most of them DNA and RNA related. One of these is periphilin-1 (PPHLN), the second most downregulated protein, which is a nuclear protein and part of the Human Silencing Hub (HUSH), suggested to be an epigenetic suppression complex responsible for mediating position effect variegation (PEV)(Tchasovnikarova *et al.*, 2015). PEV refers to the phenomenon by which the position of a gene results in enhanced or repressed expression. According to this phenomenon, genes closer to heterochromatin are more likely to present a mosaic expression, presenting activated or silenced expression even between neighbouring cells, due to its position in the genome (Reuter & Spierer, 1992). Its overexpression has also been reported to induce suppression of key proteins involved in cell cycle progression resulting in S-phase arrest (Kurita *et al.*, 2004; Kurita *et al.*, 2007). Therefore, exploring the relationship between the downregulation of perihilin-1 and G-phase arrest described in chapter 4 could be of interest. On top of this, periphilin-1 has also been identified as a potential component of the cornified envelope in keratinocytes, a structure that acts as a plasma membrane in these cells providing epidermal integrity, and therefore could play a role in epithelial differentiation (Kazerounian & Aho, 2003). These results are consistent with those presented in chapter 5, where the expression of proteins involved in response to wound and wound healing were found downregulated in ISG15$^{-/-}$ cells vs WT cells treated for 48 hours. Accordingly, the study of the role of periphilin-1 in ISG15 deficient human keratinocytes would be an interesting target to explore.

Looking at the broader picture, the gene enrichment pathway analysis of the biological processes clearly shows that upon silencing of ISG15, anti-viral immune elements get upregulated in IFN treated cells, not downregulated. This seems to occur as a result of an en-

hanced unregulated IFN response and, consequently, ISGs involved in antiviral response such as MX2, IFIT1, 2 and 3 or the MDA-5 pathway appear upregulated. This is further confirmed by the fact that biological processes such as production and regulation of- and response to- type I IFN, response to IFNβ, and immune system mediators and processes are upregulated in ISG15 deficient vs WT IFN α treated cells regardless of treatment time course. Biological process analysis in ISG15 deficient vs WT cells treated for 48 hours also revealed important immune related changes. Processes like the response and regulation of cytokine stimulus and production, IL27 mediated signalling pathway, T cell mediated immunity and cytotoxicity and positive regulation of tumour necrosis factor (TNF) are upregulated in these samples. Even though the direct ISGylation of viral proteins have been proved to inhibit viral replication and free extracellular ISG15 has been proved to enhance the immune system, it seems as if ISG15 had evolved in humans to regulate the immune response in a wider way as a regulator of the IFN response, which does not happen in mice. Altogether, the results show a clear dysregulation of the immune response in the absence of ISG15, which depending on the context could promote disease fight-back or result in over-stimulation and inflammation. As described in section 1.3.1 and subsection 1.3.4, an unbalanced ratio of free to conjugated ISG15 and excessive extracellular free ISG15 are suspected to be responsible of the cytokine storms in severe COVID-19 patients (Munnur *et al.*, 2021; Schwartzenburg *et al.*, 2022). ISG15 deficient patients are known to present inflammatory interferonopaties (Martin-Fernandez *et al.*, 2020; Buda *et al.*, 2020; Al-Mayouf *et al.*, 2021; Hayat Malik *et al.*, 2022), proving that the ratio of free extracellular, free intracellular and conjugated ISG15 can have very different consequences depending on the cell type, condition and microenvironment. In contradiction with the immune related processes detected to be upregulated, the negative regulation of the innate immune response is also upregulated in 48 hour treated samples. To further investigate this, the genes that form this term were checked. The genes comprising this GO term (HLA-A, HLA-B, HLA-E, HLA-F, STAT2, OAS1, OAS3, TREX1, TRIM21, DHX58 and METTL3) are all IFN related genes with roles in the immune response. Again, the upregulation of these genes would be expected upon removal of a negative regulator of the IFN pathway. Several HLA genes are found upregulated as part of this term, suggesting an enhanced role of the MHC class I machinery. Indeed, biological processes related to antigen processing and presentation of endogenous peptide antigens were upregulated in 48h treated KO vs WT cells, consistent with results presented in chapter 5 and in subsection 6.4.1. Interestingly, protein and peptide metabolic processes and proteolysis were found upregulated after 24h of treatment in ISG15 deficient vs WT cells, which could be linked to this enhanced antigen presentation system. On the other hand, some of the other proteins expressed by the genes found in this list, such as OAS1 and OAS3, have been found to be involved in the negative regulation of IFN responsive genes (Lee *et al.*, 2019). Finally, regulation of programmed cell death and positive regulation of cell killing were also upregulated in 24h and 48h IFN treated samples respectively. Although the analysis to detect activated apoptotic caspases 3 and 7 carried

out by FACS in ISG15$^{-/-}$ SiHa cells did not reveal a significant increase in apoptotic cells, and the literature suggest that is the loss of USP18 that results in increased apoptotic cells (Cai *et al.*, 2017; Vuillier *et al.*, 2019), confirming this in ISG15 deficient glioblastoma cells would be of interest.

Agreeing with the results presented in chapter 5, the dysregulation of protein metabolic and catabolic processes and proteolysis along with the upregulation antigen presentation processes suggested alterations in the MHC system machinery in ISG15 KO cells compared to WT cells. A more in depth analysis of the cellular origin of the proteins differentially expressed identified via whole proteomic analysis of ISG15 deficient vs WT cells was performed to be compared with the cellular origin of the enriched and underrepresented MHC class I bound peptides identified my immunopeptidomic analysis. As seen in Figure 6.21 and Figure 6.22, proteins belonging to the mitochondrial protein-containing complex were found upregulated in untreated ISG15 KO vs WT GSC cells, and yet peptides originated from these proteins were underrepresented at the plasma membrane. This could suggest that the upregulated proteins were not being degraded as in WT cells, or that they do get degraded but the processing and transport to the membrane is somehow disrupted.

NDUA4, also known as NDUFA4 or COXFA4, was the top significantly upregulated protein in untreated ISG15 KO vs WT cells. First identified as an NADH dehydrogenase, NDUFA4 is actually a subunit of the cytochrome c oxidase, part of the electron transport chain in humans (Balsa *et al.*, 2012; Kadenbach, 2017; Pitceathly & Taanman, 2018). This protein was selected to further investigate the underrepresented peptides originated from upregulated mitochondrial proteins and, indeed, all the peptides identified in untreated ISG15KO vs WT condition were underrepresented even though the mitochondrial proteins seemed to be upregulated in this condition. Interestingly, once treated with IFNα for 24h the same mitochondrial proteins get downregulated in ISG15 deficient cells when compared to treated WT cells, but no significant change in the peptides originated from mitochondrial proteins was detected upon IFN treatment. These results are consistent with the data presented by Baldanta *et al.* (2017), who reported that IFN treatment of ISG15 deficient macrophages resulted in disrupted oxidative phosphorylation and mitochondrial pathways through the downregulation of mitochondrial respiration and lowered production of ATP and ROS. They also reported upregulated NDUFA4 in IFN-treated ISG15$^{-/-}$ vs ISG15 WT murine bone marrow derived macrophages with a fold change of 22.94. As noticed in section 5.5, IFNs have been shown to have the ability to alter metabolic processes, including lipid metabolism and mitochondrial pathways. Similarly, Yim *et al.* (2012) reported that the IFN mediated mitochondrial apoptotic pathway was upregulated in USP18 deficient human leukaemia monocytic (THP-1) and mouse bone marrow cells. Based on the information reviewed here, it could be hypothesised that ISG15 may modify NDUFA4 for its regulation, the absence of which results in dysregulated upregulation. This potential

interaction has not been described to date, and would be an interesting target to validate.

The relation of ISG15 with autophagy and mitophagy could provide an explanation for the difference between upregulated proteins and their correspondent underrepresented peptides in untreated ISG15 KO vs WT cells. As discussed in subsection 1.3.4, ISG15 has been reported to upregulate autophagy, either to compensate for downregulated protein degradation (Desai *et al.*, 2013) or to aid clear disease upon pathogenic infection (Zhang *et al.*, 2019; Bhushan *et al.*, 2020). ISG15 has also been related to mitophagy, the autophagic quality control mechanism responsible of degrading unnecessary or defective mitochondrial elements for the renewal of its components and maintenance (Pickles *et al.*, 2018). Upon mitochondrial damage, the PTEN induced putative kinase (PINK1) is gathered on the mitochondrial outer membrane to promote the recruitment and translocation of Parkin, an E3 ligase that initiates the ubiquitination of mitochondrial proteins aiding with the maintenance of mitochondrial homeostasis (Wang *et al.*, 2020b). At the same time, ISG15 has been shown to ISGylate parkin enhancing its ligase activity (Im *et al.*, 2016), and therefore the absence of ISG15 could result in impaired mitophagy. Interestingly, Alcalá *et al.* (2020) reported that the decrease of ISGylation resultant from knocking down ISG15 in pancreatic stem cells led to altered mitochondrial metabolisms, accumulation of impaired mitochondria and reduced mitophagy without increased levels of apoptotic cells. Recently, Fakhar-Ul-Hassnain Waqas *et al.* (2022) reported that induced pluripotent stem cell-derived macrophages also presented defective mitochondrial respiration. They showed that the transduction of WT ISG15 restored the defective pathway, and that protein ISGylation is at at least partially responsible of this recovery, since the transduction of a mutated ISG15 incapable of ISGylating only recovered the pathway partially, and they suggested from their conclusions that the loss of ISG15 could increase autophagy and mitophagy, although they did not further explore this possibility. The mass spectrometry analysis presented in this chapter detected large amount of upregulated proteins related to mitochondrial processes in untreated ISG15 deficient vs WT cells. Although the functionality of such mitochondria was not assessed, the significant downregulation of mitochondria derived peptides suggest mitophagic dysregulation, and further research is required to determine the mitochondrial state and the effect of IFN in the absence of ISG15.

Another meaningful event is the upregulation of secretory granule related proteins in untreated ISG15 deficient cells when compared to WT. No significant down- or upregulation of these proteins was detected upon IFN treatment. Yet, peptides originated from proteins belonging to the secretory granule lumen were found both underrepresented and enriched in untreated and IFN treated for 24h KO vs WT cells. Hypothetically, this dysregulated pathway in untreated and treated for 24 hour samples could account for the upregulated cytokine response and regulation of biological processes observed in samples treated for 48 hours. Lastly, it is worth noting that one of the only two downregulated cel-

lular compartments found in ISG15 KO vs WT samples treated with IFN for 48h was the astrocyte end-foot, a structural element thought to provide integrity to brain blood vessels. Since these were patient-derived glioblastoma stem cells, it would be of interest to further research if the knock down of ISG15 leads to structural damage in tumour cells, and if this happens even in healthy neuronal cells.

After being processed inside the cell, endogenous and exogenous peptides bind to MHC class I and II molecules attached to the cell surface so they can be recognised by $CD8^+$ and $CD4^+$ T cells respectively. However, peptide binding to MHC is not sufficient by itself for proper induction of the immune response – peptide processing, abundance and affinity are key factors as well, and the optimal conditions might vary between HLA alleles (Paul *et al.*, 2013). The optimal length for naturally occurring peptide epitopes binding to the MHC class I antigen-binding groove was determined to be 7-10 amino acids (Bleek & Nathenson, 1991), and because of the higher abundance of ninemers, many studies focus in the study of these peptides. Trolle *et al.* (2016) studied the natural length distribution of the peptide epitopes and the binding preference of the HLA class I alleles in HeLa cells. Although they did find diversity in the binding preference of the different alleles, ranging from 8 to 10, there was a common motif in the length distribution profile of the peptides naturally presented by each of them, as seen in Figure 6.26. Similarly, Schellens *et al.* (2015) studied the length distribution of peptides eluted from HLA-A-B-C molecules in four B lymphoblastoid cell-lines. A piece of their results, presented in Figure 6.27, shows a distribution profile very similar to the one reported by Trolle *et al.* (2016).

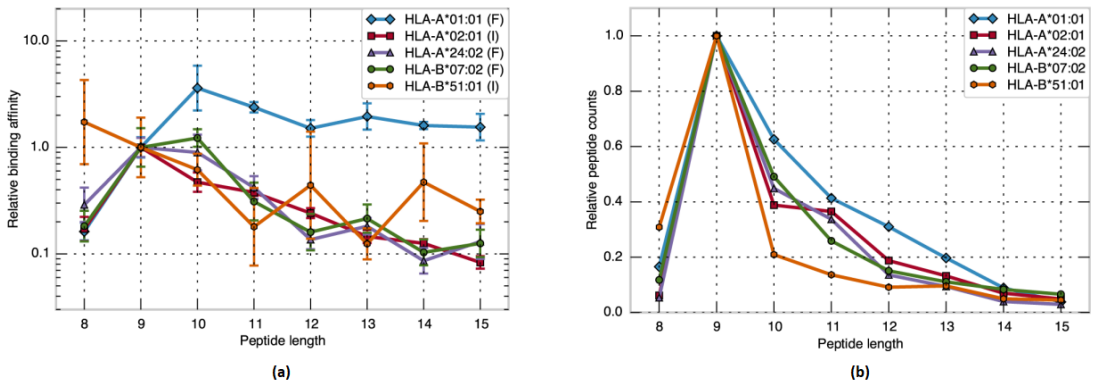

Figure 6.26: (a) Length of the peptides preferred for binding of different HLA class I alleles, measured in affinity. **(b)** Length distribution profiles of the peptides naturally presented by the different HLA alleles tested. The count of peptides of each length was normalised by the number of ninemers. Figures by Trolle *et al.* (2016).

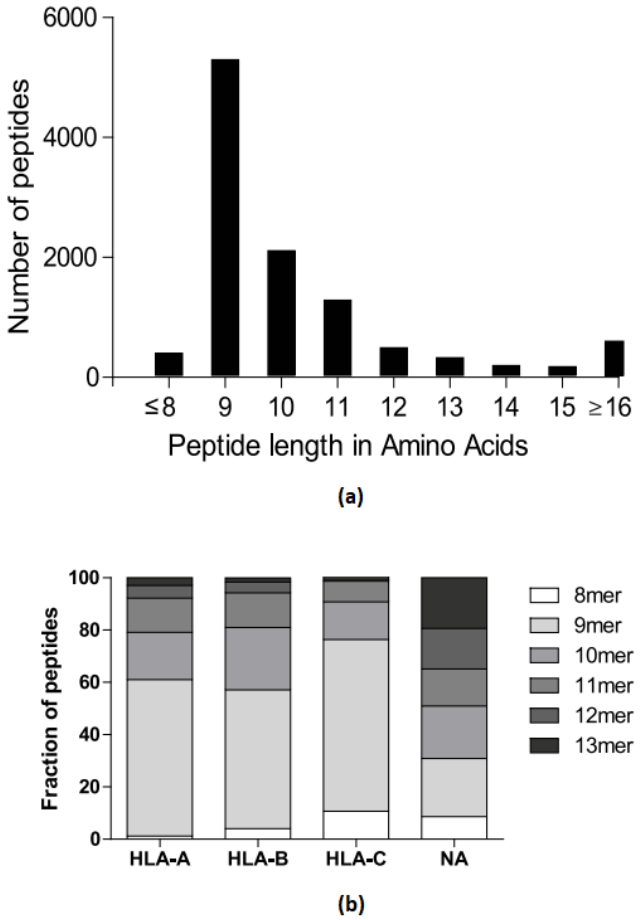

Figure 6.27: **(a)** Length distribution of the peptides naturally presented by HLA-A-B-C in B lymphoblastoid cells. **(b)** Fraction of the peptides specific to the different alleles, separated by length. Figures by Schellens *et al.* (2015).

In order to determine if there was a particular peptide length distribution among the peptides differently enriched in ISG15 deficient vs WT cells, the number of residues per peptide were counted. Results show a significant downregulation of peptides in untreated ISG15 KO vs WT samples that does not follow the standard length distribution presented by other groups, suggesting it could be due to the general protein downregulation observed in this condition in the whole proteomic results, most noticeable in the volcano plots presented here. This overall peptide downregulation significantly attenuates upon IFN treatment and as the treatment time increases, suggesting IFN recovers the protein expression diminished by the lack of ISG15. On the other hand, peptide enrichment, subtle in untreated and treated for 24 hours, significantly increases be tween 24 and 48 hours upon IFNα treatment. In this case, it does seem to follow the common length distribution generally observed in the MHC class I machinery. Because these distributions were obtained using only the peptides found in ISG15 KO samples relative to those found in WT samples in each condition, the underrepresented and enriched peptides identified during the first

24 hours after treatment (treated for 24h vs untreated) and the ones identified 24 to 48 hours after treatment (treated for 24h vs treated for 48h) were evaluated in both ISG15 KO and WT cells. These comparisons allow for the analysis of the effect of the IFN treatment on peptide length distribution and abundance, which revealed that the treatment in WT GSC resulted in the underrepresentation of a number of peptides, and the peptides enriched during the first 24 hours after treatment decline when the treatment is maintained for 48 hours. In the absence of ISG15, a larger number of peptides are enriched during the first 24 hours of treatment than in the presence of ISG15. Most importantly, this peptide enrichment is maintained throughout the treatment, quite possibly due to the absence of an important negative regulator of the IFN pathway. Overall, the peptide length distribution does not seem to be altered in treated samples in the absence of ISG15. Nevertheless, the state of the enriched peptides in WT untreated and ISG15 KO untreated samples could not be determined independently, which could show different results to the ones observed under IFN treatment.

As a final effort to identify potential differences in the peptides presented in ISG15 KO vs WT samples, the number of significant peptides per protein were counted to identify which proteins produced the most differentially enriched peptides. GAPDH (noted as G3P) was identified as the protein with the most peptides underrepresented in the absence of ISG15 when untreated, and the most peptides enriched 48h after IFN treatment. The expression of GAPDH, routinely used to normalise the expression of other proteins in immunoblotting experiments, has been reported to be inconstant in damaged vs healthy epidermal samples (Wu & Rees, 2000). As with PPHLN, this finding is noteworthy bearing in mind that one of the main symptoms of ISG15$^{-/-}$ patients is the occurrence of ulcerative skin lesions (Buda *et al.*, 2020; Martin-Fernandez *et al.*, 2020; Al-Mayouf *et al.*, 2021; Hayat Malik *et al.*, 2022). Similarly, the expression of this housekeeping gene has been described to be dysregulated in various types of cancer, including lung cancer, renal cancer, breast cancer, gastric cancer, glioma, liver cancer, colorectal cancer, melanoma, prostate cancer, pancreatic cancer and bladder cancer, as reported by Guo *et al.* (2013). Although the whole proteomic state of the targets of interest could not be confirmed due to poor p-values, further research such as expression analysis can be carried out to confirm these findings. The analysis of the enriched and underrepresented peptides identified in WT and ISG15 KO samples independently could also help determine if the origin of the peptides within the proteins changes in the absence of ISG15.

In conclusion, the lack of ISG15 has proved to have several consequences, the main one being the effects of the loss of an important IFN pathway negative regulator. Although this loss does not affect the expression of HLA in humans unless treated with type I IFN, treatment time dependant upregulation occurs upon triggering of the IFN response. The uncontrolled upregulation of the IFN pathway also results in enhanced expression of many

immune response related ISGs. Depending on the background and environment, this could enhance a beneficial anti-pathogen and malignancy response, as reported in many studies, or trigger pro-inflammatory autoimmune responses. The upregulation of a mitochondrial protein as part of the top ten hits in all conditions suggested upregulation of this biological pathway. Indeed, the whole proteomic analysis showed many metabolic pathways upregulated, and proteins originating from the mitochondrial protein-containing complex were over-expressed in untreated ISG15 deficient vs WT cells. Nonetheless, the peptides belonging to this exact term show to be significantly underrepresented under the same conditions. On the other hand, it seems as if the IFN treatment recovered the general peptide downregulation and promoted enhanced MHC class I antigen presentation, which is maintained for a much longer time in ISG15 KO cells that in WT cells. Moreover, the peptide length distribution does not seem to be altered in treated samples in the absence of ISG15. These results could have promising implications for the treatment of glioblastoma, since the expression of MHC class I has been reported to be low in these patients hampering the development of cancer vaccines (Keskin *et al.*, 2018), and ISG15 has been reported to be overexpressed in relation with glioblastoma progression (Tecalco-Cruz *et al.*, 2022) and treatment resistance (Weichselbaum *et al.*, 2008). Anti-ISG15 targeted therapies could help address the negative effects related to its overexpression and boost the MHC-I machinery sustaining HLA expression and peptide processing and presentation. At the same time, further analysis of the GSC WT immunopeptidomic data along with genomic and RNA-sequencing analysis could lead to the identification of neoantigens, which is one of the challenges in malignancies with a lower mutational burden, as discussed in the introduction of this chapter (section 6.1).

Chapter 7

Future work

7.1 Additional analyses to complement results

7.1.1 Examination of the impact of a background gene list in gene enrichment analysis

In chapter 5, the idea of the use of a background list when doing gene enrichment analysis was discussed (section 5.5). In order to determine to what extent the list of biological processes identified could change if a background list was used, a test was performed with the list of significantly dysregulated genes identified in ISG15$^{-/-}$ SiHa cells when compared to WT cells after 48 hours of IFNα treatment. To this end, a file containing Transcript Per Million (TPM) gene expression values of the protein coding genes inferred from RNA sequencing for all the cell lines within the DepMap database (OmicsExpressionProteinCodingGenesTPMLogp1.csv) was downloaded from the DepMap Portal (https://depmap.org/portal/). All the genes expressed within the SiHa cell line (Depmap ID: ACH-000556) were selected and fed into ShinyGO, a gene enrichment analysis tool that allows for the insertion of a background list prior the analysis (Xijin Ge *et al.*, 2020). The significantly downregulated and upregulated biological processes identified using ShinyGO and the SiHa gene expression background list are shown in Table 7.1 and Table 7.2 respectively.

Table 7.1: Downregulated biological processes identified by ShinyGO in ISG15 KO vs WT SiHa samples treated with IFNα for 48 hours.

Downregulated biological processes in ISG15 KO vs WT SiHa treated for 48h		
Biological process	**Fold Enrichment**	**Enrichment FDR**
Glycoside metabolic processes	58.296	0.028
Response to wounding	4.932	0.028
Neg. reg. of phospholipase A2 activity	145.74	0.049

Table 7.2: Upregulated biological processes identified by ShinyGO in ISG15 KO vs WT SiHa samples treated with IFNα for 48 hours.

Upregulated biological processes in ISG15 KO vs WT SiHa treated for 48h		
Biological process	**Fold Enrichment**	**Enrichment FDR**
Antigen processing and presentation of peptide antigen	13.485	1.75E-05
Antigen processing and presentation	11.654	1.75E-05
Antigen processing and presentation of exogenous peptide antigen	13.474	7.66E-05
Cell cycle	2.892	0.003
Cellular macromolecule catabolic processes	3.415	0.003
Antigen processing and presentation of peptide antigen via MHC class I	14.791	0.005
Viral processes	3.642	0.005
Macromolecule catabolic processes	3.029	0.005
Cellular protein catabolic processes	3.867	0.009
Protein catabolic processes	3.504	0.01
Exosomal secretion	34.612	0.013
Extracellular exosome biogenesis	32.964	0.013
Antigen processing and presentation of exogenous peptide antigen via MHC class I	16.482	0.013
Pos. reg. of extracellular exosome assembly	115.373	0.013
Extracellular vesicle biogenesis	30.097	0.014
Reg. of cell cycle	3.144	0.019
Innate immune response	3.458	0.025

To make the data clear, the results were not analysed by Revigo, and the similar results were not manually combined. Although there are some differences in the results obtained using this method, most of the processes identified in the analysis performed with g:Profiler and without a background list were also identified here. There are, however, inconsistencies between the two methods on the common identified processes. The top upregulated and downregulated processes according to their enrichment scores / fold enrichment are different in each method. While the combination of g:Profiler and Revigo led to quite consistent enrichment scores (ranging between 1 and 4), the processes identified by ShinyGO have fold enrichment values ranging 3-4 to 115-145, suggesting a significant difference in the dysregulation level among each of them. Although further research is required to understand the differences in the statistical approaches taken by each of these methods, preliminary data suggests that the results obtained via gene enrichment analysis in this thesis are valid and meaningful.

7.1.2 Comparison of the results obtained through mass spectrometry analysis in SiHa cells (SILAC) and in GSC cells (whole proteomics)

A table summarising the results obtained through SILAC and whole proteomic mass spectrometry (MS) analysis in SiHa and GSC cells respectively was prepared to compare the top down- and upregulated proteins identified with each method Table 7.3. Hits identified in untreated samples through SILAC MS analysis were combined, since there is no IFN treatment in them to discern the samples collected at 24 hours from the ones collected at 48 hours. The proteins identified in samples collected at 48 hours that were synthesised during the first 24 hours after treatment (R10K8 proteins) were included in the 24 hour category. ISG15 (shown in red) is the only commonly downregulated protein in all the categories except untreated samples analysed through SILAC MS. Apart from IFIT1, identified to be upregulated both in SILAC and whole proteomic analysis in ISG15 KO samples treated for 24 hours, no other common proteins were identified between the two methods. It must be borne in mind that while whole proteomic MS analyses the steady state levels of proteins in the proteome, SILAC analysis only detects the newly synthesised proteins. Therefore, the fact that not many proteins match as the top dysregulated proteins is not surprising. A further step into understanding the differences in the proteomic landscape in SiHa and GSC ISG15 KO cells could be to search for the expression state of hits of interest identified in one of the analysis, in the other one. For example, CMPK2, found significantly upregulated in ISG15 KO GSC cells treated with IFNα for 24h, was found downregulated in ISG15 KO SiHa cells treated for 24 hours (R10K8), although with a very poor p-value (FC 0.46, p-value 0.915). This kind of differences could be validates using experimental approaches.

Table 7.3: Summary table of the results obtained through SILAC and whole proteomic mass spectrometry analysis in SiHa and GSC cells respectively, showing the top down- and upregulated proteins identified in ISG15 KO vs WT cells through each method. ISG15 is shown in red, and the proteins found through both methods are shown in green.

	SILAC		**Whole proteomics**	
	Downregulated	**Upregulated**	**Downregulated**	**Upregulated**
Untreated	EXT1	NQO1	NFIC	NDUA4
	EIF3M	TKT	PPHLN	CATD
	PML	ACTR3	HMGA1	
	CEBPD	MT1G	TM41B	
	MTERF		ADA	
	IFI35		ADPPT	
	SNTA1		ROA0	
	G3BP1		**ISG15**	
	CPS1			
	RPS24			
	DAB2			
	RPS6			
	ZW10			
IFNα 24h	EXT1	MX1	**ISG15**	IFIT2
	ISG15	FGB		IFIT3
	UBE2K	NQO1		IFIH1
	CNN2	MT1G		CMPK2
	EIF1	MT1F		SYWC
	MTERF	ACTR3		CD151
	DAB2	MX1		IFIT1
		ATM		DHX58
		IFIT1		5NTD
		PABPC1		
IFNα 48h	**ISG15**	WARS	**ISG15**	IFIT2
	ATAD2	FGB		CMPK2
		MX1		IFIT3
		ACTR3		LG3BP
		MTG1		MX2
				IFIT1
				DHX58
				IFIH1
				CD151

7.1.3 Further analysis of the immunopeptides identified in glioblastoma stem cells

Peptide clustering

The work presented in chapter 6 provides initial steps towards the HLA presented peptide prediction in WT and ISG15 KO glioblastoma stem cells. The enrichment of ninemers observed in the peptide length distribution analysis and the significant increase in detected peptides upon 48 hour IFNα treatment, correlating with the upregulation of HLA measured by flow cytometry, suggest a good rate of immunopeptide identification. Nevertheless, a more in-depth assessment of the peptides identified would be required, including the use of *in silico* approaches to further filter the peptides identified to remove non-HLA eluted peptides and aid the prediction of potential T cell epitopes, since peptide binding to HLA does not equal to antigen presentation and induction of the immune response.

The peptide-binding groove on HLA molecules has pockets where specific residues of the bound peptide anchor, and those anchoring amino acids are especially important when analysing strong binders and potential presented peptides. The fact that many different peptides are capable of binding to HLA molecules often translates in conserved sequence motifs that ensure receptor specificity (Klein & Sato, 2000). HLA-A, B and C molecules usually have two or three pockets where anchoring residues bind the groove (Figure 7.1). However, each MHC allotype has a distinctly shaped and charged binding groove, resulting from their particular polymorphisms. Hence, the peptides and motifs that will bind most strongly to each allotype will also vary (Bassani-Sternberg *et al.*, 2017).

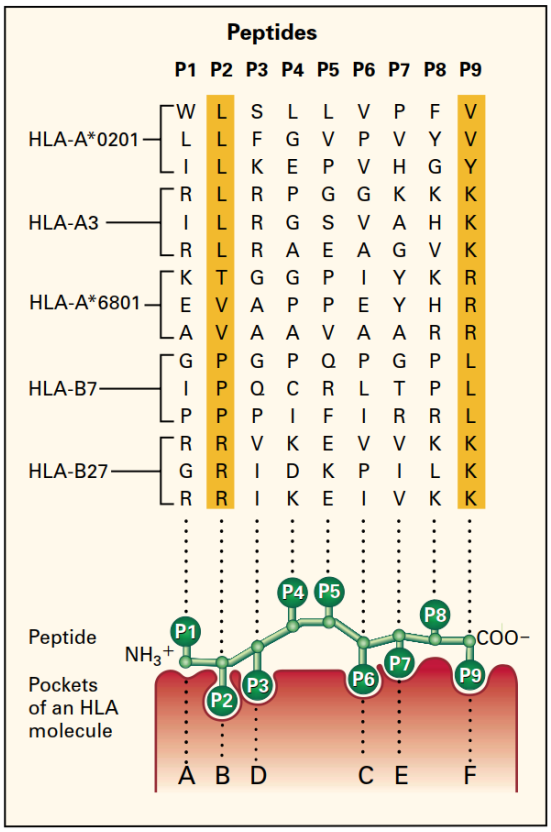

Figure 7.1: Binding peptide motifs in HLA molecule. Example ninemers illustrating peptide motifs in critical anchoring residues (P2 and P9), which change in different HLA allotypes. Non-anchoring residues (P1, P4, P5 and P8) are not decisive in determining the binding specificity. Figure by Klein & Sato (2000).

Online tools like GibbsCluster (Andreatta *et al.*, 2013; Andreatta *et al.*, 2017) can be used to identify MHC-specific sequence motifs to help determine which peptides are more likely to be strong binders for these molecules. This server is capable of aligning and clustering the peptides introduced to search for conserved sequence motifs, thus helping with the filtering of non-HLA eluted and non-specific ligand peptides. As an example of such analysis, all the ninemers with a p-value < 0.05 identified in each treatment category (untreated, treated for 24 hours and treated for 48 hours) in chapter 6 were fed to GibbsCluster (https://services.healthtech.dtu.dk/services/GibbsCluster-2.0/) separated in two categories – peptides overrepresented (FC > 2) and underrepresented in ISG15 KO vs WT cells (FC < 0.67), selecting the parameters for MHC class I ligands of same length.

Comparing the obtained motifs with known HLA binding motifs found in data bases, such as the Imunne Epitope Database (https://www.iedb.org/), can help discern what HLA alleles could the peptides have been eluted from. Further analysis would include the use of machine learning techniques to estimate proteasomal cleavage sites, and T-cell functional assays could be carried out to assess the ability of T-cells to respond to selected immunopeptides.

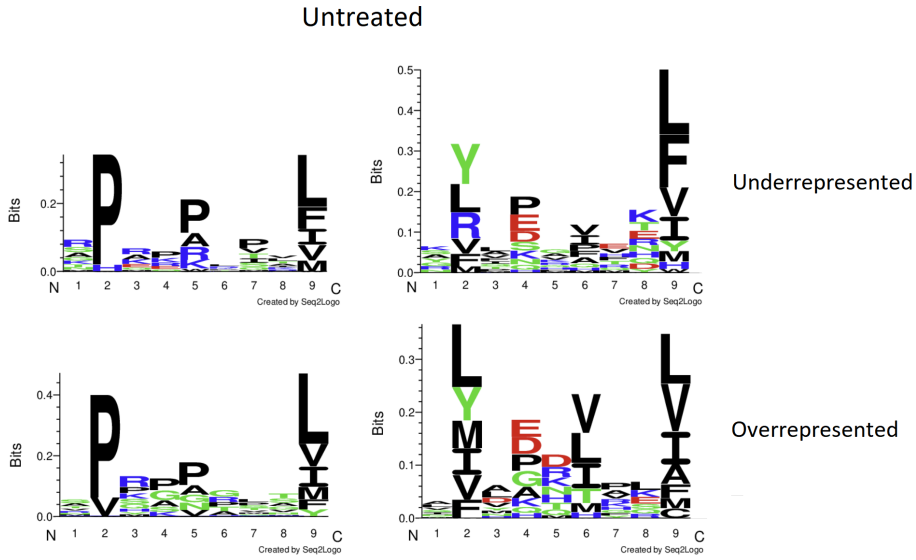
Untreated
Underrepresented
Overrepresented
Bits
N 1 2 3 4 5 6 7 8 9 C
Created by Seq2Logo

(a)

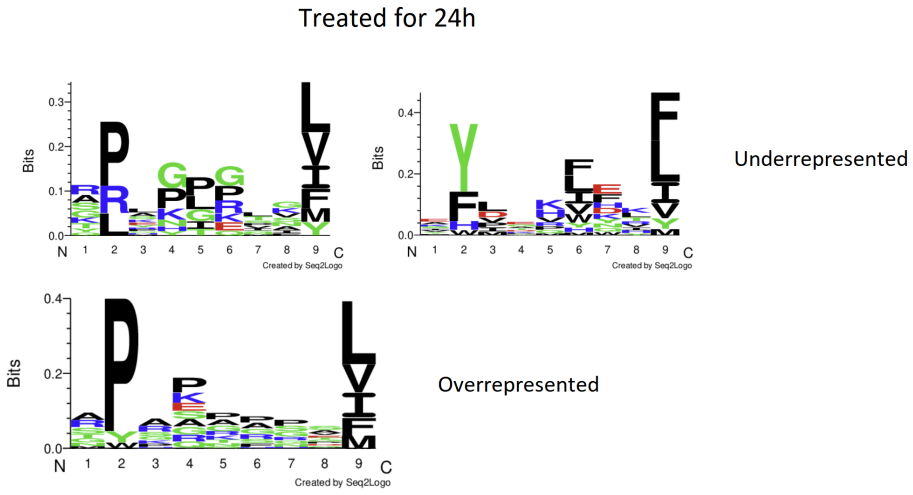
Treated for 24h
Underrepresented
Overrepresented
Bits
N 1 2 3 4 5 6 7 8 9 C
Created by Seq2Logo

(b)

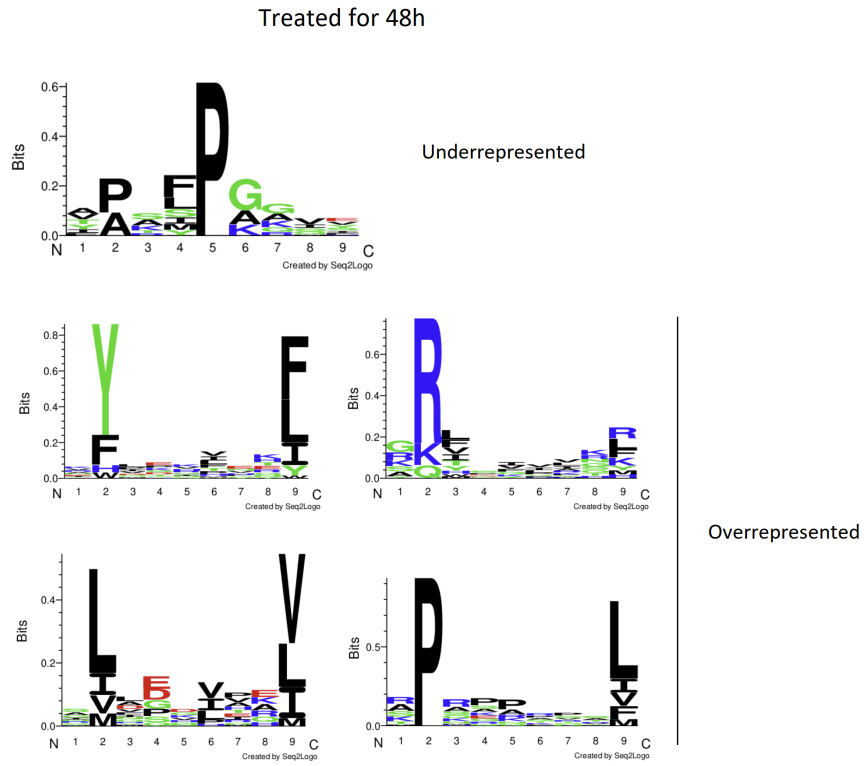

(c)

Figure 7.2: Clustering analysis on ninemer peptides (p-value < 0.05) identified in chapter 6. The ninemers significantly overrepresented (FC > 2) and underrepresented (FC < 0.67) identified in ISG15 KO vs WT cells in each treatment category were fed to GibbsCluster, selecting the parameters for MHC class I ligands of same length.

Analysis of the peptide distribution within the sequences of targets of interest

A large number of GAPDH (G3P) peptides were found significantly underrepresented in ISG15 KO vs WT untreated cells and significantly enriched in ISG15 KO vs WT cells treated for 48 hours. This sparked interest in further research of these peptides. To this end, all the peptides identified in each of these conditions were aligned with the sequence of GAPDH, to determine where within the protein the peptides were coming from. COBALT, a multiple sequence alignment tool available at the National Center for Biotechnology Information (NCBI) (https://www.ncbi.nlm.nih.gov/tools/cobalt/re_cobalt.cgi), was used to generate maps showing the alignment of each peptide within the protein's sequence. This revealed an interesting pattern - while the peptides enriched upon IFN treatment show a more dispersed arrangement along the sequence (see Figure 7.4), nearly all the peptides found underrepresented in ISG15 KO vs WT untreated samples (51 out of 55) originated from a very limited section of the C-terminal of the protein (Figure 7.3). This opens the

question of whether the loss of ISG15 causes changes in the antigen processing machinery that result in a significant change on the origin of peptides within the protein. Further analysis to determine the peptide pattern within the protein of origin of all the peptides identified enriched and underrepresented in WT samples vs the pattern within the same protein in all the peptides identified to be enriched and underrepresented in ISG15 KO samples could help answer this question. At the same time, further investigating those peptides found only in ISG15 KO samples and not in WT samples might result in the identification of unique peptides presented only in the absence of ISG15. In samples treated with IFNα for 48 hours, 32 of the 44 peptides identified to be enriched were found solely in ISG15 KO samples, and not in WT samples.

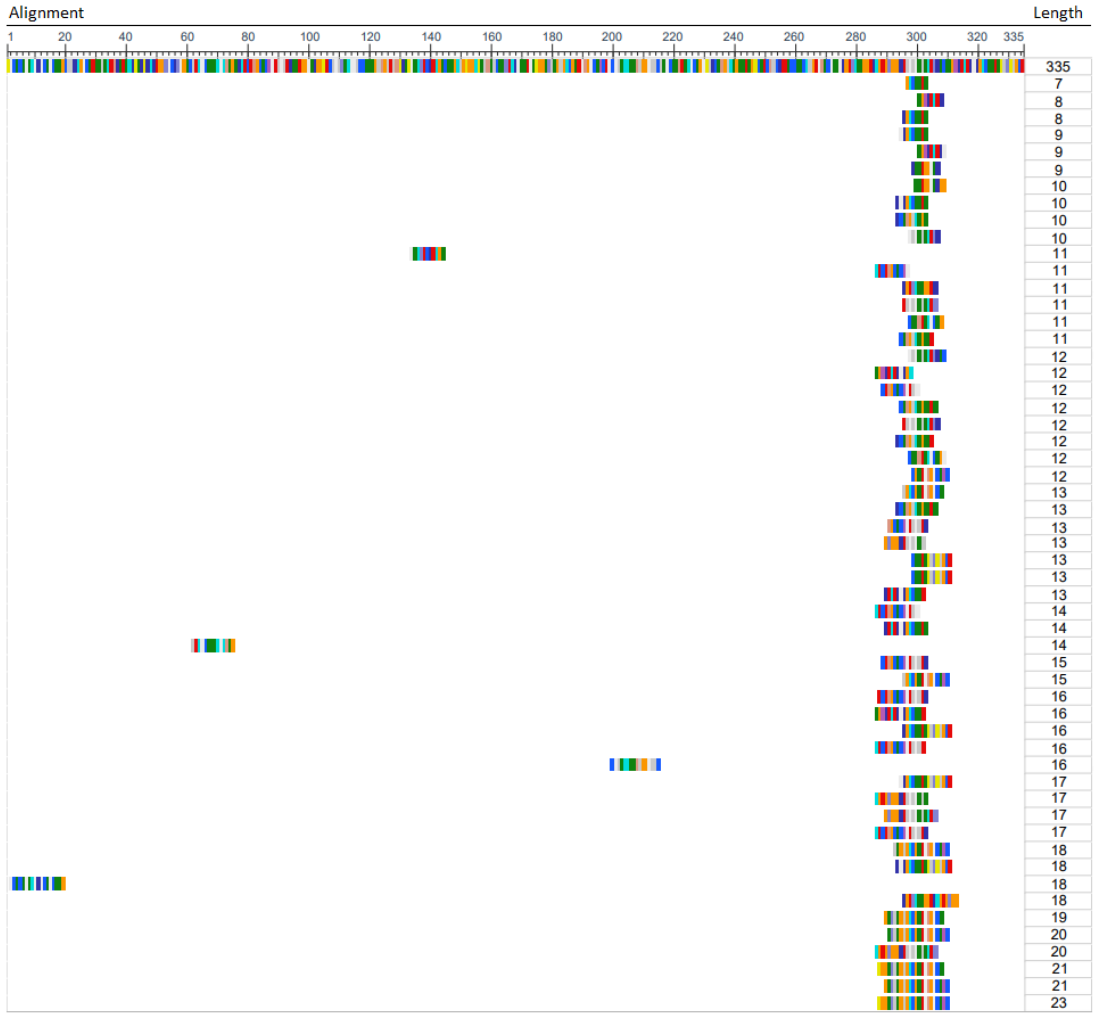

Figure 7.3: GAPDH peptides identified to be underrepresented in untreated ISG15 KO vs WT samples, aligned against the GAPDH protein sequence.

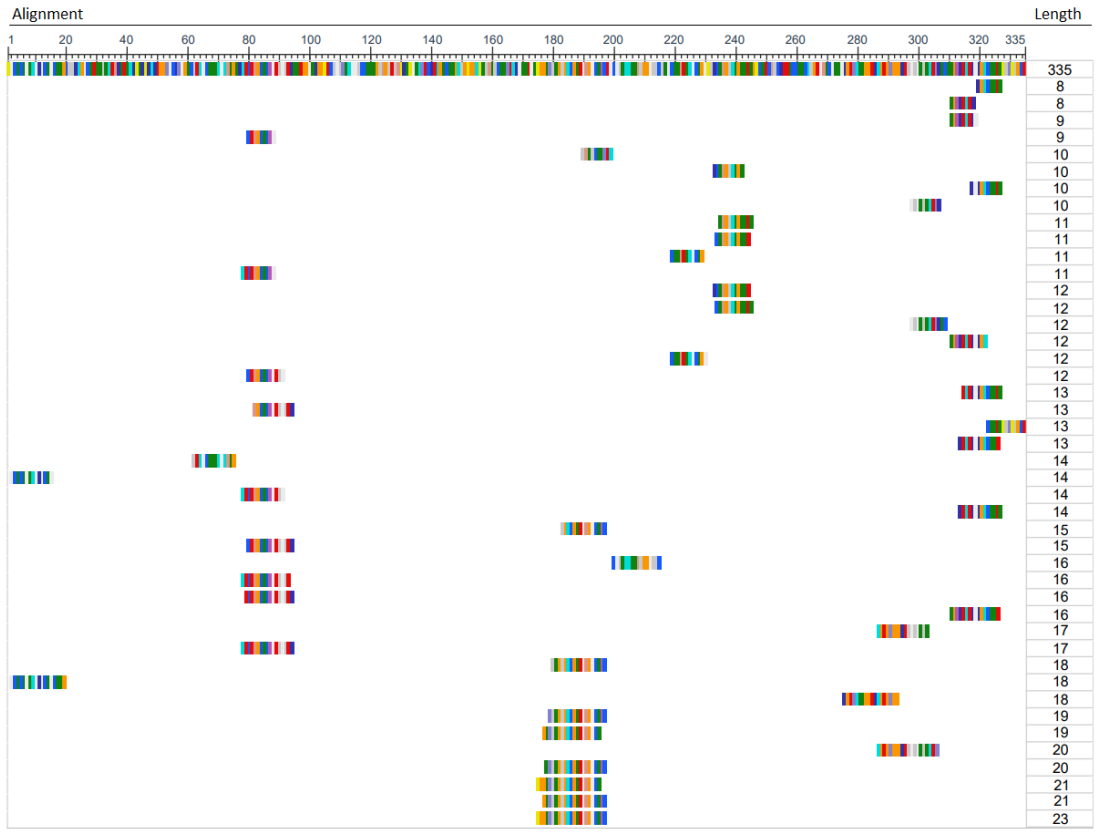

Figure 7.4: GAPDH peptides identified to be enriched in ISG15 KO vs WT samples treated with IFNα for 48 hours, aligned against the GAPDH protein sequence.

A slight preference of MHC class I molecules towards peptides derived from helical peptides was reported in 2019 by Perez *et al.* In their analysis of nonameric peptides identified by MS and searched on databases revealed that peptides originated from helical structures within the proteins were enriched among the peptides presented by human MHC-I. Similarly, peptides derived from human transmembrane helices have been reported to be over-presented in MHC-I compared to that which would be expected from their abundance (Bianchi *et al.*, 2017). This is suggested to be due to the relatively hydrophobic nature of the groove in most of the MHC class I alleles and the hydrophobicity of these regions (Bilderbeek *et al.*, 2022). Therefore, identifying the origin of the peptides within the structure of the protein could be of interest as part of the this study. As an example of the kind of structural analysis that could be carried out to determine the origin of the peptides within the protein structure, the 55 underrepresented peptides identified in ISG15 KO vs WT untreated samples were aligned with each other looking for common motifs (as the one seen in Figure 7.5 and Appendix E) that could help identify peptide editing patterns. The minimal peptide from each aligned set plus single peptides were highlighted in the structure of GAPDH using the PyMOL Molecular Graphics System, by Schrödinger LLC

(https://pymol.org/). As seen in Figure 7.5, the majority of the peptide (shown in lilac) described here are not found in hydrophobic regions of the protein but are found in loop structures and are therefore more solvent exposed and less hydrophobic. In fact, only one of the overlapping peptide series was from a helical segment of the structure (shown in cyan, SNRVVDL), and of note this was the most overlapping series of peptides identified. The results presented in this thesis provide exciting possibilities to further investigate the increased and sustained general peptide expression on MHC-I molecules upon loss of ISG15, as well as the significant number of dysregulated peptides originated from specific proteins of interest such as GAPDH or B2M.

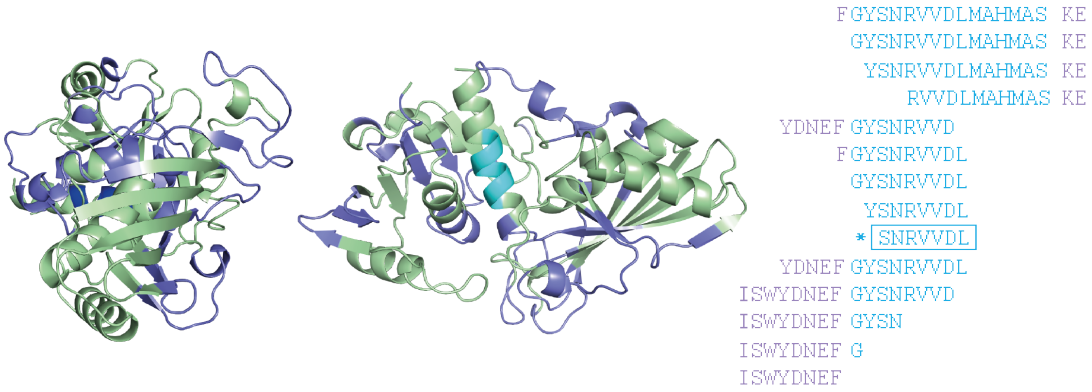

Figure 7.5: The origin of the underrepresented peptides identified in ISG15 KO vs WT GSC cells within the GAPDH sequence. All the peptides were aligned and arranged in groups of nested peptides, which were then located within the structure of GAPDH using Pymol. A group of 14 nested peptides were selected out of the 55 found underrepresented in ISG15 KO vs WT GSC cells to be aligned to each other looking for common motifs that could help identify peptide editing patterns. SNRVVDL, an heptamer found to be in the centre of its nested peptide group (marked with a box and an asterisk) was plotted in blue to show its location in the centre of an alpha-helix. Figure by Professor Kathryn Ball.

7.1.4 The use of other IFN types and subtypes in future research

The aim of this thesis was to study the role of ISG15 in cancer cell models. ISG15 is one of the most upregulated proteins upon IFN treatment, and although there is a degree of cross-talk between type I and type II signalling, its expression is primarily triggered by type I IFNs (Zhang & Zhang, 2011). The only experiment performed at the beginning of this project with both type I and type II IFNs in WT and ISG15 KO SiHa cells (Figure 4.9) showed that the loss of ISG15 did not lead to the same sensitivity to treatment in IFNα and γ treated cells. In order to further study this response, IFNα was selected to induce the expression of ISG15 in WT cell lines and compare it with also treated ISG15 KO cell lines. Even though some experiments in chapter 4 were carried out with a range of IFNα subtypes in order to elucidate if they generated a different response to the commonly used IFNα2, commercial

IFNα2 was selected for the mass spectrometry analysis for easier reproducibility. Future mass spectrometry experiments could be carried out to compare results upon treatment with selected IFNα subtypes or other type I IFNs such as IFNβ. However, and since results on chapter 6 suggest a role of ISG15 in peptide processing and presentation with important implications in cancer immunology, further experiments with IFNγ, reported to be highly involved both in protumour and antitumour activities (Gocher *et al.*, 2022), should be reconsidered in future research approaches.

7.2 Exploration of new research directions

Some interesting ideas to extend the results presented in this thesis include:

- Further study of the between NQO1, MT1F and MT1G with ISG15 and the role of ISG15 in the response to oxidative stress.
- Examining the mitochondrial state in ISG15 deficient cells.
- Further research the autophagy and mitophagy pathways in glioblastoma ISG15 deficient cells to determine the reason for the underrepresented mitochondrial peptides, and answer whether IFN treatment can rescue these defects.
- Further study the role of NDUFA4 in relation to ISG15.
- Determine the role of ISG15 in wound response and recovery, analysing the genes grouped in these biological processes.
- Study the state of the enriched peptides in WT untreated and ISG15 KO untreated samples independently to better understand the effects of the loss of ISG15 in the absence of IFN.
- Analyse the enriched and underrepresented peptides originated from interesting targets such as GAPDH, VIME or B2M in WT cells, and compare them with those enriched in ISG15 KO cells to determine if there is any variability in the origin of the peptides within the protein (sequence section or structure).
- Combine the data obtained from the immunopeptidomic analysis performed on GSC WT cells with genomic and RNA-sequencing data to try to identify new neoantigens that can be studied for vaccines for the treatment of glioblastoma.

Appendices

Appendix A

Supplementary data for chapter 3: Generation of isogenic ISG15 knock out cell models

Full ISG15 gene amplicon sequences

SiHa WT and ISG15$^{-/-}$ clones

WT

5'…GCAGATTCATGAACACGGTGCTCAGGGGCTTGAGGCCGTACTCCCCCAGCGGGA
GCTGGTCCTCCAGGGGCTTCCCCTCGAAGGTCAGCCAGAACAGGTCGTCCTGCACACCC
TCCAGCCCGCTCACTTGCTGCTTCAGGTGGGCCACGGTCTGCGTCAGCCGTACCTCGTA
GGTGCTGCTGCGGCCCTTGTTATTCCTCACCAGGATGCTCAGAGGTTCGTCGCATTTGT
CCACCACCAGCAGGACCGTGCTGCCGGGGCCCAGGCCCTGGCTGGCAAGGGGGACCCTG
TCCTGCAGCGCCACACCGCTCGGGTGGACAGCCAGACGCTGCTGGAAGGCGTGCACGCC
GATCTTCTGGGTGATCTGCGCCTTCAGCTCTGACACCGACATGGAGCTGCTCAGGGACA
CCTGGAATTCGTTGCCCGCCAGCATCTTCACCGTCAGGTCCCA…3'

Clone #3 - Edit 1

5'…GCAGATTCATGAACACGGTGCTGCATCTTCACCGTCAGGTCCCA…3'

Clone #3 - Edit 2

5'...GCAGATTCATGAACACGGTGCAGGGGCTTGAGGCCGTACTCCCCCAGCGGGAGCT
GGTCCTCCAGGGGCTTCCCCTCGAAGGTCAGCCAGAACAGGTCGTCCTGCACACCCTCCA
GCCCGCTCACTTGCTGCTTCAGGTGGGCCACGGTCTGCGTCAGCCGCACCTCGTAGGTGC
TGCTGCGGCCCTTGTTATTCCTCACCAGGATGCTCAGAGGTTCGTCGCATTTGTCCACCA
CCAGCAGGACCGTGCTGCCGGGGCCCAGGCCCTGGCTGGCAAGGGGGACCCTGTCCTGCA
GCGCCACACCGCTCGGGTGGACAGCCAGACGCTGCTGGAAGGCGTGCACGCCGATCTTCT
GGGTGATCTGCGCCTTCAGCTCTGACACCGACATGGAGCTGCTCAGGGACACCTGGAATT
CGTTGCCCGCATCTTCACCGTCAGGTCCCA...3'

Clone #3 - Edit 3

5'...GCAGATTCATGAACACGGTGCTTCAGGGGCTTGAGGCCGTACTCCCCCAGCGGGA
GCTGGTCCTCCAGGGGCTTCCCCTCGAAGGTCAGCCAGAACAGGTCGTCCTGCACACCCT
CCAGCCCGCTCACTTGCTGCTTCAGGTGGGCCACGGTCTGCGTCAGCCGCACCTCGTAGG
TGCTGCTGCGGCCCTTGTTATTCCTCACCAGGATGCTCAGAGGTTCGTCGCATTTGTCCA
CCACCAGCAGGACCGTGCTGCCGGGGCCCAGGCCCTGGCTGGCAAGGGGGACCCTGTCCT
GCAGCGCCACACCGCTCGGGTGGACAGCCAGACGCTGCTGGAAGGCGTGCACGCCGATCT
TCTGGGTGATCTGCGCCTTCAGCTCTGACACCGACATGGAGCTGCTCAGGGACACCTGGA
ATCAGGTCCCA...3'

Clone #4 - Edit 1

5'...GCAGATTCATGAACACGGTGGTCAGGGGCTTGAGGCCGTACTCCCCCAGCGGGAG
CTGGTCCTCCAGGGGCTTCCCCTCGAAGGTCAGCCAGAACAGGTCGTCCTGCACACCCTC
CAGCCCGCTCACTTGCTGCTTCAGGTGGGCCACGGTCTGCGTCAGCCGCACCTCGTAGGT
GCTGCTGCGGCCCTTGTTATTCCTCACCAGGATGCTCAGAGGTTCGTCGCATTTGTCCAC
CACCAGCAGGACCGTGCTGCCGGGGCCCAGGCCCTGGCTGGCAAGGGGGACCCTGTCCTG
CAGCGCCACACCGCTCGGGTGGACAGCCAGACGCTGCTGGAAGGCGTGCACGCCGATCTT
CTGGGTGATCTGCGCCTTCAGCTCTGACACCGACATGGAGCTGCTCAGGGACACCTGGAA
TTCACCGTCAGGTCCCA...3'

Clone #4 - Edit 2

'5...GCAGATTCATGAACACGGTGCTTCAGGGGCTTGAGGCCGTACTCCCCCAGCGGGA
GCTGGTCCTCCAGGGGCTTCCCCTCGAAGGTCAGCCAGAACAGGTCGTCCTGCACACCCT
CCAGCCCGCTCACTTGCTGCTTCAGGTGGGCCACGGTCTGCGTCAGCCGCACCTCGTAGG
TGCTGCTGCGGCCCTTGTTATTCCTCACCAGGATGCTCAGAGGTTCGTCGCATTTGTCCA
CCACCAGCAGGACCGTGCTGCCGGGGCCCAGGCCCTGGCTGGCAAGGGGGACCCTGTCCT
GCAGCGCCACACCGCTCGGGTGGACAGCCAGACGCTGCTGGAAGGCGTGCACGCCGATCT
TCTGGGTGATCTGCGCCTTCAGCTCTGACACCGACATGGAGCTGCTCAGGGACACCTGGA
ATTCGTTGCCCGCCAAGCATCTTCACCGTCAGGTCCCA...3'

Clone #4 - Edit 3

5'...GCAGATTCATGAACACGGTGCAGGGGCTTGAGGCCGTACTCCCCCAGCGGGAGCT
GGTCCTCCAGGGGCTTCCCCTCGAAGGTCAGCCAGAACAGGTCGTCCTGCACACCCTCCA
GCCCGCTCACTTGCTGCTTCAGGTGGGCCACGGTCTGCGTCAGCCGCACCTCGTAGGTGC
TGCTGCGGCCCTTGTTATTCCTCACCAGGATGCTCAGAGGTTCGTCGCATTTGTCCACCA
CCAGCAGGACCGTGCTGCCGGGGCCCAGGCCCTGGCTGGCAAGGGGGACCCTGTCCTGCA
GCGCCACACCGCTCGGGTGGACAGCCAGACGCTGCTGGAAGGCGTGCACGCCGATCTTCT
GGGTGATCTGCGCCTTCAGCTCTGACACCGACATGGAGCTGCTCAGGGACACCTGGAATT
CGTTGCCCGCCACGCATCTTCACCGTCAGGTCCCA...3'

Clone #4 - Edit 4

5'...GCAGATTCATGAACACGTCAGGGGCTTGAGGCCGTACTCCCCCAGCGGGAGCTGG
TCTTCACCGTCAGGTCCCA...3'

Clone #9 - Edit 1

5'...GCAGATTCATGAACACGGTGCTTCAGGGGCTTGAGGCCGTACTCCCCCAGCGGGA
GCTGGTCCTCCAGGGGCTTCCCCTCGAAGGTCAGCCAGAACAGGTCGTCCTGCACACCCT
CCAGCCCGCTCACTTGCTGCTTCAGGTGGGCCACGGTCTGCGTCAGCCGCACCTCGTAGG

TGCTGCTGCGGCCCTTGTTATTCCTCACCAGGATGCTCAGAGGTTCGTCGCATTTGTCCA
CCACCAGCAGGACCGTGCTGCCGGGGCCCAGGCCCTGGCTGGCAAGGGGGACCCTGTCCT
GCAGCGCCACACCGCTCGGGTGGACAGCCAGACGCTGCTGGAAGGCGTGCACGCCGATCT
TCTGGGTGATCTGCGCCTTCAGCTCTGACACCGACATGGAGCTGCTCAGGGACACCTGGA
ATTCGTTGCCCGCCAGGCATCTTCACCGTCAGGTCCCA...3'

Clone #9 - Edit 2

5'...GCAGATTCATGAACACGGTGCTTCAGGGGCTTGAGGCCGTACTCCCCCAGCGGGA
GCTGGTCCTCCAGGGGCTTCCCCTCGAAGGTCAGCCAGAACAGGTCGTCCTGCACACCCT
CCAGCCCGCTCACTTGCTGCTTCAGGTGGGCCACGGTCTGCGTCAGCCGCACCTCGTAGG
TGCTGCTGCGGCCCTTGTTATTCCTCACCAGGATGCTCAGAGGTTCGTCGCATTTGTCCA
CCACCAGCAGGACCGTGCTGCCGGGGCCCAGGCCCTGGCTGGCAAGGGGGACCCTGTCCT
GCAGCGCCACACCGCTCGGGTGGACAGCCAGACGCTGCTGGAAGGCGTGCACGCCGATCT
TCTGGGTGATCTGCGCCTTCAGCTCTGACACCGACATGGAGCTGCTCAGGGACACCTGGA
ATTCGTTGCCCGCCATCTTCACCGTCAGGTCCCA...3'

Clone #9 - Edit 3

5'...GCAGATTCATGAACACGGTGCCGCATCTTCACCGTCAGGTCCCA...3'

Clone #9 - Edit 4

5'...GCAGATTCATGAACACGGTGCTTCAGGGGCTTGAGGCCGTACTCCCCCAGCGGGA
GCTGGTCCTCCAGGGGCTTCCCCTCGAAGGTCAGCCAGAACAGGTCGTCCTGCACACCCT
CCAGCCCGCTCACTTGCTGCTTCAGGTGGGCCACGGTCTGCGTCAGCCGCACCTCGTAGG
TGCTGCTGCGGCCCTTGTTATTCCTCACCAGGATGCTCAGAGGTTCGTCGCATTTGTCCA
CCACCAGCAGGACCGTGCTGCCGGGGCCCAGGCCCTGGCTGGCAAGGGGGACCCTGTCCT
GCAGCGCCACACCGCTCGGGTGGACAGCCAGACGCTGCTGGAAGGCGTGCACGCCGATCT
TCTGGGTGATCTGCGCCTTCAGCTCTGACACCGACATGGAGCTGCTCAGGGACACCTGGA
ATTCGTTGCCCGCCAGTCAGGGGCTTGAGGCCGTACTCCCCCAGCGGGAGCTGGTCCTCC
AGGGGCTTCCCCTCGAAGGTCAGCCAGAACAGGTCGTCCTGCACACCCTCCAGCCCGCTC
ACTTGCTGCTTCAGGTGGGCCACGGTCTGCGTCAGCCGCACCTCGTAGGTGCTGCTGCGG
CCCTTGTTATTCCTCACCAGGATGCTCAGAGGTTCGTCGCATTTGTCCACCACCAGCAGG
ACCGTGCTGCCGGGGCCCAGGCCCTGGCTGGCAAGGGGGACCCTGTCCTGCAGCGCCACA
CCGCTCGGGTGGACAGCCAGACGCTGCTGGAAGGCGTGCACGCCGATCTTCTGGGTGATC
TGCGCCTTCAGCTCTGACACCGACATGGAGCTGCTCAGGGACACCTGGAATTCGTTGCAT
CTTCACCGTCAGGTCCCA...3'

Clone #10 - Edit 1

5'...GCAGATTCATGAACACGGTGCTCAGGGGCTTGAGGCCGTACTCCCCCAGCGGGAG
CTGGTCCTCCAGGGGCTTCCCCTCGAAGGTCAGCCAGAACAGGTCGTCCTGCACACCCTC
CAGCCCGCTCACTTGCTGCTTCAGGTGGGCCACGGTCTGCGTCAGCCGCACCTCGTAGGT
GCTGCTGCGGCCCTTGTTATTCCTCACCAGGATGCTCAGAGGTTCGTCGCATTTGTCCAC
CACCAGCAGGACCGTGCTGCCGGGGCCCAGGCCCTGGCTGGCAAGGGGGACCCTGTCCTG
CAGCGCCACACCGCTCGGGTGGACAGCCAGACGCTGCTGGAAGGCGTGCACGCCGATCTT
CTGGGTGATCTGCGCCTTCAGCTCTGACACCGACATGGAGCTGCTCAGGGACACCTGGAA
TTCGTTGCCCGCCAGGCATCTTCACCGTCAGGTCCCA...3'

Clone #10 - Edit 2

5'...GCAGATTCATGAACACGGTGCTTGGCGGGCAACGAATTCCAGGTGTCCCTGAGCA
GCTCCATGTCGGTGTCAGAGCTGAAGGCGCAGATCACCCAGAAGATCGGCGTGCACGCCT
TCCAGCAGCGTCTGGCTGTCCACCCGAGCGGTGTGGCGCTGCAGGACAGGGTCCCCCTTG
CCAGCCAGGGCCTGGGCCCCGGCAGCACGGTCCTGCTGGTGGTGGACAAATGCGACGAAC
CTCTGAGCATCCTGGTGAGGAATAACAAGGGCCGCAGCAGCACCTACGAGGTGCGGCTGA
CGCAGACCGTGGCCCACCTGAAGCAGCAAGTGAGCGGGCTGGAGGGTGTGCAGGACGACC
TGTTCTGGCTGACCTTCGAGGGGAAGCCCCTGGAGGACCAGCTCCCGCTGGGGGAGTACG
GCCTCAAGCCCCTGCATCTTCACCGTCAGGTCCCA...3'

GSC WT and ISG15$^{-/-}$ clones #2

WT

5'...GCAGATTCATGAACACGGTGCTCAGGGGCTTGAGGCCGTACTCCCCCAGCGGGAG
CTGGTCCTCCAGGGGCTTCCCCTCGAAGGTCAGCCAGAACAGGTCGTCCTGCACACCCTC
CAGCCCGCTCACTTGCTGCTTCAGGTGGGCCACGGTCTGCGTCAGCCGCACCTCGTAGGT
GCTGCTGCGGCCCTTGTTATTCCTCACCAGGATGNTCAGAGGTTCGTCGCATTTGTCCAC
CACCAGCAGGACCGTGCTGCCGGGGCCCAGGCCCTGGCTGGCAAGGGGGACCCTGTCCTG
CAGCGCCACACCGCTCGGGTGGACAGCCAGACGCTGCTGGAAGGCGTGCACGCCGATCTT
CTGGGTGATCTGCGCCTTCAGCTCTGACACCGACATGGAGCTGCTCAGGGACACCTGGAA
TTCGTTGCCCGCCAGCATCTTCACCGTCAGGTCCCA...3'

Clone #2 - Edit 1

5'...GCAGATTCATGAACACGGTGCTTGGCGGGCAACGAATTCCAGGTGTCCCTGAGCA
GCTCCATGTCGGTGTCAGAGCTGAAGGCGCAGATCACCCAGAAGATCGGCGTGCACGCCT
TCCAGCAGCGTCTGGCTGTCCACCCGAGCGGTGTGGCGCTGCAGGACAGGGTCCCCCTTG
CCAGCCAGGGCCTGGGCCCCGGCAGCACGGTCCTGCTGGTGGTGGACAAATGCGACGAAC

CTCTGAGCATCCTGGTGAGGAATAACAAGGGCCGCAGCAGCACCTACGAGGTGCGGCTGA
CGCAGACCGTGGCCCACCTGAAGCAGCAAGTGAGCGGGCTGGAGGGTGTGCAGGACGACC
TGTTCTGGCTGACCTTCGAGGGGAAGCCCCTGGAGGACCAGCTCCCGCTGGGGGAGTACG
GCCTCAAGCCCCTGAGCATCTTCACCGTCAGGTCCCA...3'

Clone #2 - Edit 2

5'...GCAGATTCATGAACACGGTGCTGCATCTTCACCGTCAGGTCCCA...3'

Clone #2 - Edit 3

5'...GCAGATTCATGAACACGGTGCAGGGGCTTGAGGCCGTACTCCCCCAGCGGGAGCT
GGTCTTCACCGTCAGGTCCCA...3'

Full gel containing Caki WT and ISG15 KO mixed population PCR products (lines 8 and 9)

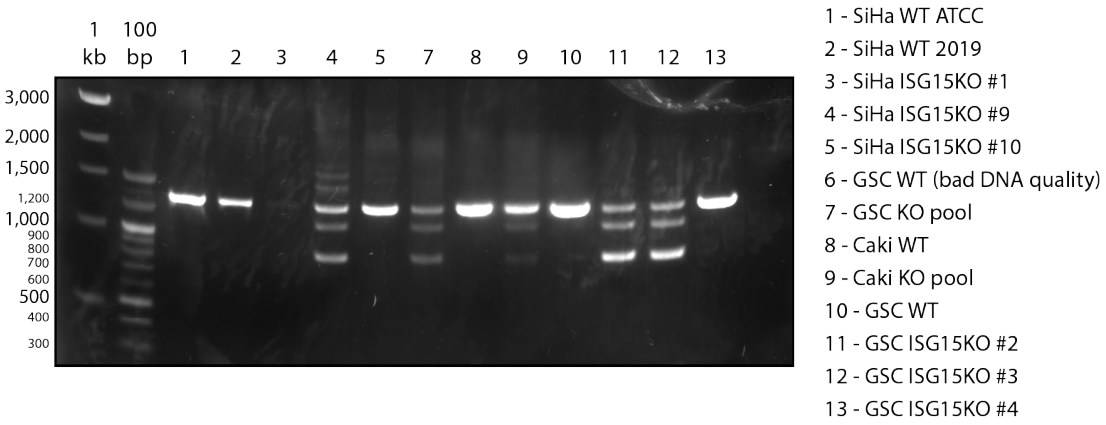

Figure A.1: PCR products of various WT and ISG15 deficient cell lines amplifying the ISG15 region in a 1.5% agarose gel.

Appendix B

Supplementary data for chapter 4: Identification of phenotypic differences between wild-type and ISG15$^{-/-}$ cells in cancer cell models

Mechanism of the Gateway Cloning System

Figure B.1: Mechanism of the Gateway Cloning System based on integration/excision cycle of bacteriophage λ mediated by site-specific recombination. V5 tagged ISG15 containing constructs were generated as part of my MScR project.

Replica of the colony formation assay on WT and ISG15$^{-/-}$ cells

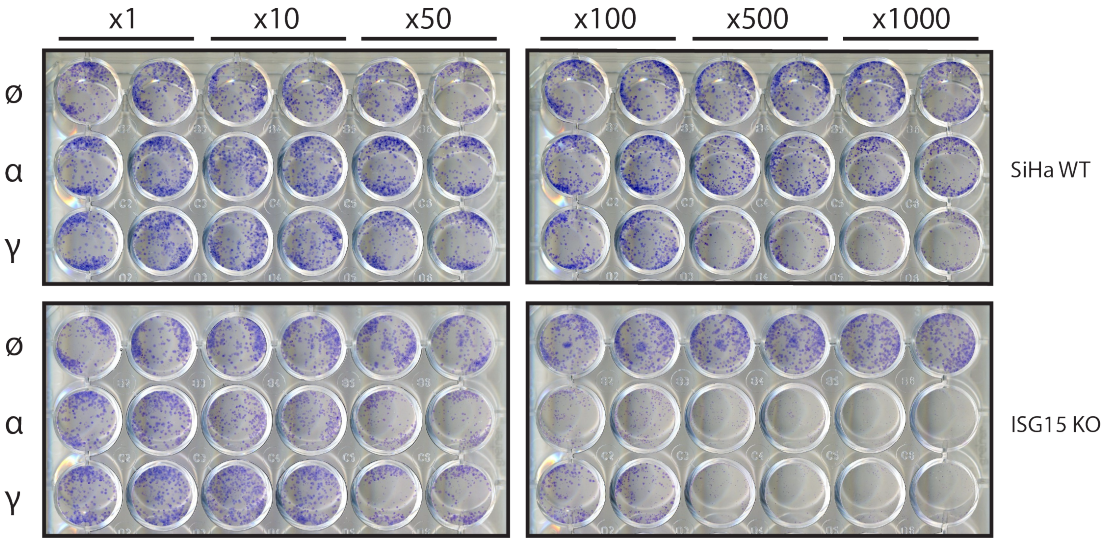

Figure B.2: Experimental replica of the colony formation assay performed on WT and ISG15$^{-/-}$ cells (Figure 4.9). The upper row of each plate was left untreated, the middle row was treated with IFNα treated and the lower row was treated with IFNγ. x1 of treatment equals to 1 U/mL IFNα and 0.2 ng/mL IFNγ and each condition was tested on duplicates. Results of this experiment are consistent with the results obtained from the first clonogenic assay performed under the same conditions. Quantitative measurement of these colonies can be found on Figure 4.10.

Details on statistical analyses

Table B.1: Linear Regression statistical analysis results for WT $\emptyset/\alpha$ presented in Figure 4.10.

	$\emptyset$	α
Equation	$y = 0.006626 \cdot x + 0.2592$	$y = -0.01359 \cdot x + 0.3700$
95% Confidence Intervals		
Slope	$(-0.01013, 0.02338)$	$(-0.03002, 0.002839)$
Y-intercept	$(0.1939, 0.3244)$	$(0.3061, 0.4340)$
X-intercept	$(-\infty, -8.490)$	$(14.17, \infty)$
Goodness of Fit		
R^2	0.07203	0.2536
RMSD	0.04449	0.04362
Are slopes equal?		
F	3.684	
DFn	1	
DFd	20	
P value	0.0693	
Comment	The differences between the slopes are not quite significant.	

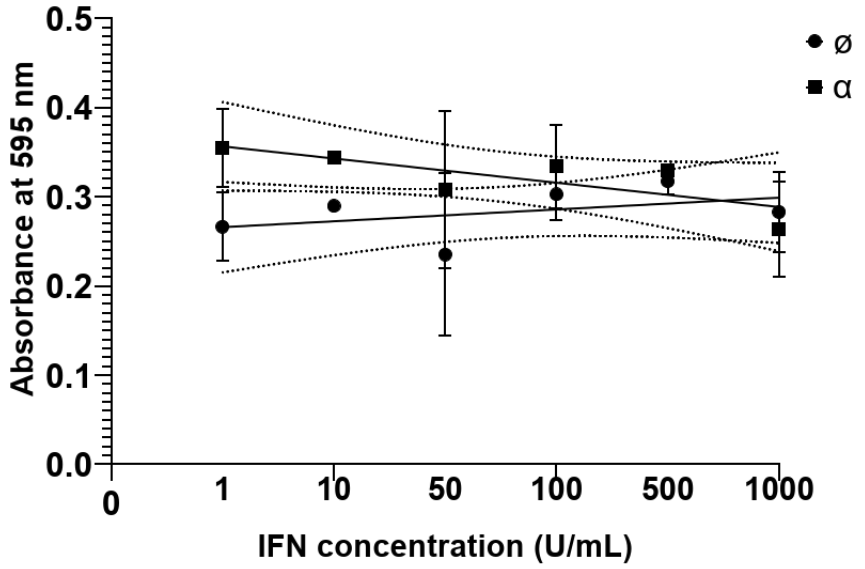

Figure B.3: Linear regression analysis for WT $\emptyset/\alpha$ cell data presented in Figure 4.10.

Table B.2: Linear Regression statistical analysis results for WT $\emptyset/\gamma$ presented in Figure 4.10.

	$\emptyset$	γ
Equation	$y = 0.006626 \cdot x + 0.2592$	$y = -0.04831 \cdot x + 0.4280$
95% Confidence Intervals		
Slope	$(-0.01013, 0.02338)$	$(-0.06124, -0.03538)$
Y-intercept	$(0.1939, 0.3244)$	$(0.3776, 0.4783)$
X-intercept	$(-\infty, -8.490)$	$(7.656, 10.89)$
Goodness of Fit		
R^2	0.07203	0.8739
RMSD	0.04449	0.03433
Are slopes equal?		
F	33.45	
DFn	1	
DFd	20	
P value	< 0.0001	
Comment	The differences between the slopes are extremely significant.	

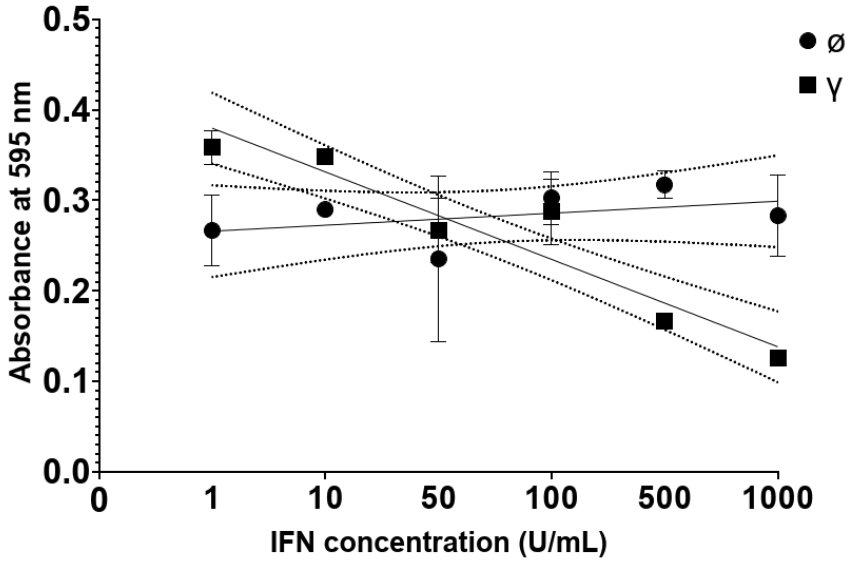

Figure B.4: Linear regression analysis for WT $\emptyset/\gamma$ cell data presented in Figure 4.10.

Table B.3: Linear Regression statistical analysis results for KO $\emptyset/\alpha$ presented in Figure 4.10.

	$\emptyset$	α
Equation	$y = 0.008214 \cdot x + 0.2266$	$y = -0.04151 \cdot x + 0.2919$
95% Confidence Intervals		
Slope	$(-0.0002867, 0.01672)$	$(-0.05206, -0.03097)$
Y-intercept	$(0.1935, 0.2597)$	$(0.2508, 0.3330)$
X-intercept	$(-\infty, -11.73)$	$(6.216, 8.334)$
Goodness of Fit		
R^2	0.3167	0.8849
RMSD	0.02257	0.02801
Are slopes equal?		
F	66.89	
DFn	1	
DFd	20	
P value	< 0.0001	
Comment	The differences between the slopes are extremely significant.	

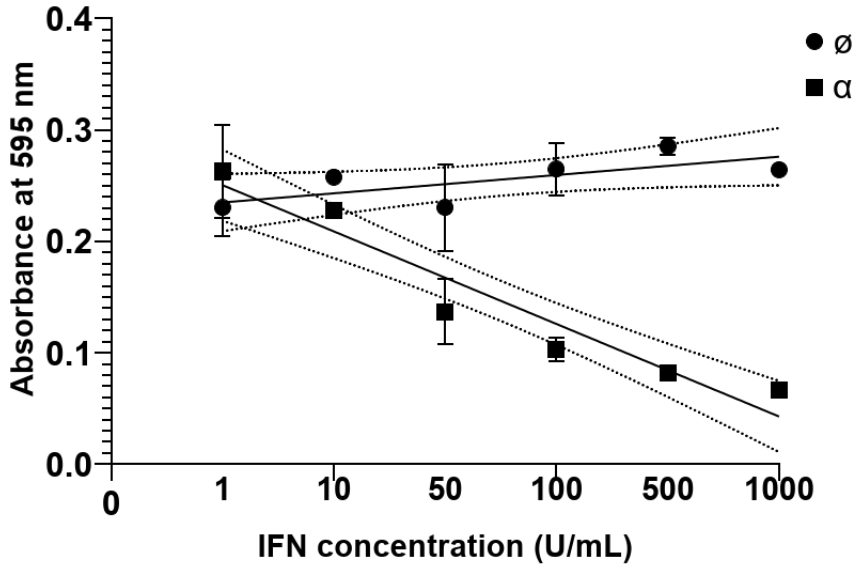

Figure B.5: Linear regression analysis for KO $\emptyset/\alpha$ cell data presented in Figure 4.10.

Table B.4: Linear Regression statistical analysis results for KO $\emptyset/\gamma$ presented in Figure 4.10.

	$\emptyset$	γ
Equation	$y = 0.008214 \cdot x + 0.2266$	$y = -0.05335 \cdot x + 0.3604$
95% Confidence Intervals		
Slope	$(-0.0002867, 0.01672)$	$(-0.0684, -0.0383)$
Y-intercept	$(0.1935, 0.2597)$	$(0.3018, 0.4190)$
X-intercept	$(-\infty, -11.73)$	$(5.920, 8.154)$
Goodness of Fit		
R^2	0.3167	0.8618
RMSD	0.02257	0.03997
Are slopes equal?		
F	62.97	
DFn	1	
DFd	20	
P value	< 0.0001	
Comment	The differences between the slopes are extremely significant.	

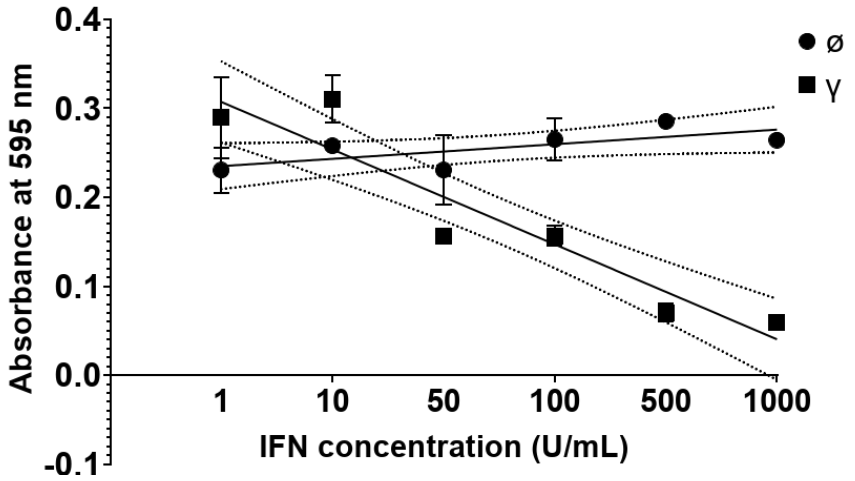

Figure B.6: Linear regression analysis for KO $\emptyset/\gamma$ cell data presented in Figure 4.10.

Table B.5: Linear Regression statistical analysis results for WT $\emptyset/c.\alpha 2$ presented in Figure 4.12.

	$\emptyset$	$c.\alpha 2$
Equation	$y = 0.005081 \cdot x + 0.5692$	$y = 0.003261 \cdot x + 0.5357$
95% Confidence Intervals		
Slope	$(-0.01745, 0.007284)$	$(-0.007255, 0.01378)$
Y-intercept	$(0.5210, 0.6173)$	$(0.4947, 0.5766)$
X-intercept	$(35.07, \infty)$	$(-\infty, -36.18)$
Goodness of Fit		
R^2	0.07735	0.04558
RMSD	0.03283	0.02792
Are slopes equal?		
F	1.311	
DFn	1	
DFd	20	
P value	0.2657	
Comment	The differences between the slopes are not quite significant.	

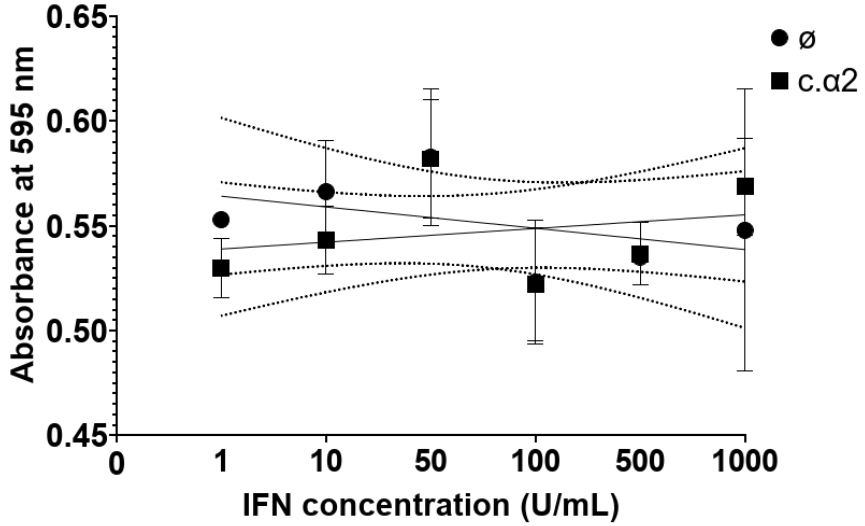

Figure B.7: Linear regression analysis for WT $\emptyset/c.\alpha 2$ cell data presented in Figure 4.12.

Table B.6: Linear Regression statistical analysis results for clone #3 $\emptyset/c.\alpha 2$ presented in Figure 4.12.

	$\emptyset$	$c.\alpha 2$
Equation	$y = -0.0005914 \cdot x + 0.4951$	$y = -0.1126 \cdot x + 0.6800$
95% Confidence Intervals		
Slope	$(-0.01679, 0.01560)$	$(-0.1488, -0.07644)$
Y-intercept	$(0.4320, 0.5582)$	$(0.5390, 0.8209)$
X-intercept	$(32.82, \infty)$	$(5.251, 7.407)$
Goodness of Fit		
R^2	0.0006616	0.8278
RMSD	0.043	0.09611
Are slopes equal?		
F	39.63	
DFn	1	
DFd	20	
P value	< 0.0001	
Comment	The differences between the slopes are extremely significant.	

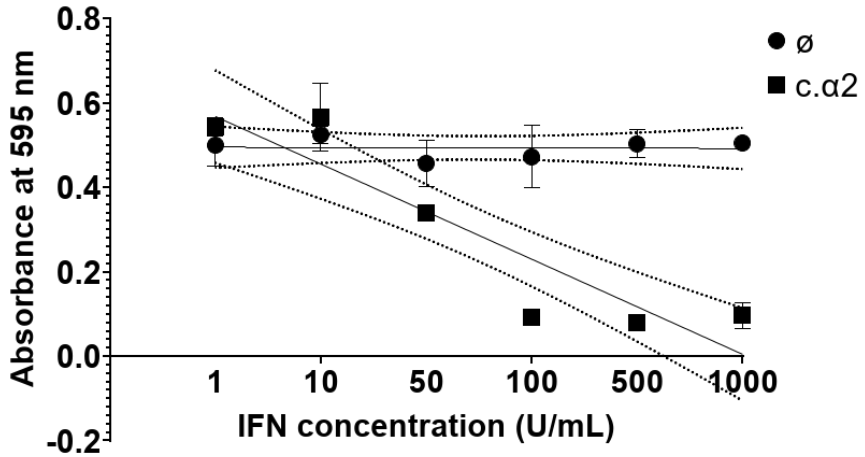

Figure B.8: Linear regression analysis for clone #3 $\emptyset/c.\alpha 2$ cell data presented in Figure 4.12.

Table B.7: Linear Regression statistical analysis results for clone #4 $\emptyset/c.\alpha 2$ presented in Figure 4.12.

	$\emptyset$	$c.\alpha 2$
Equation	$y = 0.01367 \cdot x + 1.198$	$y = -0.1770 \cdot x + 1.595$
95% Confidence Intervals		
Slope	$(-0.02279, 0.05013)$	$(-0.2291, -0.1250)$
Y-intercept	$(1.056, 1.340)$	$(1.392, 1.798)$
X-intercept	$(-\infty, -21.30)$	$(7.681, 11.38)$
Goodness of Fit		
R^2	0.06522	0.8516
RMSD	0.09682	0.1382
Are slopes equal?		
F	44.69	
DFn	1	
DFd	20	
P value	< 0.0001	
Comment	The differences between the slopes are extremely significant.	

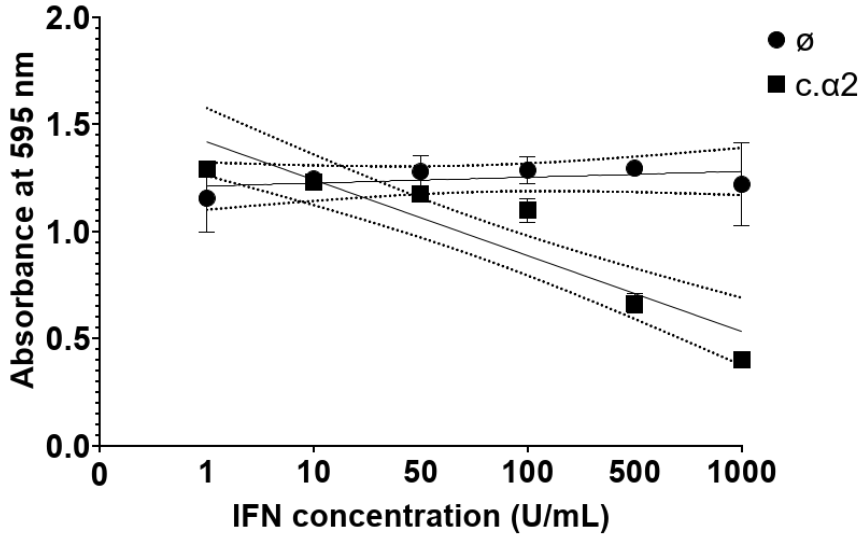

Figure B.9: Linear regression analysis for clone #4 $\emptyset/c.\alpha 2$ cell data presented in Figure 4.12.

Table B.8: Linear Regression statistical analysis results for clone #9 $\emptyset/c.\alpha 2$ presented in Figure 4.12.

	$\emptyset$	$c.\alpha 2$
Equation	$y = 0.03902 \cdot x + 0.6210$	$y = -0.1570 \cdot x + 0.8918$
95% Confidence Intervals		
Slope	$(0.01399, 0.06405)$	$(-0.2014, -0.1125)$
Y-intercept	$(0.5236, 0.7185)$	$(0.7187, 1.065)$
X-intercept	$(-50.69, -8.280)$	$(5.032, 6.712)$
Goodness of Fit		
R^2	0.5468	0.8609
RMSD	0.06645	0.118
Are slopes equal?		
F	73.27	
DFn	1	
DFd	20	
P value	< 0.0001	
Comment	The differences between the slopes are extremely significant.	

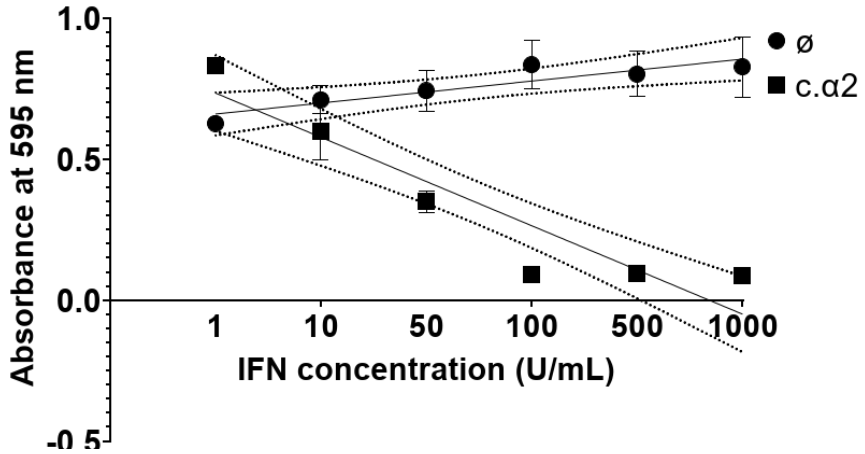

Figure B.10: Linear regression analysis for clone #9 $\emptyset/c.\alpha 2$ cell data presented in Figure 4.12.

Table B.9: Linear Regression statistical analysis results for clone #10 $\emptyset/c.\alpha 2$ presented in Figure 4.12.

	$\emptyset$	$c.\alpha 2$
Equation	$y = 0.002429 \cdot x + 0.9815$	$y = -0.1555 \cdot x + 0.8601$
95% Confidence Intervals		
Slope	$(0.03056, 0.03541)$	$(-0.2200, -0.09098)$
Y-intercept	$(0.8530, 1.110)$	$(0.6087, 1.111)$
X-intercept	$(-\infty, -24.41)$	$(4.671, 7.234)$
Goodness of Fit		
R^2	0.002684	0.7425
RMSD	0.08758	0.1713
Are slopes equal?		
F	23.58	
DFn	1	
DFd	20	
P value	< 0.0001	
Comment	The differences between the slopes are extremely significant.	

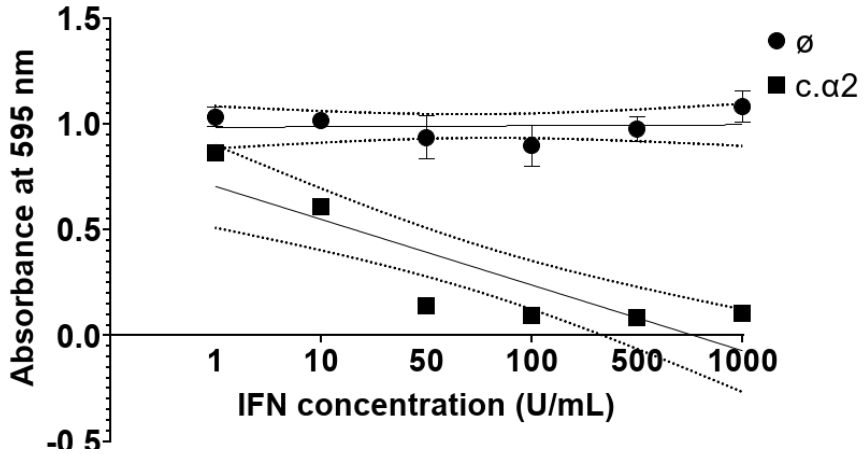

Figure B.11: Linear regression analysis for clone #10 $\emptyset/c.\alpha 2$ cell data presented in Figure 4.12.

Table B.10: Linear Regression statistical analysis results for EV$\emptyset$/*c*.α2 cells presented in Figure 4.21.

	EV$\emptyset$	**EV *c*.α2**
Equation	$y = 0.005839 \cdot x + 0.4353$	$y = -0.06491 \cdot x + 0.5298$
95% Confidence Intervals		
Slope	$(-0.002478, 0.01415)$	$(-0.07335, -0.05648)$
Y-intercept	$(0.4029, 0.4677)$	$(0.4970, 0.5627)$
X-intercept	$(-\infty, -28.67)$	$(7.587, 8.897)$
Goodness of Fit		
R^2	0.1966	0.9671
RMSD	0.02208	0.02239
Are slopes equal?		
F	177.2	
DFn	1	
DFd	20	
P value	< 0.0001	
Comment	The differences between the slopes are extremely significant.	

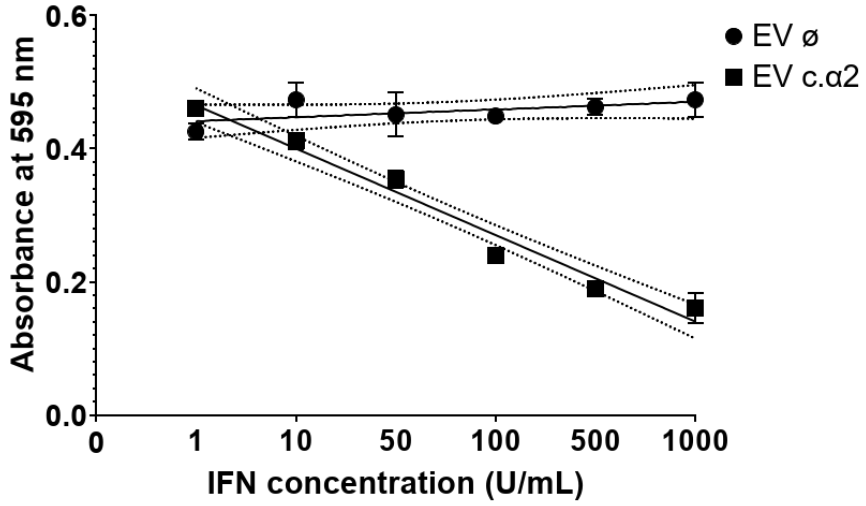

Figure B.12: Linear regression analysis for EV$\emptyset$/*c*.α2 cell data presented in Figure 4.21.

Table B.11: Linear Regression statistical analysis results for WT $\emptyset/c.\alpha 2$ cells presented in Figure 4.21.

	WT $\emptyset$	**WT** $c.\alpha 2$
Equation	$y = 0.0006 \cdot x + 0.2667$	$y = -0.02781 \cdot x + 0.2911$
95% Confidence Intervals		
Slope	$(-0.005179, 0.006379)$	$(-0.03909, -0.01652)$
Y-intercept	$(0.2442, 0.2892)$	$(0.2471, 0.335)$
X-intercept	$(-\infty, -38.61)$	$(8.373, 15.31)$
Goodness of Fit		
R^2	0.005322	0.7508
RMSD	0.01535	0.02997
Are slopes equal?		
F	24.91	
DFn	1	
DFd	20	
P value	< 0.0001	
Comment	The differences between the slopes are extremely significant.	

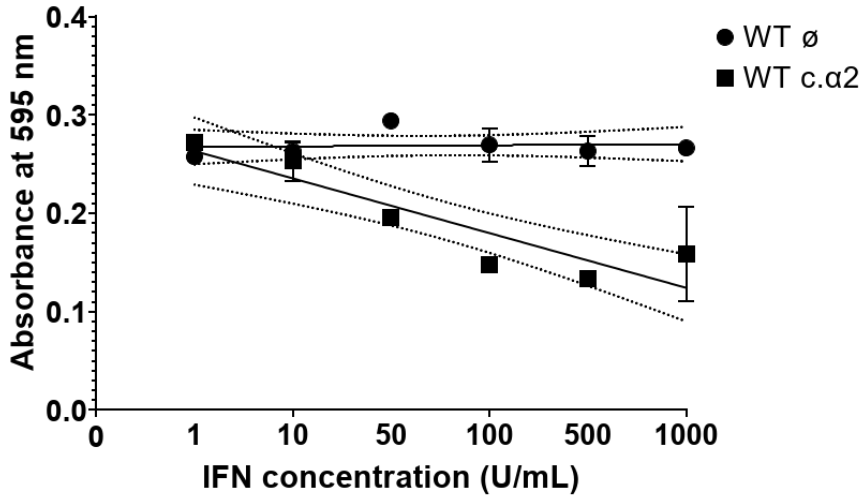

Figure B.13: Linear regression analysis for WT $\emptyset/c.\alpha 2$ cell data presented in Figure 4.21.

Table B.12: Linear Regression statistical analysis results for AA $\emptyset$/$c.\alpha 2$ cells presented in Figure 4.21.

	AA $\emptyset$	**AA $c.\alpha 2$**
Equation	$y = 0.004937 \cdot x + 0.4116$	$y = -0.05908 \cdot x + 0.4746$
95% Confidence Intervals		
Slope	$(-0.01368, 0.003808)$	$(-0.07877, -0.03940)$
Y-intercept	$(0.3775, 0.4456)$	$(0.3979, 0.5513)$
X-intercept	$(32.29, \infty)$	$(6.796, 10.40)$
Goodness of Fit		
R^2	0.1366	0.8172
RMSD	0.02322	0.05228
Are slopes equal?		
F	31.36	
DFn	1	
DFd	20	
P value	< 0.0001	
Comment	The differences between the slopes are extremely significant.	

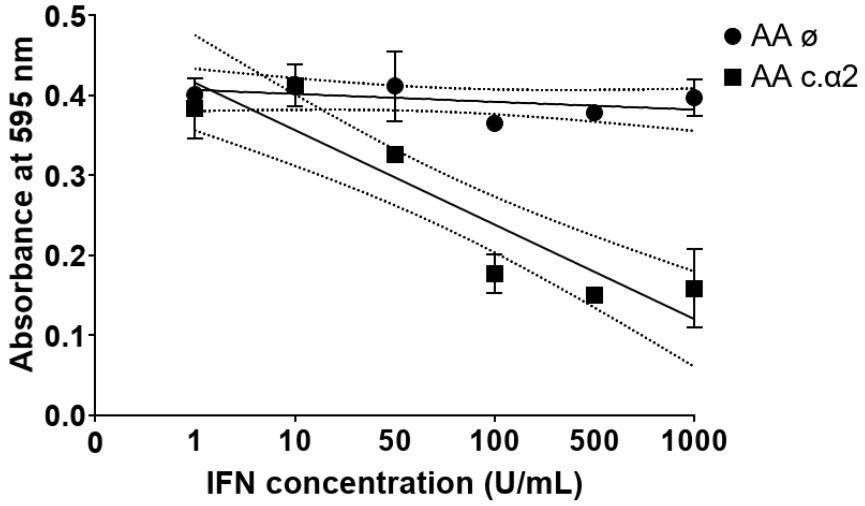

Figure B.14: Linear regression analysis for AA $\emptyset$/$c.\alpha 2$ cell data presented in Figure 4.21.

Table B.13: Linear Regression statistical analysis results for EV $\emptyset$/*c*.α2 cells presented in Figure 4.22.

	EV $\emptyset$	**EV *c*.α2**
Equation	$y = -0.009704 \cdot x + 0.3785$	$y = -0.07050 \cdot x + 0.4891$
95% Confidence Intervals		
Slope	$(-0.02720, 0.007793)$	$(-0.09041, -0.05060)$
Y-intercept	$(0.3103, 0.4466)$	$(0.4115, 0.5666)$
X-intercept	$(16.09, \infty)$	$(6.066, 8.403)$
Goodness of Fit		
R^2	0.1325	0.8616
RMSD	0.04646	0.05286
Are slopes equal?		
F	26.12	
DFn	1	
DFd	20	
P value	< 0.0001	
Comment	The differences between the slopes are extremely significant.	

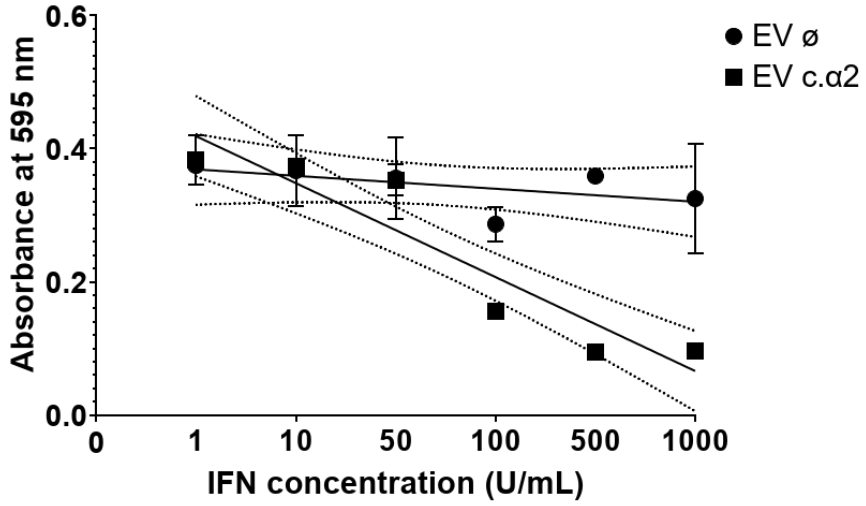

Figure B.15: Linear regression analysis for EV $\emptyset$/*c*.α2 cell data presented in Figure 4.22.

Table B.14: Linear Regression statistical analysis results for WT $\emptyset/c.\alpha 2$ cells presented in Figure 4.22.

	WT $\emptyset$	**WT** $c.\alpha 2$
Equation	$y = -0.005326 \cdot x + 0.3713$	$y = -0.06187 \cdot x + 0.4555$
95% Confidence Intervals		
Slope	$(-0.01647, 0.005821)$	$(-0.07997, -0.04378)$
Y-intercept	$(0.3279, 0.4147)$	$(0.3850, 0.5259)$
X-intercept	$(24.86, \infty)$	$(6.382, 9.063)$
Goodness of Fit		
R^2	0.1018	0.8531
RMSD	0.0296	0.04804
Are slopes equal?		
F	35.15	
DFn	1	
DFd	20	
P value	< 0.0001	
Comment	The differences between the slopes are extremely significant.	

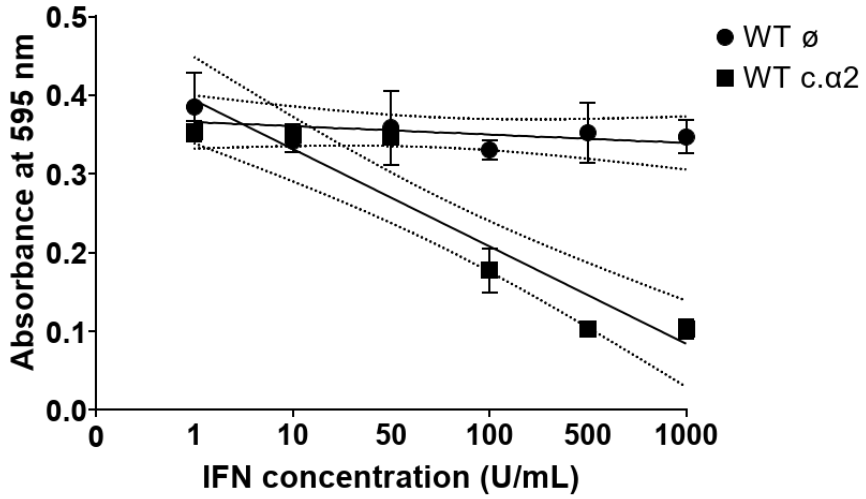

Figure B.16: Linear regression analysis for WT $\emptyset/c.\alpha 2$ cell data presented in Figure 4.22.

Table B.15: Linear Regression statistical analysis results for AA $\emptyset/c.\alpha 2$ cells presented in Figure 4.22.

	AA $\emptyset$	**AA $c.\alpha 2$**
Equation	$y = 0.004114 \cdot x + 0.5098$	$y = -0.1027 \cdot x + 0.7199$
95% Confidence Intervals		
Slope	$(-0.006315, 0.01454)$	$(-0.1318, -0.07354)$
Y-intercept	$(0.4692, 0.5504)$	$(0.6064, 0.8334)$
X-intercept	$(-\infty, -32.51)$	$(6.122, 8.514)$
Goodness of Fit		
R^2	0.07172	0.8604
RMSD	0.02769	0.07735
Are slopes equal?		
F	59.1	
DFn	1	
DFd	20	
P value	< 0.0001	
Comment	The differences between the slopes are extremely significant.	

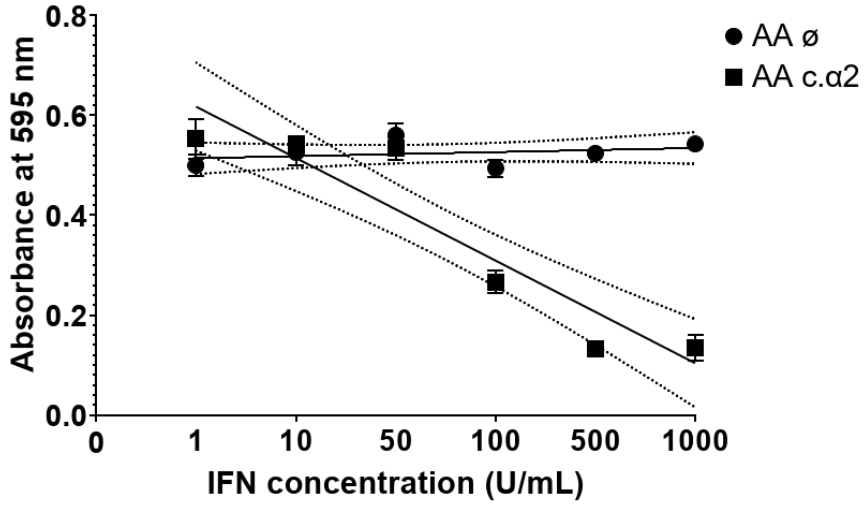

Figure B.17: Linear regression analysis for AA $\emptyset/c.\alpha 2$ cell data presented in Figure 4.22.

Appendix C

Supplementary data for chapter 5: Analysis of the proteomic landscape of ISG15$^{-/-}$ cervical cancer cells employing isotopically labelled amino acids in cell culture (SILAC)

Full lists of biological processes identified ISG15 KO vs WT samples obtained from g:profiler

Table C.1: Biological processes identified in untreated ISG15 KO vs WT samples collected at 24 hours.

Downregulated in untreated samples collected at 24 hours	
Biological process	**-log10(p-value)**
response to virus	3.90
defense response to virus	3.66
defense response to symbiont	3.65
negative regulation of cellular metabolic process	2.40
cellular response to cytokine stimulus	2.27
regulation of metabolic process	2.18
regulation of response to biotic stimulus	2.04
response to cytokine	1.87
innate immune response	1.83
regulation of primary metabolic process	1.74
organic substance metabolic process	1.72
biological process involved in interspecies interaction between organisms	1.69
viral process	1.58
regulation of cellular metabolic process	1.44
primary metabolic process	1.36
Upregulated in untreated samples collected at 24 hours	
Biological process	**-log10(p-value)**
cellular catabolic process	3.58
macromolecule catabolic process	3.44
organic substance catabolic process	2.98
catabolic process	2.87
cellular macromolecule catabolic process	2.84
regulation of primary metabolic process	2.27
regulation of catabolic process	1.67
regulation of metabolic process	1.60
protein catabolic process	1.53
proteolysis involved in protein catabolic process	1.52
cellular aldehyde metabolic process	1.45
regulation of nitrogen compound metabolic process	1.37

Table C.2: Biological processes identified in untreated ISG15 KO vs WT samples collected at 48 hours.

Downregulated in untreated samples collected at 48 hours	
Biological process	**-log10(p-value)**
cellular macromolecule metabolic process	2.76
organonitrogen compound metabolic process	2.75
response to virus	2.39
defense response to virus	2.32
defense response to symbiont	2.30
protein metabolic process	1.95
amide biosynthetic process	1.85
peptide biosynthetic process	1.73
Upregulated in untreated samples collected at 48 hours	
Biological process	**-log10(p-value)**
macromolecule localization	2.28
organic substance catabolic process	2.12
organonitrogen compound catabolic process	1.78
macromolecule catabolic process	1.77
protein catabolic process	1.67
regulation of mRNA splicing, via spliceosome	1.64
cellular macromolecule metabolic process	1.60
regulation of RNA splicing	1.40

Table C.3: Biological processes identified in IFNα treated ISG15 KO vs WT samples collected at 24 hours.

Downregulated in IFNα treated samples collected at 24 hours	
Biological process	**-log10(p-value)**
macromolecule catabolic process	1.79
organic substance catabolic process	1.46
Upregulated in IFNα treated samples collected at 24 hours	
Biological process	**-log10(p-value)**
regulation of mRNA processing	2.31
regulation of mRNA metabolic process	1.91
regulation of mRNA splicing, via spliceosome	1.77
cellular aldehyde metabolic process	1.59

Table C.4: Biological processes identified in IFNα treated ISG15 KO vs WT samples collected at 48 hours.

Downregulated in IFNα treated samples collected at 48 hours	
Biological process	**-log10 (p-value)**
response to wounding	2.00
wound healing	1.90
glycoside metabolic process	1.65
Upregulated in IFNα treated samples collected at 48 hours	
Biological process	**-log10 (p-value)**
protein catabolic process	3.10
antigen processing and presentation of peptide antigen	2.60
antigen processing and presentation of peptide antigen via MHC class I	2.47
response to stress	2.45
organonitrogen compound catabolic process	2.18
macromolecule catabolic process	2.17
proteolysis involved in protein catabolic process	2.00
proteolysis	1.99
antigen processing and presentation of endogenous peptide antigen via MHC class I	1.86
organic substance catabolic process	1.51
antigen processing and presentation	1.43
antigen processing and presentation of endogenous peptide antigen	1.33

Appendix D

Supplementary data for chapter 6: Whole proteomic and immunopeptidomic analysis on ISG15 deficient patient-derived glioblastoma stem cells upon IFNα2 treatment

Full lists of biological processes identified ISG15 KO vs WT samples obtained from Revigo - Whole proteomic analysis

Table D.1: Downregulated biological processes identified in untreated ISG15 KO vs WT samples.

Downregulated in untreated samples	
Biological process	**-log10(p-value)**
amide metabolic process	16.34
organonitrogen compound metabolic process	15.56
peptide metabolic process	15.45
cytoplasmic translation	14.56
small molecule metabolic process	12.14
catabolic process	11.51
organonitrogen compound biosynthetic process	10.06
oxoacid metabolic process	10.03
cellular macromolecule metabolic process	9.77
biosynthetic process	8.58
organic substance biosynthetic process	8.19
nucleobase-containing small molecule metabolic process	7.93
nucleotide metabolic process	7.77
cellular macromolecule biosynthetic process	7.12
protein metabolic process	6.69
organelle organization	6.40
NADH metabolic process	5.72
cellular metabolic process	5.70
metabolic process	5.19
cellular nitrogen compound biosynthetic process	5.19
organophosphate metabolic process	5.01
regulation of organelle organization	5.00
nitrogen compound metabolic process	4.93
primary metabolic process	4.76
generation of precursor metabolites and energy	4.36
sulfur compound metabolic process	4.20
RNA localization	4.16
nucleotide phosphorylation	3.93
organic substance metabolic process	3.90
purine-containing compound metabolic process	3.79
establishment of RNA localization	3.77
cellular macromolecule catabolic process	3.47

protein-containing complex disassembly	3.36
small molecule catabolic process	3.31
cytoskeleton organization	3.24
regulation of cellular component organization	3.13
actin filament organization	3.12
nucleic acid transport	3.10
carbohydrate derivative metabolic process	3.01
cellular nitrogen compound catabolic process	2.85
carbohydrate metabolic process	2.84
negative regulation of cellular process	2.84
macromolecule biosynthetic process	2.81
pyruvate metabolic process	2.76
cellular detoxification	2.72
actin polymerization or depolymerization	2.61
cellular process	2.55
positive regulation of cellular process	2.49
regulation of cellular component size	2.48
heterocycle catabolic process	2.42
positive regulation of biological process	2.39
regulation of amide metabolic process	2.36
pyridine-containing compound metabolic process	2.35
glycosyl compound metabolic process	2.3
monosaccharide metabolic process	2.11
nucleocytoplasmic transport	2.09
nuclear transport	2.09
aromatic compound catabolic process	2.08
regulation of mRNA metabolic process	2.08
nucleobase-containing compound catabolic process	2.08
regulation of chromosome organization	2.01
cellular component disassembly	2.00
negative regulation of organelle organization	1.98
nucleobase-containing compound transport	1.98
regulation of nitrogen compound metabolic process	1.97
small molecule biosynthetic process	1.89
regulation of translation	1.79
actin filament-based process	1.78
regulation of cytoskeleton organization	1.76
organic cyclic compound catabolic process	1.67
glucose 6-phosphate metabolic process	1.66

regulation of cytoplasmic translation	1.66
actin filament severing	1.64
daunorubicin metabolic process	1.54
regulation of protein metabolic process	1.44
supramolecular fiber organization	1.43
glutathione metabolic process	1.42
actin filament depolymerization	1.42
negative regulation of cellular component organization	1.41
phosphorus metabolic process	1.40
regulation of biological quality	1.34

Table D.2: Upregulated biological processes identified in untreated ISG15 KO vs WT samples.

Upregulated in untreated samples	
Biological process	**-log10(p-value)**
organonitrogen compound metabolic process	9.31
mitochondrial translation	8.40
mitochondrial gene expression	7.87
peptide metabolic process	6.06
amide metabolic process	5.96
catabolic process	5.91
protein metabolic process	4.91
organonitrogen compound biosynthetic process	4.67
cellular macromolecule metabolic process	4.66
cellular respiration	4.34
cellular macromolecule biosynthetic process	2.69
nucleic acid phosphodiester bond hydrolysis	2.52
generation of precursor metabolites and energy	2.12
cellular metabolic process	2.09
small molecule metabolic process	1.88
proteolysis	1.86
regulation of peptidase activity	1.86
nucleoside triphosphate metabolic process	1.59
cellular macromolecule catabolic process	1.57
regulation of proteolysis	1.55

Table D.3: Downregulated biological processes identified in samples treated with IFNα for 24 hours.

Downregulated in samples treated with IFNα for 24 hours	
Biological process	**-log10(p-value)**
protein localization to mitochondrion	2.89
respiratory electron transport chain	1.95
establishment of protein localization to mitochondrion	1.92

Table D.4: Upregulated biological processes identified in samples treated with IFNα for 24 hours.

Upregulated in samples treated with IFNα for 24 hours	
Biological process	**-log10(p-value)**
organonitrogen compound metabolic process	7.29
catabolic process	5.28
response to biotic stimulus	4.10
small molecule metabolic process	4.05
nucleobase-containing small molecule metabolic process	3.74
positive regulation of type I interferon production	3.62
defense response to virus	3.41
defense response to symbiont	3.39
response to virus	3.28
biological process involved in interspecies interaction between organisms	3.26
regulation of type I interferon production	3.03
type I interferon production	3.03
regulation of response to biotic stimulus	2.64
MDA-5 signaling pathway	2.36
response to stress	2.29
regulation of programmed cell death	2.25
proteolysis	2.17
nucleotide metabolic process	2.15
cell death	2.05
protein metabolic process	2.01
defense response	1.99
biosynthetic process	1.98
programmed cell death	1.72
oxoacid metabolic process	1.71
organic substance biosynthetic process	1.66

protein catabolic process	1.66
response to type I interferon	1.61
organophosphate metabolic process	1.54
response to organic substance	1.50
response to nitrogen compound	1.47
peptide metabolic process	1.41
organonitrogen compound biosynthetic process	1.40
regulation of viral process	1.39
regulation of cell death	1.35
cellular response to exogenous dsRNA	1.31

Table D.5: Upregulated biological processes identified in samples treated with IFNα for 48 hours.

Upregulated in samples treated with IFNα for 48 hours	
Biological process	**-log10(p-value)**
defense response to virus	15.94
defense response to symbiont	15.91
negative regulation of viral process	13.51
response to virus	13.35
defense response	13.12
response to biotic stimulus	13.03
antigen processing and presentation of endogenous peptide antigen	12.75
immune response	12.57
biological process involved in interspecies interaction between organisms	11.98
immune system process	11.79
regulation of viral process	10.09
negative regulation of innate immune response	10.05
regulation of response to biotic stimulus	9.84
regulation of immune response	9.8
response to external stimulus	8.36
negative regulation of response to biotic stimulus	7.96
response to type I interferon	7.8
response to stress	7.7
viral genome replication	7.39
response to cytokine	7.1
regulation of immune system process	7.09
interleukin-27-mediated signaling pathway	6.99
antigen processing and presentation	6.68

regulation of defense response	6.65
cellular response to type I interferon	6.61
regulation of response to external stimulus	5.9
negative regulation of defense response	5.63
viral process	5.59
regulation of type I interferon production	5.5
type I interferon production	5.5
T cell mediated immunity	5.31
positive regulation of T cell mediated immunity	4.71
regulation of response to stimulus	4.69
immune response-regulating signaling pathway	4.57
positive regulation of type I interferon production	4.35
positive regulation of biological process	4.26
negative regulation of response to external stimulus	4.03
cellular response to cytokine stimulus	3.9
regulation of ribonuclease activity	3.88
regulation of cytokine production	3.83
T cell mediated cytotoxicity	3.8
cytokine production	3.78
regulation of response to stress	3.12
response to interferon-beta	3.05
positive regulation of cytokine production	3
positive regulation of cell killing	2.91
response to organic substance	2.74
positive regulation of cellular process	2.73
regulation of biological process	2.62
regulation of response to cytokine stimulus	2.61
regulation of type I interferon-mediated signaling pathway	2.54
regulation of nuclease activity	2.13
response to interferon-alpha	2.13
response to stimulus	2.12
positive regulation of response to stimulus	2.11
cellular response to interferon-beta	1.97
negative regulation of immune system process	1.83
regulation of cell killing	1.8
regulation of cellular process	1.8
positive regulation of gene expression	1.72
positive regulation of tumor necrosis factor production	1.7
biological regulation	1.69

positive regulation of macromolecule metabolic process	1.68
negative regulation of biological process	1.66
production of molecular mediator of immune response	1.66
regulation of immune effector process	1.59
cellular response to interferon-alpha	1.31

Full peptide length distribution

Table D.6: Length distribution of peptides identified in untreated (∅), treated for 24 hours (24h) and treated for 48 hours (48h) ISG15 KO vs WT samples.

	Downregulated			**Upregulated**		
	∅	**24h**	**48h**	∅	**24h**	**48h**
1	0	0	0	0	0	0
2	0	0	0	0	0	0
3	0	0	0	0	0	0
4	0	0	0	0	0	0
5	0	0	0	0	0	0
6	0	0	0	0	0	0
7	48	7	2	6	3	27
8	87	13	10	5	8	68
9	200	61	16	88	67	492
10	176	38	9	33	29	217
11	162	40	8	20	19	182
12	172	44	8	9	17	135
13	175	50	8	13	11	145
14	162	45	6	14	7	129
15	119	32	4	5	4	93
16	115	27	2	2	6	93
17	98	27	1	4	2	68
18	57	34	1	3	1	55
19	44	19	1	5	2	37
20	51	19	1	1	3	34
21	30	13	2	4	1	34
22	30	7	1	0	1	20
23	22	18	0	3	0	25
24	17	13	0	1	0	17

25	15	8	0	1	1	17
26	4	4	0	1	1	7
27	9	3	0	0	1	10
28	9	5	0	1	1	9
29	8	4	0	0	0	7
30	4	2	0	0	1	3
31	8	4	0	0	0	6
32	3	1	0	0	0	3
33	3	2	0	0	0	3
34	2	2	0	1	0	2
35	1	1	0	0	0	1
36	1	2	0	1	0	0
37	1	1	0	0	0	2
38	1	2	0	1	0	1
39	1	2	0	0	0	2
40	1	2	0	1	0	1
41	0	0	0	0	0	0
42	1	0	0	0	0	1
43	1	0	0	0	0	1
44	0	0	0	1	1	1
45	1	0	0	0	0	1

Fold change and lenght of the GAPDH and B2M peptides identified in ISG15 KO vs WT samples

Table D.7: GAPDH peptides identified in untreated ISG15 KO vs WT samples, showing their length (L) and fold change (FC). "NF" stands for "not found", meaning that the peptide was only found in WT samples (hence, downregulated in ISG15 KO samples) and "Inf" means "Infinite", meaning that the peptide was only found in ISG15 KO samples (hence, upregulated in ISG15 KO samples).

Untreated ISG15 KO vs WT - GAPDH					
Downregulated			**Upregulated**		
Peptide	**L**	**FC**	**Peptide**	**L**	**FC**
MTTVHAITATQKTVDGPSGKLWR	23	NF	ISWYDNEFGYSNRVVDL	17	Inf
MTTVHAITATQKTVDGPSGKL	21	NF			
TVHAITATQKTVDGPSGKLWR	21	NF			
VHAITATQKTVDGPSGKLWR	20	NF			

TVHAITATQKTVDGPSGKL	19	NF
AITATQKTVDGPSGKLWR	18	NF
FGYSNRVVDLMAHMASKE	18	NF
GKVKVGVNGFGRIGRLVT	18	NF
YTEHQVVSSDFNSDTHSS	18	NF
GYSNRVVDLMAHMASKE	17	NF
NSDTHSSTFDAGAGIAL	17	NF
THSSTFDAGAGIALNDH	17	NF
ERDPSKIKWGDAGAEY	16	NF
ISWYDNEFGYSNRVVD	16	NF
YSNRVVDLMAHMASKE	16	NF
RDPSKIKWGDAGAEY	15	NF
QERDPSKIKWGDAG	14	NF
YDNEFGYSNRVVDL	14	NF
ATQKTVDGPSGKL	13	NF
FRVPTANVSVVDL	13	NF
PSKIKWGDAGAEY	13	NF
THSSTFDAGAGIA	13	NF
GAGIALNDHFVK	12	NF
ISWYDNEFGYSN	12	NF
RDPSKIKWGDAG	12	NF
GVNHEKYDNSL	11	NF
QERDPSKIKWG	11	NF
NSDTHSSTFDAGAGIALNDH	20	0.022
QERDPSKIKWGDAGAE	16	0.025
RVVDLMAHMASKE	13	0.025
RVPTANVSVVDL	12	0.029
QERDPSKIKWGDAGAEY	17	0.030
VVESTGVFTT	10	0.041
ISWYDNEF	8	0.050
FGYSNRVVDL	10	0.057
GYSNRVVDL	9	0.073
ISWYDNEFG	9	0.075
YTEHQVVSSDF	11	0.089
FRVPTANVSV	10	0.092
GAGIALNDHF	10	0.093
DAGAGIALNDH	11	0.094
RVVDLMAHMASKE	13	0.094
DAGAGIALNDHF	12	0.104

KVIPELNGKLT	11	0.104
YSNRVVDL	8	0.109
YVVESTGVF	9	0.113
YDNEFGYSNRVVD	13	0.133
AENGKLVINGNPIT	14	0.151
SNRVVDL	7	0.161
RVPTANVSVVD	11	0.170
FRVPTANVSVVD	12	0.177
KVIPELNGKLTG	12	0.215
ATQKTVDGPSGKLWR	15	0.228
KTVDGPSGKLWR	12	0.249
RGALQNIIPASTGAAK	16	0.259

Table D.8: GAPDH peptides identified in ISG15 KO vs WT samples treated with IFNα for 24 hours, showing their length (L) and fold change (FC). "NF" stands for "not found", meaning that the peptide was only found in WT samples (hence, downregulated in ISG15 KO samples) and "Inf" means "Infinite", meaning that the peptide was only found in ISG15 KO samples (hence, upregulated in ISG15 KO samples).

ISG15 KO vs WT treated with IFNα for 24 hours - GAPDH					
Downregulated			**Upregulated**		
Peptide	**L**	**FC**	**Peptide**	**L**	**FC**
MTTVHAITATQKTVDGPSGKLWR	23	NF	ISWYDNEFGYSNRVVDL	17	Inf
MTTVHAITATQKTVDGPSGKL	21	NF			
AITATQKTVDGPSGKLWR	18	NF			
GKVKVGVNGFGRIGRLVT	18	NF			
YTEHQVVSSDFNSDTHSS	18	NF			
ERDPSKIKWGDAGAEY	16	NF			
ATQKTVDGPSGKLWR	15	NF			
YDNEFGYSNRVVDL	14	NF			
DNEFGYSNRVVDL	13	NF			
RVVDLMAHMASKE	13	NF			
ISWYDNEFGYSN	12	NF			

Table D.9: GAPDH peptides identified in ISG15 KO vs WT samples treated with IFNα for 48 hours, showing their length (L) and fold change (FC). "NF" stands for "not found", meaning that the peptide was only found in WT samples (hence, downregulated in ISG15 KO samples) and "Inf" means "Infinite", meaning that the peptide was only found in ISG15 KO samples (hence, upregulated in ISG15 KO samples).

ISG15 KO vs WT treated with IFNα for 48 hours - GAPDH					
Downregulated			**Upregulated**		
Peptide	**L**	**FC**	**Peptide**	**L**	**FC**
ATQKTVDGPSGKL	13	NF	YSNRVVDL	8	2.997
DAGAGIALNDH	11	NF	VPTANVSVVDL	11	3.170
			APLAKVIHDN	10	3.965
			RVPTANVSVVD	11	4.246
			FRVPTANVSVVD	12	5.820
			RVPTANVSVVDL	12	5.860
			ISWYDNEFG	9	6.183
			FRVPTANVSV	10	6.516
			RGALQNIIPASTGAAK	16	9.327
			FGYSNRVVDL	10	13.688
			QERDPSKIKWGDAGAE	16	16.853
			QERDPSKIKWGDAGAEY	17	156.097
			MTTVHAITATQKTVDGPSGKLWR	23	Inf
			MTTVHAITATQKTVDGPSGKL	21	Inf
			TVHAITATQKTVDGPSGKLWR	21	Inf
			NSDTHSSTFDAGAGIALNDH	20	Inf
			VHAITATQKTVDGPSGKLWR	20	Inf
			HAITATQKTVDGPSGKLWR	19	Inf
			TVHAITATQKTVDGPSGKL	19	Inf
			AITATQKTVDGPSGKLWR	18	Inf
			GKVKVGVNGFGRIGRLVT	18	Inf
			YTEHQVVSSDFNSDTHSS	18	Inf
			NSDTHSSTFDAGAGIAL	17	Inf
			ERDPSKIKWGDAGAEY	16	Inf
			ISWYDNEFGYSNRVVD	16	Inf
			ATQKTVDGPSGKLWR	15	Inf
			RDPSKIKWGDAGAEY	15	Inf
			AENGKLVINGNPIT	14	Inf
			GKVKVGVNGFGRIG	14	Inf
			QERDPSKIKWGDAG	14	Inf
			YDNEFGYSNRVVDL	14	Inf
			DNEFGYSNRVVDL	13	Inf

PSKIKWGDAGAEY	13	Inf
RVVDLMAHMASKE	13	Inf
YDNEFGYSNRVVD	13	Inf
GAGIALNDHFVK	12	Inf
ISWYDNEFGYSN	12	Inf
KVIPELNGKLTG	12	Inf
RDPSKIKWGDAG	12	Inf
KVIPELNGKLT	11	Inf
QERDPSKIKWG	11	Inf
GAGIALNDHF	10	Inf
RDPSKIKWG	9	Inf
ISWYDNEF	8	Inf

Table D.10: B2M peptides identified in untreated ISG15 KO vs WT samples, showing their length (L) and fold change (FC). "NF" stands for "not found", meaning that the peptide was only found in WT samples (hence, downregulated in ISG15 KO samples) and "Inf" means "Infinite", meaning that the peptide was only found in ISG15 KO samples (hence, upregulated in ISG15 KO samples).

Untreated ISG15 KO vs WT - B2M					
Downregulated			**Upregulated**		
Peptide	**L**	**FC**	**Peptide**	**L**	**FC**
LKNGERIEKVEHSDLSFSKD	20	NF	IQRTPKIQVY	10	4.919
LLKNGERIEKVEHSDLSFSKD	21	NF	IQRTPKIQVYS	11	9.625
RHPAENGKSNFLN	13	NF	NGERIEKVEHSDLS	14	Inf
YYTEFTPTEKDE	12	NF	LSQPKIVKWDRDM	13	Inf
YTEFTPTEKDE	11	0.296	TEFTPTEKDEYA	12	Inf
			LSQPKIVKWDR	11	Inf
			LLKNGERIE	9	Inf
			FSKDWSFY	8	Inf

Table D.11: B2M peptides identified in ISG15 KO vs WT samples treated with IFNα for 24 hours, showing their length (L) and fold change (FC). "NF" stands for "not found", meaning that the peptide was only found in WT samples (hence, downregulated in ISG15 KO samples) and "Inf" means "Infinite", meaning that the peptide was only found in ISG15 KO samples (hence, upregulated in ISG15 KO samples).

ISG15 KO vs WT treated with IFNα for 24 hours - B2M					
Downregulated			**Upregulated**		
Peptide	**L**	**FC**	**Peptide**	**L**	**FC**
IQRTPKIQVYSRHPAENGKSNFLN	24	NF	RHPAENGKSNFLN	13	Inf
IQRTPKIQVYSRHPAENGKSNFL	23	NF			
LLKNGERIEKVEHSDLSFSKD	21	NF			
LKNGERIEKVEHSDLSFSKD	20	NF			
LLKNGERIEKVEHSDLSFS	19	NF			
LKNGERIEKVEHSDLSFS	18	NF			
NGERIEKVEHSDLSFSKD	18	NF			
LLKNGERIEKVEHSDLS	17	NF			
NGERIEKVEHSDLSFS	16	NF			
LSQPKIVKWDRDM	13	NF			
LLKNGERIEKVE	12	NF			
SQPKIVKWDRDM	12	NF			
LSQPKIVKWDR	11	NF			

Table D.12: B2M peptides identified in ISG15 KO vs WT samples treated with IFNα for 48 hours, showing their length (L) and fold change (FC). "NF" stands for "not found", meaning that the peptide was only found in WT samples (hence, downregulated in ISG15 KO samples) and "Inf" means "Infinite", meaning that the peptide was only found in ISG15 KO samples (hence, upregulated in ISG15 KO samples).

ISG15 KO vs WT treated with IFNα for 48 hours - B2M					
Downregulated			**Upregulated**		
Peptide	**L**	**FC**	**Peptide**	**L**	**FC**
			YTEFTPTEKDE	11	2.976
			IQRTPKIQVY	10	5.845
			TEFTPTEKDEYA	12	7.244
			YYTEFTPTEKDE	12	10.247
			FSKDWSF	7	15.888
			SQPKIVKWDRDM	12	17.974
			YVSGFHPSDIEVD	13	19.089
			IVKWDRDM	8	21.579
			SKDWSFY	7	25.677

NGERIEKVEHSDLS	14	30.430
IQRTPKIQ	8	41.673
FSKDWSFY	8	81.203
LSQPKIVKWDRDM	13	83.472
QPKIVKWDRDM	11	100.514
IQRTPKIQVYSRHPAENGKSNFLN	24	Inf
IQRTPKIQVYSRHPAENGKSNFL	23	Inf
LLKNGERIEKVEHSDLSFSKD	21	Inf
LLKNGERIEKVEHSDLSFS	19	Inf
LLKNGERIEKVEHSDLSF	18	Inf
NGERIEKVEHSDLSFSKD	18	Inf
LKNGERIEKVEHSDLSFS	18	Inf
IQRTPKIQVYSRHPAEN	17	Inf
LLKNGERIEKVEHSDLS	17	Inf
NGERIEKVEHSDLSFS	16	Inf
LSQPKIVKWDRDM	13	Inf
RHPAENGKSNFLN	13	Inf
SQPKIVKWDRDM	12	Inf
LSQPKIVKWDR	11	Inf
PKIVKWDRDM	10	Inf
LSQPKIVK	8	Inf
KDWSFYL	7	Inf

Details on statistical analyses

Table D.13: Linear Regression statistical analysis results for WT presented in Figure 6.7.

	Low confluency	**High confluency**
Equation	$y = 1593 \cdot x + 3035$	$y = 1728 \cdot x + 2746$
95% Confidence Intervals		
Slope	(1391, 1794)	(992.4, 2463)
Y-intercept	(2600, 3470)	(1158, 4333)
X-intercept	(−2.482, −1.456)	(−4.287, 0.4788)
Goodness of Fit		
R^2	0.9918	0.9141
RMSD	145.1	529.5
Are slopes equal?		
F	0.2419	
DFn	1	
DFd	20	
P value	0.6361	
Comment	The differences between the slopes are not significant.	

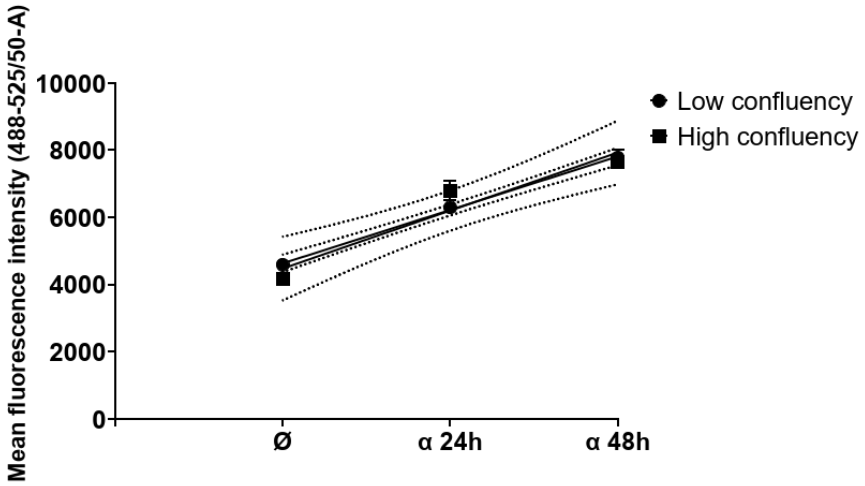

Figure D.1: Linear regression analysis for WT cell data presented in Figure 6.7.

Table D.14: Linear Regression statistical analysis results for KO presented in Figure 6.7.

	Low confluency	**High confluency**
Equation	$y = 3219 \cdot x + 1517$	$y = 3586 \cdot x + 1024$
95% Confidence Intervals		
Slope	(2816, 3623)	(2865, 4307)
Y-intercept	(645.2, 2388)	(−533.1, 2581)
X-intercept	(−0.8415, −0.1795)	(−0.8889, 0.1254)
Goodness of Fit		
R^2	0.9919	0.9795
RMSD	290.5	519.2
Are slopes equal?		
F	1.522	
DFn	1	
DFd	20	
P value	0.2523	
Comment	The differences between the slopes are not significant.	

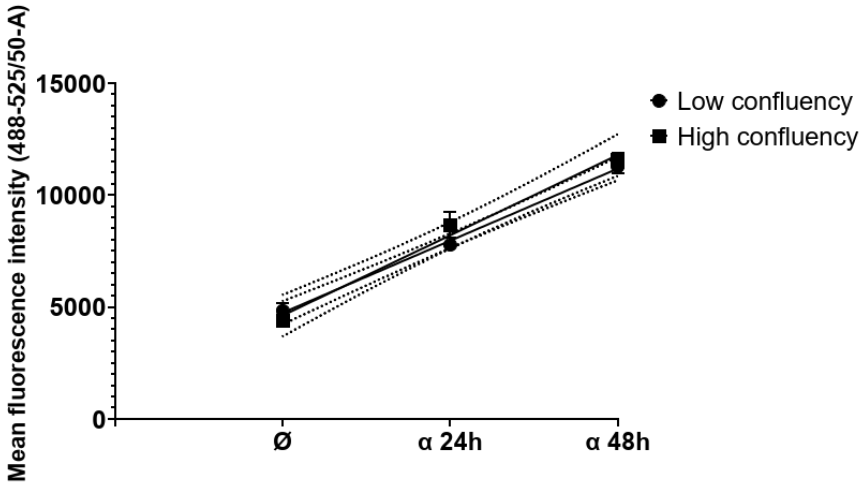

Figure D.2: Linear regression analysis for KO cell data presented in Figure 6.7.

Table D.15: Linear Regression statistical analysis results for low confluency data presented in Figure 6.7.

	WT	**KO**
Equation	$y = 1593 \cdot x + 3035$	$y = 3219 \cdot x + 1517$
95% Confidence Intervals		
Slope	(1391, 1794)	(2816, 3623)
Y-intercept	(2600, 3470)	(645.2, 2388)
X-intercept	(−2.482, −1.456)	(−0.8415, −0.1795)
Goodness of Fit		
R^2	0.9918	0.9919
RMSD	145.1	290.5
Are slopes equal?		
F	100.4	
DFn	1	
DFd	20	
P value	< 0.0001	
Comment	The differences between the slopes are extremely significant.	

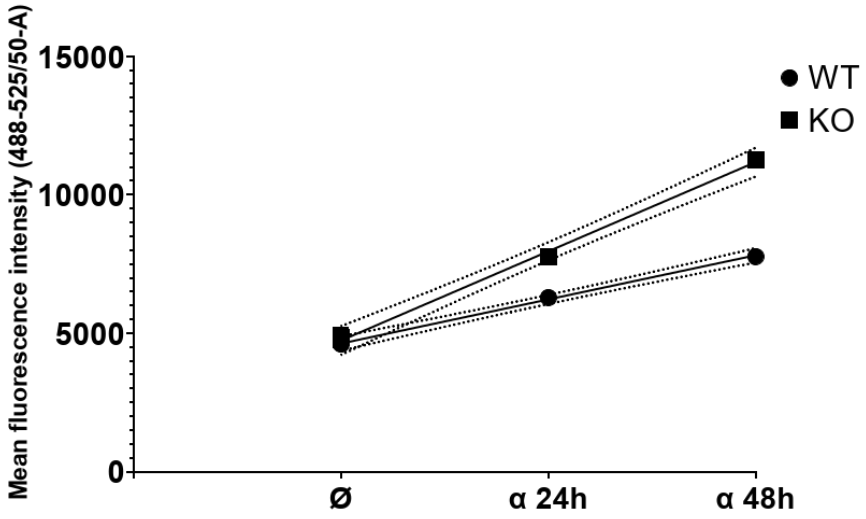

Figure D.3: Linear regression analysis for low confluency cell data presented in Figure 6.7.

Table D.16: Linear Regression statistical analysis results for high confluency data presented in Figure 6.7.

	WT	**KO**
Equation	$y = 1728 \cdot x + 2746$	$y = 3586 \cdot x + 1024$
95% Confidence Intervals		
Slope	(992.4, 2463)	(2865, 4307)
Y-intercept	(1158, 4333)	(−533.1, 2581)
X-intercept	(−4.287, −0.4788)	(−0.8889, 0.1254)
Goodness of Fit		
R^2	0.9141	0.9795
RMSD	529.5	519.2
Are slopes equal?		
F	25.13	
DFn	1	
DFd	20	
P value	0.001	
Comment	The differences between the slopes are very significant.	

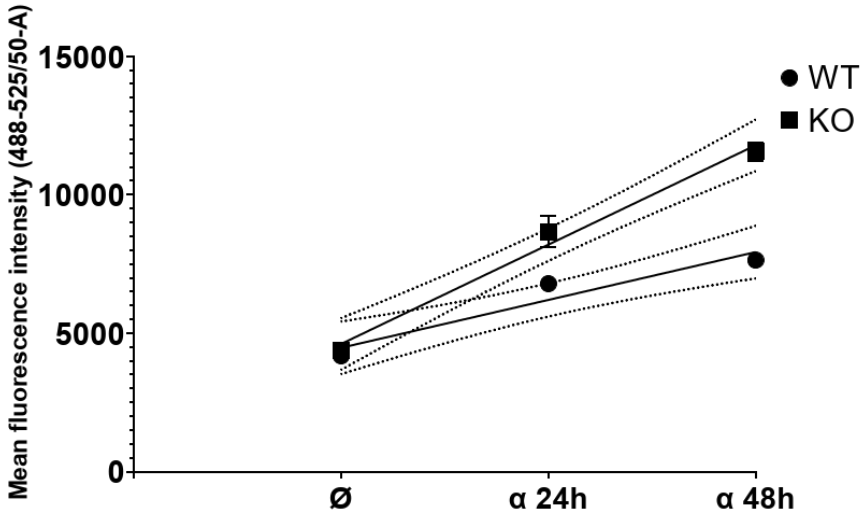

Figure D.4: Linear regression analysis for high confluency cell data presented in Figure 6.7.

Appendix E

Supplementary data for chapter 7: Future Work

Peptides originated from GAPDH found downregulated in ISG15 KO vs WT untreated GSC samples

The alignment of the 55 GAPDH-originated peptides identified allows for the identification of common motifs, performed as part of the structural analysis example provided in section 7.1.3.

```
MTTVHAITATQKTVDGPSGKLWR
MTTVHAITATQKTVDGPSGKL
  TVHAITATQKTVDGPSGKLWR
  TVHAITATQKTVDGPSGKL
   VHAITATQKTVDGPSGKLWR
     AITATQKTVDGPSGKLWR
        ATQKTVDGPSGKL
        ATQKTVDGPSGKLWR
           KTVDGPSGKLWR


YTEHQVVSSDFNSDTHSS
YTEHQVVSSDF

       FGYSNRVVDLMAHMASKE
        GYSNRVVDLMAHMASKE
         YSNRVVDLMAHMASKE
            RVVDLMAHMASKE
   YDNEFGYSNRVVD
       FGYSNRVVDL
        GYSNRVVDL
         YSNRVVDL
          SNRVVDL
   YDNEFGYSNRVVDL
ISWYDNEFGYSNRVVD
ISWYDNEFGYSN
ISWYDNEFG
ISWYDNEF
```

FRVPTANVSVVDL
FRVPTANVSVVD
 RVPTANVSVVDL
 RVPTANVSVVD
FRVPTANVSV

 VVESTGVFTT
YVVESTGVF

QERDPSKIKWGDAGAEY
QERDPSKIKWGDAGAE
QERDPSKIKWGDAG
QERDPSKIKWG
 ERDPSKIKWGDAGAEY
  RDPSKIKWGDAGAEY
  RDPSKIKWGDAG
    PSKIKWGDAGAEY

NSDTHSSTFDAGAGIALNDH
NSDTHSSTFDAGAGIAL
   THSSTFDAGAGIALNDH
   THSSTFDAGAGIA
           GAGIALNDHFVK
         DAGAGIALNDH
         DAGAGIALNDHF
           GAGIALNDHF

KVIPELNGKLTG
KVIPELNGKLT

GKVKVGVNGFGRIGRLVT
GVNHEKYDNSL
AENGKLVINGNPIT
RGALQNIIPASTGAAK

Bibliography

Abt, E. R., Le, T. M., Dann, A. M, Capri, J. R., Poddar, S., Lok, V., Li, L., Liang, K., Creech, A. L., Rashid, K., Kim, W., Wu, N., Cui, J., Cho, A., Lee, H. R., Rosser, E. W., Link, J. M., Czernin, J., Wu, T. T., Damoiseaux, R., Dawson, D. W., Donahue, T. R. & Radu, C. G. (2022). Reprogramming of nucleotide metabolism by interferon confers dependence on the replication stress response pathway in pancreatic cancer cells. *Cell reports*, 38 (2), p. 110236. DOI: 10.1016/j.celrep.2021.110236.

Alcalá, S., Sancho, P., Martinelli, P., Navarro, D., Pedrero, C., Martín-Hijano, L., Valle, S., Earl, J., Rodríguez-Serrano, M., Ruiz-Cañas, L., Rojas, K., Carrato, A., García-Bermejo, L., Fernández-Moreno, M. A., Hermann, P. C. & Sainz Jr, B. (2020). ISG15 and ISGylation is required for pancreatic cancer stem cell mitophagy and metabolic plasticity. *Nature communications*, 11 (1), p. 2682. DOI: 10.1038/s41467-020-16395-2.

Alexandrov, L. B., Nik-Zainal, S., Wedge, D. C., Aparicio, S. A., Behjati, S., Biankin, A. V., Bignell, G. R., Bolli, N., Borg, A., Børresen-Dale, A. L., Boyault, S., Burkhardt, B., Butler, A. P., Caldas, C., Davies, H. R., Desmedt, C., Eils, R., Eyfjörd, J. E., Foekens, J. A., Greaves, M., Hosoda, F., Hutter, B., Ilicic, T., Imbeaud, S., Imielinski, M., Jäger, N., Jones, D. T., Jones, D., Knappskog, S., Kool, M., Lakhani, S. R., López-Otín, C., Martin, S., Munshi, N. C., Nakamura, H., Northcott, P. A., Pajic, M., Papaemmanuil, E., Paradiso, A., Pearson, J. V., Puente, X. S., Raine, K., Ramakrishna, M., Richardson, A. L., Richter, J., Rosenstiel, P., Schlesner, M., Schumacher, T. N., Span, P. N., Teague, J. W., Totoki, Y., Tutt, A. N., Valdés-Mas, R., Buuren, M. M. van, 't Veer, L. van, Vincent-Salomon, A., Waddell, N., Yates, L. R., Zucman-Rossi, J., Futreal, P. A., McDermott, U., Lichter, P., Meyerson, M., Grimmond, S. M., Siebert, R., Campo, E., Shibata, T., Pfister, S. M., Campbell, P. J. & Stratton, M. R. (2013). Signatures of mutational processes in human cancer. *Nature*, 500 (7463), pp. 415–421. DOI: 10.1038/nature12477.

Amrhein, V., Greenland, S. & McShane, B. (2019). Scientists rise up against statistical significance. *Nature*, 567 (7748), pp. 305–307. DOI: 10.1038/d41586-019-00857-9.

Andersen, J. B., Aaboe, M., Borden, E. C., Goloubeva, O. G., Hassel, B. A. & Ømtoft, T. F. (2006). Stage-associated overexpression of the ubiquitin-like protein, ISG15, in bladder cancer. *British journal of cancer*, 94 (10), pp. 1465–1471. DOI: 10.1038/sj.bjc.6603099.

Andreatta, M., Alvarez, B. & Nielsen, M. (2017). GibbsCluster: unsupervised clustering and alignment of peptide sequences. *Nucleic acids research*, 45 (W1), pp. 458–463. DOI: 10.1093/nar/gkx248.

Andreatta, M., Lund, O. & Nielsen, M. (2013). Simultaneous alignment and clustering of peptide data using a Gibbs sampling approach. *Bioinformatics*, 29 (1), pp. 8–14. DOI: 10.1093/bioinformatics/bts621.

Apcher S. Daskalogianni, C. & Fåhraeus, R. (2015). Pioneer translation products as an alternative source for MHC-I antigenic peptides. *Molecular immunology*, 68 (2A), pp. 68–71. DOI: 10.1016/j.molimm.2015.04.019.

Asher, G., Lotem, J., Kama, R., Sachs, L. & Shaul, Y. (2002). NQO1 stabilizes p53 through a distinct pathway. *Proceedings of the National Academy of Sciences*, 99 (5), pp. 3099–3104. DOI: 10.1073/pnas.052706799.

Bade, V. N., Nickels, J., Keusekotten, K. & Praefcke, G. J. K. (2012). Covalent Protein Modification with ISG15 via a Conserved Cysteine in the Hinge Region. *PLoS One*, 7 (6), pp. 1–12. DOI: 10.1371/journal.pone.0038294.

Baldanta, S., Fernández-Escobar, M., Acín-Perez, R., Albert, M., Camafeita, E., Jorge, I., Vázquez, J., Enríquez, J. A. & Guerra, S. (2017). ISG15 governs mitochondrial function in macrophages following vaccinia virus infection. *PLoS pathogens*, 13 (10), pp. 1–30. DOI: 10.1371/journal.ppat.1006651.

Balsa, E., Marco, R., Perales-Clemente, E., Szklarczyk, R., Calvo, E., Landázuri, M. O. & Enríquez, J. A. (2012). NDUFA4 is a subunit of complex IV of the mammalian electron transport chain. *Cell metabolism*, 16 (3), pp. 378–386. DOI: 10.1016/j.cmet.2012.07.015.

Banchereau, J. & Pascual, V. (2006). Type I interferon in systemic lupus erythematosus and other autoimmune diseases. *Immunity*, 25 (3), pp. 383–392. DOI: 10.1016/j.immuni.2006.08.010.

Barrangou, R., Fremaux, C., Deveau, H., Richards, M., Boyaval, P., Moineau, S., Romero, D. A. & Horvath, P. (2007). CRISPR provides acquired resistance against viruses in prokaryotes. *Science*, 315 (5819), pp. 1709–1712. DOI: 10.1126/science.1138140.

Bassani-Sternberg, M., Chong, C., Guillaume, P., Solleder, M., Pak, H., Gannon, P. O., Kandalaft, L. E., Coukos, G. & Gfeller, D. (2017). Deciphering HLA-I motifs across HLA peptidomes improves neo-antigen predictions and identifies allostery regulating HLA specificity. *PLoS computational biology*, 13 (8), e1005725. DOI: 10.1371/journal.pcbi.1005725.

Basters, A., Geurink, P. P., El Oualid, F., Ketscher, L., Casutt, M. S., Krause, E., Ovaa, H., Knobeloch, K. P. & G., Fritz (2014). Molecular characterization of ubiquitin-specific protease 18 reveals substrate specificity for interferon-stimulated gene 15. *FEBS Journal*, 281 (7), pp. 1918–1928. DOI: 10.1111/febs.12754.

Basters, A., Geurink, P. P., Röcker, A., Witting, K. F., Tadayon, R., Hess, S., Semrau, M. S., Storici, P., Ovaa, H., Knobeloch, K. P. & Fritz, G. (2017). Structural basis of the specificity

of USP18 toward ISG15. *Nature structural molecular biology*, 24 (3), pp. 270–278. DOI: 10.1038/nsmb.3371.

Bauer, J. W., Petri, M., Batliwalla, F. M., Koeuth, T., Wilson, J., Slattery, C., Panoskaltsis-Mortari, A., Gregersen, P. K., Behrens, T. W. & Baechler, E. C. (2009). Interferon-regulated chemokines as biomarkers of systemic lupus erythematosus disease activity: a validation study. *Arthritis & Rheumatology*, 60 (10), pp. 3098–3107. DOI: 10.1002/art.24803.

Bektas, N., Noetzel, E., Veeck, J., Press, M. F., Kristiansen, G., Naami, A., Hartmann, A., Dimmler, A., Beckmann, M. W., Knüchel, R., Fasching, P. A. & Dahl, E. (2008). The ubiquitin-like molecule interferon-stimulated gene 15 (ISG15) is a potential prognostic marker in human breast cancer. *Breast cancer research*, 10 (4), R58. DOI: 10.1186/bcr2117.

Ben-David, U. & Amon, A. (2020). Context is everything: aneuploidy in cancer. *Nature reviews genetics*, 21 (1), pp. 44–62. DOI: 10.1038/s41576-019-0171-x.

Ben-David, U., Beroukhim, R. & Golub, T. R. (2019). Genomic Evolution of Cancer Models: Perils and Opportunities. *Nature reviews cancer*, 19 (2), pp. 97–109. DOI: 10.1038/s41568-018-0095-3.

Ben-David, U., Siranosian, B., Ha, G., Tang, H., Oren, Y., Hinohara, K., Strathdee, C. A., Dempster, J., Lyons, N. J., Burns, R., Nag, A., Kugener, G., Cimini, B., Tsvetkov, P., Maruvka, Y. E., O'Rourke, R., Garrity, A., Tubelli, A. A., Bandopadhayay, P., Tsherniak, A., Vazquez, F., Wong, B., Birger, C., Ghandi, M., Thorner, A. R., Bittker, J. A., Meyerson, M., Getz, G., Beroukhim, R. & Golub, T. R. (2018). Genetic and transcriptional evolution alters cancer cell line drug response. *Nature*, 560, pp. 325–330. DOI: 10.1038/s41586-018-0409-3.

Benci, J. L., Xu, B., Qiu, Y., Wu, T. J., Dada, H., Twyman-Saint Victor, C., Cucolo, L., Lee, D. S. M., Pauken, K. E., Huang, A. C., Gangadhar, T. C., Amaravadi, R. K., Schuchter, L. M., Feldman, M. D., Ishwaran, H., Vonderheide, R. H., Maity, A., Wherry, E. J. & Minn, A. J. (2016). Tumor Interferon Signaling Regulates a Multigenic Resistance Program to Immune Checkpoint Blockade. *Cell*, 167 (6), pp. 1540–1554. DOI: 10.1016/j.cell.2016.11.022.

Bhushan, J., Radke, J. B., Perng, Y. C., Mcallaster, M., Lenschow, D. J., Virgin, H. W. & Sibley, L. D. (2020). ISG15 Connects Autophagy and IFN-γ-Dependent Control of Toxoplasma gondii Infection in Human Cells. *mBio*, 11 (5), pp. 1–19. DOI: 10.1128/mBio.00852-20.

Bianchi, F., Textor, J. & Bogaart, G. van den (2017). Transmembrane Helices Are an Overlooked Source of Major Histocompatibility Complex Class I Epitopes. *Frontiers in immunology*, 8 (1118). DOI: 10.3389/fimmu.2017.01118.

Bigner, S. H., Mark, J., Burger, P. C., Mahaley Jr., M. S., Bullard, D. E., Muhlbaier, L. H. & Bigner, D. D. (1988). Specific chromosomal abnormalities in malignant human gliomas. *Cancer research*, 48 (2), pp. 405–11. DOI: Notavailable.

Bilderbeek, R. J. C., Baranov, M. V., Bogaart, G. van den & Bianchi, F. (2022). Transmembrane Helices Are an Over-Presented and Evolutionarily Conserved Source of Major Histocompatibility Complex Class I and II Epitopes. *Frontiers in immunology*, 12 (763044), pp. 1–10. DOI: 10.3389/fimmu.2021.763044.

Blanc, M., Hsieh, W. Y., Robertson, K. A., Watterson, S., Shui, G., Lacaze, P., Khondoker, M., Dickinson, P., Sing, G., Rodríguez-Martín, S., Phelan, P., Forster, T., Strobl, B., Müller, M., Riemersma, R., Osborne, T., Wenk, M. R., Angulo, A. & Ghazal, P. (2011). Host Defense against Viral Infection Involves Interferon Mediated Down-Regulation of Sterol Biosynthesis. *PLoS biology*, 9 (3), pp. 1–19. DOI: 10.1371/journal.pbio.1000598.

Bleek, G. M. van & Nathenson, S. G. (1991). The structure of the antigen-binding groove of major histocompatibility complex class I molecules determines specific selection of self-peptides. *Proceedings of the National Academy of Sciences*, 88 (24), pp. 11032–11036. DOI: 10.1073/pnas.88.24.11032.

Blomstrom, D. C., Fahey, D., Kutny, R., Korant, B. D. & Knight Jr., E. (1986). Molecular characterization of the interferon-induced 15-kDa protein. Molecular cloning and nucleotide and amino acid sequence. *The Journal of Biological Chemistry*, 261 (19), pp. 8811–8816. DOI: 10.1016/S0021-9258(19)84453-8.

Bobisse, S., Foukas, P. G., Coukos, G. & Harari, A. (2016). Neoantigen-based cancer immunotherapy. *Annals of Translational Medicine*, 4 (14), pp. 1–9. DOI: 10.21037/atm.2016.06.17.

Boelens, M. C., Wu, T. J., Nabet, B. Y., Xu, B., Qiu, Y., Yoon, T., Azzam, D. J., Victor, C. T., Wiemann, B. Z., Ishwaran, H., Brugge, P. J. ter, Jonkers, J., Slingerland, J. & Minn, A. J. (2014). Exosome Transfer from Stromal to Breast Cancer Cells Regulates Therapy Resistance Pathways. *Cell*, 159 (3), pp. 499–513. DOI: 10.1016/j.cell.2014.09.051.

Bogunovic, D., Byun, M., Durfee, L. A., Abhyankar, A., Sanal, O., Mansouri, D., Salem, S., Radovanic, I., Grant, A. V., Adimi, P., Mansouri, N., Okada, S., Bryant, V. L., Kong, X. F., Kreins, A., Velez, M. M., Boisson, B., Khalilzadeh, S., Ozcelik, U., Darazam, I. A., Schoggins, J. W., Rice, C. M., Al-Muhsen, S., Behr, M., Vogt, G., Puel, A., Bustamante, J., Gros, P., Huibregtse, J. M., Abel, L., Boisson-Dupuis, S. & Casanova, J. L. (2012). Mycobacterial disease and impaired IFN-γ immunity in humans with inherited ISG15 deficiency. *Science*, 337 (6102), pp. 1684–1688. DOI: 10.1126/science.1224026.

Bolotin, A., Quinquis, B., Sorokin, A. & Ehrlich, S. D. (2005). Clustered regularly interspaced short palindrome repeats (CRISPRs) have spacers of extrachromosomal origin. *Microbiology (Reading)*, 151 (8), pp. 2551–2561. DOI: 10.1099/mic.0.28048-0.

Bourdetsky, D., Schmelzer, C. E. H. & Admon, A. (2014). The nature and extent of contributions by defective ribosome products to the HLA peptidome. *Proceedings of the National Academy of Sciences*, 111 (16), E1591–1599. DOI: doi:10.1073/pnas.1321902111.

Buda, G., Valdez, R. M., Biagioli, G., Olivieri, F. A., Affranchino, N., Bouso, C., Lotersztein, V., Bogunovic, D., Bustamante, J. & Martí, M. A. (2020). Inflammatory cutaneous le-

sions and pulmonary manifestations in a new patient with autosomal recessive ISG15 deficiency case report. *Allergy, asthma & clinical immunology*, 16 (77), pp. 1–6. DOI: 10.1186/s13223-020-00473-7.

Burks, J., Reed, R. E. & D., Desai. S. (2015). Free ISG15 triggers an antitumor immune response against breast cancer: a new perspective. *Oncotarget*, 6 (9), pp. 7221–7231. DOI: 10.18632/oncotarget.3372.

Butiuc-Keul, A., Farkas, A., Carpa, R. & Iordache, D. (2022). CRISPR-Cas System: The Powerful Modulator of Accessory Genomes in Prokaryotes. *Microbial physiology*, 32 (1-2), pp. 2–17. DOI: 10.1159/000516643.

Cai, J., Liu, T., Jiang, X., Guo, C., Liu, A. & Xiao, X. (2017). Downregulation of USP18 inhibits growth and induces apoptosis in hepatitis B virus-related hepatocellular carcinoma cells by suppressing BCL2L1. *Experimental cell research*, 358 (2), pp. 315–322. DOI: 10.1016/j.yexcr.2017.07.006.

Carey, B. S., Poulton, K. V. & Poles, A. (2019). Factors affecting HLA expression: A review. *International journal of immunogenetics*, 46 (5), pp. 307–320. DOI: 10.1111/iji.12443.

Catic, A., Fiebiger, E., Korbel, G. A., Blom, D., Galardy, P. J. & Ploegh, H. L. (2007). Screen for ISG15-crossreactive Deubiquitinases. *PLoS One*, 2 (7), e679. DOI: 10.1371/journal.pone.0000679.

Chang, Y., Yan, X., Xie, Y., Gao, X., Song, A., Zhang, D. & Hu, H. (2008). Different Roles for Two Ubiquitin-like Domains of ISG15 in Protein Modification. *The journal of biological chemistry*, 283 (19), pp. 13370–13377. DOI: 10.1074/jbc.M800162200.

Chen, L., Borozan, I., Feld, J., Sun, J., Tannis, L. L., Coltescu, C., Heathcote, J., Edwards, A. M. & McGilvray, I. D. (2005). Hepatic gene expression discriminates responders and nonresponders in treatment of chronic hepatitis C viral infection. *Gastroenterology*, 128 (5), pp. 1437–1444. DOI: 10.1053/j.gastro.2005.01.059.

Chen, L., Borozan, I., Sun, J., Guindi, M., Fischer, S., Feld, J., Anand, N., Heathcote, J., Edwards, A. M. & McGilvray, I. D. (2010). Cell-type specific gene expression signature in liver underlies response to interferon therapy in chronic hepatitis C infection. *Gastroenterology*, 138 (3), pp. 1123–1133. DOI: 10.1053/j.gastro.2009.10.046.

Chen, L., Li, S. & McGilvray, I. (2011). The ISG15/USP18 ubiquitin-like pathway (ISGylation system) in Hepatitis C Virus infection and resistance to interferon therapy. *The international journal of biochemistry & cell biology*, 43 (10), pp. 1427–1431. DOI: 10.1016/j.biocel.2011.06.006.

Chen, R. H., Du, Y., Han, P., Wang, H. B., Liang, F. Y., Feng, G. K., Zhou, A. J., Cai, M. Y., Zhoing, Q., Zeng, M. S. & Huang, X. M. (2016). ISG15 predicts poor prognosis and promotes cancer stem cell phenotype in nasopharyngeal carcinoma. *Oncotarget*, 7 (13), pp. 6910–6922. DOI: 10.18632/oncotarget.7626.

Chen, R. H., Xiao, Z. W., Yan, X. Q., Han, P., Liang, F. Y., Wang, J. Y., Yu, S. T., Zhang, T. Z., Chen, S. Q., Zhong, Q. & Huang, X. M. (2020). Tumor Cell-Secreted ISG15 Promotes

Tumor Cell Migration and Immune Suppression by Inducing the Macrophage M2-Like Phenotype. *Frontiers in Immunology*, 11 (594775), pp. 1–13. DOI: 10.3389/fimmu.2020.594775.

Chen, Y. L., Wu, W. L., Jang, C. W., Yen, Y. C., Wang, S. H., Tsai, F. Y., Shen, Y. Y. & Chen, Y. W. (2019). Interferon-stimulated gene 15 modulates cell migration by interacting with Rac1 and contributes to lymph node metastasis of oral squamous cell carcinoma cells. *Oncogene*, 38 (23), pp. 4480–4495. DOI: 10.1038/s41388-019-0731-8.

Cheon, H., Borden, E. C. & Stark, G. R. (2014). Interferons and their stimulated genes in the tumor microenvironment. *Seminars in Oncology*, 41 (2), pp. 156–173. DOI: 10.1053/j.seminoncol.2014.02.002.

Cheon, H., Holvey-Bates, E. G., Schoggins, J. W., Forster, S., Hertzog, P., Imanaka, N., Rice, C. M., Jackson, M. W., Junk, D. J. & Stark, G. R. (2013). IFNβ-dependent increases in STAT1, STAT2, and IRF9 mediate resistance to viruses and DNA damage. *The EMBO Journal*, 32 (20), pp. 2751–2763. DOI: 10.1038/emboj.2013.203.

Cheon, H. & Stark, G. R. (2009). Unphosphorylated STAT1 prolongs the expression of interferon-induced immune regulatory genes. *Proceedings of the National Academy of Sciences of the United States of America*, 106 (23), pp. 9373–9378. DOI: 10.1073/pnas.0903487106.

Cherian, M. G., Jayasurya, A. & Bay, B. H. (2003). Metallothioneins in human tumors and potential roles in carcinogenesis. *Mutation research*, 533 (1-2), pp. 201–209. DOI: 10.1016/j.mrfmmm.2003.07.013.

Cho, S. W., Kim, S., Kim, J. M. & Kim, J. S. (2013). Targeted genome engineering in human cells with the Cas9 RNA-guided endonuclease. *Nature biotechnology*, 31 (3), pp. 230–232. DOI: 10.1038/nbt.2507.

Chong, C., Coukos, G. & Bassani-Sternberg, M. (2022). Identification of tumor antigens with immunopeptidomics. *Nature biotechnology*, 40 (2), pp. 175–188. DOI: 10.1038/s41587-021-01038-8.

Christie, M. & Igreja, C. (2023). eIF4E-homologous protein (4EHP): a multifarious cap-binding protein. *The FEBS journal*, 290 (2), pp. 266–285. DOI: 10.1111/febs.16275.

Chyuan, I. T., Tzeng, H. T. & Chen, J. Y. (2019). Signaling Pathways of Type I and Type III Interferons and Targeted Therapies in Systemic Lupus Erythematosus. *Cells*, 8 (9), pp. 1–19. DOI: 10.3390/cells8090963.

Colquhoun, D. (2017). The reproducibility of research and the misinterpretation of p-values. *Royal society open science*, 4 (12), pp. 1–22. DOI: 10.1098/rsos.171085.

Cong, L., Ran, F. A., Cox, D., Lin, S., Barretto, R., Habib, N., Hsu, P. D., Wu, X., Jiang, W., Marraffini, L. A. & Zhang, F. (2013). Multiplex genome engineering using CRISPR/Cas systems. *Science*, 339 (6121), pp. 818–823. DOI: 10.1126/science.1231143.

Crow, M. K. (2010). Type I interferon in organ-targeted autoimmune and inflammatory diseases. *Arthritis Research & Therapy*, 12 (1), pp. 1–10. DOI: 10.1186/ar2886.

Crow, M. K. & Ronnblom, L. (2019). Type I interferons in host defence and inflammatory diseases. *Lupus science & medicine*, 6 (1), pp. 1–. DOI: 10.1136/lupus-2019-000336.

Cui, C, Shu, W. & Li, P. (2016). Fluorescence In situ Hybridization: Cell-Based Genetic Diagnostic and Research Applications. *Frontiers in cell and developmental biology*, 4 (89), pp. 1–11. DOI: 10.3389/fcell.2016.00089.

D'Cunha, J., Knight Jr., E., Haas, A. L., Truitt, R. L. & Borden, E. C. (1996a). Immunoregulatory properties of ISG15, an interferon-induced cytokine. *Proceedings of the National Academy of Sciences of the United States of America*, 93 (1), pp. 211–215.

D'Cunha, J., Ramanujam, S., Wagner, R. J., Witt, P. L., Knight Jr., E. & Borden, E. C. (1996b). In vitro and in vivo secretion of human ISG15, an IFN-induced immunomodulatory cytokine. *Journal of Immunology*, 157 (9), pp. 4100–4108.

Dai, H., Wang, L., Li, L., Huang, Z. & Ye, L. (2021). Metallothionein 1: A New Spotlight on Inflammatory Diseases. *Frontiers in Immunology*, 12 (739918), pp. 1–14. DOI: 10.3389/fimmu.2021.739918.

Dai, Y., Yu, T., Yu, C., Lu, T., Zhou, L., Cheng, C. & Ni, H. (2022). ISG15 enhances glioma cell stemness by promoting Oct4 protein stability. *Environmental toxicology*, 37 (9), pp. 2133–2142. DOI: 10.1002/tox.23556.

Dastur, A., Beaudenon, S., Kelley, M., Krug, R. M. & Huibregtse, J. M. (2006). Herc5, an interferon-induced HECT E3 enzyme, is required for conjugation of ISG15 in human cells. *The Journal of Biological Chemistry*, 281 (7), pp. 4334–4338. DOI: 10.1074/jbc.M512830200.

Der, S. D., Zhou, A., Williams, B. R. G. & Silverman, R. H. (1998). Identification of genes differentially regulated by interferon alpha, beta, or gamma using oligonucleotide arrays. *Proceedings of the national academy of sciences USA*, 95 (26), pp. 15623–15628. DOI: 10.1073/pnas.95.26.15623.

Desai, S. D. (2015). ISG15: A double edged sword in cancer. *Oncoimmunology*, 4 (12). DOI: 10.1080/2162402X.2015.1052935.

Desai, S. D., Haas, A. L., Wood, L. M., Tsai, Y. C., Pestka, S., Rubin, E. H., Saleem, A., Nur-E-Kamal, A. & Liu, L. F. (2006). Elevated expression of ISG15 in tumor cells interferes with the ubiquitin/26S proteasome pathway. *Cancer research*, 66 (2), pp. 921–928. DOI: 10.1158/0008-5472.CAN-05-1123.

Desai, S. D., Reed, R. E., Babu, S. & Lorio, E. A. (2013). ISG15 Deregulates Autophagy in Genotoxin-treated Ataxia Telangiectasia Cells. *Journal of Biological Chemistry*, 288 (4), pp. 2388–2402. DOI: 10.1074/jbc.M112.403832.

Desai, S. D., Wood, L. M., Tsai, Y.C., Hsieh, T. S., Marks, J. R., Scott, G. L., Giovanella, B. C. & Liu, L. F. (2008). ISG15 as a novel tumor biomarker for drug sensitivity. *Molecular Cancer Therapeutics*, 7 (6), pp. 1430–1439. DOI: 10.1158/1535-7163.MCT-07-2345.

Dinkova-Kostova, A. T. & Talalay, P. (2010). NAD(P)H:quinone acceptor oxidoreductase 1 (NQO1), a multifunctional antioxidant enzyme and exceptionally versatile cytopro-

tector. *Archives of biochemistry and biophysics*, 501 (1), pp. 116–123. DOI: 10.1016/j.abb.2010.03.019.

Doherty, M. K., Hammond, D. E., Clague, M. J., Gaskell, S. J. & Beynon, R. J. (2009). Turnover of the human proteome: determination of protein intracellular stability by dynamic SILAC. *Journal of proteome research*, 8 (1), pp. 104–112. DOI: 10.1021/pr800641v.

Durfee, L. A., Lyon, N., Seo, K. & Huibregtse, J. M. (2010). The ISG15 conjugation system broadly targets newly synthesized proteins: implications for the antiviral function of ISG15. *Molecular Cell*, 38 (5), pp. 722–732. DOI: 10.1016/j.molcel.2010.05.002.

Eder, K. & Kalman, B. (2014). Molecular Heterogeneity of Glioblastoma and its Clinical Relevance. *Pathology Oncology Research*, 20 (4), pp. 777–787. DOI: 10.1007/s12253-014-9833-3.

Elsen, P. J. van den, Holling, T. M., Kuipers, H. F. & Stoep, N. van der (2004). Transcriptional regulation of antigen presentation. *Current opinion in immunology*, 16 (1), pp. 67–75. DOI: 10.1016/j.coi.2003.11.015.

Erdal, E., Haider, S., Rehwinkel, J., Harris, A. L. & McHugh, P. J. (2017). A prosurvival DNA damage-induced cytoplasmic interferon response is mediated by end resection factors and is limited by Trex1. *Genes & Development*, 31 (4), pp. 353–369. DOI: 10.1101/gad.289769.116.

Espada, C. E., Lummertz da Rocha, E., Santos, A. A. dos, Guerra Soares, Z., Malaquias, G., Oliveira Patrício, D., Gonzalez Kozlova, E., Fernandes dos Santos, P., Bordignon, J., Sanford, T. J., Fajardo, T., Sweeney, T. R., Báfica, A. & Santos Mansur, D (2019). ISG15/USP18/STAT2 is a molecular hub regulating autocrine IFN I-mediated control of Dengue and Zika virus replication. *bioRxiv*. DOI: 10.1101/784678.

Everley, P. A., Bakalarski, C. E., Elias, J. E., Waghorne, C. G., Beausoleil, S. A., Gerber, S. A., Faherty, B. K., Zetter, B. R. & Gygi, S. P. (2006). Enhanced Analysis of Metastatic Prostate Cancer Using Stable Isotopes and High Mass Accuracy Instrumentation. *Journal of proteome research*, 5 (5), pp. 1224–1231. DOI: 10.1021/pr0504891.

Everley, P. A., Krijgsveld, J., Zetter, B. R. & Gygi, S. P. (2004). Quantitative cancer proteomics: Stable isotope labeling with amino acids in cell culture (SILAC) as a tool for prostate cancer research. *Molecular and cellular proteomics*, 3 (7), pp. 729–735. DOI: 10.1074/mcp.M400021-MCP200.

Ewing, R. M., Chu, P., Elisma, F., Li, H., Taylor, P., Climie, S., McBroom-Cerajewski, L., Robinson, M. D., O'Connor, L., Li, M., Taylor, R., Dharsee, M., Ho, Y., Heilbut, A., Moore, L., Zhang, S., Ornatsky, O., Bukhman, Y. V., Ethier, M., Sheng, Y., Vasilescu, J., Abu-Farha, M., Lambert, J. P., Duewel, H. S., Stewart, I. I., Kuehl, B., Hogue, K., Colwill, K., Gladwish, K., Muskat, B., Kinach, R., Adams, S. L., Moran, M. F., Morin, G. B., Topaloglou, T. & Figeys, D. (2007). Large-scale mapping of human protein–protein interactions by mass spectrometry. *Molecular Systems Biology*, 3 (89), pp. 1–17. DOI: 10.1038/msb4100134.

Fakhar-Ul-Hassnain Waqas, S., Sohail, A., Nguyen, A. H. H., Usman, A., Ludwig, T., Wegner, A., Malik, M. N. H., Schuchardt, S., Geffers, R., Winterhoff, M., Merkert, S., Martin,

U., Olmer, R., Lachmann, N. & Pessler, F. (2022). ISG15 deficiency features a complex cellular phenotype that responds to treatment with itaconate and derivatives. *Clinical and translational medicine*, 12 (7), pp. 1–27. DOI: 10.1002/ctm2.931.

Fallet, B., Narr, K., Ertuna, Y. I., Remy, M., Sommerstein, R., Cornille, K., Kreutzfeldt, M., Page, N., Zimmer, G., Geier, F., Straub, T., Pircher, H., Larimore, K., Greenberg, P. D., Merkler, D. & Pinschewer, D. D. (2016). Interferon-driven deletion of antiviral B cells at the onset of chronic infection. *Science Immunology*, 1 (4), pp. 1–23. DOI: 10.1126/sciimmunol.aah6817.

Falvey, C. M., O'Donovan, T. R., El-Mashed, S., Nyhan, M. J., O'Reilly, S. & McKenna, S. L. (2017). UBE2L6/UBCH8 and ISG15 attenuate autophagy in esophageal cancer cells. *Oncotarget*, 8 (14), pp. 23479–23491. DOI: 10.18632/oncotarget.15182.

Fan, J. B., Arimoto, K., Motamedchaboki, K., Yan, M., Wolf, D. A. & Zhang, D. E. (2015a). Identification and characterization of a novel ISG15-ubiquitin mixed chain and its role in regulating protein homeostasis. *Scientific reports*, 5 (12704), pp. 1–11. DOI: 10.1038/srep12704.

Fan, J. B., Miyauchi-Ishida, S., Arimoto, K., Liu, D., Yan, M., Liu, C. W., Győrffy, B. & Zhang, D. E. (2015b). Type I IFN induces protein ISGylation to enhance cytokine expression and augments colonic inflammation. *Proceedings of the national academy of sciences of the united states of america*, 112 (46), pp. 14313–14318. DOI: 10.1073/pnas.1505690112.

Farrell, P. J., Broeze, R. J. & Lengyel, P. (1979). Accumulation of an mRNA and protein in interferon-treated Ehrlich ascites tumour cells. *Nature*, 279 (5713), pp. 523–525. DOI: 10.1038/279523a0.

Ferrantini, M., Capone, I. & Belardelli, F. (2007). Interferon-alpha and cancer: mechanisms of action and new perspectives of clinical use. *Biochimie*, 89 (6-7), pp. 884–893. DOI: 10.1016/j.biochi.2007.04.006.

Freitas, B. T., Durie, I. A., Murray, J., Longo, J. E., Miller, H. C., Crich, D., Hogan, R. J., Tripp, R. A. & Pegan, S. D. (2020a). Characterization and Noncovalent Inhibition of the Deubiquitinase and deISGylase Activity of SARS-CoV-2 Papain-Like Protease. *ACS infectious diseases*, 6 (8), pp. 2099–2109. DOI: 10.1021/acsinfecdis.0c00168.

Freitas, B. T., Scholte, F. E. M., Bergeron, E. & Pegan, S. D. (2020b). How ISG15 combats viral infection. *Virus research*, 286 (198036), pp. 1–22. DOI: 10.1016/j.virusres.2020.198036.

Friedman, R. M. (2008). Clinical uses of interferons. *British Journal of Clinical Pharmacology*, 65 (2), pp. 158–162. DOI: 10.1111/j.1365-2125.2007.03055.x.

Giannakopoulos, N. V., Arutyunova, E., Lai, C., Lenschow, D. J., Haas, A. L. & Virgin, H. W. (2009). ISG15 Arg151 and the ISG15-Conjugating Enzyme UbE1L Are Important for Innate Immune Control of Sindbis Virus. *Journal of virology*, 83 (4), pp. 1602–1610. DOI: 10.1128/JVI.01590-08.

Giannakopoulos, N. V., Luo, J. K., Papov, V., Zou, W., Lenschow, D. J., Jacobs, B. S., Borden, E. C., Li, J., Virgin, H. W. & Zhang, D. E. (2005). Proteomic identification of proteins conjugates to ISG15 in mouse and human cells. *Biochemical and Biophysical Research Communications*, 336 (2), pp. 496–506. DOI: 10.1016/j.bbrc.2005.08.132.

Gibbert, K., Schlaak, J. F., Yang, D. & Dittmer, U. (2013). IFN-α subtypes: distinct biological activities in anti-viral therapy. *British journal of pharmacology*, 168 (5), pp. 1048–1058. DOI: 10.1111/bph.12010.

Gilbert, L. A, Horlbeck, M. A., Adamson, B., Villalta, J. E., Chen, Y., Whitehead, E. H., Guimaraes, C., Panning, B., Ploegh, H. L., Bassik, M. C., Qi, L. S., Kampmann, M. & Weissman, J. S. (2014). Genome-Scale CRISPR-Mediated Control of Gene Repression and Activation. *Cell*, 159 (3), pp. 647–661. DOI: 10.1016/j.cell.2014.09.029.

Gilbert, L. A., Larson, M. H., Morsut, L., Liu, Z., Brar, G. A., Torres, S. E., Stern-Ginossar, N., Brandman, O., Whitehead, E. H., Doudna, J. A., Lim, W. A., Weissman, J. S. & Qi, L. S. (2013). CRISPR-Mediated Modular RNA-Guided Regulation of Transcription in Eukaryotes. *Cell*, 154 (2), pp. 442–451. DOI: 10.1016/j.cell.2013.06.044.

Gocher, A. M., Workman, C. J. & Vignali, D. A. A. (2022). Interferon-γ: teammate or opponent in the tumour microenvironment? *Nature reviews immunology*, 22 (3), pp. 158–172. DOI: 10.1038/s41577-021-00566-3.

Goedhart, J. & Luijsterburg, M. S. (2020). VolcaNoseR is a web app for creating, exploring, labeling and sharing volcano plots. *Scientific report*, 10 (1), pp. 1–5. DOI: 10.1038/s41598-020-76603-3.

González-Amor, M., García-Redondo, A. B., Jorge, I., Zalba, G., Becares, M., Ruiz-Rodríguez, M. J., Rodríguez, C., Bermeo, H., Rodrigues-Díez, R., Rios, F. J., Montezano, A. C., Martínez-González, J., Vázquez, J., Redondo, J. M., Touyz, R. M., Guerra, S., Salaices, M. & Briones, A. M. (2022). Interferon-stimulated gene 15 pathway is a novel mediator of endothelial dysfunction and aneurysms development in angiotensin II infused mice through increased oxidative stress. *Cardiovascular research*, 118 (16), pp. 3250–3268. DOI: 10.1093/cvr/cvab321.

González-Navajas, J. M., Lee, J., David, M. & Raz, E. (2012). Immunomodulatory functions of type I interferons. *Nature reviews*, 12 (2), pp. 125–135. DOI: 10.1038/nri3133.

Graham, D. B. & Root, D. E. (2015). Resources for the design of CRISPR gene editing experiments. *Genome biology*, 16 (260), pp. 1–21. DOI: 10.1186/s13059-015-0823-x.

Griffin, C. A., Hawkins, A. L., Packer, R. J., Rorke, L. B. & Emanuel, B. S. (1988). Chromosome abnormalities in pediatric brain tumors. *Cancer research*, 48 (1), pp. 175–180. DOI: Notavailable.

Guan, W., Ni, Z., Hu, Y., Liang, W., Ou, C., He, J., Liu, L., Shan, H., Lei, C., Hui, D.S.C., Du, B., Li, L., Zeng, G., Yuen, K. Y., Chen, R., Tang, C., Wang, T., Chen, P., Xiang, J., Li, S., Wang, J. L., Liang, Z., Peng, Y., Wei, L., Liu, Y., Hu, Y. H., Peng, P., Wang, J. M., Liu, J., Chen, Z., Li, G., Zheng, Z., Qiu, S., Luo, J., Ye, C., S., Zhu & N., Zhong (2020). Clinical Character-

istics of Coronavirus Disease 2019 in China. *The journal of emergency medicine*, 58 (4), pp. 711–712. DOI: 10.1016/j.jemermed.2020.04.004.

Guo, C., Liu, S. & Sun, M. Z. (2013). Novel insight into the role of GAPDH playing in tumor. *Clinical and translational oncology*, 15 (3), pp. 167–172. DOI: 10.1007/s12094-012-0924-x.

Haas, A. L., Ahrens, P., Bright, P. M. & Ankel, H. (1987). Interferon induces a 15-kilodalton protein exhibiting marked homology to ubiquitin. *Journal of biological chemistry*, 262 (23), pp. 11315–11323. DOI: 10.1016/S0021-9258(18)60961-5.

Hadjadj, J., Yatim, N., Barnabei, L., Corneau, A., Boussier, J., Smith, N., Péré, H., Charbit, B., Bondet, V., Chenevier-Gobeaux, C., Breillat, P., Carlier, N., Gauzit, R., Morbieu, C., Pène, F., Marin, N., Roche, N., Szwebel, T. A., Merkling, S. H., Treluyer, J. M., Veyer, D., Mouthon, L., Blanc, C., Tharaux, P. L., Rozenberg, F., Fischer, A., Duffy, D., Rieux-Laucat, F., Kernéis, S. & Terrier, B. (2020). Impaired type I interferon activity and inflammatory responses in severe COVID-19 patients. *Science*, 369 (6504), pp. 718–724. DOI: 10.1126/science.abc6027.

Haft, D. H., Selengut, J., Mongodin, E. F. & Nelson, K. E. (2005). A guild of 45 CRISPR-associated (Cas) protein families and multiple CRISPR/Cas subtypes exist in prokaryotic genomes. *PLoS Computational Biology*, 1 (6), pp. 1–10. DOI: 10.1371/journal.pcbi.0010060.

Hall, J. C. & Rosen, A. (2010). Type I interferons: crucial participants in disease amplification in autoimmunity. *Nature Reviews Rheumatology*, 6 (1), pp. 40–49. DOI: 10.1038/nrrheum.2009.237.

Halsey, L. G. (2019). The reign of the p-value is over: what alternative analyses could we employ to fill the power vacuum? *Biology letters*, 15 (5), pp. 1–8. DOI: 10.1098/rsbl.2019.0174.

Halsey, L. G., Curran-Everett, D., Vowler, S. L. & Drummond, G. B. (2015). The fickle P value generates irreproducible results. *Nature methods*, 12 (3), pp. 179–185. DOI: 10.1038/nmeth.3288.

Hanahan, D. & Weinberg, R. A. (2011). Hallmarks of Cancer: The Next Generation. *Cell*, 144 (5), pp. 646–674. DOI: 10.1016/j.cell.2011.02.013.

Harty, R. N., Pitha, P. M. & Okumura, A. (2009). Antiviral activity of innate immune protein ISG15. *Journal of Innate Immunity*, 1 (5), pp. 397–404. DOI: 10.1159/000226245.

Hayat Malik, M. N., Fakhar-Ul-Hassnain Waqas, S., Zeitvogel, J., Cheng, J., Geffers, R., Abu-Elbaha Gouda, Z., Mahrous Elsaman, A., Radwan, A. R., Schefzyk, M., Braubach, P., Auber, B., Olmer, R., Müsken, M., Roesner, L. M., Gerold, G., Schuchardt, S., Merkert, S., Martin, U., Meissner, F., Werfel, T. & Pessler, F. (2022). Congenital deficiency reveals critical role of ISG15 in skin homeostasis. *Journal of clinical investigation*, 132 (3), pp. 1–19. DOI: 10.1172/JCI141573.

Held, T., Basler, M., Knobeloch, K. P. & Groettrup, M. (2020). Evidence for an involvement of the ubiquitin-like modifier ISG15 in MHC class I antigen presentation. *European Journal of Immunology*, 51 (1), pp. 138–150. DOI: 10.1002/eji.202048646.

Hermeking, H., Lengauer, C., Polyak, K., He, T. C., Zhang, L., Thiagalingam, S., Kinzler, K. W. & Vogelstein, B. (1997). 14-3-3sigma is a p53-regulated inhibitor of G2/M progression. *Molecular cell*, 1 (1), pp. 3–11. DOI: 10.1016/s1097-2765(00)80002-7.

Holland, A. J. & Cleveland, D. W. (2009). Boveri revisited: chromosomal instability, aneuploidy and tumorigenesis. *Nature reviews molecular cell biology*, 10 (7), pp. 478–487. DOI: 10.1038/nrm2718.

Hu, Y., Hong, X. Y., Yang, X. F., Ma, R. H., Wang, X., Zhang, J. F., Feng, Q., Li, X. G., Sun, D. S., Li, X., Wan, H. L., Li, T., Wang, Q., Ke, D., Wang, J. Z. & Liu, G. P. (2019). Inflammation-dependent ISG15 upregulation mediates MIA-induced dendrite damages and depression by disrupting NEDD4/Rap2A signaling. *Biochimica et biophysica acta, molecular basis of disease*, 1865 (6), pp. 1477–1489. DOI: 10.1016/j.bbadis.2019.02.020.

Huang, Y. F., Wee, S., Gunaratne, J., Lane, D. P. & Bulavin, D. V (2014). Isg15 controls p53 stability and functions. *Cell cycle*, 13 (14), pp. 2199–2209. DOI: 10.4161/cc.29209.

Huo, Y., Zong, Z., Wang, Q., Zhang, Z. & Deng, H. (2017). ISG15 silencing increases cisplatin resistance via activating p53-mediated cell DNA repair. *Oncotarget*, 8 (64), pp. 107452–107461. DOI: 10.18632/oncotarget.22488.

Hwang, W. Y., Fu, Y., Reyon, D., Maeder, M. L., Tsai, S. Q., Sander, J. D., Peterson, R. T., Yeh, J. R. J. & Joung, J. K. (2013). Efficient genome editing in zebrafish using a CRISPR-Cas system. *Nature biotechnology*, 31 (3), pp. 227–229. DOI: 10.1038/nbt.2501.

Im, E., Yoo, L., Hyun, M., Shin, W. H. & Chung, K. C. (2016). Covalent ISG15 conjugation positively regulates the ubiquitin E3 ligase activity of parkin. *Open biology*, 6 (8), pp. 1–15. DOI: 10.1098/rsob.160193.

Isaacs, A. & Lindenmann, J. (1957). Virus interference. I. The interferon. *Proceedings of the Royal Society B: Biological Sciences*, 147 (927), pp. 258–267. DOI: 10.1098/rspb.1957.0048.

Ivashkiv, L. B. & Donlin, L. T. (2014). Regulation of type I intereferon responses. *Nature Reviews Immunology*, 14, pp. 36–49. DOI: 10.1038/nri3581.

Jeon, Y. J., Jo, M. G., Yoo, H. M., Hong, S. H., Park, J. M., Ka, S. H., Oh, K. H., Seol, J. H., Jung, Y. K. & Chung, C. H. (2012). Chemosensitivity is controlled by p63 modification with ubiquitin-like protein ISG15. *The journal of clinical investigation*, 122 (7), pp. 2622–2636. DOI: 10.1172/JCI61762.

Jin, R., Bay, B. H., Chow, V. T. & Tan, P. H. (2001). Metallothionein 1F mRNA expression correlates with histological grade in breast carcinoma. *Breast cancer research and treatment*, 66 (3), pp. 265–272. DOI: 10.1023/a:1010658907462.

Jinek, M., Chylinski, K., Fonfara, I., Hauer, M., Doudna, J. A. & Charpentier, E. (2012). A programmable dual-RNA-guided DNA endonuclease in adaptive bacterial immunity. *Science*, 337 (6096), pp. 816–821. DOI: 10.1126/science.1225829.

Jinek, M., East, A., Cheng, A., Lin, S., Ma, E. & Doudna, J. (2013). RNA-programmed genome editing in human cells. *eLife*, 2 (e00471), pp. 1–9. DOI: 10.7554/eLife.00471.

Johnston, C., Jiang, W., Chu, T. & Levine, B. (2001). Identification of Genes Involved in the Host Response to Neurovirulent Alphavirus Infection. *Journal of Virology*, 75 (21), pp. 10431–10445. DOI: 10.1128/JVI.75.21.10431-10445.2001.

Jumper, J., Evans, R., Pritzel, A., Green, T., Figurnov, M., Ronneberger, O., Tunyasuvunakool, K., Bates, R., Žídek, A., Potapenko, A., Bridgland, A., Meyer, C., Kohl, S. A. A., Ballard, A. J., Cowie, A., Romera-Paredes, B., Nikolov, S., Jain, R., Adler, J., Back, T., Petersen, S., Reiman, D., Clancy, E., Zielinski, M., Steinegger, M., Pacholska, M., Berghammer, T., Bodenstein, S., Silver, D., Vinyals, O., Senior, A. W., Kavukcuoglu, K., Kohli, P. & Hassabis, D. (2021). Highly accurate protein structure prediction with AlphaFold. *Nature*, 596 (7873), pp. 583–589. DOI: 10.1038/s41586-021-03819-2.

Juncker, M., Kim, C., Reed, R., Haas, A., Schwartzenburg, J. & Desai, S. (2021). ISG15 attenuates post-translational modifications of mitofusins and congression of damaged mitochondria in Ataxia Telangiectasia cells. *Biochimica et Biophysica Acta, Molecular Basis of Disease*, 1867 (6), pp. 1–14. DOI: 10.1016/j.bbadis.2021.166102.

Jurczyszak, D., Manganaro, L., Buta, S., Gruber, C., Martin-Fernandez, M., Taft, J., Patel, R. S., Cipolla, M., Alshammary, H., Mulder, L. C. F., Sachidanandam, R., Bogunovic, D. & Simon, V. (2022). ISG15 deficiency restricts HIV-1 infection. *18*, 3 (PLoS), e1010405. DOI: 10.1371/journal.ppat.1010405.

Kadenbach, B. (2017). Regulation of Mammalian 13-Subunit Cytochrome c Oxidase and Binding of other Proteins: Role of NDUFA4. *Trends in endocrinology and metabolism*, 28 (11), pp. 761–770. DOI: 10.1016/j.tem.2017.09.003.

Kazerounian, S. & Aho, S. (2003). Characterization of periphilin, a widespread, highly insoluble nuclear protein and potential constituent of the keratinocyte cornified envelope. *The journal of biological chemistry*, 278 (38), pp. 36707–36717. DOI: 10.1074/jbc.M303896200.

Keane, L., Cheray, M., K., Blomgren. & Joseph, B. (2021). Multifaceted microglia - key players in primary brain tumour heterogeneity. *Nature reviews neurology*, 17 (4), pp. 243–259. DOI: 10.1038/s41582-021-00463-2.

Kennedy, W. P., Maciuca, R., Wolslegel, K., Tew, W., Abbas, A. R., Chaivorapol, C., Morimoto, A., McBride, J. M., Brunetta, P., Richardson, B. C., Davis, J. C. Jr., Behrens, T. W. & Townsend, M. J. (2015). Association of the interferon signature metric with serological disease manifestations but not global activity scores in multiple cohorts of patients with SLE. *Lupus, Science & Medicine*, 2 (1), pp. 1–11. DOI: 10.1136/lupus-2014-000080.

Keskin, D. B., Anandappa, A. J., Sun, J., Tirosh, I., Mathewson, N. D., Li, S., Oliveira, G., Giobbie-Hurder, A., Felt, K., Gjini, E., Shukla, S. A., Hu, Z., Li, L., Le, P. M., Allesøe, R. L., Richman, A. R., Kowalczyk, M. S., Abdelrahman, S., Geduldig, J. E., Charbonneau, S., Pelton, K., Iorgulescu, J. B., Elagina, L., Zhang, W. & Reardon, D. A. (2018). Neoantigen

vaccine generates intratumoral T cell responses in phase Ib glioblastoma trial. *Nature*, 565 (7738), pp. 234–239. DOI: 10.1038/s41586-018-0792-9.

Khodarev, N. N., Beckett, M., Labay, E., Darga, T., Roizman, B. & Weichselbaum, R. R. (2004). STAT1 is overexpressed in tumors selected for radioresistance and confers protection from radiation in transduced sensitive cells. *Proceedings of the National Academy of Sciences*, 101 (6), pp. 1714–1719. DOI: 10.1073/pnas.0308102100.

Khodarev, N. N., Minn, A. J., Efimova, E. V., Darga, T. E., Labay, E., Beckett, M., Mauceri, E. J., Roizman, B. & Weichselbaum, R. R. (2007). Signal transducer and activator of transcription 1 regulates both cytotoxic and prosurvival functions in tumor cells. *Cancer research*, 67 (19), pp. 9214–9220. DOI: 10.1158/0008-5472.CAN-07-1019.

Kim, K. I., Giannakopoulos, N. V., Virgin, H. W. & Zhang, D. (2004). Interferon-Inducible Ubiquitin E2, Ubc8, Is a Conjugating Enzyme for Protein ISGylation. *Molecular and Cellular Biology*, 24 (21), pp. 9592–9600. DOI: 10.1128/MCB.24.21.9592-9600.2004.

Kim, K. I., Yan, M., Malakhova, O., Luo, J. K., Shen, M. F., Zou, W., Torre, J. C. de la & Zhang, D. E. (2006). Ube1L and protein ISGylation are not essential for alpha/beta interferon signaling. *Molecular and Cellular Biology*, 26 (2), pp. 472–479. DOI: 10.1128/MCB.26.2.472-479.2006.

Kim, M. S. & Kim, K. H. (2019). Effect of CRISPR/Cas9-mediated knockout of either Mx1 or ISG15 gene in EPC cells on resistance against VHSV infection. *Fish and Shellfish Immunology*, 93, pp. 1041–1046. DOI: 10.1016/j.fsi.2019.08.058.

Klein, J. & Sato, A. (2000). The HLA system. First of two parts. *The New England journal of medicine*, 343 (10), pp. 702–709. DOI: 10.1056/NEJM200009073431006.

Knight Jr., E. & Cordova, B. (1991). IFN-induced 15-kDa protein is released from human lymphocytes and monocytes. *Journal of Immunology*, 146 (7), pp. 2280–2284.

Knight Jr., E., Fahey, D., Cordova, B., Hillman, M., Kutny, R., Reich, N. & Blomstrom, D. (1988). A 15-kDa interferon-induced protein is derived by COOH-terminal processing of a 17-kDa precursor. *The Journal of Biological Chemistry*, 263 (10), pp. 4520–4522. DOI: 10.1016/S0021-9258(18)68812-X.

Ko, S. S., Kim, J. Y., Jeong, J., Lee, J. E., Yang, W. I. & Jung, W. H. (2014). The role and regulatory mechanism of 14-3-3 sigma in human breast cancer. *Journal of breast cancer*, 7 (3), pp. 207–218. DOI: 10.4048/jbc.2014.17.3.207.

Komander, D. (2009). The emerging complexity of protein ubiquitination. *Biochemical society transactions*, 37 (5), pp. 937–953. DOI: 10.1042/BST0370937.

Kong, E. B., Kim, H. D. & Kim, J. (2020). Deleting key autophagy elongation proteins induces acquirement of tumor-associated phenotypes via ISG15. *Cell death and differentiation*, 27 (8), pp. 2517–2530. DOI: 10.1038/s41418-020-0519-y.

Korant, B. D., Blomstrom, D. C., Jonak, G. J. & Knight Jr., E. (1984). Interferon-induced proteins. Purification and characterization of a 15,000-dalton protein from human

and bovine cells induced by interferon. *The journal of biological chemistry*, 259 (23), pp. 14835–1489. DOI: 10.1016/S0021-9258(17)42679-2.

Kote, S., Pirog, A., Bedran, G., Alfaro, J. & Dapic, I. (2020). Mass Spectrometry-Based Identification of MHC-Associated Peptides. *Cancers*, 12 (535), pp. 1–14. DOI: 10.3390/cancers12030535.

Kotenko, S. V. (2011). IFN-λs. *Current opinion in immunology*, 23 (5), pp. 583–590. DOI: 10.1016/j.coi.2011.07.007.

Kunzi, M. S. & Pitha, P. M. (1996). Role of Interferon-Stimulated Gene ISG-15 in the Interferon-ω-Mediated Inhibition of Human Immunodeficiency Virus Replication. *Journal of Interferon & Cytokine Research*, 16 (11), pp. 919–927. DOI: 10.1089/jir.1996.16.919.

Kurita, M., Suzuki, H., Kawano, Y., Aiso, S. & Matsuoka, M. (2007). CR/periphilin is a transcriptional co-repressor involved in cell cycle progression. *Biochemical and biophysical research communications*, 364 (4), pp. 930–6. DOI: 10.1016/j.bbrc.2007.10.090.

Kurita, M., Suzuki, H., Masai, H., Mizumoto, K., Ogata, E., Nishimoto, I., Aiso, S. & Matsuoka, M. (2004). Overexpression of CR/periphilin downregulates Cdc7 expression and induces S-phase arrest. *Biochemical and biophysical research communications*, 324 (2), pp. 554–561. DOI: 10.1016/j.bbrc.2004.09.083.

Labrada, L., Liang, X. H, Zheng, W., Johnston, C. & Levine, B. (2002). Age-dependent resistance to lethal alphavirus encephalitis in mice: analysis of gene expression in the central nervous system and identification of a novel interferon-inducible protective gene, mouse ISG12. *Journal of Virology*, 76 (22), pp. 11688–11703. DOI: 10.1128/jvi.76.22.11688-11703.2002.

Labun, K., Montague, T. G., Krause, M., Torres Cleuren, Y. N., Tjeldnes, H. & Valen, E. (2019). CHOPCHOP v3: expanding the CRISPR web toolbox beyond genome editing. *Nucleic Acids Research*, 47 (W1), W171–W174. DOI: 10.1093/nar/gkz365.

Lahm, H. W. & Langen, H. (2000). Mass spectrometry: A tool for the identification of proteins separated by gels. *Electrophoresis*, 21 (11), pp. 2105–2114. DOI: 10.1002/1522-2683(20000601)21:11<2105::AID-ELPS2105>3.0.CO;2-M.

Laukens, D., Waeytens, A., Bleser, P. D., Cuvelier, C. & De Vos, M. (2009). Human metallothionein expression under normal and pathological conditions: mechanisms of gene regulation based on in silico promoter analysis. *Critical reviews in eukaryotic gene expression*, 19 (4), pp. 301–317. DOI: 10.1615/critreveukargeneexpr.v19.i4.40.

Lavoie, T. B., Kalie, E., Crisafulli-Cabatu, S., Abramovich, R., DiGioia, G., Moolchan, K., Pestka, S. & Schreiber, G. (2011). Binding and activity of all human alpha interferon subtypes. *Cytokine*, 56 (2), pp. 282–289. DOI: 10.1016/j.cyto.2011.07.019.

Lee, W. B., Choi, W. Y., Lee, D. H., Shim, H., Kim-Ha, J. & Kim, Y. J. (2019). OAS1 and OAS3 negatively regulate the expression of chemokines and interferon-responsive genes in

human macrophages. *BMB reports*, 52 (2), pp. 133–138. DOI: 10.5483/BMBRep.2019.52.2.129.

Lefebvre, S., Berrih-Aknin, S., Adrian, F., Moreau, P., Poea, S., Gourand, L., Dausset, J., Carosella, E. D. & Paul, P. (2001). A Specific Interferon (IFN)-stimulated Response Element of the Distal HLA-G Promoter Binds IFN-regulatory Factor 1 and Mediates Enhancement of This Nonclassical Class I Gene by IFN-beta. *The journal of biological chemistry*, 276 (9), pp. 6133–6139. DOI: 10.1074/jbc.M008496200.

Lenschow, D. J., Giannakopoulos, N. V., Gunn, L. J., Johnston, C., O'Guin, A. K., Schmidt, R. E., Levine, B. & Virgin IV, H. W. (2005). Identification of Interferon-Stimulated Gene 15 as an Antiviral Molecule during Sindbis Virus Infection In Vivo. *Journal of Virology*, 79 (22), pp. 13974–13983. DOI: 10.1128/JVI.79.22.13974âĂŞ13983.2005.

Lenschow, D. J., Lai, C., Frias-Staheli, N., Giannakopoulos, N. V., Lutz, A., Wolff, T., Osiak, A., Levine, B., Schmidt, R. E., García-Sastre, A., Leib, D. A., Pekosz, A., Knobeloch, K. P., Horak, I. & Virgin, H. W. (2007). IFN-stimulated gene 15 functions as a critical antiviral molecule against influenza, herpes, and Sindbis viruses. *Proceedings of the National Academy of Sciences of the United States of America*, 104 (4), pp. 1371–1376. DOI: 10.1073/pnas.0607038104.

Li, Y., Ma, M. X., Qin, B., Lin, L. T., Richardson, C. D., Feld, J., McGilvray, I. D. & Chen, L. (2019). The Ubiquitin-Specific Protease 18 Promotes Hepatitis C Virus Production by Increasing Viral Infectivity. *Mediators of inflammation*, 2019 (3124745), pp. 1–12. DOI: 10.1155/2019/3124745.

Li, Y., Wen, B., Chen, R., Jiang, F., Zhao, X. & Deng, X. (2015). Promotion of expression of interferon-stimulated genes in U937 monocytic cells by HIV RNAs, measured using stable isotope labeling with amino acids in cell culture (SILAC). *Archives of cirology*, 160 (5), pp. 1249–1258. DOI: 10.1007/s00705-015-2372-8.

Liang, R., Li, X. & Zhu, X. (2020). Deciphering the Roles of IFITM1 in Tumors. *Molecular diagnosis and therapy*, 24 (4), pp. 433–441. DOI: 10.1007/s40291-020-00469-4..

Liu, G., Lee, J., Parker, Z. M., Acharya, D., Chiang, J. J., Gent, M. van, Riedl, W., Davis-Gardner, M. E., Wies, E., Chiang, C. & Gack, M. U. (2021). ISG15-dependent activation of the sensor MDA5 is antagonized by the SARS-CoV-2 papain-like protease to evade host innate immunity. *Nature microbiology*, 6 (4), pp. 467–478. DOI: 10.1038/s41564-021-00884-1.

Liu, M., Hummer, B. T., Li, X. & Hassel, B. A. (2004). Camptothecin induces the ubiquitin-like protein, ISG15, and enhances ISG15 conjugation in response to interferon. *Journal of interferon & cytokine research*, 24 (11), pp. 647–654. DOI: 10.1089/jir.2004.24.647.

Loeb, K. R. & Haas, A. L. (1992). The interferon-inducible 15-kDa ubiquitin homolog conjugates to intracellular proteins. *The Journal of Biological Chemistry*, 267 (11), pp. 7806–7813. DOI: 10.1016/S0021-9258(18)42585-9.

López de Padilla, C. M. & Niewold, T. B. (2016). The Type I Interferons: Basic Concepts and Clinical Relevance in Immune-mediated Inflammatory Diseases. *Gene*, 576 (1), pp. 14–21. DOI: 10.1016/j.gene.2015.09.058.

Lu, D. D., Chen, Y. C., Zhang, X. R., Cao, X. R., Jiang, H. Y. & Yao, L. (2003). The relationship between metallothionein-1F (MT1F) gene and hepatocellular carcinoma. *Yale journal of biology and medicine*, 76 (2), pp. 55–62. DOI: Notavailable.

Lukhele, S., Boukhaled, G. M. & Brooks, D. G. (2019). Type I interferon signaling, regulation and gene stimulation in chronic virus infection. *Seminars in Immunology*, 43 (101277), pp. 1–15. DOI: 10.1016/j.smim.2019.05.001.

Ma, Y., Shan, S., Luo, C., Mo, J., Hu, Z. & Jing, R. (2023). Identification of Potential Biomarkers for Nonsurvivor Sepsis Patients via Microarray Technology: A Study Based on GEO Datasets. *Research square - preprint*, pp. 1–23. DOI: 10.21203/rs.3.rs-2548567/v1.

Makarova, K. S. & Koonin, E. V. (2015). Annotation and Classification of CRISPR-Cas Systems. *Methods in Molecular Biology*, 1311, pp. 47–75. DOI: 10.1007/978-1-4939-2687-9_4.

Malakhova, O. A., Kim, K. I., Luo, J. K., Zou, W., Kumar, K. G. S., Fuchs, S. Y., Shuai, K. & Zhang, D. E. (2006). UBP43 is a novel regulator of interferon signaling independent of its ISG15 isopeptidase activity. *The EMBO journal*, 25 (11), pp. 2358–2367. DOI: 10.1038/sj.emboj.7601149.

Malakhova, O. A., Yan, M., Malakhov, M. P., Yuan, Y., Ritchie, K. J., Kim, K. I., Peterson, L. F., Shuai, K. & Zhang, D. E. (2003). Protein ISGylation modulates the JAK-STAT signaling pathway. *Genes & development*, 17 (4), pp. 455–460. DOI: 10.1101/gad.1056303.

Mali, P., Yang, L., Esvelt, K. M., Aach, J., Guell, M., DiCarlo, J. E., Norville, J. E. & Church, G. M. (2013). RNA-guided human genome engineering via Cas9. *Science*, 339 (6121), pp. 823–826. DOI: 10.1126/science.1232033.

Marrack, P., Kappler, J. & Kotzin, B. L. (2001). Autoimmune disease: why and where it occurs. *Nature Medicine*, 7 (8), pp. 899–905. DOI: 10.1038/90935.

Marraffini, L. A. (2015). CRISPR-Cas immunity in prokaryotes. *Nature*, 525 (7571), pp. 55–61. DOI: 10.1038/nature15386.

Martin-Fernandez, M., Bravo García-Morato, M., Gruber, C., Murias Loza, S., Nasir Hayat Malik, M., Alsohime, F., Alakeel, A., Valdez, R., Buta, S., Buda, G., Marti, M. A., Larralde, M., Boisson, B., Feito Rodriguez, M., Qiu, X., Chrabieh, M., Al Ayed, M., Al Muhsen, S., Desai, J. V., Ferre, E. M. N., Rosenzweig, S. D., Amador-Borrero, B., Bravo-Gallego, L. Y., Olmer, R., Merkert, S., Bret, M., Sood, A. K., Al-Rabiaah, A., Hani Temsa, M., Halwani, R., Hernandez, M., Pessler, F., Casanova, J. L., Bustamante, J., Lionakis, M. S. & Bogunovic, D. (2020). Systemic Type I IFN Inflammation in Human ISG15 Deficiency Leads to Necrotizing Skin Lesions. *Cell reports*, 31 (6), pp. 1–37. DOI: 10.1016/j.celrep.2020.107633.

Mathieu, N. A., Paparisto, E., Barr, S. D. & Spratt, D. E. (2021). HERC5 and the ISGylation Pathway: Critical Modulators of the Antiviral Immune Response. *Viruses*, 13 (1102), pp. 1–18. DOI: 10.3390/v13061102.

Al-Mayouf, S. M., Akbar, L., AlEnazi, A. & Al-Mousa, H. (2021). Autosomal Recessive ISG15 Deficiency Underlies Type I Interferonopathy with Systemic Lupus Erythematosus and Inflammatory Myositis. *Journal of clinical immunology*, 41 (6), pp. 1361–1364. DOI: 10.1007/s10875-021-01019-1.

Merkert, S., Jaboreck, M. C., Engels, L., Malik, M. N. H., Göhring, G., Pessler, F., Martin, U. & Olmer, R. (2020). Generation of two human ISG15 knockout iPSC clones using CRISPR/Cas9 editing. *Stem cell research*, 50 (102135), pp. 1–5. DOI: 10.1016/j.scr.2020.102135.

Metzger, M. B., Hristova, V. A. & Weissman, A. M. (2012). HECT and RING finger families of E3 ubiquitin ligases at a glance. *Journal of Cell Science*, 125 (3), pp. 531–537. DOI: 10.1242/jcs.091777.

Mocchegiani, E., Bertoni-Freddari, C., Marcellini, F. & Malavolta, M. (2005). Brain, aging and neurodegeneration: Role of zinc ion availability. *Progress in neurobiology*, 75 (6), pp. 367–390. DOI: 10.1016/j.pneurobio.2005.04.005.

Mojica, F. J. M., Díez-Villaseñor, C., García-Martínez, J. & Soria, E. (2005). Intervening sequences of regularly spaced prokaryotic repeats derive from foreign genetic elements. *Journal of molecular evolution*, 60 (2), pp. 174–182. DOI: 10.1007/s00239-004-0046-3.

Mondaza-Hernandez, J. L., Moura, D. S., Lopez-Alvarez, M., Sanchez-Bustos, P., Blanco-Alcaina, E., Castilla-Ramirez, C., Collini, P., Merino-Garcia, J., Zamora, J., Carrillo-Garcia, J., Maestro, R., Hindi, N., Garcia-Foncillas, J. & Martin-Broto, J. (2022). ISG15 as a prognostic biomarker in solitary fibrous tumour. *Cellular and molecular life sciences*, 79 (8), pp. 1–18. DOI: 10.1007/s00018-022-04454-4.

Morales, D. J. & Lenschow, D. J. (2013). The Antiviral Activities of ISG15. *Journal of Molecular Biology*, 425 (24), pp. 4995–5008. DOI: 10.1016/j.jmb.2013.09.041.

Munnur, D., Teo, Q., Eggermont, D., Lee, H. H. Y., Thery, F., Ho, J., Leur, S. W. van, Ng, W. W. S., Siu, L. Y. L., Beling, A., Ploegh, H., Pinto-Fernandez, A., Damianou, A., Kessler, B., Impens, F., Mok, C. K. P. & Sanyal, S. (2021). Altered ISGylation drives aberrant macrophage-dependent immune responses during SARS-CoV-2 infection. *Nature immunology*, 22 (11), pp. 1416–1427. DOI: 10.1038/s41590-021-01035-8.

Murira, A> & Lamarre, A. (2016). Type-I Interferon Responses: From Friend to Foe in the Battle against Chronic Viral Infection. *Frontiers in Immunology*, 7 (609), pp. 1–8. DOI: 10.3389/fimmu.2016.00609.

Narasimhan, J., Wang, M., Fu, Z., Klein, J. M., Haas, A. L. & Kim, J. J. (2005). Crystal Structure of the Interferon-induced Ubiquitin-like Protein ISG15. *The Journal of Biological Chemistry*, 280 (29), pp. 27356–27365. DOI: 10.1074/jbc.M502814200.

Neefjes, J., Jongsma, M. L. M., Paul, P. & Bakke, O. (2011). Towards a systems understanding of MHC class I and MHC class II antigen presentation. *Nature Reviews Immunology*, 11 (12), pp. 823–836. DOI: 10.1038/nri3084.

Nelde, A., Maringer, Y., Bilich, T., Salih, H. R., Roerden, M., Heitmann, J. S., Marcu, A., Bauer, J., Neidert, M. C., Denzlinger, C., Illerhaus, G., Aulitzky, W. E., Rammensee, H. G. & Walz, J. S. (2021). Immunopeptidomics-Guided Warehouse Design for Peptide-Based Immunotherapy in Chronic Lymphocytic Leukemia. *Frontiers in immunology*, 12 (705974), pp. 1–12. DOI: 10.3389/fimmu.2021.70597.

Nguyen, A., Jing, Z., Mahoney, P. S., Davis, R., Sikka, S. C., Agrawal, K. C. & Abdel-Mageed, A. B. (2000). In vivo gene expression profile analysis of metallothionein in renal cell carcinoma. *Cancer letters*, 160 (2), pp. 133–140. DOI: 10.1016/s0304-3835(00)00534-6.

Nguyen, H. M., Oladejo, M., Paulishak, W. & Wood, L. M. (2022). A Listeria-based vaccine targeting ISG15 exerts anti-tumor efficacy in renal cell carcinoma. *Cancer immunology, immunotherapy*, Online issue, pp. 1–5. DOI: 10.1007/s00262-022-03352-9.

Ningrum, A. R. (2014). Human Interferon Alpha-2b: A Therapeutic Protein for Cancer Treatment. *Scientifica (Cairo)*, 2014 (970315), pp. 1–8. DOI: 10.1155/2014/970315.

Nurk, S., Koren, S., Rhie, A., Rautiainen, M., Bzikadze, A. V., Mikheenko, A., Vollger, M. R., Altemose, N., Uralsky, L., Gershman, A., Aganezov, S., Hoyt, S. J., Diekhans, M., Logsdon, G. A., Alonge, M., Antonarakis, S. E., Borchers, M., Bouffard, G. G., Brooks, S. Y., Caldas, G. V., Cheng, H., Chin, C., Chow, W., Lima, L. G. de, Dishuck, P. C., Durbin, R., Dvorkina, T., Fiddes, I. T., Formenti, G., Fulton, R. S., Fungtammasan, A., Garrison, E., Grady, P. G. S., Graves-Lindsay, T. A., Hall, I. M., Hansen, N. F., Hartley, G. A., Haukness, M., Howe, K., Hunkapiller, M. W., Jain, C., Jain, M., Jarvis, E. D., Kerpedjiev, P., Kirsche, M., Kolmogorov, M., Korlach, J., Kremitzki, M., Li, H., Maduro, V. V., Marschall, T., McCartney, A. M., McDaniel, J., Miller, D. E., Mullikin, J. C., Myers, E. W., Olson, N. D., Paten, B., Peluso, P., Pevzner, P. A., Porubsky, D., Potapova, T., Rogaev, E. I., Rosenfeld, J. A., Salzberg, S. L., Schneider, V. A., Sedlazeck, F. J., Shafin, K., Shew, C. J., Shumate, A., Sims, Y., Smit, A. F. A., Soto, D. C., Sović, I., Storer, J. M., Streets, A., Sullivan, B. A., Thibaud-Nissen, F., Torrance, J., Wagner, J., Walenz, B. P., Wenger, A., Wood, J. M. D., Xiao, C., Yan, S. M., Young, A. C, Zarate, S., Surti, U., McCoy, R. C., Dennis, M. Y., Alexandrov, I. A., Gerton, J. L., O'Neill, R. J., Timp, W., Zook, J. M., Schatz, M. C., Eichler, E. E., Miga, K. H. & Phillippy, A. M (2022). The complete sequence of a human genome. *Science*, 376 (6588), pp. 44–53. DOI: 10.1126/science.abj6987.

Nuzzo, R. (2014). Scientific method: statistical errors. *Nature*, 506 (7487), pp. 150–152. DOI: 10.1038/506150a.

O'Neill, L. A. J. (2015). How Low Cholesterol Is Good for Anti-viral Immunity. *Cell*, 163 (7), pp. 1572–1574. DOI: 10.1016/j.cell.2015.12.004.

O'Connor, H. F., Lyon, N., Leung, J. W., Agarwal, P., Swaim, C. D., Miller, K. M. & M., Huibregtse. J. (2015). Ubiquitin-Activated Interaction Traps (UBAITs) identify E3 lig-

ase binding partners. *EMBO reports*, 16 (12), pp. 1699–1712. DOI: 10.15252/embr.201540620.

Okumura, F., Zou, W. & Zhang, D. E. (2007). ISG15 modification of the eIF4E cognate 4EHP enhances cap structure-binding activity of 4EHP. *Genes & Development*, 21 (3), pp. 255–260. DOI: 10.1101/gad.1521607.

Ong, S. E., Blagoev, B., Kratchmarova, I., Bach Kristensen, D., Steen, H., Pandey, A. & Mann, M. (2002). Stable isotope labeling by amino acids in cell culture, SILAC, as a simple and accurate approach to expression proteomics. *Molecular and cellular proteomics*, 1 (5), pp. 376–386. DOI: 10.1074/mcp.m200025-mcp200.

Ong, S. E. & Mann, M. (2006). A practical recipe for stable isotope labeling by amino acids in cell culture (SILAC). *Nature protocols*, 1, pp. 2650–2660. DOI: 10.1038/nprot.2006.427.

Østvik, A. E., Svendsen, T. D., Granlund, A. V. B., Doseth, B., Skovdahl, H. K., Bakke, I., Thorsvik, S., Afroz, W., Walaas, G. A., Mollnes, T. E., Gustafsson, B. I., Sandvik, A. K. & Bruland, T. (2020). Intestinal Epithelial Cells Express Immunomodulatory ISG15 During Active Ulcerative Colitis and Crohn's Disease. *Journal of Crohn's and Colitis*, 14 (7), pp. 920–934. DOI: 10.1093/ecco-jcc/jjaa022.

Padariya, M., Sznarkowska, A., Kote, S., Gómez-Herranz, M., Mikac, S., Pilch, M., Alfaro, J., Fahraeus, R., Hupp, T. & Kalathiya, U. (2021). Functional Interfaces, Biological Pathways, and Regulations of Interferon-Related DNA Damage Resistance Signature (IRDS) Genes. *Biomolecules*, 11 (5), p. 622. DOI: 10.3390/biom11050622.

Park, J. H., Yang, S. W., Park, J. M., Ka, S. H., Kim, J. H., Kong, Y. Y., Jeon, Y. J., Seol, J. H. & Chung, C. H. (2016). Positive feedback regulation of p53 transactivity by DNA damage-induced ISG15 modification. *Nature communications*, 7 (12513), pp. 1–13. DOI: 10.1038/ncomms12513.

Park, J. M., Yang, S. W., Yu, K. R., Ka, S. H., Lee, S. W., Seol, J. H., J., Jeon Y. & Chung, C. H. (2014). Modification of PCNA by ISG15 plays a crucial role in termination of error-prone translesion DNA synthesis. *Molecular Cell*, 54 (4), pp. 626–638. DOI: 10.1016/j.molcel.2014.03.031.

Paul, S., Weiskopf, D., Angelo, M. A., Sidney, J., Peters, B. & Sette, A. (2013). HLA class I alleles are associated with peptide binding repertoires of different size, affinity and immunogenicity. *Journal of immunology*, 191 (12), pp. 5831–5839. DOI: 10.4049/jimmunol.1302101.

Pedersen, M. Ø., Larsen, A., Stoltenberg, M. & Penkowa, M. (2009). The role of metallothionein in oncogenesis and cancer prognosis. *Progress in histochemistry and cytochemistry*, 44 (1), pp. 29–64. DOI: 10.1016/j.proghi.2008.10.001.

Perez, M. A. S., Bassani-Sternberg, M., Coukos, G., Gfeller, D. & Zoete, V. (2019). Analysis of Secondary Structure Biases in Naturally Presented HLA-I Ligands. *Frontiers in immunology*, 10 (2731), pp. 1–18. DOI: 10.3389/fimmu.2019.02731.

Perng, Y. C. & Lenschow, D. J. (2018). ISG15 in antiviral immunity and beyond. *Nature Reviews Microbiology*, 16 (7), pp. 423–439. DOI: 10.1038/s41579-018-0020-5.

Petri, M., Singh, A., Tesfasyone, H., Dedrick, R., Fry, K., Lal, P. G., Williams, G., Bauer, J. W., Gregersen, P. K., Behrens, T. W. & Baechler, E. C. (2009). Longitudinal expression of type I interferon responsive genes in systemic lupus erythematosus. *Lupus*, 18 (11), pp. 980–989. DOI: 10.1177/0961203309105529.

Pickart, C. M. (2001). Mechanisms underlying ubiquitination. *Annual Review of Biochemistry*, 70 (1), pp. 503–533. DOI: 10.1146/annurev.biochem.70.1.503.

Pickles, S., Vigié, P. & Youle, R. J. (2018). Mitophagy and Quality Control Mechanisms in Mitochondrial Maintenance. *Current biology*, 28 (4), R170–R185. DOI: 10.1016/j.cub.2018.01.004.

Pinto-Fernandez, A., Salio, M., Partridge, T., Chen, J., Vere, G., Greenwood, H., Olie, C. S., Damianou, A., Scott, H. C., Pegg, H. J., Chiarenza, A., Díaz-Saez, L., Smith, P., Gonzalez-Lopez, C., Patel, B., Anderton, E., Jones, N., Hammonds, T. R., Huber, K., Muschel, R., Borrow, P., Cerundolo, V. & Kesslert, B. M. (2021). Deletion of the deISGylating enzyme USP18 enhances tumour cell antigenicity and radiosensitivity. *British journal of cancer*, 124 (4), pp. 817–830. DOI: 10.1038/s41416-020-01167-y.

Pitceathly, R. D. S. & Taanman, J. W. (2018). NDUFA4 (Renamed COXFA4) Is a Cytochrome-c Oxidase Subunit. *Trends in endocrinology and metabolism*, 29 (7), pp. 452–454. DOI: 10.1016/j.tem.2018.03.009.

Platanias, L. C. (2005). Mechanisms of type-I- and type-II-interferon-mediated signalling. *Nature Reviews Immunology*, 5 (5), pp. 375–386. DOI: 10.1038/nri1604.

Potter, J. L., Narasimhan, J., Mende-Mueller, L. & Haas, A. L. (1999). Precursor Processing of Pro-ISG15/UCRP, an Interferon-β-induced Ubiquitin-like Protein. *The Journal of Biological Chemistry*, 274 (35), pp. 25061–25068. DOI: 10.1074/jbc.274.35.25061.

Pourcel, C., Salvignol, G. & Vergnaudy, G. (2005). CRISPR elements in Yersinia pestis acquire new repeats by preferential uptake of bacteriophage DNA, and provide additional tools for evolutionary studies. *Microbiology (Reading)*, 151 (3), pp. 656–663. DOI: 10.1099/mic.0.27437-0.

Prokunina-Olsson, L., Muchmore, B., Tang, W., Pfeiffer, R. M., Park, H., Dickensheets, H., Hergott, D., Porter-Gill, P., Mumy, A., Kohaar, I., Chen, S., Brand, N., Tarway, M., Liu, L., Sheikh, F., Astemborski, J., Bonkovsky, H. L., Edlin, B. R., Howell, C. D., Morgan, T. R., Thomas, D. L., Rehermann, B., Donnelly, R. P. & O'Brien, T. R. (2013). A variant upstream of IFNL3 (IL28B) creating a novel interferon gene IFNL4 is associated with impaired clearance of hepatitis C virus. *Nature genetics*, 45 (2), pp. 164–171. DOI: 10.1038/ng.2521.

Purcell, A. W., Ramarathinam, S. H. & Ternette, N. (2019). Mass spectrometry–based identification of MHC-bound peptides for immunopeptidomics. *Nature protocols*, 14 (6), pp. 1687–1707. DOI: 10.1038/s41596-019-0133-y.

Radoshevich, L., Impens, F., Ribet, D., Quereda, J. J., Tham, T. N., Nahori, M. A., Bierne, H., Dussurget, O., Pizarro-Cerdá, J., Knobeloch, K. P. & Cossart, P. (2015). ISG15 counteracts *Listeria monocytogenes* infection. *eLife*, 4 (e06848), pp. 1–23. DOI: 10.7554/eLife.06848.

Rashid, M. H., Babu, D. & Siraki, A. G. (2021). Interactions of the antioxidant enzymes NAD(P)H: Quinone oxidoreductase 1 (NQO1) and NRH: Quinone oxidoreductase 2 (NQO2) with pharmacological agents, endogenous biochemicals and environmental contaminants. *Chemico-biological interactions*, 345 (109574), pp. 1–24. DOI: 10.1016/j.cbi.2021.109574.

Raught, B. & Gingras, A. C. (1999). eIF4E activity is regulated at multiple levels. *The international journal of biochemistry & cell biology*, 31 (1), pp. 43–57. DOI: 10.1016/s1357-2725(98)00131-9.

Recht, M., Borden, E. C. & Knight Jr., E. (1991). A human 15-kDa IFN-induced protein induces the secretion of IFN-gamma. *Journal of Immunology*, 147 (8), pp. 2617–2623.

Reuter, G. & Spierer, P. (1992). Position effect variegation and chromatin proteins. *Bioessays*, 14 (9), pp. 605–612. DOI: 10.1002/bies.950140907.

Ritchie, K. J., Hahn, C. S., Kim, K. I., Yan, M., Rosario, D., Li, L., Torre, J. C. de la & Zhang, D. (2004). Role of ISG15 protease UBP43 (USP18) in innate immunity to viral infection. *Nature Medicine*, 10 (12), pp. 1374–1378. DOI: 10.1038/nm1133.

Rock, K. L., Reits, E. & Neefjes, J. (2016). Present Yourself! By MHC Class I and MHC Class II Molecules. *Trends in immunology*, 37 (11), pp. 724–737. DOI: 10.1016/j.it.2016.08.010.

Rooij, N. van, Buuren, M. M. van, Philips, D., Velds, A., Toebes, M., Heemskerk, B., Dijk, L. J. van, Behjati, S., Hilkmann, H., El Atmioui, D., Nieuwland, M., Stratton, M. R., Kerkhoven, R. M., Kesmir, C., Haanen, J. B., Kvistborg, P. & Schumacher, T. N. (2013). Tumor Exome Analysis Reveals Neoantigen-Specific T-Cell Reactivity in an Ipilimumab-Responsive Melanoma. *Journal of Clinical Oncology*, 31 (32), pp. 1–8. DOI: 10.1200/JCO.2012.47.7521.

Rosewicz, S., Detjen, K., Scholz, A. & Marschall, Z. V. (2004). Interferon-alpha: regulatory effects on cell cycle and angiogenesis. *Neuroendocrinology*, 80 (Suppl 1), pp. 85–93. DOI: 10.1159/000080748.

Sainz, B., Martín, B., Tatari, M., Heeschen, C. & Guerras, S. (2014). ISG15 Is a Critical Microenvironmental Factor for Pancreatic Cancer Stem Cells. *Cancer Research*, 74 (24), pp. 7309–7320. DOI: 10.1158/0008-5472.CAN-14-1354.

Salzberg, S., Hacohen, D., David, S., Dovrat, S., Ahwan, S., Gamliel, H. & Birnbaum, M. (1990). Involvement of interferon-system in the regulation of cell growth and differentiation. *Scanning Microscopy*, 4 (2), pp. 479–89. DOI: Notavailable.

Sandler, N. G., Bosinger, S. E., Estes, J. D., Zhu, R. T. R., Tharp, G. K., Boritz, E., Levin, D., Wijeyesinghe, S., Makamdop, K. N., Prete, G. Q. del, Hill, B. J., Timmer, J. K., Reiss, E., Yarden, G., Darko, S., Contijoch, E., Todd, J. P., Silvestri, G., Nason, M., Norgren, R. B. Jr.,

Keele, B. F., Rao, S., Langer, J. A., Lifson, J. D., Schreiber, G. & Douek, D. C. (2014). Type I interferon responses in rhesus macaques prevent SIV infection and slow disease progression. *Nature*, 511 (7511), pp. 601–605. DOI: 10.1038/nature13554.

Sangfelt O. andErickson, S., Castro, J., Heiden, T., Gustafsson, A., Einhorn, S. & Grandér, D. (1999). Molecular mechanisms underlying interferon-alpha-induced G0/G1 arrest: CKI-mediated regulation of G1 Cdk-complexes and activation of pocket proteins. *Oncogene*, 18 (18), pp. 2798–2810. DOI: 10.1038/sj.onc.1202609.

Satake, H., Tamura, K., Furihata, M., Anchi, T., Sakoda, H., Kawada, C., Iiyama, T., Ashida, S. & Shuin, T. (2010). The ubiquitin-like molecule interferon-stimulated gene 15 is overexpressed in human prostate cancer. *Oncology reports*, 23 (1), pp. 11–16. DOI: 10.3892/or_00000600.

Schellens, I. M. M., Hoof, I., Meiring, H. D., Spijkers, S. N. M., Poelen, M. C. M., Gaans-van den Brink, J. A. M. van, Poel, K. van der, Costa, A. I., Els, C. A. C. M. van, Baarle, D. van & Kesmir, C. (2015). Comprehensive Analysis of the Naturally Processed Peptide Repertoire: Differences between HLA-A and B in the Immunopeptidome. *PLoS one*, 10 (9), pp. 1–18. DOI: 10.1371/journal.pone.0136417.

Schoggins, J. W. (2019). Interferon-stimulated genes: What do they all do. *Annual review of virology*, 6 (1), pp. 567–584. DOI: 10.1146/annurev-virology-092818-015756.

Schumacher, T. N., Scheper, W. & Kvistborg, P. (2019). Cancer Neoantigens. *Annual Review of Immunology*, 37, pp. 173–200. DOI: 10.1146/annurev-immunol-042617-053402.

Schwanhäusser, B., Gossen, M., Dittmar, G. & Selbach, M. (2009). Global analysis of cellular protein translation by pulsed SILAC. *Proteomics*, 9 (1), pp. 205–209. DOI: 10.1002/pmic.200800275.

Schwartzenburg, J., Juncker, M., Reed, R. & Desai, S. (2019). Increased ISGylation in Cases of TBI-Exposed ALS Veterans. *Journal of Neuropathology & Experimental Neurology*, 78 (3), pp. 209–218. DOI: 10.1093/jnen/nly129.

Schwartzenburg, J., Reed, R., Koul, H., Zea, A. H., Shellito, J., Miele, L., Crabtree, J. S. & Desai, S. (2022). ISGylation is increased in the peripheral blood mononuclear cells derived from symptomatic COVID-19 patients. *Experimental biology and medicine (Maywood, NJ)*, 247 (10), pp. 842–847. DOI: 10.1177/15353702221075606.

Segal, N. H., Parsons, D. W., Peggs, K. S., Velculescu, V., Kinzler, K. W., Vogelstein, B. & Allison, J. P. (2008). Epitope landscape in breast and colorectal cancer. *Cancer research*, 68 (3), pp. 889–892. DOI: 10.1158/0008-5472.CAN-07-3095.

Shaw, A. E., Hughes, J., Gu, Q., Behdenna, A., Singer, J. B., Dennis, T., Orton, R. J., Varela, M., Gifford, R. J., Wilson, S. J. & Palmarini, M. (2017). Fundamental properties of the mammalian innate immune system revealed by multispecies comparison of type I interferon responses. *PLoS Biology*, 15 (12), e2004086. DOI: 10.1371/journal.pbio.2004086.

Shi, H. X., Yang, K., Liu, X., Liu, X. Y., Wei, B., Shan, Y. F., Zhu, L. H. & Wang, C. (2010). Positive Regulation of Interferon Regulatory Factor 3 Activation by Herc5 via ISG15 Modification. *Molecular and cellular biology*, 30 (10), pp. 2424–2436. DOI: 10.1128/MCB.01466-09.

Shi, W. Y., Cao, C. & Liu, L. (2016). Interferon α Induces the Apoptosis of Cervical Cancer HeLa Cells by Activating both the Intrinsic Mitochondrial Pathway and Endoplasmic Reticulum Stress-Induced Pathway. *International journal of molecular sciences*, 17 (1832), pp. 1–13. DOI: 10.3390/ijms17111832.

Shin, D., Mukherjee, R., Grewe, D., Bojkova, D., Baek, K., Bhattacharya, A., Schulz, L., Widera, M., Mehdipour, A. R., Tascher, G., Geurink, P. P., Wilhelm, A., Heden van Noort, G. J. van der, Ovaa, H., Müller, S., Knobeloch, K. P., Rajalingam, K., Schulman, B. A., Cinatl, J., Hummer, G., Ciesek, S. & Dikic, I. (2020). Papain-like protease regulates SARS-CoV-2 viral spread and innate immunity. *Nature*, 587 (7835), pp. 657–662. DOI: 10.1038/s41586-020-2601-5.

Si, M. & Lang, J. (2008). The roles of metallothioneins in carcinogenesis. *Journal of hematology & oncology*, 11 (107), pp. 1–20. DOI: 10.1186/s13045-018-0645-x.

Singh, V., Prakhar, P., Rajmani, R. S., Mahadik, K., Borbora, S. M. & Balaji, K. N. (2017). Histone Methyltransferase SET8 Epigenetically Reprograms Host Immune Responses to Assist Mycobacterial Survival. *The Journal of Infectious Diseases*, 216 (4), pp. 477–488. DOI: 10.1093/infdis/jix322.

Sjöblom, T., Jones, S., Wood, L. D., Parsons, D. W., Lin, J., Barber, T. D., Mandelker, D., Leary, R. J., Ptak, J., Silliman, N., Szabo, S., Buckhaults, P., Farrell, C., Meeh, P., Markowitz, S. D., Willis, J., Dawson, D., Willson, J. K., Gazdar, A. F., Hartigan, J., Wu, L., Liu, C., Parmigiani, G., Park, B. H., Bachman, K. E., Papadopoulos, N., Vogelstein, B., Kinzler, K. W. & Velculescu, V. E. (2006). The consensus coding sequences of human breast and colorectal cancers. *Science*, 314 (5797), pp. 268–274. DOI: 10.1126/science.1133427.

Skaug, B. & Chen, Z. J. (2010). Emerging Role of ISG15 in Antiviral Immunity. *Cell*, 143 (2), pp. 187–190. DOI: 10.1016/j.cell.2010.09.033.

Smith, C. C., Selitsky, S. R., Chai, S., Armistead, P. M., Vincent, B. G. & Serody, J. S. (2019). Alternative tumour-specific antigens. *Nature Reviews: Cancer*, 19 (8), pp. 465–478. DOI: 10.1038/s41568-019-0162-4.

Smits, A. H., Ziebell, F., Joberty, G., Zinn, N., Mueller, W. F., Clauder-Münster, S., Eberhard, D., Fälth Savitski, M., Grandi, P., Jakob, P., Michon, A. M., Sun, H., Tessmer, K., Bürckstümmer, T., Bantscheff, M., Steinmetz, L. M., Drewes, G. & Huber, W. (2019). Biological plasticity rescues target activity in CRISPR knock outs. *Nature methods*, 16 (11), pp. 1087–1093. DOI: 10.1038/s41592-019-0614-5.

Snell, L. M., McGaha, T. L. & Brooks, D. G. (2017). Type I Interferon in Chronic Virus Infection and Cancer. *Trends in immunology*, 38 (8), pp. 542–557. DOI: 10.1016/j.it.2017.05.005.

Snyder, A., Makarov, V., Merghoub, T., Yuan, J., Zaretsky, J. M., Desrichard, A., Walsh, L. A., A., Postow. M., Wong, P., Ho, T. S., Hollmann, T. J., Bruggeman, C., Kannan, K., Li, Y., Elipenahli, C., Liu, C., Harbison, C. T., Wang, L., Ribas, A., Wolchok, J. D. & Chan, T. A. (2014). Genetic basis for clinical response to CTLA-4 blockade in melanoma. *The New England journal of medicine*, 371 (23), pp. 2189–2199. DOI: 10.1056/NEJMoa1406498.

Sontheimer, E. J. & Barrangou, R. (2015). The Bacterial Origins of the CRISPR Genome-Editing Revolution. *Human gene therapy*, 26 (7), pp. 413–424. DOI: 10.1089/hum.2015.091.

Speer, S. D., Li, Z., Buta, S., Payelle-Brogard, B., Qian, L., Vigant, F., Rubino, E., Gardner, T. J., Wedeking, T., Hermann, M., Duehr, J., Sanal, O., Tezcan, I., Mansouri, N., Tabarse, P., Mansouri, D., Francois-Newton, V., Daussy, C. F., Rodriguez, M. R., Lenschow, D. J., N., Freiberg A., Tortorella, D., Piehler, J., Lee, B., García-Sastre, A., Pellegrini, S. & Bogunovic, D. (2016). ISG15 deficiency and increased viral resistance in humans but not mice. *Nature Communications*, 7 (11496), pp. 1–10. DOI: 10.1038/ncomms11496.

Stetson, D. B. & Medzhitov, Ruslan (2006). Type I interferons in host defense. *Immunity*, 25 (3), pp. 373–381. DOI: 10.1016/j.immuni.2006.08.007.

Subramaniam, P. S. & Johnson, H. M. (1997). A role for the cyclin-dependent kinase inhibitor p21 in the G1 cell cycle arrest mediated by the type I interferons. *Journal of Interferon & Cytokine Research*, 17 (1), pp. 11–15. DOI: 10.1089/jir.1997.17.11.

Supek, F., Bošnjak, M., Škunca, N. & Šmuc, T. (2011). REVIGO Summarizes and Visualizes Long Lists of Gene Ontology Terms. *PLoS one*, 6 (7), e21800. DOI: 10.1371/journal.pone.0021800.

Swaim, C. D., Canadeo, L. A., Monte, K. J., Khanna, S., Lenschow, D. J. & Huibregtse, J. M. (2020). Modulation of Extracellular ISG15 Signaling by Pathogens and Viral Effector Proteins. *Cell reports*, 31 (11), p. 107772. DOI: 10.1016/j.celrep.2020.107772.

Swaim, C. D., Scott, A. F., Canadeo, L. A. & Huibregtse, J. M. (2017). Extracellular ISG15 Signals Cytokine Secretion Through the LFA-1 Integrin Receptor. *Molecular Cell*, 68 (3), pp. 581–590. DOI: 10.1016/j.molcel.2017.10.003.

Swatek, K. N. & Komander, D. (2016). Ubiquitin modifications. *Cell research*, 26, pp. 399–422. DOI: 10.1038/cr.2016.39.

Takeuchi, T., Inoue, S. & Yokosawa, H. (2006). Identification and Herc5-mediated ISGylation of novel target proteins. *Biochemical and Biophysical Research Communications*, 348 (2), pp. 473–477. DOI: 10.1016/j.bbrc.2006.07.076.

Tang, Y., Zhong, G., Zhu, L., Liu, X., Shan, Y., Feng, H., Bu, Z., Chen, H. & Wang, C. (2010). Herc5 Attenuates Influenza A Virus by Catalyzing ISGylation of Viral NS1 Protein. *The Journal of Immunology*, 184 (10), pp. 5777–5790. DOI: 10.4049/jimmunol.0903588.

Tao, P., Sun, L., Sun, Y., Wang, Y., Yang, Y., Yang, B. & Li, F. (2022). ISG15 is associated with cervical cancer development. *Oncology letters*, 24 (4), pp. 1–9. DOI: 10.3892/ol.2022.13500.

Tarhini, A. A., Gogas, H. & Kirkwood, J. M. (2012). IFN-α in the Treatment of Melanoma. *The journal of Immunology*, 189 (8), pp. 3789–3793. DOI: 10.4049/jimmunol.1290060.

Tchasovnikarova, I. A., Timms, R. T., Matheson, N. J., Wals, K., Antrobus, R., Göttgens, B., Dougan, G., Dawson, M. A. & Lehner, P. J. (2015). Epigenetic silencing by the HUSH complex mediates position-effect variegation in human cells. *Science*, 348 (6242), pp. 1481–1485. DOI: 10.1126/science.aaa7227.

Tecalco Cruz, A. C. & Mejía-Barreto, K. (2017). Cell type-dependent regulation of free ISG15 levels and ISGylation. *Journal of cell communication and signaling*, 11 (2), pp. 127–135. DOI: 10.1007/s12079-017-0385-7.

Tecalco-Cruz, A. C., Velasco-Loyden, G., Robles-Villarruel, L., Cortes-González, C. C., Zepeda-Cervantes, J., Pineda, B. & Chagoya de Sánchez, V. (2022). Interferon-stimulated gene 15 and ISGylation are upregulated in glioblastoma. *Biochemical and biophysical research communications*, 621, pp. 144–150. DOI: 10.1016/j.bbrc.2022.07.011.

Teijaro, J. R., Ng, C., Lee, A. M., Sullivan, B. M., Sheehan, K. C. F., Welch, M., Schreiber, R. D., Torre, J. C. de la & Oldstone, M. B. A. (2013). Persistent LCMV infection is controlled by blockade of type I interferon signaling. *Science*, 340 (6129), pp. 207–211. DOI: 10.1126/science.1235214.

Terawaki, S., Chikuma, S., Shibayama, S., Hayashi, T., Yoshida, T., Okazaki, T. & Honjo, T. (2011). IFN-α directly promotes programmed cell death-1 transcription and limits the duration of T cell-mediated immunity. *Journal of Immunology*, 186 (5), pp. 2772–2779. DOI: 10.4049/jimmunol.1003208.

Theofilopoulos, A. N., Baccala, R., Beutler, B. & Kono, D. H. (2005). Type I interferons (alpha/beta) in immunity and autoimmunity. *Annual review of immunology*, 23, pp. 307–336. DOI: 10.1146/annurev.immunol.23.021704.115843.

Timmons, J. A., Szkop, K. J. & Gallagher, I. J. (2015). Multiple sources of bias confound functional enrichment analysis of global -omics data. *Genome biology*, 16 (186), pp. 1–3. DOI: 10.1186/s13059-015-0761-7.

Tracz, M. & Bialek, W. (2021). Beyond K48 and K63: non-canonical protein ubiquitination. *Cellular Molecular Biology Letters*, 26 (1), pp. 1–17. DOI: 10.1186/s11658-020-00245-6.

Tran, E., Turcotte, S., Gros, A., Robbins, P. F., Lu, Y. C., Dudley, M. E., Wunderlich, J. R., Somerville, R. P., Hogan, K., Hinrichs, C. S., Parkhurst, M. R., Yang, J. C. & Rosenberg, S. A. (2014). Cancer immunotherapy based on mutation-specific CD4+ T cells in a patient with epithelial cancer. *Science*, 344 (6184), pp. 641–645. DOI: 10.1126/science.1251102.

Trolle, T., McMurtrey, C. P., Sidney, J., Bardet, W., Osborn, S. C., Kaever, T., Sette, A., Hildebrand, W. H., Nielsen, M. & Peters, B. (2016). The Length Distribution of Class I-Restricted T Cell Epitopes Is Determined by Both Peptide Supply and MHC Allele-

Specific Binding Preference. *Journal of immunology*, 196 (4), pp. 1480–1487. DOI: 10.4049/jimmunol.1501721.

Urano, T., Saito, T., Tsukui, T., Fujita, M., Hosoi, T., Muramatsu, M., Ouchi, Y. & Inoue, S. (2002). Efp targets 14-3-3 sigma for proteolysis and promotes breast tumour growth. *Nature*, 417 (6891), pp. 871–875. DOI: 10.1038/nature00826.

Urionabarrenetxea, A. G., Fahraeus, R., Hupp, T. & Ball, K. (2019). Neo-antigen peptide vaccines as emerging cancer therapeutics. *The Biochemist*, 41 (1), pp. 16–21. DOI: 10.1042/BIO04101016.

Varadi, M., Anyango, S., Deshpande, M., Nair, S., Natassia, C., Yordanova, G., Yuan, D., Stroe, O., Wood, G., Laydon, A., Žídek, A., Green, T., Tunyasuvunakool, K., Petersen, S., Jumper, J., Clancy, E., Green, R., Vora, A., Lutfi, M., Figurnov, M., Cowie, A., Hobbs, N., Kohli, P., Kleywegt, G., Birney, E., Hassabis, D. & Velankar, S. (2022). AlphaFold Protein Structure Database: massively expanding the structural coverage of protein-sequence space with high-accuracy models. *Nucleic acids research*, 50 (D1), pp. D439–D444. DOI: 10.1093/nar/gkab1061.

Vasou, A., Nightingale, K., Cetkovská, V., Bamford, C. G. G., Andrejeva, J., Randall, R. E., McLauchlan, J., Weekes, M. P. & Hughes, D. J. (2021). A co-opted ISG15-USP18 binding mechanism normally reserved for deISGylation controls type I IFN signalling. *BioRxiv*, pp. 1–38. DOI: 10.1101/2021.06.01.446527.

Vigneron, N., Ferrari, V., Stroobant, V., Habib, J. A. & Van den Eynde, B. J. (2017). Peptide splicing by the proteasome. *Journal of Biological Chemistry*, 292 (51), pp. 21170–21179. DOI: 10.1074/jbc.R117.807560.

Voinsky, I., Zoabi, Y., Shomron, N., Harel, M., Cassuto, H., Tam, J., Rose, S., Scheck, A. C., Karim, M. A., Frye, R. E., Aran, A. & Gurwitz, D. (2022). Blood RNA Sequencing Indicates Upregulated BATF2 and LY6E and Downregulated ISG15 and MT2A Expression in Children with Autism Spectrum Disorder. *International journal of molecular sciences*, 23 (17), pp. 1–14. DOI: 10.3390/ijms23179843.

Vuillier, F., Li, Z., Commere, P. H., Dynesen, L. T. & Pellegrini, S. (2019). USP18 and ISG15 coordinately impact on SKP2 and cell cycle progression. *Scientific reports*, 9 (1), pp. 1–11. DOI: 10.1038/s41598-019-39343-7.

Wang, B., Y., Li., Wang, H., Zhao J. Zhao, Y., Liu, Z. & Ma, H. (2020a). FOXO3a is stabilized by USP18-mediated de-ISGylation and inhibits TGF-β1-induced fibronectin expression. *Journal of Investigative Medicine*, 68 (3), pp. 786–791. DOI: 10.1136/jim-2019-001145.

Wang, L., Lu, G. & Shen, H. M. (2020b). The Long and the Short of PTEN in the Regulation of Mitophagy. *Frontiers in cell and developmental biology*, 8 (299), pp. 1–10. DOI: 10.3389/fcell.2020.00299.

Wang, X., Liu, Y., Han, A., Tang, C., Xu, R., Feng, L., Yang, Y., Chen, L. & Lin, Z. (2022). The NQO1/p53/SREBP1 axis promotes hepatocellular carcinoma progression and metas-

tasis by regulating Snail stability. *Oncogene*, 41 (47), pp. 5107–5120. DOI: 10.1038/s41388-022-02477-6.

Wang, Y., Ding, Q., Xu, T., Li, C. Y., Zhou, D. D. & Zhang, L. (2017). HZ-6d targeted HERC5 to regulate p53 ISGylation in human hepatocellular carcinoma. *Toxicology and applied pharmacology*, 334, pp. 180–191. DOI: 10.1016/j.taap.2017.09.011.

Wasserstein, R. L. & Lazar, N. A. (2016). The ASA's Statement on p-Values: Context, Process, and Purpose. *The American Statistician*, 70 (2), pp. 129–133. DOI: 10.1080/00031305.2016.1154108.

Weerd, N. A. de, Samarajiwa, S. A. & Hertzog, P. J. (2007). Type I Interferon Receptors: Biochemistry and Biological Functions. *The journal of biological chemistry*, 282 (28), pp. 20053–20057. DOI: 10.1074/jbc.R700006200.

Weichselbaum, R. R., Ishwaran, H., Yoon, T., Nuyten, D. S., Baker, S. W., Khodarev, N., Su, A. W., Shaikh, A. Y., Roach, P., Kreike, B., Roizman, B., Bergh, J., Pawitan, Y., Vijver, M. J. van de & Minn, A. J. (2008). An interferon-related gene signature for DNA damage resistance is a predictive marker for chemotherapy and radiation for breast cancer. *Proceedings of the National Academy of Sciences*, 105 (47), pp. 18490–18495. DOI: 10.1073/pnas.0809242105.

Welle, K. A., Zhang, T., Hryhorenko, J. R., Shen, S., Qu, J. & Ghaemmaghami, S. (2016). Time-resolved Analysis of Proteome Dynamics by Tandem Mass Tags and Stable Isotope Labeling in Cell Culture (TMT-SILAC) Hyperplexing. *Molecular and cellular proteomics*, 15 (12), pp. 3551–3563. DOI: 10.1074/mcp.M116.063230.

Wenger, S. L., Senft, J. R., Sargent, L. M., Bamezai, R., Bairwa, N. & Grant, S. G. (2004). Comparison of established cell lines at different passages by karyotype and comparative genomic hybridization. *Bioscience reports*, 24 (6), pp. 631–639. DOI: 10.1007/s10540-005-2797-5.

Wijesooriya, K., Jadaan, S. A., Perera, K. L., Kaur, T. & Ziemann, M. (2022). Urgent need for consistent standards in functional enrichment analysis. *PLoS computational biology*, 18 (3), pp. 1–14. DOI: 10.1371/journal.pcbi.1009935.

Wilson, E. B., Yamada, D. H., Elsaesser, H., Herskovitz, J., Deng, J., Cheng, G., Aronow, B. J., Karp, C. L. & Brooks, D. G. (2013). Blockade of chronic type I interferon signaling to control persistent LCMV infection. *Science*, 340 (6129), pp. 202–207. DOI: 10.1126/science.1235208..

Wong, J. J., Pung, Y. F., Sze, N. S. & Chin, K. C. (2006). HERC5 is an IFN-induced HECT-type E3 protein ligase that mediates type I IFN-induced ISGylation of protein targets. *Proceedings of the National Academy of Sciences of the United States of America*, 103 (28), pp. 10735–10740. DOI: 10.1073/pnas.0600397103.

Wood, L. M., Pan, Z. K., Seavey, M. M., Muthukumaran, G. & Paterson, Y. (2012). The ubiquitin-like protein, ISG15, is a novel tumor-associated antigen for cancer immunotherapy. *Cancer immunology, immunotherapy*, 61 (5), pp. 689–700. DOI: 10.1007/S00262-011-1129-9.

Wu, D., Sanin, D. E, Everts, B., Chen, Q., Qiu, J., Buck, M. D., Patterson, A., Smith, A. M., Chang, C. H., Liu, Z., Artyomov, M. N., Pearce, E. L., Cella, M. & Pearce, E. J. (2016). Type 1 Interferons Induce Changes in Core Metabolism that Are Critical for Immune Function. *Immunity*, 44 (6), pp. 1325–1336. DOI: 10.1016/j.immuni.2016.06.006.

Wu, Y. Y. & Rees, J. L. (2000). Variation in epidermal housekeeping gene expression in different pathological states. *Acta dermato-venereologica*, 80 (1), pp. 2–3. DOI: 10.1080/000155500750012397.

Xijin Ge, S. X., Jung, D. & Yao, R. (2020). ShinyGO: a graphical gene-set enrichment tool for animals and plants. *Bioinformatics*, 36 (8), pp. 2628–2629. DOI: 10.1093/bioinformatics/btz931.

Ye, Y., Akutsu, M., Reyes-Turcu, F., Enchev, R. I, Wilkinson, K. D. & Komander, D. (2011). Polyubiquitin binding and cross-reactivity in the USP domain deubiquitinase USP21. *EMBO reports*, 12 (4), pp. 350–357. DOI: 10.1038/embor.2011.17.

Yeung, T. L., Tsai, C. C., Leung, C. S., Yeung, C. L. A., Thompson, M. S., Lu, K. H., Freedman, R. S., Birrer, M. J., Wong, K. K. & Mok, S. C. (2018). ISG15 Promotes ERK1 ISGylation, CD8+ T Cell Activation and Suppresses Ovarian Cancer Progression. *Cancers*, 10 (12), pp. 1–21. DOI: 10.3390/cancers10120464.

Yim, H. Y., Yang, Y., Lim, J. S., Lee, M. S., Zhang, D. E. & Kim, K. I. (2012). The mitochondrial pathway and reactive oxygen species are critical contributors to interferon-α/β-mediated apoptosis in Ubp43-deficient hematopoietic cells. *Biochemical and biophysical research communications*, 423 (2), pp. 436–440. DOI: 10.1016/j.bbrc.2012.05.154.

Yoo, L., Yoon, A. R., Yun, C. O. & Chung, K. C. (2018). Covalent ISG15 conjugation to CHIP promotes its ubiquitin E3 ligase activity and inhibits lung cancer cell growth in response to type I interferon. *Cell death & disease*, 9 (2), pp. 1–14. DOI: 10.1038/s41419-017-0138-9.

York, A. G., Williams, K. J., Argus, J. P., Zhou, Q. D., Brar, G., Vergnes, L., Gray, E. E., Zhen, A., Wu, N. C., Yamada, D. H., Cunningham, C. R., Tarling, E. J., Wilks, M. Q., Casero, D., Gray, D. H., Yu, A. K., Wang, E. S., Brooks, D. G., Sun, R., Kitchen, S. G., Wu, T. T., Reue, K., Stetson, D. B. & Bensinger, S. J. (2015). Limiting Cholesterol Biosynthetic Flux Spontaneously Engages Type I IFN Signaling. *Cell*, 163 (7), pp. 1716–1729. DOI: 10.1016/j.cell.2015.11.045.

Yuan, W. & Krug, R. M. (2001). Influenza B virus NS1 protein inhibits conjugation of the interferon (IFN)-induced ubiquitin-like ISG15 protein. *The EMBO Journal*, 20 (3), pp. 362–371. DOI: 10.1093/emboj/20.3.362.

Zaretsky, J. M., Garcia-Diaz, A., Shin, D. S., Escuin-Ordinas, H., Hugo, W., Hu-Lieskovan, S., Torrejon, D. Y., Abril-Rodriguez, G., Sandoval, S., Barthly, L., Saco, J., Homet Moreno, B., Mezzadra, R., Chmielowski, B., Ruchalski, K., Shintaku, I. P., Sanchez, P. J., Puig-Saus, C., Cherry, G., Seja, E., Kong, X., Pang, J., Berent-Maoz, B., Comin-Anduix, B., Graeber, T. G., Tumeh, P. C., Schumacher, T. N., Lo, R. S. & Ribas, A. (2016). Mutations Associated

with Acquired Resistance to PD-1 Blockade in Melanoma. *The New England Journal of Medicine*, 375 (9), pp. 819–829. DOI: 10.1056/NEJMoa1604958.

Zhang, C., Zou, Y., Zhu, Y., Liu, Y., Feng, H., Niu, F., He, P. & Liu, H. (2021a). Three Immune-Related Prognostic mRNAs as Therapeutic Targets for Pancreatic Cancer. *Frontiers in Medicine*, 8 (649326), pp. 1–13. DOI: 10.3389/fmed.2021.649326.

Zhang, D. & Zhang, D. E. (2011). Interferon-Stimulated Gene 15 and the Protein ISGylation System. *Journal of Interferon & Cytokine Research*, 31 (1), pp. 119–130. DOI: 10.1089/jr.2010.0110.

Zhang, Q., Wang, J., Qiao, H., Huyan, L., Liu, B., Li, C., Jiang, J., Zhao, F., Wang, H. & Yan, J. (2021b). ISG15 is downregulated by KLF12 and implicated in maintenance of cancer stem cell-like features in cisplatin-resistant ovarian cancer. *Journal of cellular and molecular medicine*, 25 (9), pp. 4395–4407. DOI: 10.1111/jcmm.16503.

Zhang, T., Sun, H. C., Zhou, H. Y., Luo, J. T., Zhang, B. L., Wang, P., Wang, L., Qin, L. X., Ren, N., Ye, S. L., Li, Q. & Tang, Z. Y. (2010). Interferon alpha inhibits hepatocellular carcinoma growth through inducing apoptosis and interfering with adhesion of tumor endothelial cells. *Cancer letters*, 290 (2), pp. 204–210. DOI: 10.1016/j.canlet.2009.09.009.

Zhang, X., Bogunovic, D., Payelle-Brogard, B., Francois-Newton, V., Speer, S. D., Yuan, C., Volpi, S., Li, Z., Sanal, O., Mansouri, D., Tezcan, I., Rice, G. I., Chen, C., Mansouri, N., Alireza Mahdaviani, S., Itan, Y., Boisson, B., Okada, S., Zeng, Lu, Wang, X., Jiang, H., Liu, W., Han, T., Liu, D., Ma, T., Wang, B., Liu, M., Liu, J. Y., Wang, Q. K., Yalnizoglu, D., Radoshevich, L., Uzé, G., Gros, P., Rozenberg, F., Zhang, S. Y., Jouanguy, E., Bustamante, J., García-Sastre, A., Abel, L., Lebon, P., Notarangelo, L. D., Crow, Y. J., Boisson-Dupuis, S., Casanova, J. L. & Pellegrini, S. (2015). Human intracellular ISG15 prevents interferon-α/β over-amplification and auto-inflammation. *Nature*, 517 (7532), pp. 89–93. DOI: 10.1038/nature13801.

Zhang, Y., Burke, C. W., Ryman, K. D. & Klimstra, W. B. (2007). Identification and characterization of interferon-induced proteins that inhibit alphavirus replication. *Journal of virology*, 81 (20), pp. 11246–11255. DOI: 10.1128/JVI.01282-07.

Zhang, Y., Thery, F., Wu, N. C., Luhmann, E. K., Dussurget, O., Foecke, M., Bredow, C., Jiménez-Fernández, D., Leandro, K., Beling, A., Knobeloch, K. P., Impens, F., Cossart, P. & Radoshevich, L. (2019). The in vivo ISGylome links ISG15 to metabolic pathways and autophagy upon Listeria monocytogenes infection. *Nature communications*, 10 (1), pp. 1–15. DOI: 10.1038/s41467-019-13393-x.

Zhang, Y. & Yu, C. (2020). Prognostic characterization of OAS1/OAS2/OAS3/OASL in breast cancer. *BMC Cancer*, 20 (575), pp. 1–12. DOI: 10.1186/s12885-020-07034-6.

Zhang, Z., Lu, M., Qin, Y., Gao, W., Tao, L., Su, W. & Zhong, J. (2021c). Neoantigen: A New Breakthrough in Tumor Immunotherapy. *Frontiers in Immunology*, 12 (672356), pp. 1–9. DOI: 10.3389/fimmu.2021.672356.

Zhao, C., Beaudenon, S. L., Kelley, M. L., Waddell, M. B., Yuan, W., Schulman, B. A., Huibregtse, J. M. & Krug, R. M. (2004). The UbcH8 ubiquitin E2 enzyme is also the E2 enzyme for ISG15, an IFN-α/β-induced ubiquitin-like protein. *Proceedings of the National Academy of Sciences of the United States of America*, 101 (20), pp. 7578–7582. DOI: 10.1073/pnas.0402528101.

Zhao, C., Denison, C., Huibregtse, J. M., Gygi, S. & Krug, R. M. (2005). Human ISG15 conjugation targets both IFN-induced and constitutively expressed proteins functioning in diverse cellular pathways. *Proceedings of the National Academy of Sciences of the United States of America*, 102 (29), pp. 10200–10205. DOI: 10.1073/pnas.0504754102.

Zhao, Z., Li, C., Tong, F., Deng, J., Huang, G. & Sang, Y. (2021). Review of applications of CRISPR-Cas9 gene-editing technology in cancer research. *Biological procedures online*, 23 (14), pp. 1–13. DOI: 10.1186/s12575-021-00151-x.

Zhou, Q. & Zhang, J. (2022). K27-linked noncanonic ubiquitination in immune regulation. *Journal of leukocyte biology*, 111 (1), pp. 223–235. DOI: 10.1002/JLB.4RU0620-397RR.

Zou, W. & Zhang, D. E. (2006). The interferon-inducible ubiquitin-protein isopeptide ligase (E3) EFP also functions as an ISG15 E3 ligase. *The Journal of Biological Chemistry*, 281 (7), pp. 3989–3994. DOI: 10.1074/jbc.M510787200.